Study of photo-induced and radical reactions between CH4 and NH3 : astrochemical applications

Mindaugas Jonušas

THESE DE DOCTORAT DE SORBONNE UNIVERSITÉ

Spécialité : Chimie physique et théorique

Ecole doctorale de Chimie Physique et Chimie Analytique. Paris Centre (ED 388)

Présentée par

Mindaugas Jonušas

Pour obtenir le grade de *DOCTEUR de SORBONNE UNIVERSITÉ*

Study of photo-induced and radical reactions between CH_4 and NH_3: astrochemical applications

28 May 2018

Jury de thèse composé de :

Mme. Claudine Crépin	Rapporteur
M. Fabrice Duvernay	Rapporteur
M. Justinas Čeponkus	Examinateur
M. François Dulieu	Examinateur
M. Loïc Journel	Examinateur
M. Lahouari Krim	Directeur de Thèse

Table of Contents

“The fact that we live at the bottom of a deep gravity well, on the surface of a gas covered planet going around a nuclear fireball 90 million miles away and think this to be normal is obviously some indication of how skewed our perspective tends to be.”

— Douglas Adams, the Salmon of Doubt: Hitchhiking the Galaxy One Last Time

From a dream of a child to a scientific reality:

It is hardly that one can find a child who would not have been looking at the stars in the night without trying to imagine the possibilities of extraterrestrial. Knowing there is no limits to a child's imagination, probably everyone has at least once thought about the formation of stars and galaxies, planetal diversity, their structure and, of course, a life beyond the planet Earth. This has been much more expanded in these recent decades with advances in science, cinematography and CGI (Computer-generated imagery) through movies about space, scientific discoveries and artistic imagery.

I am also one of those who fall into this category. Since I was a child I always was fascinated by the world of science. Mostly I am grateful to my physics teacher in middle school who introduced me to wonders of science, from the Newton's laws of motion across the Maxwell's equations of classical electrodynamics until the Einstein's theory of relativity. Of course, like any other child in school, I was not also very keen on studying, but not physics in particular. Physics always has been my most favorite subject, because mainly not that you had to understand it through hard studying, but rather through a logical thinking, especially, when most theories could be explained through easy experiments. For a child any kind of visual presentation is much more appealing and interesting than reading about it in a book. The same was for me from soldering electric schemes till night sky observations using a telescope. And this fascination never died even in my university days. Especially even now that I am doing the thing I love the most – try to explain the unknown.

I, being the first student to work with this particular experimental equipment, have written the experimental section with greater attention to detail because this thesis might be used by future students working with this system. Upon my arrival the system has been greatly improved by enhancing the ramping and injection systems and also introduced with new equipment (UV lamp, microwave discharge). Further on, some hardships were overcome of the laboratory movement to a new building and setting up a new work place environment followed by an equipment realignment and recalibration.

On the same note, I would like to express a great deal gratitude to my supervisor Lahouari Krim with his valuable advices and insights during these three years that we were working together. I would like also to show appreciation to the whole MONARIS laboratory team, especially to my work colleagues Cairedine and Alejandro not only for scientific discussions but also for providing a daily dose of entertainment even on the dullest moments. I should also not forget my Master thesis supervisor Justinas Čeponkus, who introduced me to the fascinating world of IR spectrometry and low temperature studies.

And last but not least, I would like to dedicate this work to my parents, brothers and a sister, who always supported me through my crazy scientific obsession and always believed and encouraged me.

On this accord, I want to say a huge AČIŪ ([ˈaːtʃuː] it is not a sneeze, it is thank you in lithuanian) to everyone mentioned and not only here on their direct or indirect help that lead me to this moment.

Chapter I:

Introduction

Probably one of the most common questions that people ask is: Why is there life on Earth? Or why is Earth so special? Well it depends on numerous aspects like: having an atmosphere, having a magnetic field, mass of the earth, mass of the sun, the distance from the sun, having a satellite (the moon). But thinking that there are billions of other stars with their own planets; does not it mean that there should be another planet similar to Earth? And would it also have life on it? Well the short answer would be: it is hard to tell. But at least we can try to analyze some possibilities. The question how life has been formed is one of the challenging problems of our time, because that is the question of our origin.[1] There are two alternative different hypotheses concerning the formation of life, or in more precise case, the formation of biotic and prebiotic structures that consists in all the living organisms, that could lead to the living organisms. The first one is about the formation of precursors on the planet itself, i.e. the in situ formation.[2] The second one is on the molecular formation in the interstellar environment. From this interstellar environment, there is a possibility of transferring these precursors via meteoritic or cometary impacts to the surface of the planet.[3] While the first hypothesis is quite plausible, we will be focusing on the second one about the molecular formation in the interstellar medium.

I.1. Chemical evolution

It is very obvious that physical and chemical evolutionary processes in interstellar space are very complex. This complex interstellar chemical evolution may be classified into different stages:[4]

1. The Big Bang is the obvious first stage. With it appeared matter as we know it, in the form of elementary particles. After that proceeded the formation processes of stars and planets, to continue synthesizing the essential chemical elements like carbon, nitrogen, and oxygen via nuclear fusion within the stars.

2. The second stage characterizes the formation of first organic molecular structures, which condensed on the surface of grains and in the gas phase of circumstellar shells of evolved stars. That later were transferred to the interstellar medium, comets, meteorites and planetary atmospheres.

3. On the third stage more complex building block molecules are produced up to prebiotic structures like the simplest amino acids, precursors of proteins and nucleic acids in the astrophysical scenarios mentioned above.

4. The next step is represented by the molecular evolution on early earth or similar environments like extraterrestrial planets right to the development of precellular structures. Chirality, self-organization, self reproduction, and the genetic code begin to play an essential role on that primitive biological stage.

5. Finally the advanced fifth level of life, perhaps more advanced than we know it so far from unicellular structures (microorganisms) to multicellular organisms.

This thesis focuses on the second stage, explaining the formation of complex molecular structures and bringing insights into molecular complexity in the interstellar medium.

I.2. Interstellar medium (ISM)

The interstellar medium is the matter that exists in the space between the stars in a galaxy. This matter includes gases (ionic, atomic and molecular species: 99%), dusts (1%) and cosmic rays. The gas composition is 90% of hydrogen, 9% of helium and 1% heavier elements.[5] Hydrogen and helium are primarily a result of protonucleosynthesis, a production of nuclei during the early phases of the Universe. The heavier elements in the ISM are mostly a result of enrichment in the process of stellar evolutions. Complex molecules are composed also out of oxygen, carbon and nitrogen in addition to hydrogen. Their relative abundances are presented in table I-1. It has to be noted that these values are given for the gas phase. However by taking into account all the species trapped in the interstellar grains, then these abundances should be higher.

Table I-1: Abundances of the three most important elements relative to atomic hydrogen.

Element	Abundance relative to hydrogen	Reference
Carbon (C)	1.4×10^{-4}	Cardelli et al, 1996[6]
Nitrogen (N)	7.5×10^{-5}	Meyer et al., 1997[7]
Oxygen (O)	3.2×10^{-4}	Meyer et al., 1998[8]

The ISM can be divided into few different environments that are shown in table I-2.[9] These environments could be grouped into two regions: hot and cold regions. The hot region, called also diffuse region, consists of gases having temperatures above 50K with densities ranging from 10 particles per cm^3 to as low as 10^{-4} particles per cm^3. The second region, called dense and cold region, is characterized by temperatures lower than 50K and high densities, which may reach up to 10^6 particles per cm^3.

Table I-2. Temperature and density distributions in the ISM.

Phase	**Temperature, K**	**Density, cm^{-3}**	**Volume, (%)**
Coronal gas (HIM)	$10^{5.5}$–10^7	0.004	50
Warm ionized medium (WIM)	~10^4	0,3	10
HII regions	10^4	10^2-10^4	0,01
Warm neutral medium (WNM)	~5000	0,6	40
Cold neutral medium	40-100	~30	1
Diffuse molecular gas	30-100	30-300	0,1
Dense molecular cores	10-20	10^3-10^6	0,01

Coronal gas or sometimes referred to as Hot Ionized Medium (HIM). This coronal cloud is the cloud of hot plasma gas surrounding a coronal mass ejection. This hot gas is often buoyant and appears as bubbles and fountains high above the protostellar disk. It mostly consists of protons and electrons, with traces of other larger elements. The densities in these clouds are very low raging between 10^{-4} to 10^{-2} particles per cm^3, so it is kind of obvious that it is the biggest by volume. Having in mind that the thermal kinetic energy is $E = \frac{3}{2}kT$ (where Boltzmann constant $k \approx 8.6 \times 10^{-5}$ eV/K) we can use the temperature range to roughly estimate the kinetic energy range. The thermal kinetic energy in this region is between ~50eV up to ~1300eV. Just for comparison the ionization of hydrogen is 13.6eV, so that means that all the elements in this medium are highly ionized.

Warm ionized medium (WIM) is a medium where hydrogen still mainly exists in ionized form. The temperatures in this region can range from 6000K up to 10000K, while densities from 0.1 to 0.4 cm^{-3}. To explore the density and distribution of diffuse plasma in this region Hα emission (visible emission corresponding to H atomic Balmer transition n=3 → n=2; λ=6563Å) and pulsar dispersion measures are used for astronomical observations. Nearly 90% of the H^+ in the Galaxy resides in the WIM, with the remaining 10% in the bright high-density HII regions that occupy a tiny fraction of the ISM.

HII regions are used to describe ionized atomic hydrogen (II is roman numerical 2), while HI stands for neutral atomic hydrogen. In comparison these regions are very similar to warm ionized medium regions having the similar temperatures. The difference is the density is much higher. These are the clouds where star formation has recently taken place. The observations are also the same as to WIM regions though emissions of Hα and pulsar dispersion.

Warm neutral medium (WNM) temperatures and densities are similar to WIM region, but this medium mainly consists of neutral atomic hydrogen. This region is located mainly in photodissociation regions on the boundaries of HII regions and molecular clouds, because of this in some older papers it can be found called “warm intercloud medium”. Primary observations are made by HI (λ=21cm and ν=1.42GHz) emission lines. This line is very useful in astronomy because the microwaves can penetrate the large clouds of interstellar cosmic dust that are opaque to visible light.

Cold neutral medium (CNM) is a medium with temperatures around 50 to 100K and densities between 20 to 50 particles per cm^3. It is mainly composed by neutral atomic Hydrogen. The main tracers are UV and optical absorption lines seen towards bright stars or quasars. The most common observation is using the HI 21 cm line absorption.

Diffuse molecular gas is like cold neutral medium in similar temperature range (30-100K) with a slightly higher density up to 300 particles per cm^3. This is a region where atomic species recombine forming molecules. As the density increases, diffuse clouds gradually turn into the clouds referred to as translucent and then to the dense. The physics and chemistry of diffuse

clouds may be studied by observing the absorption lines produced in the spectra of the background stars.

Dense molecular cores are referred to that portion of molecular clouds with densities exceeding 10^2 atoms per cm^3. These clouds are around the temperatures lower than 20K. Most molecular clouds are gravitationally bound. Molecular clouds with densities of 10^5 particles per cm^3 or greater are the sources of star formation. The gas phase of a dense interstellar cloud consists almost entirely of molecular hydrogen, and with an admixture of interstellar dust. The main tracers are millimeter and micro wavelength molecular emission lines.

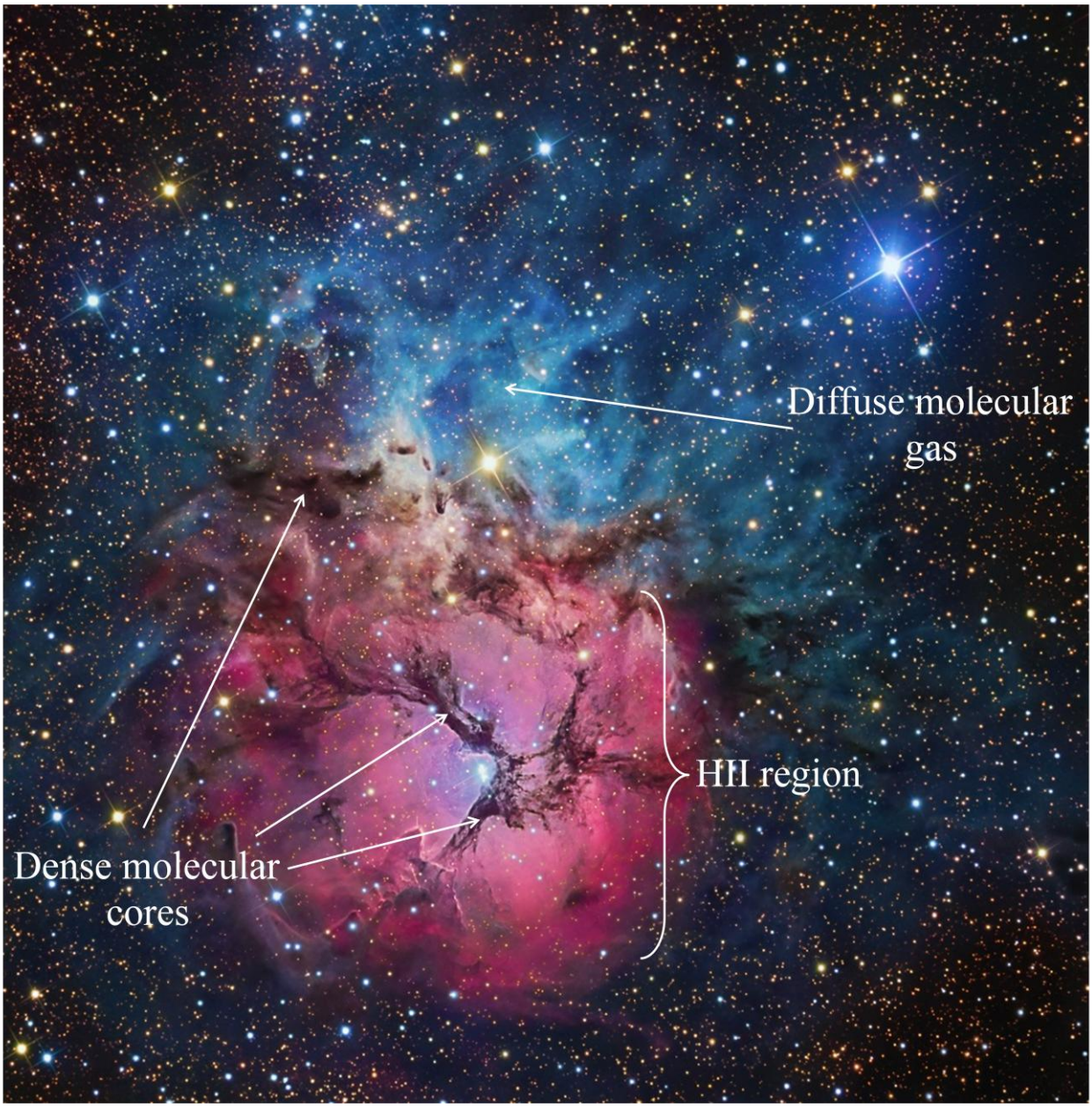

Figure I-1. Triffid Nebula (M 20). H II region is distinguished by the red-pinkish glow. Dark areas mainly consist of dust that blocks light. Bluish regions are not always seen around H II regions. These regions consist of mixture of gases and dust and are visible due to the reflection of blue light.

I.3. Formation of stars and planets

Stars and planets are formed from the same interstellar cloud. An interstellar cloud is just an accumulation of gas and dust in the universe. Average region of the interstellar medium is not completely empty, but consists of a hard vacuum containing a low density of particles (predominantly of hydrogen and helium), as well as electromagnetic radiation, neutrinos, dust, and cosmic rays.[10] An interstellar cloud is a denser than this average region of the interstellar

medium. There are a few types of clouds depending on the density, size, and temperature of a given cloud. The hydrogen in these regions can be neutral (HI regions), ionized (HII regions) or molecular (molecular clouds). Neutral and ionized clouds are sometimes also called diffuse clouds, while molecular clouds are sometimes also referred to dense clouds. Due to the low temperature and density of these clouds the reaction rates in interstellar clouds were expected to be very slow, with minimal products. However, many organic molecules were observed from the analysis of spectra given from several observations. Scientists would not have expected to find, under these extreme conditions, large complex molecules such as formaldehyde, methanol and vinyl alcohol.[11] The reactions needed to create such species are known to need much higher temperatures and requires higher quantity of materials (density and pressure). The formation of these organic species in the diluted regions of interstellar medium indicates that other chemical reaction pathways should be taken into account, such as heterogeneous processes involving solid-phase and probably gas-phase reactions unfamiliar to organic chemistry as observed on earth.

Diffuse clouds consist mainly of the material blown off from other stars. The accumulation of gas and dust creates low density clouds. Due to the gravity, further accumulation of material creates dense clouds. When the interstellar cloud reaches sufficient mass it collapses by self gravitation, leading to the formation of protostellar systems. The region surrounding a newborn massive star is called hot molecular core. The observations have revealed that the hot molecular cores show significantly different chemical compositions as compared to similar dense clouds.[12] In particular, the results suggest that simple organic molecules such as methanol are detected in lower abundances, in contrast with other large organic species showing high abundances in hot cores and never detected in dense molecular clouds. From these observations it has been suggested that the environment should affect the formation processes of molecules around a newborn star. Later on, the protostellar systems further contract forming a central protostar and a rotating disk of gas and dust accreting much more material. At this stage planets and comets are formed from the material in the outer disk. Due to the temperature and density increase in the central star, the thermonuclear reactions begin. Radiations from a newborn star drive the remaining dust and gas away from the system. At the same time planets, comets and other interplanetary material stay in the orbits of the star. Large complex molecules and eventually prebiotic species, formed during the evolution of the star, are carried to the planets by dust particles, meteorites and comets. In the end, the star becomes unstable due to the depleted nuclear fuel, blowing up in a supernova explosion and creating many chemical species, which are injected into the interstellar medium to form diffuse clouds. This is the cycle of the interstellar process is depicted in figure I-2.

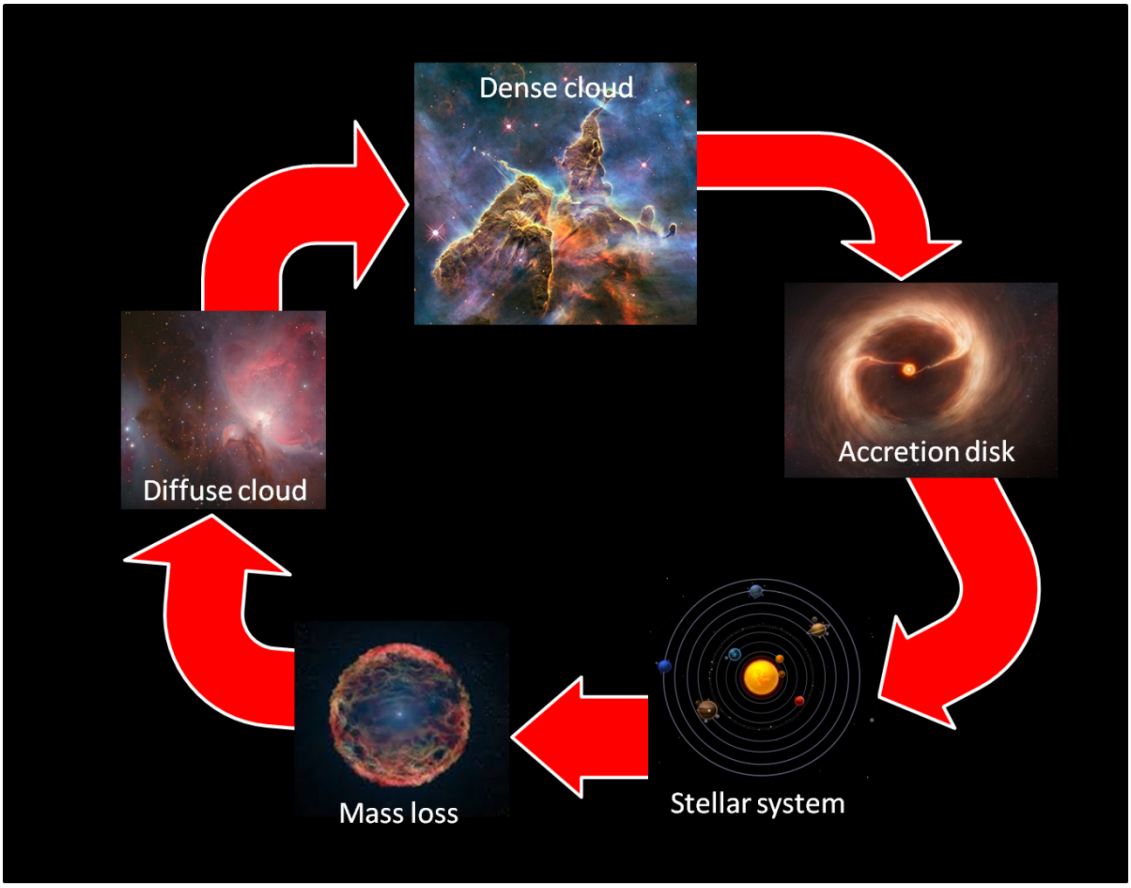

Figure I-2. Stellar system formation.

I.4. Interstellar chemistry

Presently, as of now, there are more than 200 molecules identified in the ISM. Table I-3 presents all the species already detected in the interstellar medium or circumstellar shells. The most complex species detected till now contain more than 12 atoms. In 2018 an unsaturated species C_6H_5CN has been detected and it is considered as the most complex organic molecule containing carbon, hydrogen and nitrogen ever detected. While simpler molecules can be formed by gas phase chemistry, it is well established that complex molecules are mainly formed on the surfaces of the dust grains. Dust grains play a role of a recipient by trapping several reactants and increasing the probability of their interactions. Dust grains are also considered as catalysts, which induce much more complex chemistry not feasible in gas phase. The principle chemical reactions that can occur in the dense molecular clouds and in the star forming environments are a bit different and they are going to be explained in the following paragraphs.

Table I-3. Detected and identified molecules in the Interstellar Medium or Circumstellar Shells

2 atoms		3 atoms		4 atoms	5 atoms	6 atoms	7 atoms	8 atoms	9 atoms	10 atoms
H_2	SiS	C_3 *	*c*-SiC_2	*c*-C_3H	C_5 *	C_5H	C_6H	CH_3C_3N	CH_3C_4H	CH_3C_5N
AlF	CS	C_2H	CO_2 *	*l*-C_3H	C_4H	*l*-H_2C_4	CH_2CHCN	$HC(O)OCH_3$	CH_3CH_2CN	$(CH_3)_2CO$
AlCl	HF	C_2O	NH_2	C_3N	C_4Si	C_2H_4*	CH_3C_2H	CH_3COOH	$(CH_3)_2O$	$(CH_2OH)_2$
C_2**	HD	C_2S	H_3^+(*)	C_3O	*l*-C_3H_2	CH_3CN	HC_5N	C_7H	CH_3CH_2OH	CH_3CH_2CHO
CH	FeO ?	CH_2	SiCN	C_3S	*c*-C_3H_2	CH_3NC	CH_3CHO	C_6H_2	HC_7N	CH_3CHCH_2O
CH^+	O_2	HCN	AlNC	C_2H_2*	H_2CCN	CH_3OH	CH_3NH_2	CH_2OHCHO	C_8H	2016
CN	CF^+	HCO	SiNC	NH_3	CH_4 *	CH_3SH	*c*-C_2H_4O	*l*-HC_6H *	$CH_3C(O)NH_2$	CH_3OCH_2OH
CO	SiH ?	HCO^+	HCP	HCCN	HC_3N	HC_3NH^+	H_2CCHOH	CH_2CHCHO (?)	C_8H^-	2017
CO^+	PO	HCS^+	CCP	$HCNH^+$	HC_2NC	HC_2CHO	C_6H^-	CH_2CCHCN	C_3H_6	
CP	AlO	HOC^+	AlOH	HNCO	HCOOH	NH_2CHO	CH_3NCO	H_2NCH_2CN	CH_3CH_2SH	**11 atoms**
SiC	OH^+	H_2O	H_2O^+	HNCS	H_2CNH	C_5N	HC_5O	CH_3CHNH	(?)	HC_9N
HCl	CN^-	H_2S	H_2Cl^+	$HOCO^+$	H_2C_2O	*l*-HC_4H *	2017	CH_3SiH_3	CH_3NHCHO ?	CH_3C_6H
KCl	SH^+	HNC	KCN	H_2CO	H_2NCN	*l*-HC_4N		2017	2017	C_2H_5OCHO
NH	SH	HNO	FeCN	H_2CN	HNC_3	*c*-H_2C_3O			HC_7O	$CH_3OC(O)CH_3$?
NO	HCl^+	MgCN	HO_2	H_2CS	SiH_4 *	H_2CCNH (?)			2017	
NS	TiO	MgNC	TiO_2	H_3O^+	H_2COH^+	C_5N^-				**12 atoms**
NaCl	ArH^+	N_2H^+	C_2N	*c*-SiC_3	C_4H^-	HNCHCN				*c*-C_6H_6 *
OH	N_2	N_2O	Si_2C	CH_3 *	HC(O)CN	SiH_3CN				*n*-C_3H_7CN
PN	NO^+ ?	NaCN	HS_2	C_3N^-	HNCNH	2017				*i*-C_3H_7CN
SO	NS^+	OCS	2017	PH_3	CH_3O					$C_2H_5OCH_3$?
SO^+	2018	SO_2		HCNO	NH_4^+					
SiN				HOCN	H_2NCO^+ (?)					**>12 atoms**
SiO				HSCN	$NCCNH^+$					C_{60} *
				H_2O_2	CH_3Cl					C_{70} *
				C_3H^+	2017					C_{60}^+ *
				HMgNC						*c*-C_6H_5CN
				HCCO						2018

All molecules have been detected by rotational spectroscopy in the radiofrequency to far-infrared regions.

* indicates molecules that have been detected by their rotation-vibration spectrum,

** those detected by electronic spectroscopy only.

"?" are indicated by tentative detections, which have a reasonable chance to be correct.

"(?)" are indicated detections that have been reported as secure, because the number of observed transitions have a small overlap.

The year most relevant to the detection is given for recent results.

Data provided from: https://www.astro.uni-koeln.de/cdms/molecules

I.4.1. Gas phase reactions

As noted before there are two regions in which interstellar chemistry may take place. Closer to protostars (hot cores), although the density and temperature are high (T ~ 100-500K) to favor the formation of many chemical species, the simplest molecule as H_2 cannot be formed efficiently. In the low temperature (<50K) and density regions (cold molecular cores or molecular clouds), unimolecular or bimolecular reaction pathways may be the source of simple and complex molecular species.[13,14] Reactions involved in gas phase imply that the molecules are so dispersed and far from each other that the possibility of interaction is very small and consequently processes involved in the gas phase cannot be the only source of the molecular composition in the ISM. Radical–radical and ion-molecule reactions are dominant over neutral-neutral reactions. Radical-radical reactions are possible because of the tendency to pair the electrons and because they have small energies of activation. While the ion-molecule reactions may take place due to the attraction-repulsion of charge that induces the movement of the ions increasing their kinetic energy. This kinetic energy is enough to overcome activation barriers showed by a given chemical reaction.[15] Neutral-neutral reactions are discarded due to the fact that nearly all exothermic reactions involving neutral species possess large activation energies.

As already noted before, the most abundant molecule in the ISM is H_2, which can be ionized by cosmic rays to produce electrons, H^+ and H_2^+. Through subsequent reaction an H_3^+ ion can be created, that easily transfers protons to other molecules. The synthesis of interstellar molecules may be started by charge transfer between H_3^+ and other species such as atomic oxygen, to form H_2 and OH^+, two chemical precursors for the formation of water molecules. Similar reactions may lead to the formation of CO, NH_3, and N_2 as the most abundant molecules after H_2. [16,17] The timescale to form these species under ISM have been calculated on the order of several million years. During this time almost all the atomic such as C and O are converted into molecular species CO and O_2.[18]

I.4.2. Grain surface reactions

In a previous paragraph the existence of cosmic dust was also mentioned. These microscopic particles are mainly composed of a mixture of carbonaceous material or silicates. The average size of these particles has been estimated around 0.1 μm. Dust grains play an important role in the ISM chemistry. Infrared observations of dark clouds and subsequent interpretations indicate that ice mantles cover interstellar dust grains and suggest that a rich catalytic chemistry is possible.[19]

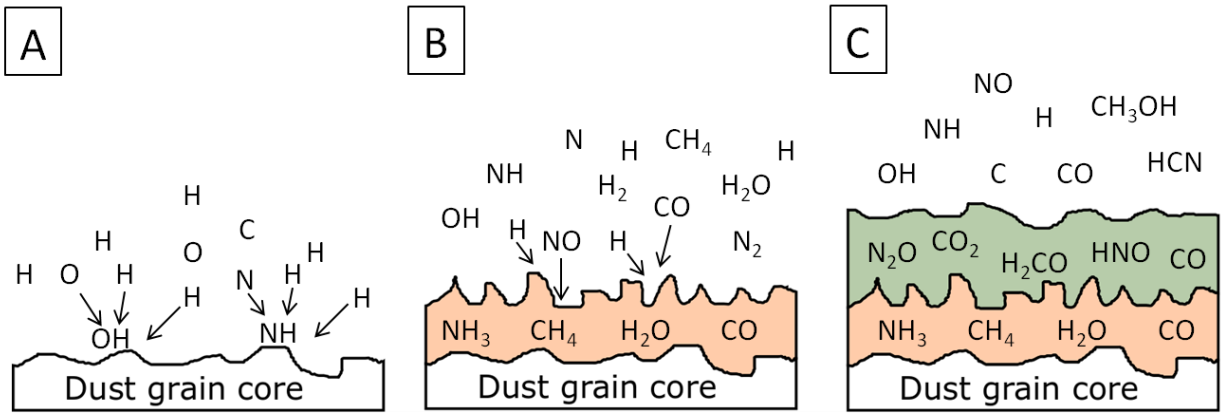

Figure I-3. Increase of molecular variety on dust grain surface chemistry going from diffuse (A) through translucent (B) into dense (C) clouds

Cold grain-surface reactions occur in two steps. First, atoms and molecules stick to the surface, and then subsequently diffuse on to the surface binding sites by quantum mechanical tunneling. Considering most of the gases in dense clouds consist of atomic species predominantly H, but also heavier: O, N, C. Diffusion of light atoms is many times faster than that of heavier molecules; therefore the chemistry is dominated by atom-atom reactions and atom-molecular radical reactions.[20] Considering the long lifetime of clouds (10^6-10^8 years) the atoms or fragments of molecules are transformed into the stable molecules such as H_2O, NH_3 and CH_4, through atomic hydrogenation processes. Surface chemistry is the source of the huge variety of molecules, which could not be explained through simple gas phase chemistry. Figure I-3 shows the different steps of dust grain evolution in dense molecular clouds. Although H addition reaction can be predominant, surface reaction involving atomic species such as C, N and O can lead to many known interstellar molecules containing N, O, C and H such as amines, aldehydes, ketones, alcohols, sugars.[21,22] Figure I-4 shows an example of chemical reaction pathways adopted by astrophysical models for the solid phase transformation of CO molecule.

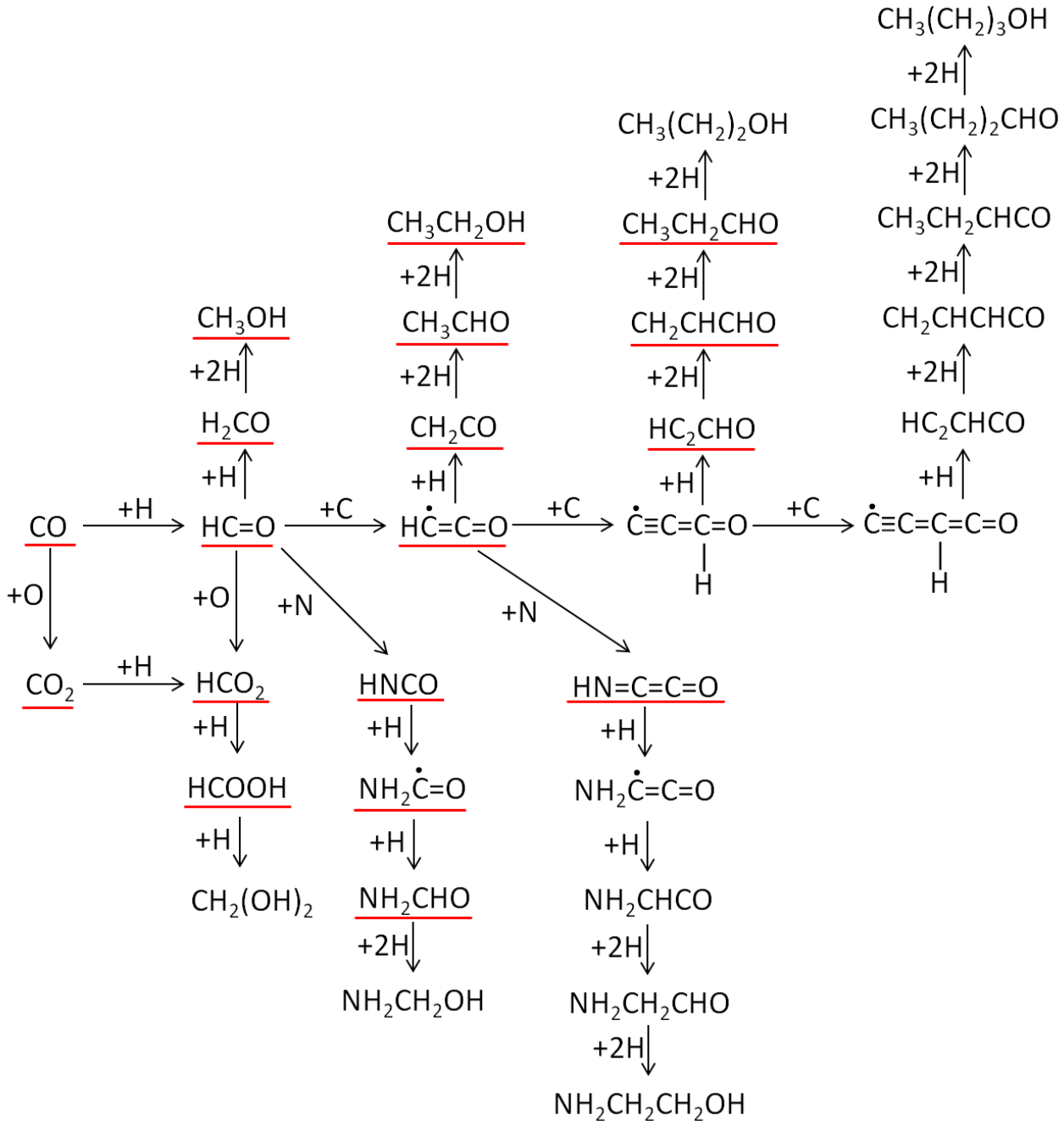

Figure I-4. A basic CO solid phase transformation sequence involving C, N and H atoms, underlined species are detected in the ISM

As mentioned before the surfaces of dust grains operate as catalysts, bringing together reactants that might otherwise rarely interact due to low density of the gas phase. For example, with the conditions present in molecular clouds, it is quite rare that two colliding hydrogen atoms would recombine to form H_2 molecule. However, H_2 molecules can form when the atoms are attached to the sticky surface of a dust grain which is able to absorb the excess energy derived from the exothermic H-H recombination. Additionally to the atomic addition reactions occurring

on the surface of dust grains, energetic processing involving UV photons and cosmic-rays may induce other chemical reactions. These energetic chemical processes are equilibrium between molecular fragmentations, formation of large complex molecules and desorptions at low temperature induced by UV light. Additional excess energy may be used in breaking the weak surface bond thus leading to direct ejection of molecules from the mantle into the gas phase.[25] The dust grains may also be a source of stability of molecules by absorbing the ionising UV radiations to protect molecules already formed.[23] Dust grains also keep interstellar gas clouds cool by absorbing the energy from both gas-grain collisions and UV radiation. Processes on the interstellar dust grain due to the environmental impact are shown in figure I-5.

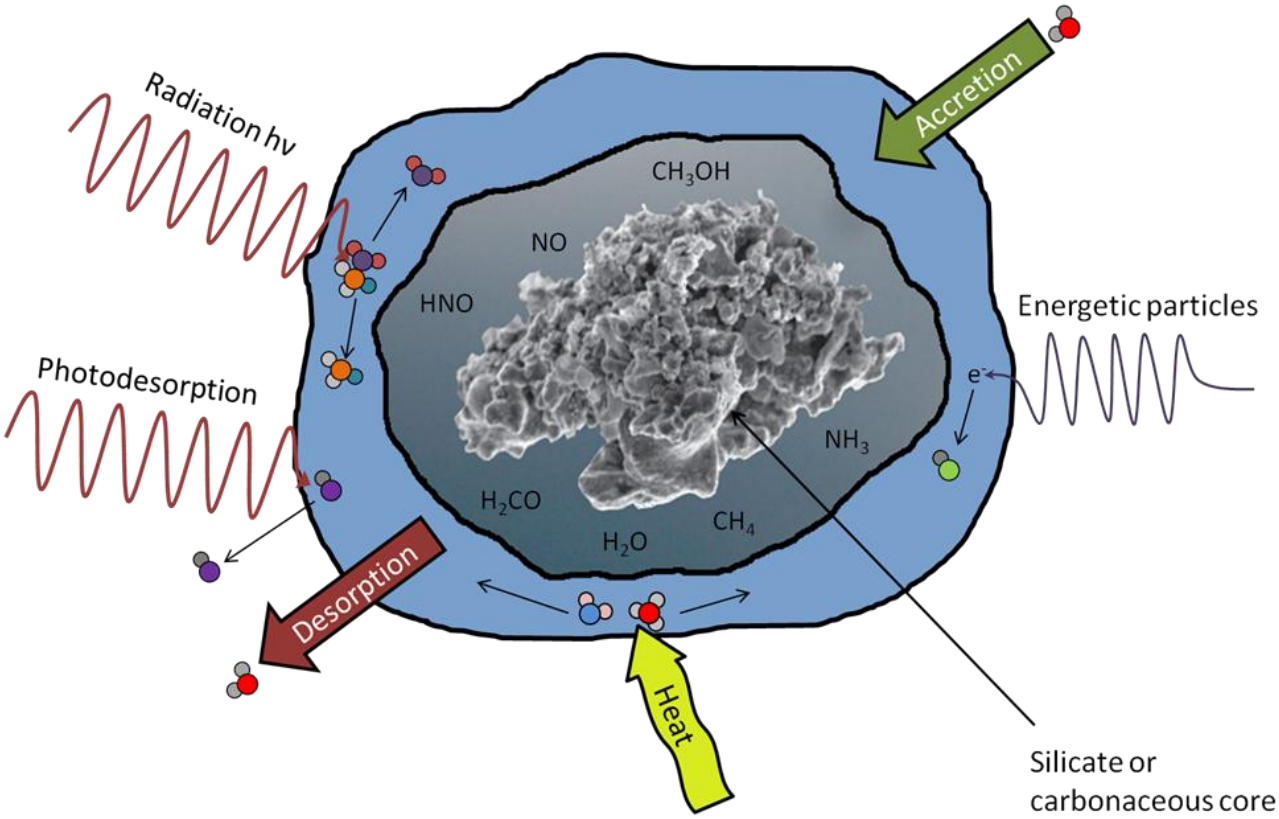

Figure I-5. Astrophysical processes leading to the formation of complex molecules on interstellar grain surfaces

The annealing process also can be viewed as one of the energetic processes. This can lead to molecular rearrangement and thus a formation of complexes like clathrates as H_2O-CH_3OH.[24] At lower temperatures a possibility of desorption is possible though absorption of UV photons or other cosmic rays in contrast to a thermal desorption which may occur only by sublimation of the interstellar ice covering the dust grain. Protostellar shock waves can also induce the nonthermal sputtering causing the desorption of ice mantles.[26] Consequently, the external physical environment determines the nature of desorption of grain mantle materials from the solid to the gas phase. Cold gases are mainly due to the mainly of UV induced desorption while hot gases are

due to the thermal desorption. The cloud temperature surrounding the hot core gradiently decreases the further away from the center of the core, thus inducing desorption of discrete molecules at different temperatures (figure I-6). It is possible that many complex organics detected in protostellar gas such as C_2H_5OH, CH_3CHO, CH_3CH_2CHO, C_2H_5OCHO may have also formed on dust grains, but they could have also been formed, post-evaporation, by chemical reactions in the hot gas. Many of the large interstellar molecules could be created through grain-surface chemistry, solid-gas interface, ion-molecule reactions or induced by energetic particles. The richness of the organic chemistry found in molecular clouds, particularly in the environments of massive protostars, has long been suspected as a source for many of the precursor complex molecules on meteoritic bodies.[27]

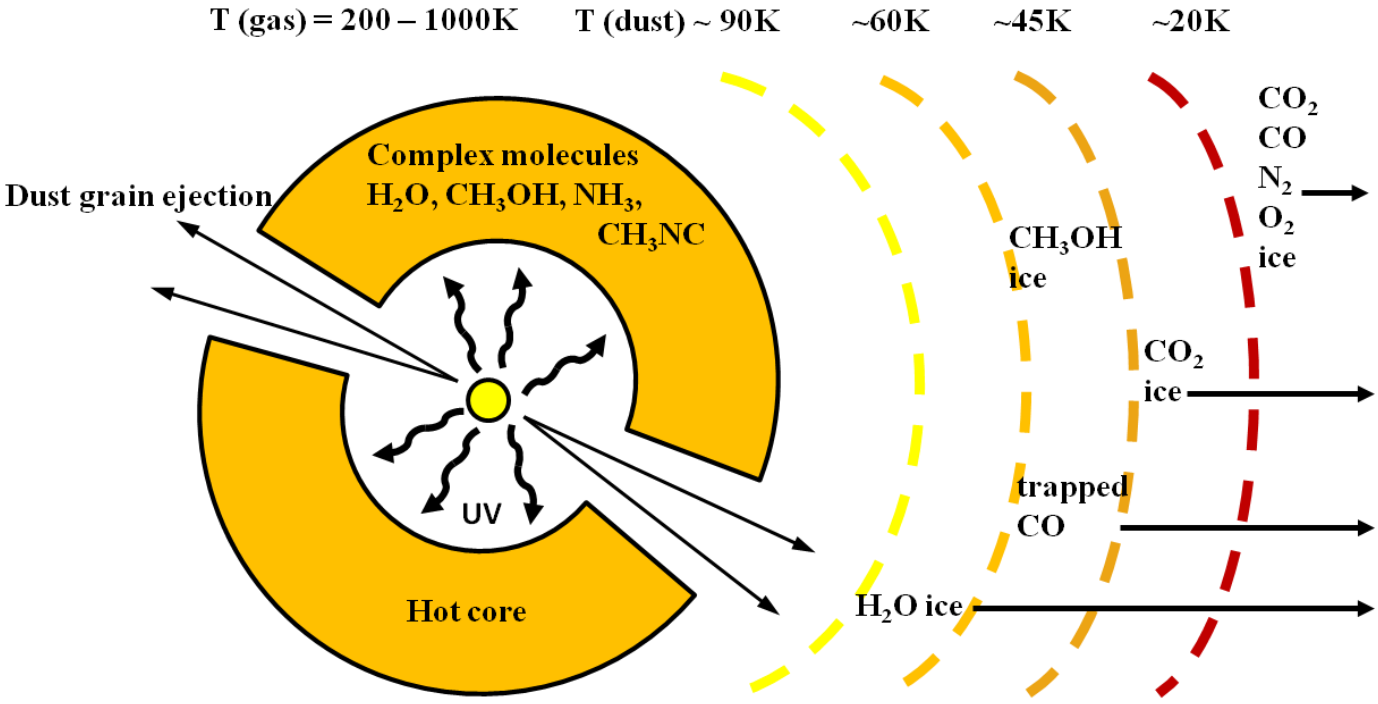

Figure I-6. Gradient temperature evolution of regions surrounding a hot core

I.5. Thesis planning and description

To sum up as mentioned above the interstellar medium contains many simple species CO, CO_2, NH_3, N_2… and also some well-known complex organic molecules such as acetone and dimethyl ether, glycolaldehyde $HOCH_2COH$, ethylene glycol $HOCH_2CH_2OH$, and the simplest amino acid glycine (NH_2CH_2COOH), which its detection in the ISM should be taken with caution (glycine has been detected for sure in meteorites).[28] The formation of these simple and complex molecules could be a key step in the prebiotic chemistry and the origin of life. Even when it seems that interstellar medium has very unfavorable conditions for the formation of such complex molecules (low temperature T=10K, low density, presence of energetic particles) such and even more complex molecules have been detected in space. The purpose of this thesis is to

experimentally mimic the conditions of the interstellar medium and study either of photo-induced or radical reactions of two most basic and common molecules: methane (CH_4) and ammonia (NH_3) in order to have a molecular description of the formation of large complex molecules already detected in the interstellar medium or not yet. The main concept is to study the influence of the water molecules introduced by small amounts into the samples. Such experiments are very useful to characterize some water catalytic effects that may occur in interstellar clouds on the surface of icy dust grains or to promote more complex chemical reactions. This can greatly help identifying reaction intermediates for creating more complex molecules. This thesis consists of six more chapters in addition to this introduction part:

- Chapter II: Experimental section: ice formation, infrared spectroscopy, mass spectroscopy.

- Chapter III: Photochemistry of NH_3-H_2O ice: N/H radical reaction vs photochemistry for the formation of NH, NH_2 and NH_2OH.

- Chapter IV: Thermal stability of NH_2OH: desorption of interstellar ice analog NH_2OH-H_2O.

- Chapter V: Photochemistry of CH_4-H_2O ice: formation of aldehydes and alcohols.

- Chapter VI: Hydrogenation of C_3H_nO species (n=2, 4, 6): H addition surface reaction vs photochemistry

- Chapter VII: Photochemistry of CH_4-NH_3-H_2O ice: formation of organic complex comlecules.

- Conclusions and projects

Bibliography

[1] Mojzsis S.J., Arrhenius G., McKeegan K.D., Harrison T.M., Nutman A.P. and Friend C.R., 1996, Nature 384, 55.
[2] Miao Y., Snyder L.E., Kuan Y.-J. and Lovas F.J., 1994. B.A.A.S., 26, 906.
[3] Chyba C. and Sagan C., 1992. Nature 355, 125.
[4] Heidmann J. and Klein M.J. (eds), Bioastronomy | Search for Extraterrestial Life, Springer Verlag 1991
[5] Ferriere K., 2001. Reviews of Modern Physics, 73 (4): 1031.
[6] Cardelli J. A., Meyer D.M., Jura M., Savage B.D., 1996. Astrophysical Journal, 467, 334.
[7] Meyer D. M., Cardelli J.A., Sofia U. J., 1997. The Astrophysical Journal, 490:L103.
[8] Meyer D. M., Jura M., Cardelli J.A., 1998. Astrophysical Journal, 493, 222.
[9] Draine B., 2011. Physics of the interstellar and intergalactic medium, Princeton series in astrophysics. Princeton University Press, Princeton
[10] Chuss, David T. (June 26, 2008), Cosmic Background Explorer, NASA Goddard Space Flight Center,
[11] Ohishi M., 2016. J. Phys.: Conf. Ser. 728;052002.
[12] Tornow C., Kührt E., Motschmann U., 2005. Astrobiology, 5, 632.
[13] Goldsmith P. F. and Langer W. D., 1978. Astrophys. J., 222, 881.
[14] Hollenbach D. J. and Salpeter E. E., 1971. Astrophys. J., 163, 155.
[15] Gas Phase Ion Chemistry, M.T. Bowers, ed., 1979, Academic Press.
[16] Prasad S.S. and Tarafdar S.P., 1983. Astrophys. J., 267, 603.
[17] Shul R. J., Passarella R., DiFazio Jr. L.T., Keesee R.G., Castleman Jr. A.W., 1988. J. Phys. Chem., 92 (17), 4947.
[18] Elmegreen B.G., 2000. Astrophys. J., 530, 277.
[19] Ehrenfreund P. and Charnley S.B., 2000. Annu. Rev. Astron. Astrophys., 38, 427.
[20] Charnley S.B., 2001. Astrophys. J. Lett., 562, L99.
[21] Charnley S. B., 2001. Interstellar organic chemistry. In The Bridge Between the Big Bang and Biology (F. Giovannelli, ed.), pp. 139–149. Consiglio Nazionale delle Ricerche President Bureau Special Volume, Rome, Italy
[22] Charnley S.B., 1997. On the nature of interstellar organic chemistry. In Astronomical and Biochemical Origins and the Search for Life in the Universe (C. B. Cosmovici et al., eds.), pp. 89–96. Editrice Compositori, Bologna
[23] Draine B.T., Interstellar Dust Grains, Princeton University Observatory, Princeton, NJ 08544 USA.
[24] Blake D., Allamandola L., Sandford S., Hudgins D. and Freund F., 1991. Science, 254, 548.
[25] Willacy K. and Millar T. J., 1998. MNRAS, 298, 562.
[26] Draine B. T., Roberge W. G. and Dalgarno A., 1983. ApJ., 264, 485.
[27] Cronin J. R. and Chang S., 1993. Organic matter in meteorites:Molecular and isotopic analyses of the Murchison meteorite. In The Chemistry of Life's Origins (J. M. Greenberg et al.,eds.), pp. 209–258. Kluwer, Dordrecht.
[28] Kuan Y.-J., Charnley S. B., Huang H.-C., Tseng W.-L. and Kisiel Z., 2003. ApJ, 593, 848.

Chapter II:

Experimental section

II.1. Laboratory studies

The most common laboratory studies to analyze samples and materials are through spectroscopy. Spectroscopy is the study of the interaction between matter and electromagnetic radiation.[1] Historically, spectroscopy studies started through the study of the visible light dispersed by a prism to its different wavelengths. Later the concept was expanded greatly to include any interaction with any radiative energy as a function of its wavelength or frequency. Spectroscopy is used in physical and analytical chemistry because each atom and molecule has their unique spectrum. As a result, these spectra can be used to detect, identify and quantify information about the atoms and molecules.[2]

One of the central concepts in spectroscopy is a resonance and its corresponding resonant frequency. In quantum mechanical systems, the resonance happens between the two quantum stationary states of one system, such as an atom, and an oscillatory source of energy such as a photon. It is strongest when the energy of the source matches the energy difference between the two states. The energy (E) of a photon is related to its frequency (v) by $E=hv$ where h is Planck's constant. The system response vs. photon frequency will peak at the resonant frequency or energy producing a line in the atomic or molecular spectrum. Spectra of atoms and molecules often consist of a series of spectral lines, each one representing a resonance between two different quantum states.[3]

Spectroscopy can be distinguished into two groups by the nature of the interaction between the energy and the material.[4] These interactions are as shown in figure II-1:

Absorption occurs when energy from the radiative source is absorbed by the material.

Emission indicates that radiative energy is released by the material. A material's blackbody spectrum is a spontaneous emission spectrum determined by its temperature; this feature can be measured in the infrared.

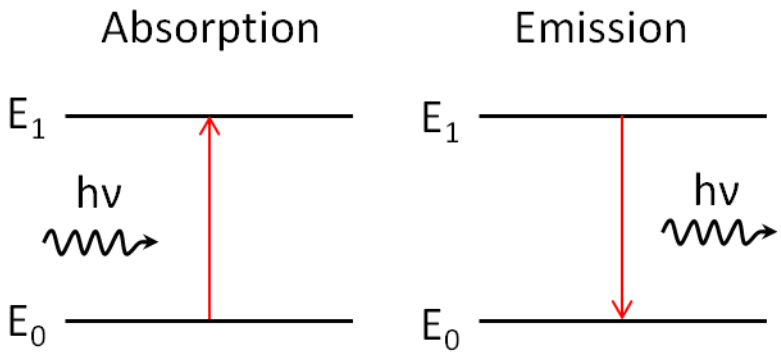

Figure II-1. Absorption and emission transitions

Electromagnetic radiation is the source of energy used for spectroscopic studies.[5] Techniques that employ electromagnetic radiation are typically classified by the wavelength region of the spectrum and include microwave, terahertz, infrared, near infrared, visible and ultraviolet, x-ray and gamma spectroscopy.[6] Evidently different spectroscopic techniques induce different types of transitions in the molecular system.

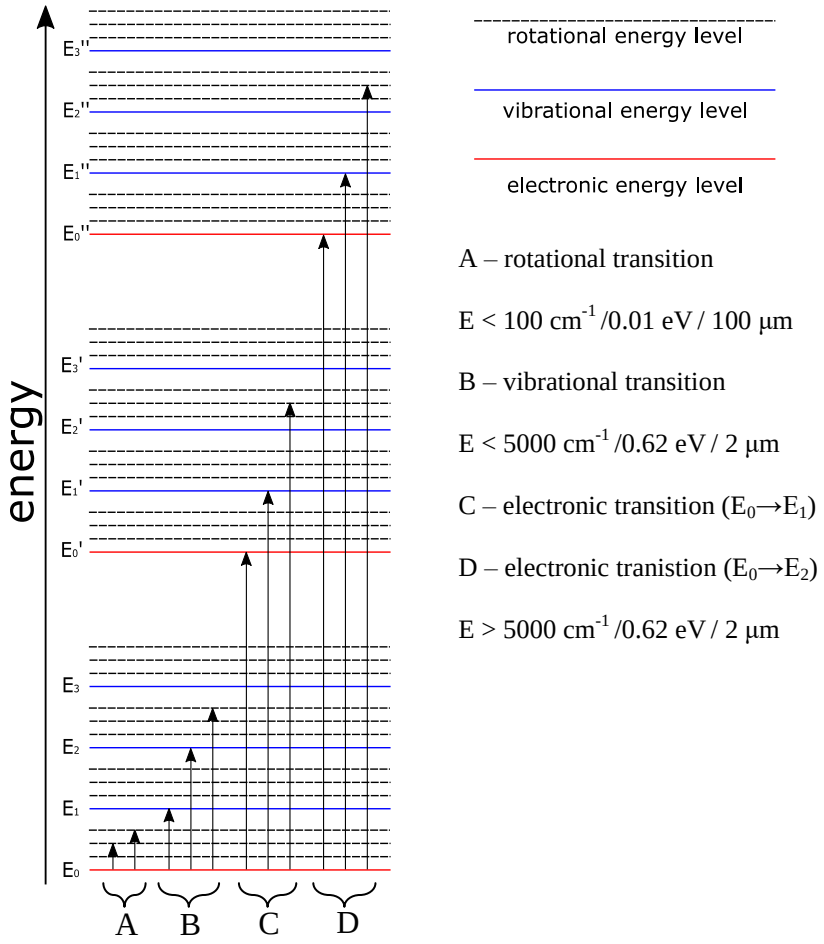

Figure II-2. Possible energy transitions in a molecular system with their appropriate energetic value ranges

Figure II-2 shows a simplified molecular system's energy transition diagram. As seen the highest energy required is for the electronic transitions and the lowest for the rotational. So it seems evident that different wavelengths induce different transitions: visible and ultraviolet – electronic transitions, infrared – vibrational transitions and microwave – rotational transitions.[7] Each of these techniques theoretically work on the same principle, but practically requires different approaches to be implemented to use in laboratory conditions.

For our studies we have used infrared spectroscopy to characterize samples and reactivity in the solid phase. All processes involved in gas phase, such as compositions of chemical

mixtures, interface solid phase gas interactions, ice sublimations have been studied using mass spectroscopy.

II.2. Infrared spectrometry

II.2.1. Vibrations, absorbance, interferogram, fourier transformation

Infrared spectroscopy (IR spectroscopy or vibrational spectroscopy) is one of the techniques that involve the interaction of infrared radiation with matter. From vibrational spectra of molecules it is possible find out the structure and properties of the derivatives that carry out both quantitative and qualitative analysis of materials. The infrared portion of the electromagnetic spectrum is usually divided into three regions; the near-, mid- and far- infrared, in relation to the visible spectrum. The higher-energy near-IR, approximately 14000–4000 cm^{-1} can excite overtone or harmonic vibrations. The mid-infrared, approximately 4000–400 cm^{-1} may be used to study the fundamental vibrations and associated rotational-vibrational structure. The vibrational transitions of most molecules are in this region. The far-infrared, approximately 400–10 cm^{-1}, adjacent to the microwave region, has low energy and may be used for rotational spectroscopy and low frequency vibrations.[8]

II.2.2. Molecular vibrations

Infrared spectroscopy may be the right probe to characterize the structures of many chemical species. As explained in the previous chapter these absorptions occur at resonant frequencies, which mean that the frequency of the absorbed radiation matches the vibrational frequency. Using the Born–Oppenheimer and harmonic approximations the molecular Hamiltonian by a harmonic oscillator and those resonant frequencies can be associated with the normal modes.[9] A given molecular vibrational mode can be IR measurable, only if it correspond with the changes in the dipole moment of the molecule. The rule requires only a change in dipole moment, so a permanent dipole is not necessary for polyatomic molecules. For molecules with N atoms, linear molecules have 3N – 5 degrees of vibrational modes, where nonlinear molecules have 3N – 6 degrees of vibrational modes.[10] These vibrational modes are also called vibrational degrees of freedom. These molecular vibrations can be grouped and are shown in figure II-3. It consists of two main groups: fundamental and non-fundamental vibrations as shown below.[11]

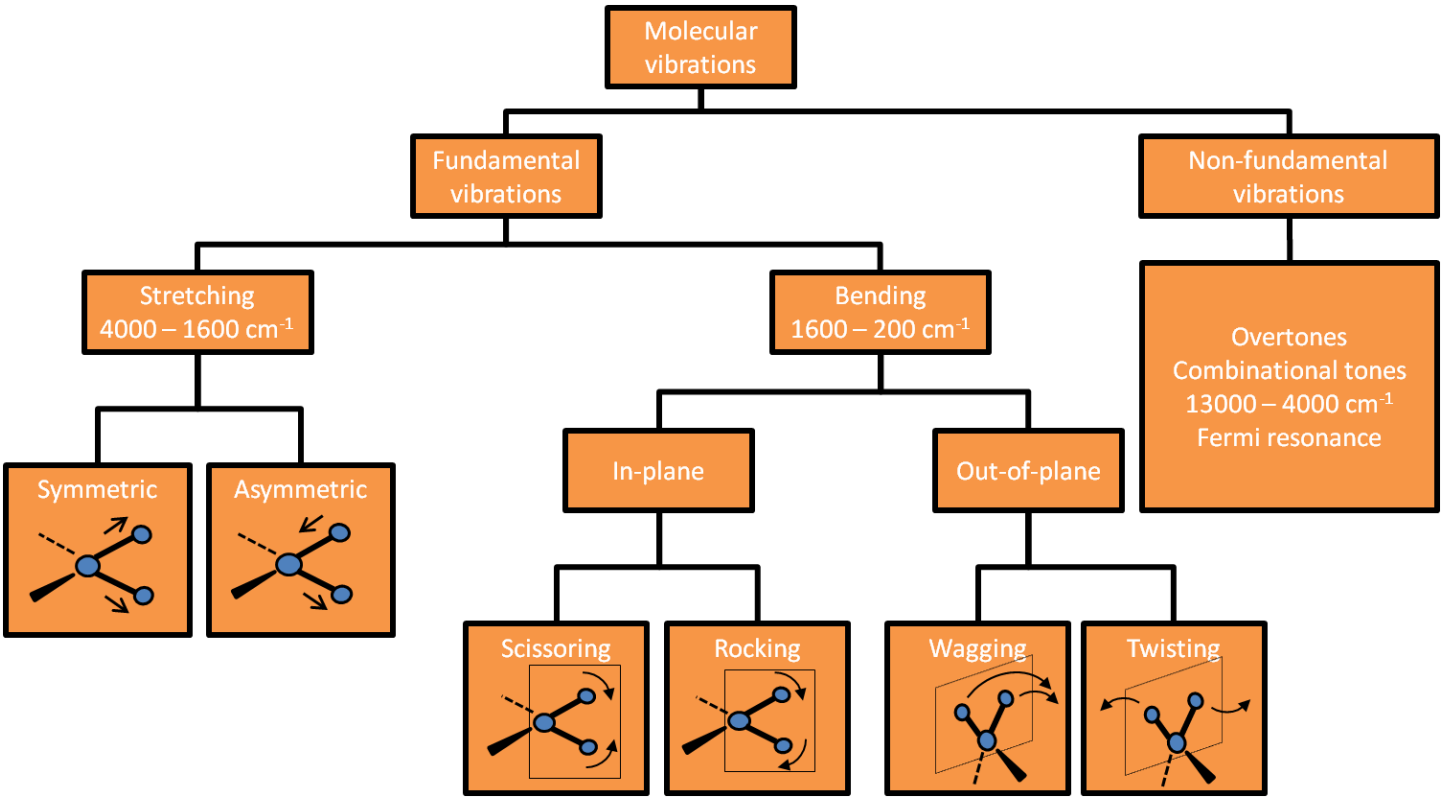

Figure II-3. Molecular normal vibrations

Fundamental vibrations consist of two groups: stretching and bending modes.

Stretching modes are vibrations in which the bond length is altered (increasing and/or decreasing). Stretching vibration is further divided into: symmetric – where both bonds increase and decrease in length symmetrically; asymmetric – one bond length increases while other one decrease. Approximately most of the stretching modes absorb in 4000 – 1600 cm^{-1} region. It is sometimes called "functional group" regions. For larger molecules some of the C-C, C-O, C-N stretches can appear at lower wavenumbers also (CO stretching in alcohols are around 1000 cm^{-1}).

Bending modes are characterized by changes in molecular bond angles. Bending modes are divided into two groups each having two vibrations. Usually bending modes absorb in 1600 – 200 cm^{-1} region. It is sometimes called "fingerprint" region. Among the bending modes we can distinguish the **In-plane** and **Out-of-plane** bending modes. The in-plane modes contain both **Scissoring** and **Rocking** while the out-of-plane modes contain **Wagging** and **Twisting** as shown in the figure II-3.

Non-fundamental vibrational modes consist of overtones, combination tones and Fermi resonance. The first **overtone** mode arises from the absorption of a photon leading to a direct transition from the ground state to the second excited vibrational state, which correspond to approximately twice the frequency of the fundamental mode. There are possibilities to induce

higher overtone modes. **Combination** modes, involve simultaneous excitation of more than one normal mode. Combination and overtone most usually appear in the region above 4000 cm^{-1}, even though it is possible to have them at lower wavenumbers also. They are usually weak bands. The phenomenon of **Fermi resonance** can arise when two modes are similar in energy; Fermi resonance results in an unexpected shift in energy and intensity of the bands, usually it is the interaction between the fundamental modes and overtone or combination modes.

II.2.3. Infrared absorption

Vibrational spectra can be recorded either through the absorption of light or the emission. In order to record a vibrational emission spectrum, molecules would have to be thermally exited to higher vibrational states. This can lead to a dissociation of the molecule.[12] Considering this, the vibrational transitions are mostly observed through the absorption.

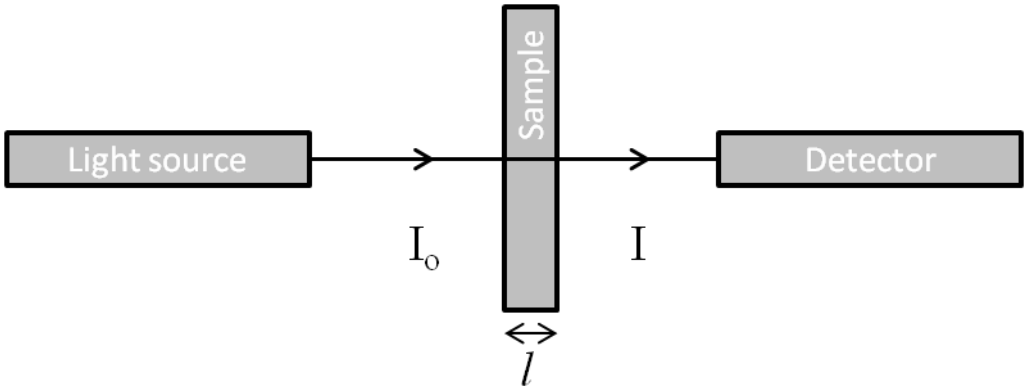

Figure II-4. Infrared absorption experiment principal scheme

The infrared spectrum of a sample is recorded by passing a beam of infrared light through the sample. When the frequency of the IR is the same as the vibrational frequency of a bond, the absorption occurs. Examinations of the transmitted light reveal how much energy was absorbed at each wavelength.[13] The principal scheme of the infrared absorption is shown in figure II-4. Experimentally it was noticed that during the absorption in the sample, the intensity difference decrease $-dI/I$ is proportional to the length of the sample l, on which the light passes. It can be expressed:

$$-\frac{\mathrm{d}I}{I} = b\mathrm{d}l, \qquad \text{(II-1)}$$

where b correspond to the coefficient of absorptivity. By solving this differential equation we get:

$$\ln\frac{I_0}{I} = bl. \qquad \text{(II-2)}$$

J.H. Lambert and P. Bouguer where the first ones to make this expression and is called Lambert-Bouguer law.[14] They also found out that the coefficient does not depend on the intensity

of light and the light beam length in the material. More commonly this intensity ratio is expressed through the common logarithm of a base of 10:

$$\log_{10} \frac{I_0}{I} = al, \qquad \text{(II-3)}$$

where *a* here is a decimal coefficient of absorptivity.

During the registration of infrared absorption spectrum the value measured is transmittance $T = I/I_o$ or more commonly absorbance:

$$A = -\log_{10} T = -\log_{10} \frac{I}{I_0} \qquad \text{(II-4)}$$

II.2.4. Infrared Fourier spectrometry (FTIR)

We know that spectroscopy studies the light absorption in the sample at different wavelengths. At first it was done by dispersing the light through a prism to different wavelengths and scanning the sample. Due to the fact that it takes long time to scan the whole diapason of wavelengths and requires good prisms and gratings, it is not used anymore.[15] Right know Fourier spectrometers are used. They are based on electromagnetic wave interference. The negative aspects of the Fourier spectrometers are that they require difficult computations in calculating absorption spectra. At the present this is not an issue anymore since the science in computers is very advanced and the Fourier transformation takes a couple of seconds to calculate.

The main part of Fourier spectrometer is the interferometer. The most common are the Michelson interferometers (figure II-5a).[16] It consists of light source, a beam splitter, a one fixed and one moving mirror system and a detector. Ideally 50% of the light is transmitted towards the fixed mirror and 50% is refracted towards the moving mirror. Light is reflected from the two mirrors back to the beam splitter and towards the sample and to the detector after that. The difference in optical path length between the two arms to the interferometer is known as the retardation or optical path difference Δx. An interferogram is obtained by varying the delay and recording the signal from the detector for various values of Δx. This results in a maximum at $\Delta x = 0$, when there is constructive interference at all wavelengths, followed by series of "wiggles"[17] (as shown in figure II-5b). The interferogram has to be measured from zero path difference to a maximum length that depends on the resolution required. In practice the scan can be on either side of zero resulting in a double-sided interferogram from $-\Delta x_{max}$ to Δx_{max}. For the interferogram to be converted to a spectrum a Fourier transformation is needed to be done.[18]

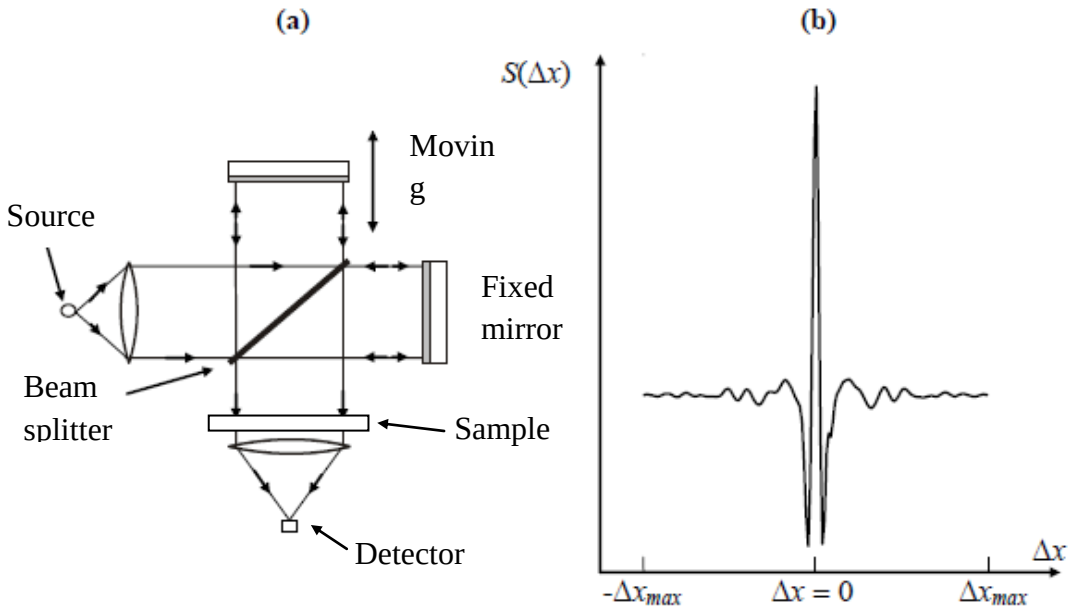

Figure II-5. a) principal scheme of Michelson interferometer; b) the recoded signal by the detector (interferogram)

II.2.5. Advantages of Fourier transform spectroscopy

There are three main advantages for an FT spectroscopy compared to a scanning (dispersive) classical method:[19]

Fellgett's or multiplex advantage. One of the reasons FT spectrometers are much better than dispersive it that the information from all wavelengths is collected simultaneously. Obviously it allows shorter scan times. In practice multiple scans are often averaged where in the same time it would take for a single scan of a dispersive spectrometer.

Jacquinot's or throughput advantage. This results from the fact that in a dispersive instrument, the monochromator has entrance and exit slits which restrict the amount of light that passes through it. The interferometer throughput is determined only by the diameter of the collimated beam coming from the source. That means that the energy throughput in an interferometer can be higher than in a dispersive spectrometer. This combined with Fellgett's advantage gives the ability to achieve the same signal-to-noise ratio as a dispersive instrument in a much shorter time.

Connes' or the wavelength accuracy advantage. The wavelength scale is calibrated by a laser beam of known wavelength derived from a He-Ne (helium neon) laser that passes through the interferometer. This is much more stable and accurate than in dispersive instruments where the scale depends on the mechanical movement of diffraction gratings. The wavenumber of He-Ne laser is known very accurately and is very stable. As a result, the wavenumber calibration of

interferometers is much more accurate and has much better long term stability than the calibration of dispersive instruments.

II.2.6. Calculation of absorbance spectrum of a sample

It was shown previously that using Lamber-Bouguer law $A = -\log_{10}\frac{I}{I_0}$, it is possible to calculate absorbance for a specific wavelength. In ideal world it would be great, but in real world the spectrometers consists of parts (beam splitter, IR windows) that absorb some of the light in different wavelengths. So recording a reference spectrum is required.[20] The reference measurement makes it possible to eliminate this instrument influence. The reference spectrum is a spectrum recorded without samples. Lamber-Bouguer law consists of two components referred as intensity, and these are obtained by recording reference and sample spectra. Later on using the same law the absorbance spectrum is calculated. All of this is shown in Figure II-6.

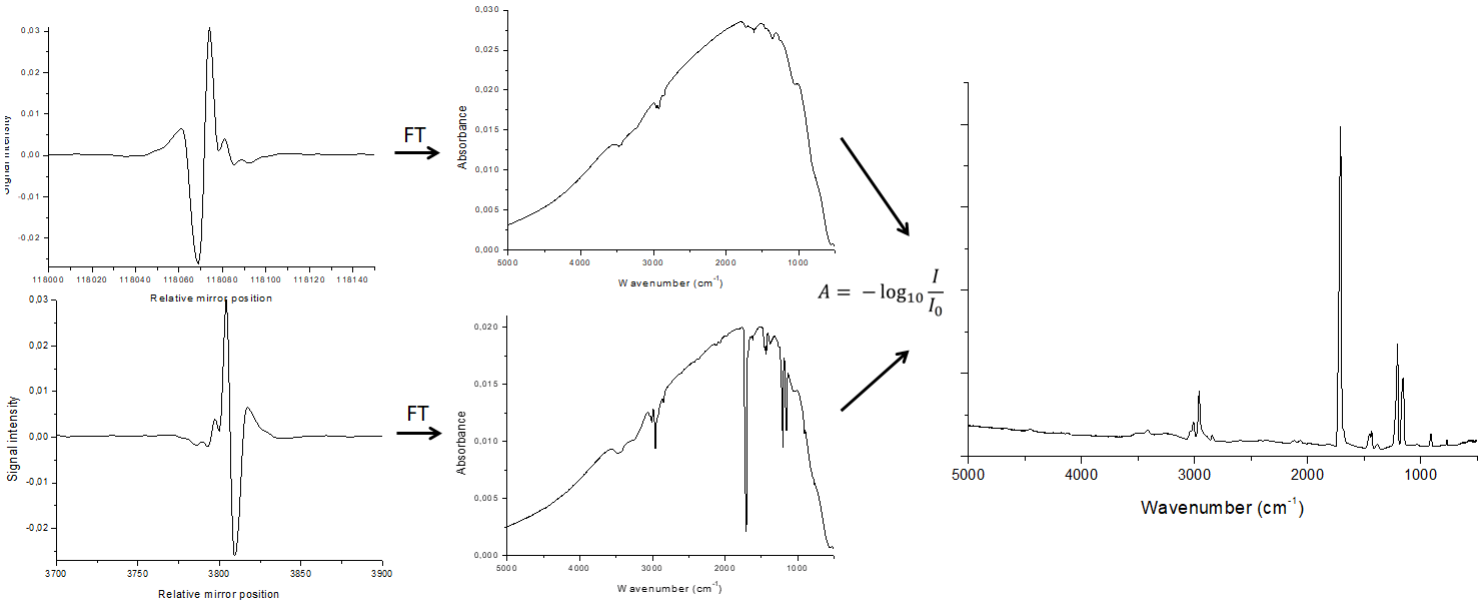

Figure II-6. Recorded interferogram using FTIR spectral signal processing transformed into a single channel spectrum for reference (upper) and sample (lower). Using a Lamber-Bouguer law an absorption spectrum is calculated

II.3. Mass spectrometry

Mass spectrometry is an analytical technique to characterize chemical species and sort them based on their masses. In simpler terms, a mass spectrum measures the masses of molecular species involved in gas phase.[21] Most usually mass spectrometry is used to analyze pure gases and also complex mixtures. Mass spectrometers works on very basic principle: If something is moving and you subject it to a sideways force, instead of moving in a straight line, it will move in a curve - deflected out of its original path by the sideways force.

II.3.1 Mass selection

In mass spectrometry the moving subjects are atoms and molecules. They can be deflected by magnetic fields – if at first they turned into an ion. Electrically charged particles are affected by a magnetic field but electrically neutral ones are not.[22] So the most basic construction would consist of 4 main parts:

1. **Ionisation.** The atom or molecule is ionized by knocking one or more electrons off to give a positive ion.
2. **Acceleration.** The ions are accelerated so that they all have the same kinetic energy.
3. **Deflection.** The ions are then deflected by a magnetic field according to their masses. The lighter they are, the more they are deflected.
4. **Detection.**The beam of ions passing through the machine is detected electrically giving a direct current that is equal to the amount of ions detected.

Mass spectrometer output signal is simplified into a column chart. This shows the relative current produced by ions of varying mass/charge ratio. You may find diagrams in which the vertical axis is labeled as either "relative abundance" or "relative intensity". Mass spectrum of methane (CH_4) is given as an example in figure II-7. Usually molecular ion (MI) should be the ion of highest mass in the spectrum. In this case mass of methane is 16 u. However for many species in addition to the main ion (MI) mass of molecular fragments are also detected due to the molecular fragmentation in the mass spectrometer.

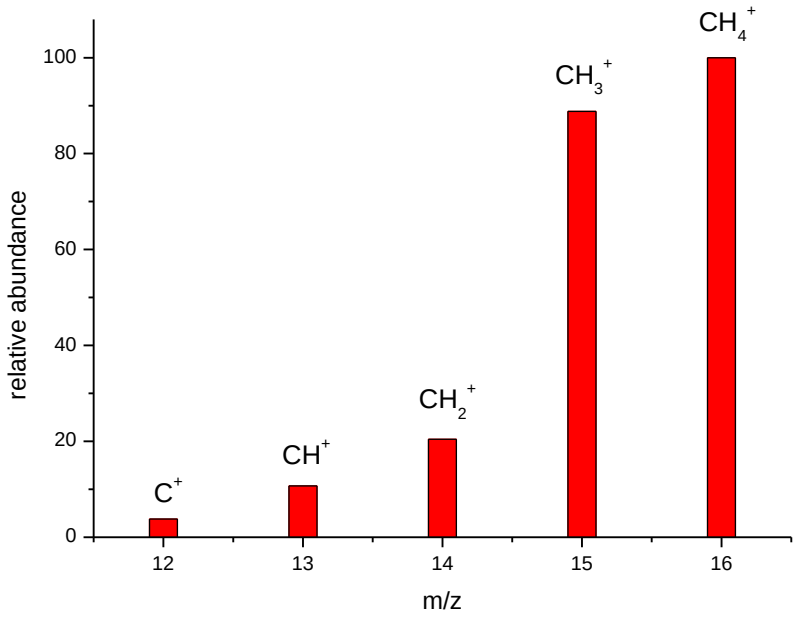

Figure II-7. Mass spectrum of methane (CH_4 m=16u) and fragmentation pattern

II.3.2. Molecular fragmentation

The ionization process can produce the molecular ion - same molecular weight and elemental composition of the starting analyte [M^+] and fragment ions corresponding to smaller pieces of the analyte molecule ([M^+-1] and so on). Fragmentation process can complicate the analysis process of the sample because the amount of fragment ions and highest intensity might not be corresponding to the highest mass.[23] This can be clearly seen in figure II-8 depicting ethane (M=30u) and propane (M=44u) mass spectra.

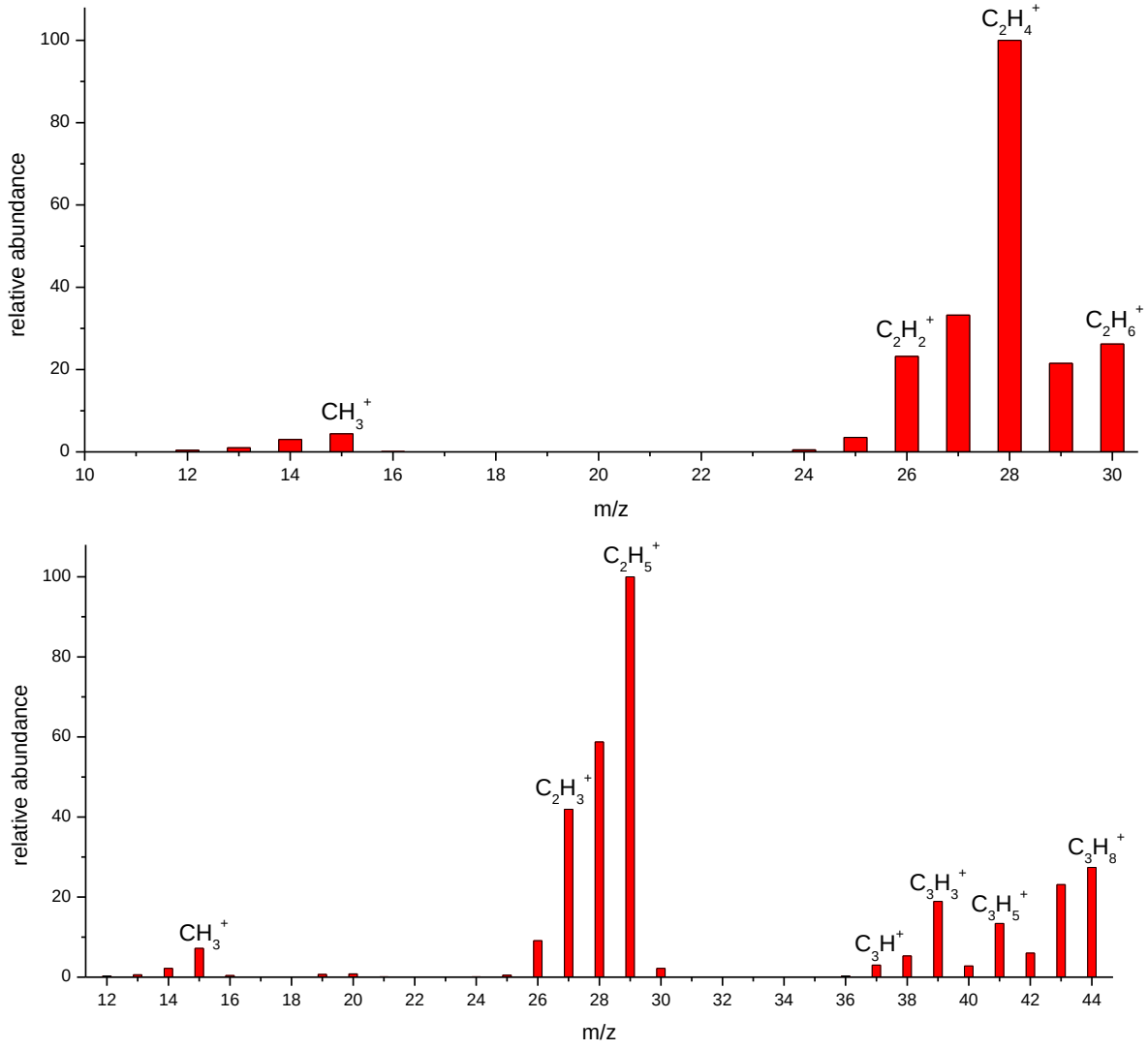

Figure II-8. Mass spectra of ethane (top, C_2H_6, M=30u) and propane (bottom, C_3H_8, M=44u)

The molecular ions are energetically unstable, and some of them will break up into smaller fragments.[24] The simplest case is that a molecular ion breaks into two parts - one of which is another positive ion, and the other is an uncharged free radical.

$$M^+ = X^+ + \bullet Y \qquad \text{(II-5)}$$

The uncharged free radical won't produce a line on the mass spectrum. Only charged particles will be accelerated, deflected and detected by the mass spectrometer. These uncharged particles will simply get lost in the machine - eventually, they will get removed by the vacuum pump. The ion, X^+, will travel through the mass spectrometer just like any other positive ion - and will produce a line on the column diagram. All sorts of fragmentations of the original molecular ion are possible - and that means that a whole host of lines in the mass spectrum will be produced.[25] The highest intensity line in the mass spectra (in the case of propane m/z = 29) is called the base peak. This is usually given an arbitrary height of 100, and the height of everything else is measured relative to this. The base peak is the highest intensity peak because it represents the most common fragment ion to be formed - either because there are several ways in which it could be produced during fragmentation of the parent ion, or because it is a particularly stable ion.

All the peaks can be explained with the (II-5) formula. Propane molecular ion $[M^+]$ = 44u and the base peak is 29u. So what causes the line at 29 m/z?

$$[CH_3\text{-}CH_2\text{-}CH_3]^+ \rightarrow [CH_3\text{-}CH_2]^+ + \bullet CH_3 \qquad \text{(II-6)}$$

The produced methyl radical will simply get lost in the machine. And similarly all the other lines can be explained in the similar way.

II.4. Experimental setup

In this section the experimental setup used for all the subsequent described results is presented. During my Ph.D. work I have participated in the development and the creation of an experimental setup which connect infrared spectroscopy to mass spectrometry. The experimental setup is called MASSIR and used to mimic the interstellar medium conditions: where the low vacuum and temperature is required. For that to happen a vacuum chamber connected to a cryogenerator was used.[26] Cryogenerator is connected to sample holder where the temperature as low as 3K could be maintained. The top side view of the system is shown in figure II-9. In the center we have a spherical vacuum chamber (Kurt J. Lesker)[27] with variety of different ports for the connection of the desired equipment. On top of it there is a 1-axis motor controlled rotational manipulator with a differential pumping (Prevac).[28] Onto this manipulator we have a cold head unit which is connected to our sample holder. Sample holder contains six mirrors and due to rotational manipulator these mirrors can be rotated as needed to a specific device depending on the experiment. For sample analysis we have two spectrometers: Fourier Transform Infrared spectrometer (FTIR) for analyzing samples in the solid phase and a quadrupole mass spectrometer for analysis of desorption into a gas phase. The vacuum chamber is connected to two microwave dischargers and a VUV light source. The two microwave dischargers are used to generate atomic or radical species in order to study atomic or radical addition reactions, while the vacuum ultraviolet light source is used for photochemically induced reactions.

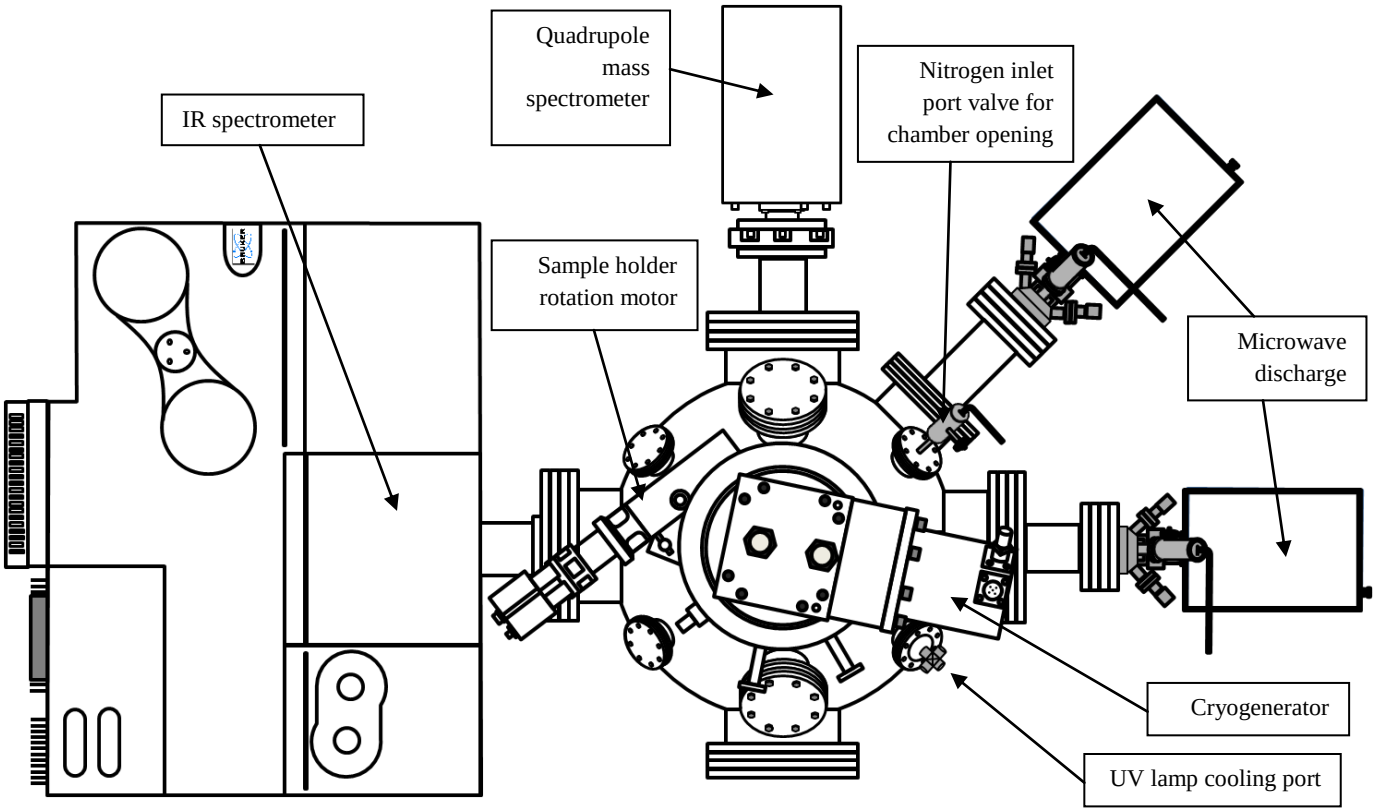

Figure II-9. Top-side view schematic of the MASSIR experimental setup and a real life photo

Figure II-10 shows the left side view of the experimental setup. Below middle section of the chamber we can see two injection ports. The one on the left is for formation of simple ices and the one on the right is used for a codeposition experiments with a discharge at the same time. Beneath it we have a two turbo molecular pumping units for reaching high vacuum ~10^{-10} mbar

conditions with a few valves and inlets connected to a differential pumping on the rotational unit. A more detailed description of all the parts of this system are in the following paragraphs

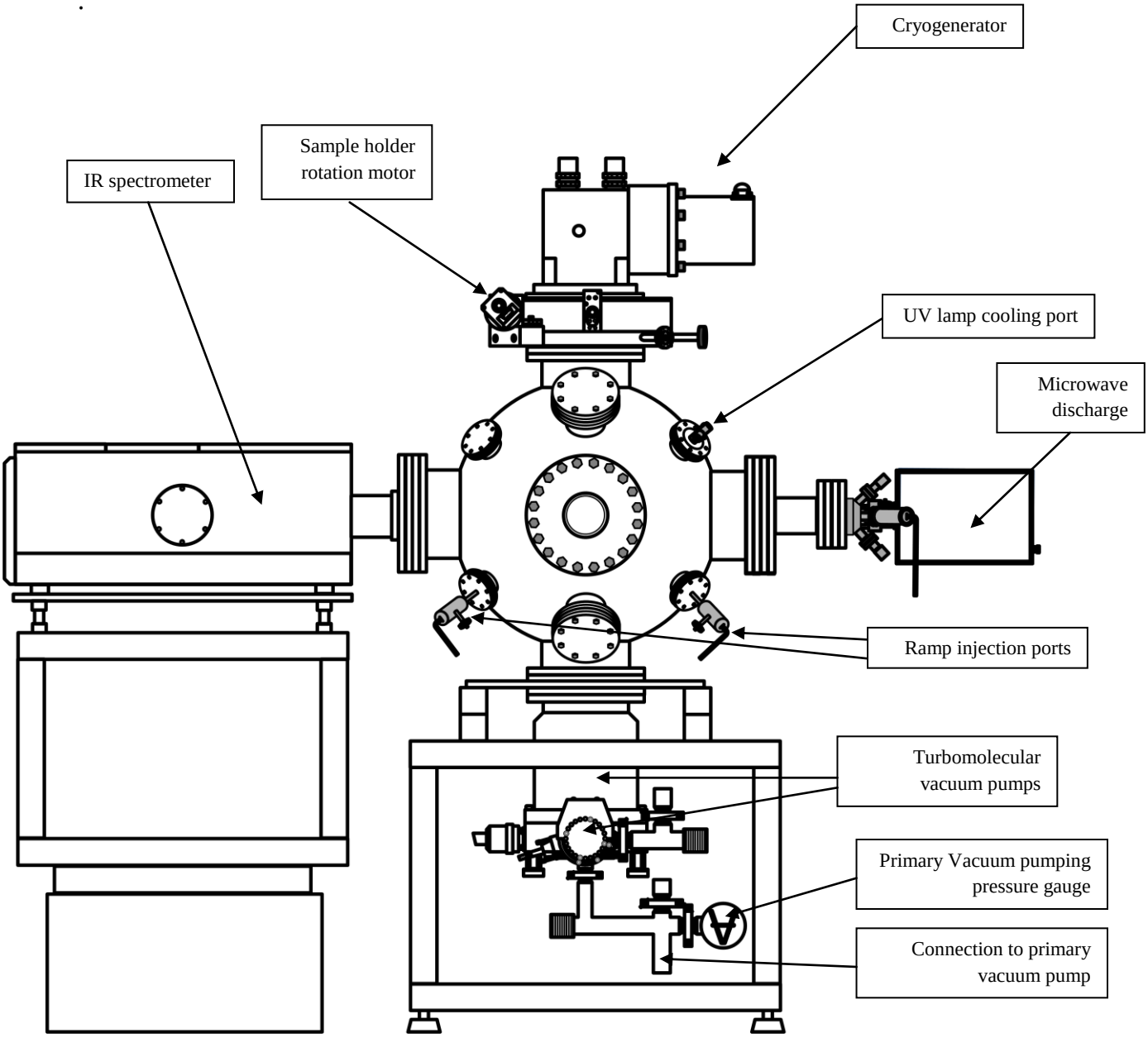

Figure II-10. Left-side view of the MASSIR experimental setup

II.4.1. Pumping system

To reach as low temperatures as 3K and at the same time to avoid contaminants in the sample from the outside impurities, it is necessary to attain low pressures not only in the sample chamber but in the mixing ramps too. For simplicity and easier manipulation both systems (chamber and ramps) have their own separate pumping systems. The main pumping configuration

of the chamber system is shown figure II-11. The system is quite simple: there are two secondary turbomolecular vacuum pumps sequentially connected to a primary rotary vane pump.

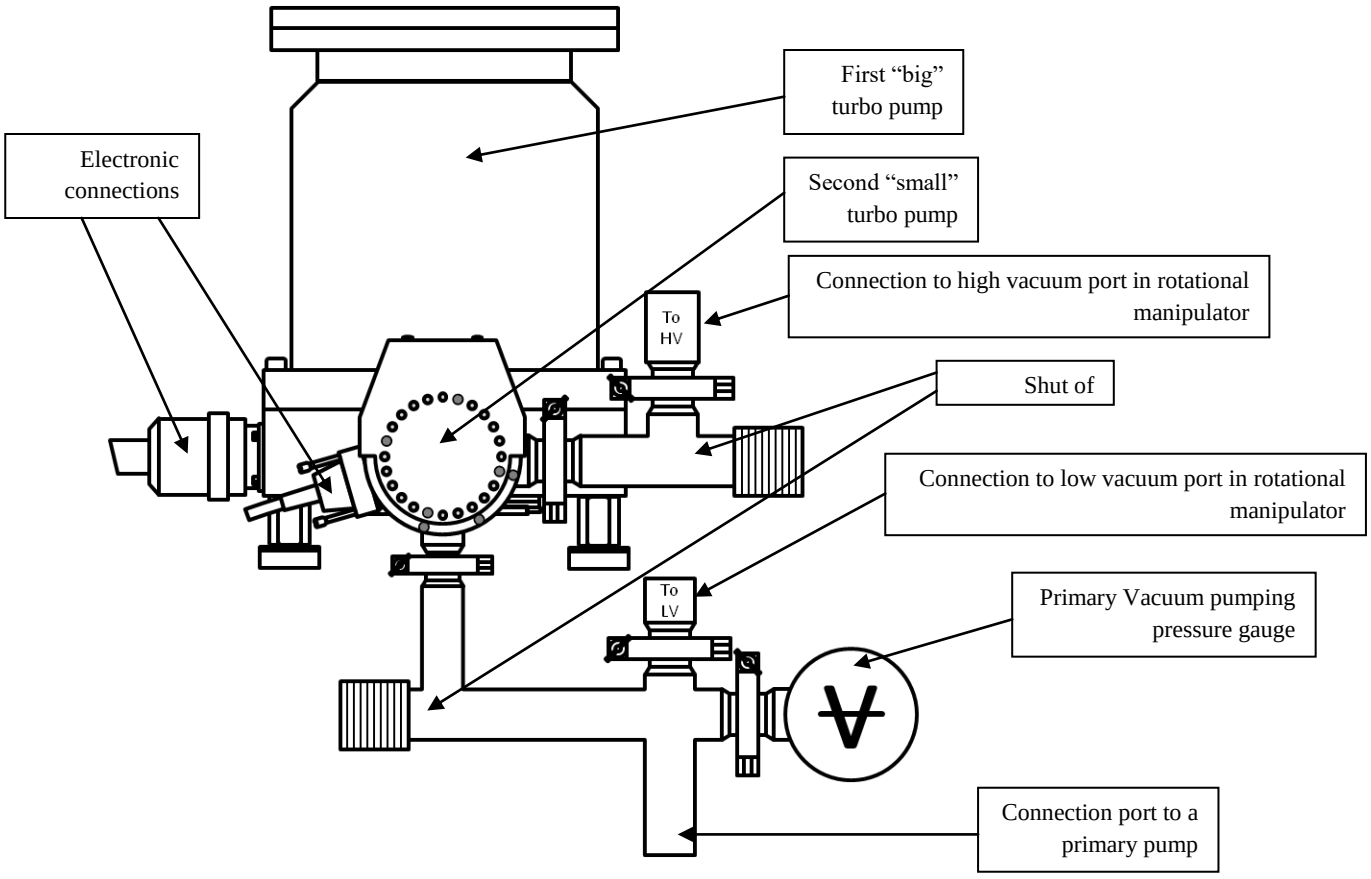

Figure II-11. Chamber vacuum system

There are two turbomolecular vacuum pumps labeled "big" and "small" not only because of their size but also of the possible attainable vacuum pressure. These pumps work on quite simple principle that gas molecules with a repeated collision with a moving solid surface can be given momentum to the desirable direction. In a turbomolecular pump, a rapidly spinning fan rotor hitting gas molecules creates a flow from the inlet of the pump towards the exhaust thus creating and maintaining vacuum.[29] To avoid damage to rotor blades these pumps cannot be operated from the atmospheric pressure. Firstly to reduce pressure a simple primary rotary vane pump is used. A rotary vane pump (Adixen PASCAL 2015SD by Pfeiffer vacuum)[30] is a positive-displacement pump that consists of vanes mounted to a rotor that rotates inside of a cavity thus creating partial vacuum. The vacuum pressure attained only with a primary pump is ~10^{-3} mbar. Then it is sequentially connected to a "small" turbo pump (Turbovac SL80)[31] reaching ~10^{-6} mbar pressure. And the lastly the "big" turbo (Edwards STP-603C)[32] obtaining 10^{-10} mbar.

Another specific piece of equipment requiring pumping is a rotational cold head manipulator. There are two ports shown in figure II-11. that are connected to the manipulator.

Low vacuum (LV) port is only pumped through primary pump, and high vacuum (HV) before the "small" turbo pump. This setup assures that no addition contaminants enter the vacuum chamber during the rotation of the sample holder assembly.

Ramp vacuum system is similar with just one exception of not having a "big" turbomolecular pump. The reachable pressure is around 10^{-5} mbar which is enough to form clean samples without impurities (H_2O, CO, CO_2, O_2 and N_2). During energetic processing (microwave discharge and UV light) CO and CO_2 can be detected as traces in our samples. Considering most of the sample formations take around or less than 30min the whole amount of all the impurities can be negligible and then dismissed.

II.4.2. Cryostat

Figure II-12. Cryostat

The cryogenerator used in this system is a "closed" cycle cryogenerator (Sumitomo 082-B)[33] reaching temperature of 3K. This cooling system is designed in such a way that the vibrations during the cooling would be greatly reduced (2^{nd} stage cooling ±9 microns). This greatly helps during infrared spectrum recording to avoid disturbances in optical calibration of the spectrometer. The cryogenic system consists of a compressor connected through flexible pressurized tubes (24 bar) to the end of the cryogenic module called "cold head" where the sample holder is connected. The cryostat shown in figure II-12 is inserted in the vacuum chamber as illustrated in figure II-10.

A "Closed" cycle means that cryogenic liquid helium is not consumed for cooling process. The top tube consists of a piston for gas compression and several heat exchangers.[34] During the movement of the piston the helium gas moves changing the pressure (from 10 to 24 bar) in the system resulting in a successive decrease of the temperature through adiabatic processes.[35] 90 minutes are needed to cool down the sample holder from room temperature to 3K. As seen in the figure II-12 the cryostat itself is made from two cooling stages with tubes in series. The first stage (reaching the temperature around 40K) is connected to a protective copper shield to reduce thermal radiation. The second stage is connected to the sample holder reaching the temperature as low as 3K. The sample holder is connected using a temperature controller (Lakeshore Model 336)[36] to two Si-diodes and one resistor. The Si-diodes measure the temperature of the sample while the resistor is used to control the heating of the sample with accuracy of 0.1K.

II.4.3. Sample holder

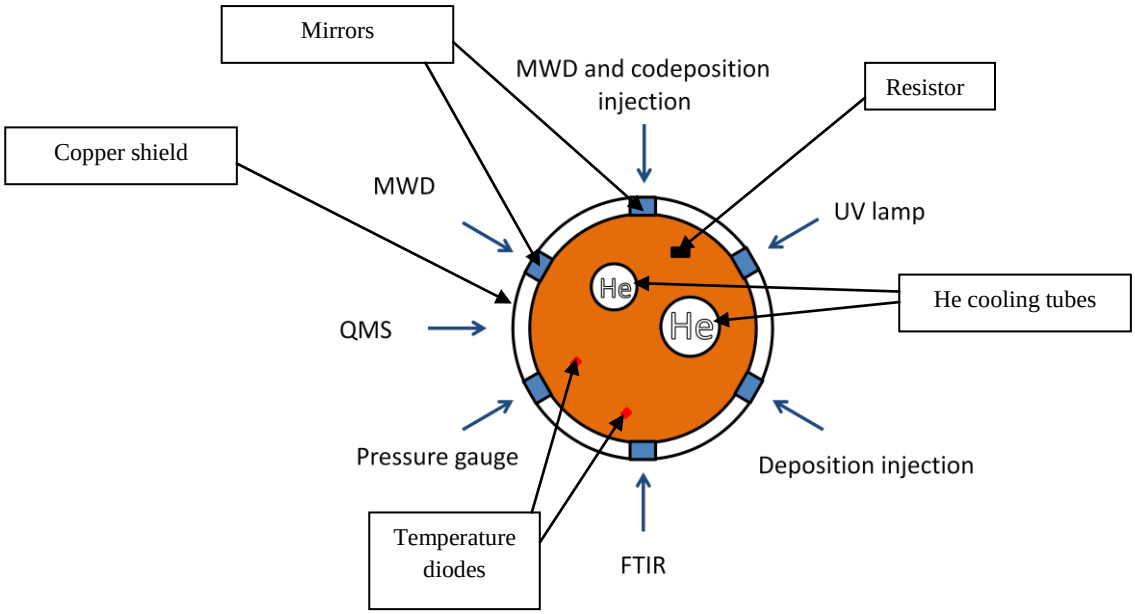

Figure II-13. Sample holder

The sample holder itself consists of six copper mirrors coated by a layer of rhodium. Rhodium has high reflectance in IR region also resistant to extreme conditions like exposure to corrosive gases. All of the mirrors are mounted in a hexagonal pattern on the surface of the second level cooling of the cryostat as shown in figure II-13. The sample holder is inside a copper shield mounted on the head of the cryostat. This makes sure that the temperature of the shield is around 40K providing thermal stabilization for the sample holder. This way the sample mirrors are protected from outside heating sources and radiation. Also during the cooling of the system, the impurities found in the chamber are first condensed on the shield instead of the mirrors.[37] Considering the pressure of the chamber (10^{-10} mbar), this also minimizes the temperature rise. The sample holder with a shield can be rotated with a cryostat itself, thus getting to the desired position on the required experiment (deposition, codeposition, UV irradiation, infrared and mass spectrometry measurements…). The equipment positions are shown in figure II-13 with a mirror configuration with addition of the temperature sensors and resistor for heating.

The sample holder rotation is controlled through the computer using 1-axis manipulator. All the mirrors are numerated from F1 to F6 (F from the French word fenêtre). Rotating the sample holder clockwise positive values is used, anti-clockwise negative. The position diagram is shown in figure II-14. For example, at 0^{o} window F3 is in front of the FTIR spectrometer to record IR spectra in transmission-reflection mode, while at -60^{o} the mirror F3 is in front of one of the injection lines. There is no difference in the final position between 180^{o} and -180^{o} only the direction of rotation.

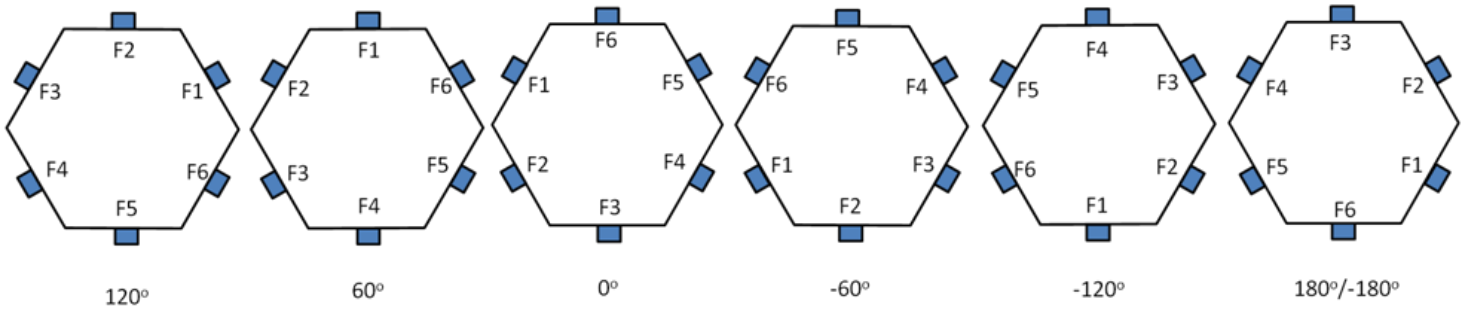

Figure II-14. Mirror position diagram

II.4.4. Sample formation system (Ramps)

For the formation and injection of the samples a custom stainless steel tubing system was used (Figure II-15). This sample formation system is divided into three specific sections called ramps.

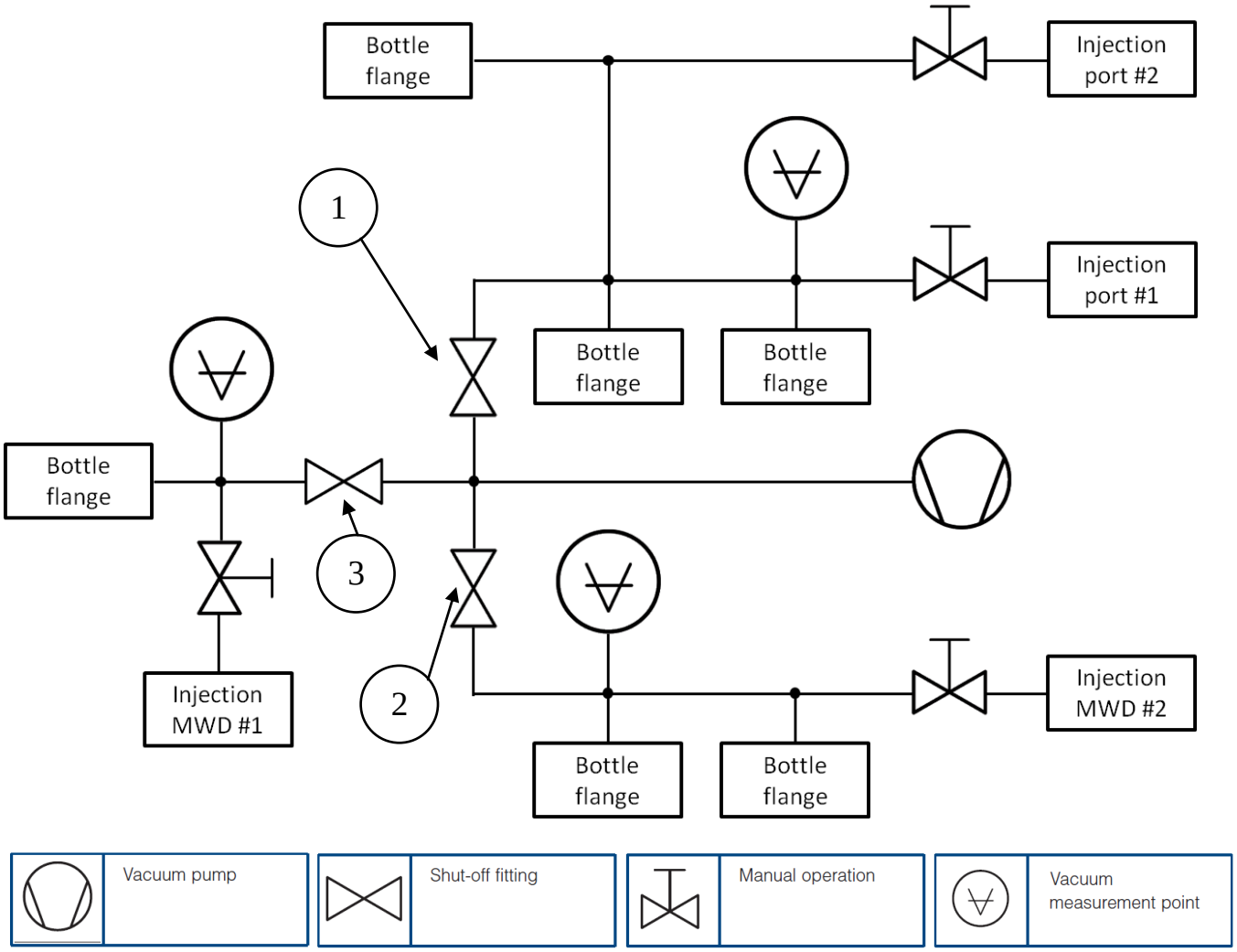

Figure II-15. Sample preparation unit scheme with their corresponding symbols

Each of the ramps is separated by a shut-off valve connected to the main pumping unit in a figure referred simply by their numbers. Obviously each section has a connected pressure gauge to determine the amount of material deposited. These ramps are connected to the main chamber through manually operated precision valves. This allows injection of gas on to the mirrors with very high pressure accuracy.

Ramp #1 is the main formation and mixing ramp mainly used for sample ice depositions. It consists of 3 bottle flanges, so up to 3 different materials can be mixed in the ramp. Most of the time one of the materials is neon for matrix isolation experiments. This ramp connects to the main chamber through two manually operated precision valves. Injection port #1 is the mainly used for ice depositions. It is situated 60^{o} to the right of the FTIR spectrometer. The injection tube is very close to the mirror so high sticking of the material to the cold mirror is achieved. Unlike injection port #1 a port #2 is a bit further away from the mirror. This port is used for the co-deposition experiments when sample material is simultaneously deposited with discharged atomic species. This port is located on the opposite site of the FTIR spectrometer, the same as one of the micro wave dischargers.

Ramps #2 and #3 are for holding gases used by micro wave discharges. The ports connected to injection ports on the discharges itself can be switched over if needed. The only difference between those two ramps is the bottle flange connection count. Ramp #2 has two gas tank connection flanges for the experiments where mixture species can be used for the discharge (For example discharge into N_2-H_2 mixture). Figure II-16 shows how some injection lines (ramp #1, #2 and #3) are connected to the sample holder.

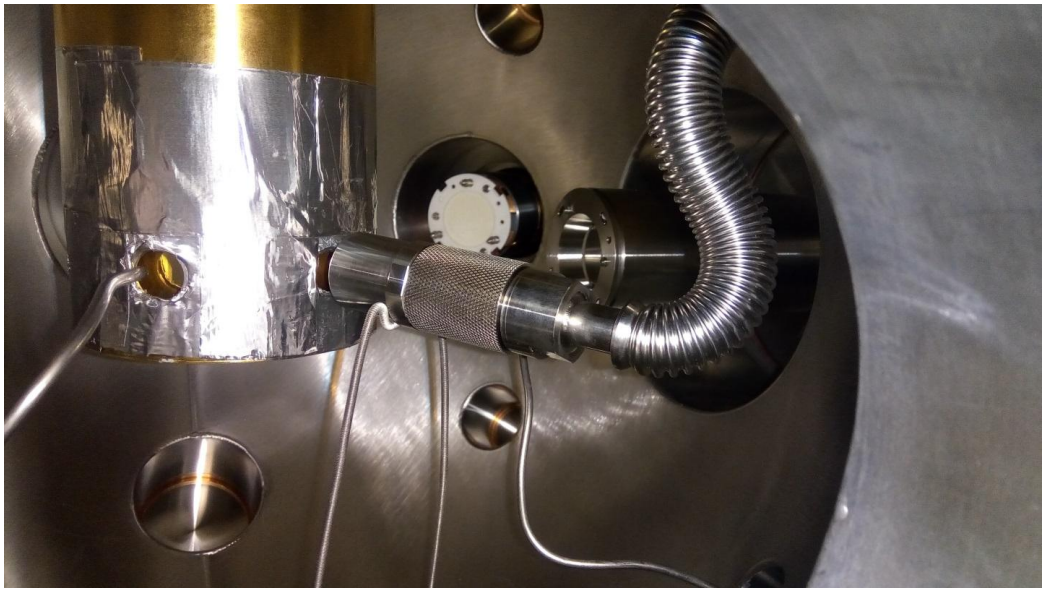

Figure II-16. The inside of the MASSIR chamber: we distinguish one injection line on the left, UV source and two microwave discharges.

II.4.5. UV source unit

In MASSIR equipment as a UV source a deuterium arc lamp (Hamamatsu L10706)[38] is used. It is a vacuum ultra-violet (VUV) light source mounted on a flexible tube with a vacuum flange. By this design this unit allows irradiating samples at a close distance (~1cm, as shown in figure II-16) inside vacuum chamber itself. These lamps are notable for having a high output photon flux (~10^{15} photons*s^{-1}*cm^{-2}) in ultraviolet light range and low at visible and infrared. Deuterium lamp is used over simple hydrogen because of the higher emissivity in a shortwave UV range (figure II-17). A continuous UV spectrum is produced ranging from 115nm up to 400nm. The highest relative intensity is around 160nm (100%) but also intensity at lower wave number is sufficient (~120nm, 30%). There is a great decrease of the intensity after 160nm due to the construction of the housing and material itself (MgF_2). Inside the lamp itself there is a filament which actually is not a source of light. An arc is created from this filament producing extensive heat. This arc excites the molecular deuterium inside the bulb to a higher energy state. Deuterium emits light when it transitions back to its initial state.[39] This is a continuous cycle thus producing a continuous UV radiation. Because lamp operates at high temperatures normal glass cannot be used as a gas housing material. Instead a magnesium fluoride (MgF_2) is used. It is also cooled externally by air.

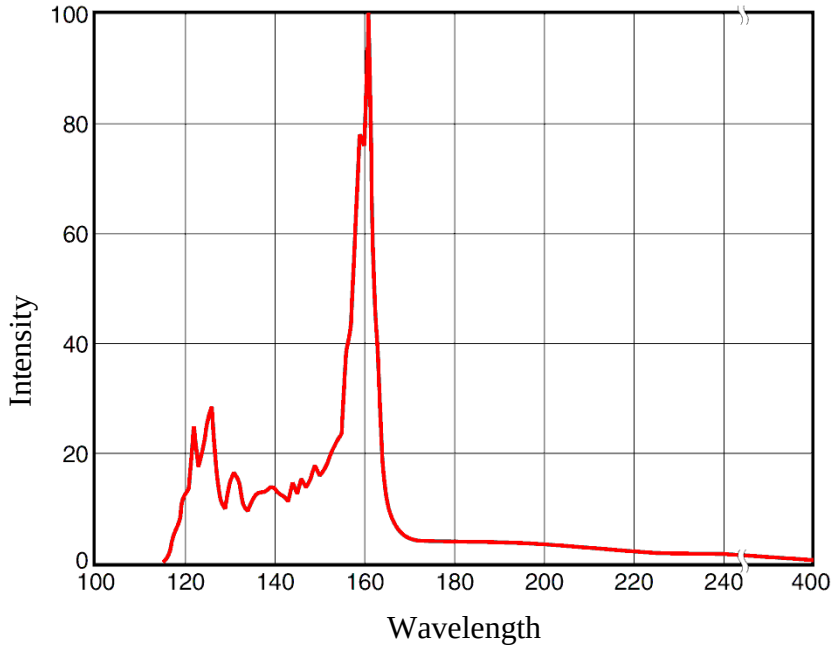

Figure II-17. UV spectrum produced with Hamamatsu L10706 deuterum arc lamp[38]

II.4.6. Microwave discharge source (MWD)

For some experiments atomic species were needed. These species were produced in a plasma source using a microwave discharge (SPECS, Plasma cracker source – Electron cyclotron resonance (PCS-ECR)[40] shown in figure II-16 and in figure II-18. The plasma source is compatible for use in ultrahigh vacuum conditions due to the possibility of working in wide range

of pressures and generates a continuous flux of radical species. It is compatible with most gases like nitrogen, hydrogen, oxygen and water vapor. The injection flow is regulated with a precise micro-leakage valve.

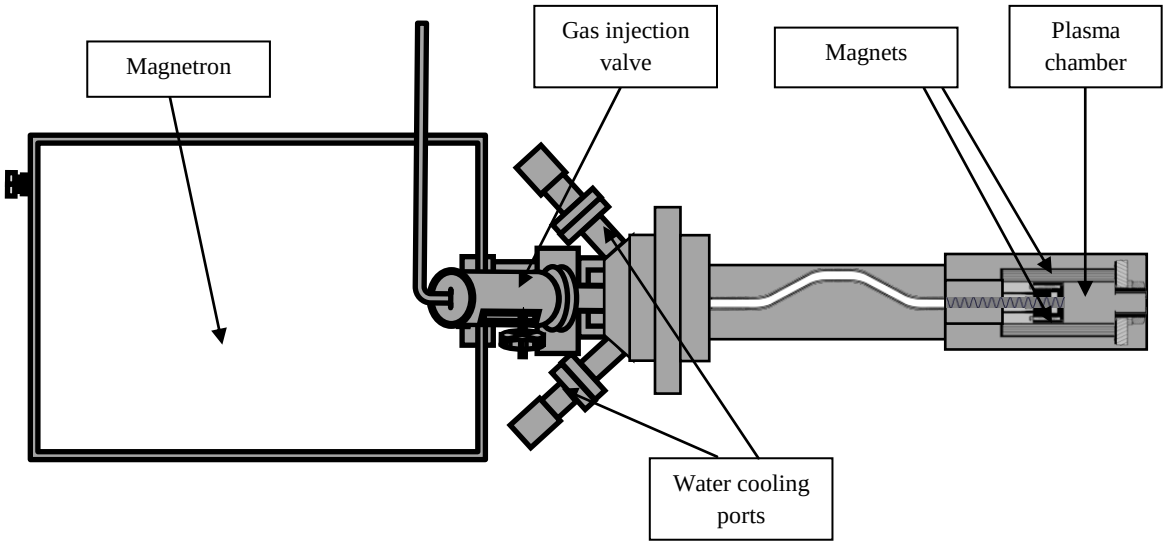

Figure II-18. Microwave discharge from SPECS (PCS-ECR)[40]

Plasma source works on the principle of the electron cyclotron resonance phenomena.[41] An electron in a static and uniform magnetic field will move in a circle due to the Lorentz force. The ionization starts when neutral gas and microwaves are introduced into the plasma chamber. When an external rapidly changing electric field is generated by the microwaves, electrons can gain energy if their frequency equals the frequency of the applied electromagnetic waves, thus a resonance. In our case electromagnetic microwaves are produced by an external magnetron generator with a frequency of 2.45 GHz. To meet resonance criteria a constant magnetic field of 87 mT is required. This magnetic field is created by quadruple magnets around the plasma chamber. This way the electrons are heated and the plasma is ignited as electrons collide with the neutral gases and ionize them. Since the mass of the electrons are low they retain their energy, thus making heavy molecules to dissociate.[42] This source is configured in the manner so that it produces not ions but a thermal energy neutrals radicals (< 1eV). The formed radicals lose their energy through multiple collisions with each other or the walls of the plasma chamber. Because of this also recombinations occur, therefore the source emits a mixture of the atomic and molecular species.

The whole discharge assembly is mounted on the side of the vacuum chamber with a tube of the plasma chamber inside the vacuum chamber. In total two microwave discharge sources are equipped in MASSIR system at an angle of 60^{o} as shown in figure II-13. such geometrical configuration allows radical –radical injection. The end of the discharge tube is at a distance of 10 cm from the sample holder. The radical species are introduced into the chamber through a plate with circular orifices placed at the corners of a rectangle and additional in the middle (5 in total) with diameters of 0.2 mm. Also this plate prevents the spread of photons emitted by

plasma. The pressure difference between the plasma chamber and the vacuum chamber creates a constant flux of material. This flux is not directly focused to the mirror in front of the discharge but is introduced at an angle (at 20°). Even though the highest radical flux is on the mirror in front of the discharge, a few amounts of radical species might also reach other mirrors of the sample holder. This can be used to study the given reaction with different radical fluxes during the same measurement.

Considering that atomic species used are nitrogen, oxygen and hydrogen and their counter molecular parts cannot be directly measured using IR spectrometry, mass spectrometry was used. The dissociation ratios have been calculated to be: N_2 ~ 5%, H_2 ~ 15%, O_2 ~ 10%.

II.4.7. FTIR (Fourier Transform Infrared) spectrometer

In this equipment, all the infrared spectra were recorded using high resolution Bruker Vertex 80v[43] Fourier transform spectrometer. For ice studies a mid-infrared (500 – 5000 cm^{-1}) range is sufficient for vibrational identification of species. Most stretching and bending modes lie in this region. Optionally, if needed, this spectrometer is equipped with additional optical components to cover the whole spectral range from far infrared to ultraviolet (5 – 50000 cm^{-1}). As spectrometer is used under vacuum all the unwanted atmospheric interferents (water vapor, CO_2) are eliminated from the spectrometer and there is no need for spectral manipulations like atmospheric compensation.[44] Under these conditions measured IR spectrum will not contain residual H_2O and CO_2 features which could mask weak spectral bands of the sample. IR spectrometer compartment is separated from the vacuum chamber by a KBr window. The connected vacuum pump is oil-free in order to prevent oil vapor from entering the spectrometer optics interior.

This spectrometer works on principle of classical Michelson interferometer concept. The internal components are shown in figure II-19. Bruker Vertex 80v spectrometer consists of these components:

Light Source: The instrument is equipped with a MIR (mid infrared) source (H in figure II-19). The MIR light source is a globar (silicon carbide) that emits mid-infrared light.[45] Optionally it can be equipped by other light sources (G in figure II-19) like mercury, tungsten or xenon sources.

Detector: Same as a light source, a detector can be chosen depending on the study of the spectral region needed. This spectrometer is equipped with two detectors: MCT (HgCdTe) and InSb (B in figure II-19). For this study a MCT, liquid N_2 cooled, detector was used because of its operating spectral range of 500 – 5000 cm^{-1}. InSb detector is used for studies in near-infrared range (1850 – 10000 cm^{-1}). Other detectors can be used for different spectral regions: Far Infrared – Bolometer (8 – 600 cm^{-1}) or Visible and UV – Silicon diode (9000 – 25000 cm^{-1}), GaP diode (18000 – 50000 cm^{-1}).[46]

Beamsplitter: Beamsplitter is the last component with a light source and detector to determine the IR measurement range. Beamsplitter is an optical device made from semi reflecting plates used for splitting a single beam of light into two. This spectrometer is equipped with standard KBr beamsplitter (F in figure II-19) which covers a spectra range from 350 – 8000 cm^{-1}. Apart from this standard beamsplitter, evidently other beamsplitters are needed for different spectral regions: for near-infrared CaF_2 and Mylar for far-infrared.[47]

Interferometer: The interferometer itself consists of the main components: a fixed mirror, a beamsplitter and a moving mirror. A moving mirror is based on a linear scanner (A in figure II-19) which ensures highest possible spectral resolution (as standard 0.5 cm^{-1} was used). The linear scanner is supported by an air bearing which requires the connection to a compressed-air line. This line is connected to a source of dry and clean nitrogen gas installed in the laboratory having the pressure about 1bar with a flow rate around 100 L/h.

Laser: Vertex 80v is equipped with a He-Ne laser that emits red light with a wavelength of 632.8 nm[48] (D in figure II-19). The laser controls the position of the moving interferometer mirror (the scanner) and is used to determine the data sampling positions. The monochromatic beam produced by He-Ne laser is modulated by the interferometer to generate a sinusoidal signal.

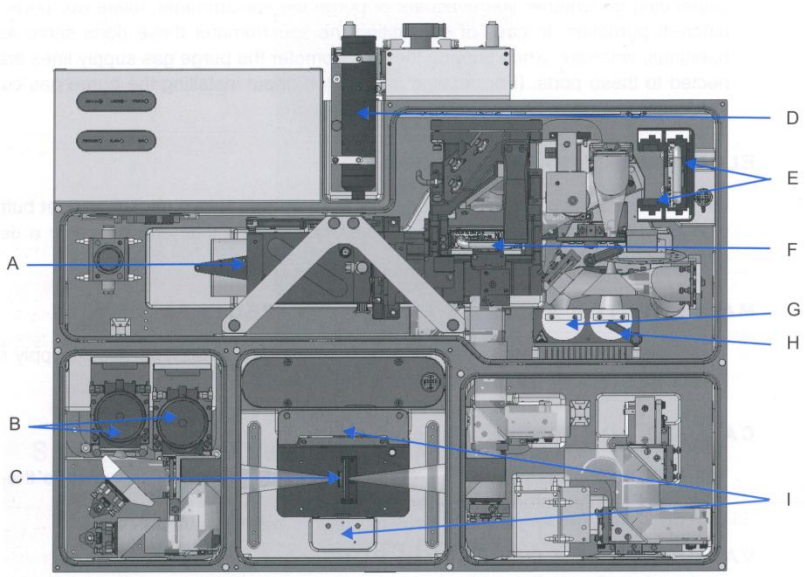

	Component
A	Linear air bearing scanner (UltraScan, true-aligned)
B	DigiTect Detectors
C	Sample holder (exchangeable for other optional accessories)
D	Laser
E	Two beamsplitters storage positions
F	Beamsplitter (operation position)
G	Optional NIR source (operating position)
H	MIR source (operating position)
I	QuickLock clamping device (including connectors)

Figure II-19. Internal components of the Bruker Vertex 80v FTIR spectrometer

II.4.8. QMS – Quadrupole mass spectrometer

Figure II-20. Hidden analytical quadruple mass spectrometer[49]

For detection of species during the desorption in gas phase a mass spectrometer is used. In this equipment a quadrupole mass spectrometer (Hidden analytical HAL7,[49] figure II-20) is used. It is named quadrupole because for mass selection a quadrupole mass filter is used. As any other mass spectrometer this one also consists of three main parts: an ion source, a mass analyzer and detector.[50]

Ion source: Before gases can be analyzed in a mass filter, they must first be ionized in an ion source by means of electron bombardment[51] (the tip in figure II-20). Electrons are emitted from an electrically heated cathode (filament). A voltage is applied between anode and cathode, which accelerates the electrons. Neutral gas molecules that are present in the formation space between the anode and cathode are ionized by collisions between electrons, forming single and multiple positive ions. The energy of the colliding electrons exerts a significant influence on both the number and type of ions that will be formed. Negative thing is that it works only up to $5x10^{-6}$mbar, because the filament of the ionizer can burn up.

Mass analyzer: As the name states the quadruple mass analyzer consists of four 4 rods (figure II-21). The principle of operation is quite simple. The opposite rods have different polarity and are connected together to a constant voltage U and a radio frequency voltage (with amplitude V and frequency ω). The ions propagate through the rods along the z axis. Depending on the U/V ratio only certain ions with mass-to-charge ratio will reach the detector. The other ions will have unstable trajectories and will hit the rods. The negative aspect of this type of the mass analyzer is that the ions should enter the analyzer exactly at the center to pass through. This can be avoided by using small center clits at the entrance, but this would reduce the amount of ions drastically. This particular mass spectrometer consists of a triple mass filter system containing a pre-filter (figure II-22, light green in the beginning), a mass selective primary filter (red in the middle) and a post filter (dark green in the end). All those 3 filters work on the same principle, but do not require a usage of centered slits. Triple mass filter increases sensitivity with enhanced contamination resistance.[52]

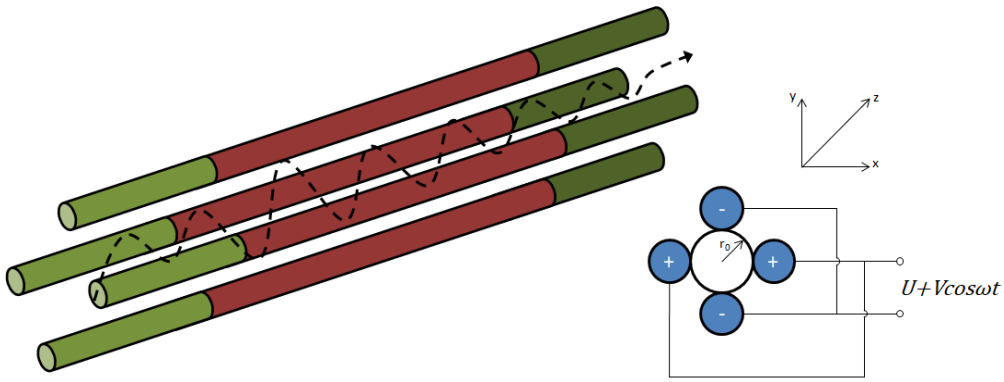

Figure II-21. Quadrupole mass analyzer principle scheme

Detector: The ions selected in the rod due to their mass-to-charge ratio can be electrically detected with the means of a Faraday cup.[53] Faraday cup directly measures the ion current using an electrometer. The ions strike a Faraday collector (Faraday cup), where they give up their electrical charge. The resulting current is converted to a voltage that is proportional to the ion current by means of a sensitive current-to-voltage converter (electrometer amplifier).

II.5. Interstellar ice analog formation

Due to the physical and chemical properties of the materials, experiments can be carried out in any state of the matter: gas, liquid or solid, depending on the experimental requirements. Atmospheric and interstellar studies used mainly solid and gas phase and eventually the interface solid-gas. The analysis of the investigated samples depends strongly on the temperature. At room temperature gas phase molecular spectra are complicated due to the high rotational and vibrational density states, which show numerous ro-vibrational transitions. This can be avoided by decreasing the temperature which strongly simplifies the structure of the molecular spectra. Solid phase molecular spectra show wide absorption bands which might overlap in different spectral regions. The transitions identified in solid phase are mainly vibrational transitions. Matrix isolation technique is usually used in order to reduce the environmental interactions and then to avoid overlapping band absorptions.[54]

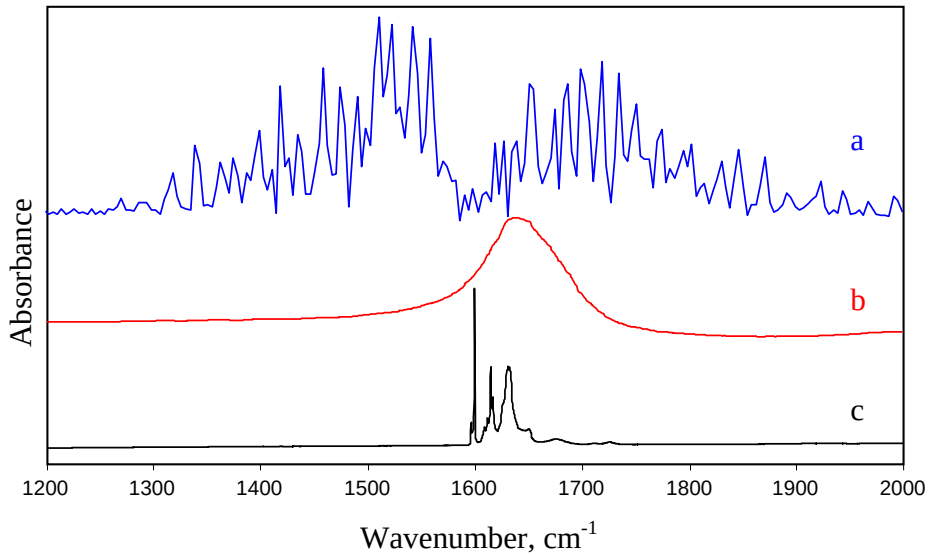

Figure II-22. IR absorption spectra of ν_2 water bending mode:
a) gas; b) solid; c) water molecule in 3K Ne matrix.

As an example in figure II-22 it is shown the difference of IR absorption spectra of water. Spectrum **a,** recorded at room temperature, shows the ro-vibrational transitions of the bending mode of water in gas phase. Spectrum **b,** recorded at 3K**,** shows the vibrational transition of the bending mode of the water ice. Spectrum **c**, recorded at 3K, shows the bending mode of water isolated in solid neon matrix. We notice that in neon matrix the infrared signals are narrow and we can distinguish the vibrational and ro-vibrational transitions of water trapped in solid neon. Usually the matrix isolation technique is associated to the study of interstellar ice analogs in order to characterize the solid state reactions taking place on the surface of the ice or inside the bulk ice.

II.5.1. Pure ices

The formation of solid ice samples itself is possible using precursors taken from the gas phase. For liquids and solid materials, at room temperature, we use evaporation techniques. In a closed system at a given temperature vapor is in thermodynamic equilibrium with its condensed phases (solid or liquid) defined by the pressure also known as vapor pressure.[55] Mixing vapors or gases using ramping system (discussed in II.4.4) it is possible to form samples by quickly condensing them on the mirror on the sample holder (discussed in II.4.3) cooled at a low temperature (around 3-10K). This process is called deposition. During the material deposition layers of ice are formed which later on can be probed using IR spectroscopy. There are two possible ice structures: amorphous and crystalline. Amorphous ices have an irregular geometry with molecules arranged in an indefinite manner. This ice can be formed at very low temperatures (3-10K) depending on materials. They are formed like that because molecules do not have enough time to rearrange on the mirror before freezing. These types of ices formed at very low temperature are mostly found in the interstellar medium. On the other hand crystalline ices have a regular geometry with atoms arranged in a definite manner. These kinds of ices are formed at relatively higher temperatures (50-100K), depending on the studied species.

Amorphous to crystalline transformations can also be induces by heating an amorphous ice formed at low temperature (10K) to higher temperatures (>50K).[56]

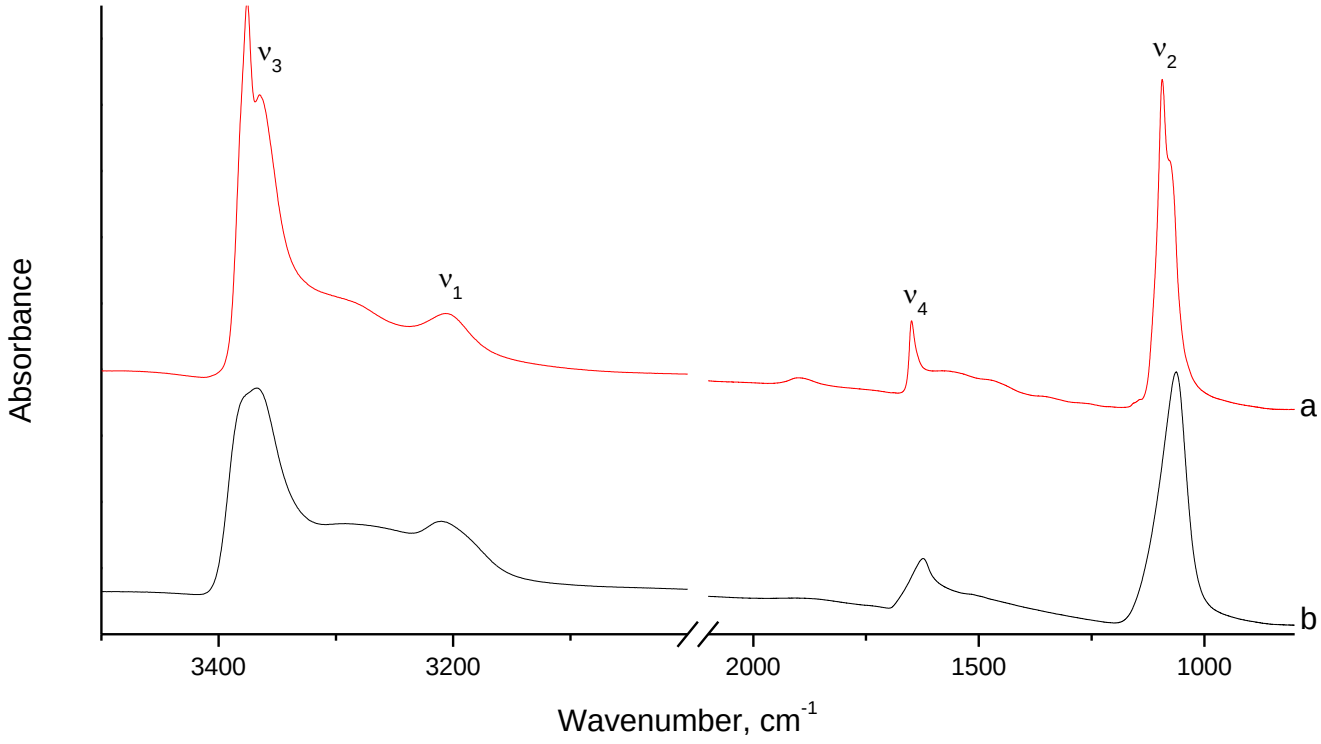

Figure II-23. NH_3 IR absorption spectra: a) crystalline ice at 100K; b) amorphous ice at 10K

As an example in figure II-23 it is shown both crystalline and amorphous IR absorption spectra of NH_3 ice. At first glance both spectra look alike, but upon closer inspection in crystalline ice it is visible more structured bands. The crystalline ice's absorption spectrum usually has more sharp vibrational bands. However analysis of reaction products in solid phase vs temperature should be taken great cautions as during the heating of the sample the IR signals due to the amorphous-crystalline transformations can be easily mistaken with the IR signals derived from newly formed species.

II.5.2. Matrix isolation

Matrix isolation technique is used to greatly reduce the wideness of the vibrational bands for easier IR absorption spectrum analysis. The samples are formed similarly as trying to get pure ices just that they are mixed upon with any neutral gases inactive in IR region. It can be inert atomic gases: He, Ne, Ar, Xe; or diatomic molecule gases: H_2, N_2, O_2. Noble gases are mainly used because of their unreactivity, especially if combined with subsequent irradiation experiments. Mono-atomic gases also have relatively simple face-centered cubic crystal structure, which can make interpretations of the site occupancy of the guest molecules easier (figure II-24). Most important usage of the matrix isolation technique is that short-lived, highly-reactive species (radicals or ions) and reaction intermediates can also be entrapped in inert crystals and later on

may be observed and identified by spectroscopic means.[57] The matrix molecule ratio with sample molecules are usually around 10^2 - 10^5:1. By condensing this kind of mixture on a cold mirror sample molecules are surrounded and isolated in inert matrix thus reducing intermolecular interactions.

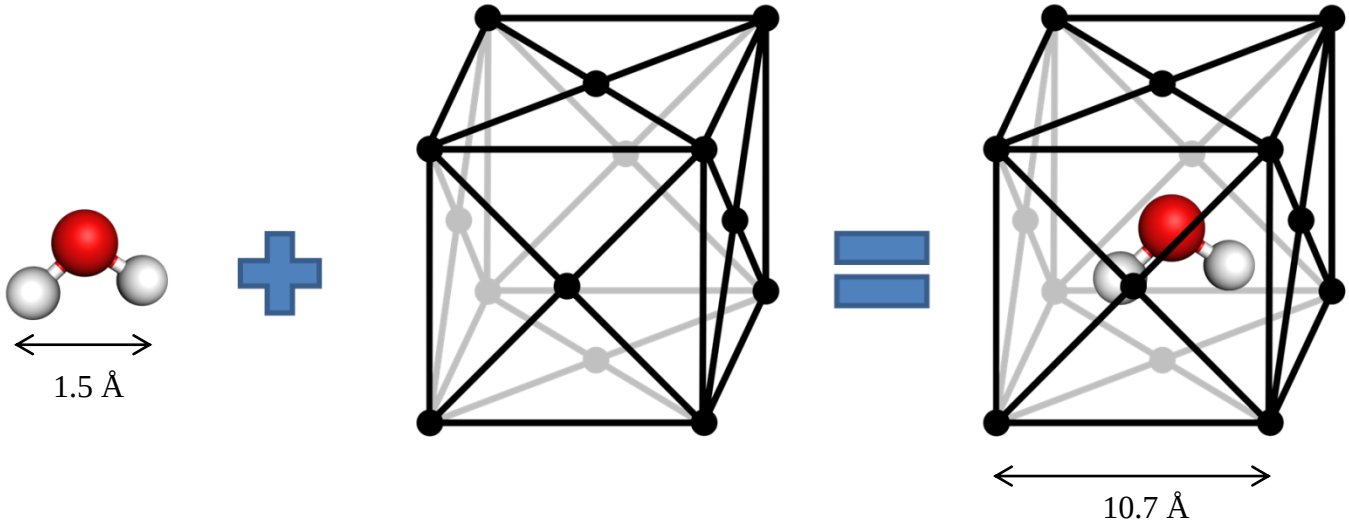

Figure II-24. Molecule entrapment in inert gas fcc (face centered cubic) crystal matrix with length of water molecule and size of the lattice (roughly estimated using neon atomic radius)

II.6. Samples and materials: preparation and composition

There are two possible ways of sample formation. The one deposition process was briefly mentioned in section II.5.1. It consists of just condensing gases on the cold mirror. It is the most simple and commonly used method. Just after deposition, the sample can be manipulated by the needs of the experiment: UV irradiation, atomic bombardment or temperature variation. Bombardment of sample by atomic species (H, N, O) is an interesting experiment to investigate atom addition surface reactions. The only negative aspect is that it works like a surface treatment. The penetration depth is not that great and the success of the experiment depend strongly on the ice thickness. Thin ice samples on the mirrors can be removed due to reactive aspects and thick ice samples, even after bombardment, might produce too wide IR absorption bands to see any significant change. In this case another experimental method might be used: the co-deposition.

As the name suggests co-deposition (or sometimes co-injection) means that sample material is deposited at the same time as the discharged atomic species.[58] The co-deposition method is shown in figure II-25. Preparing samples this way the reactant is mixed with atomic species. Naturally this method has its own advantages and disadvantages. The obvious advantage is that reactants are mixed with atomic species increasing the probability of the reaction in the sample in comparison with only surface bombardment. The disadvantages would be the difficulty of sample formation. Firstly the dissociation ratio of molecular species using microwave

discharge is not efficient (lower than 20%). What this means is that both molecular and atomic species are mixed with the reactant. This does not bring too much trouble because the molecular species are not reacting and they are IR inactive so not visible in IR absorption spectra. The second difficulty comes from working with heavy IR absorbing (e.g. NH_3) molecules. And consequently very low amount of reactants should be co-deposited to avoid the opaque IR spectra. Even though most of the difficulties can be overcome through good preparation and experimental experience, it sometimes might be difficult to set the correct low flux of reactants and maintain it during the whole co-deposition with radicals.

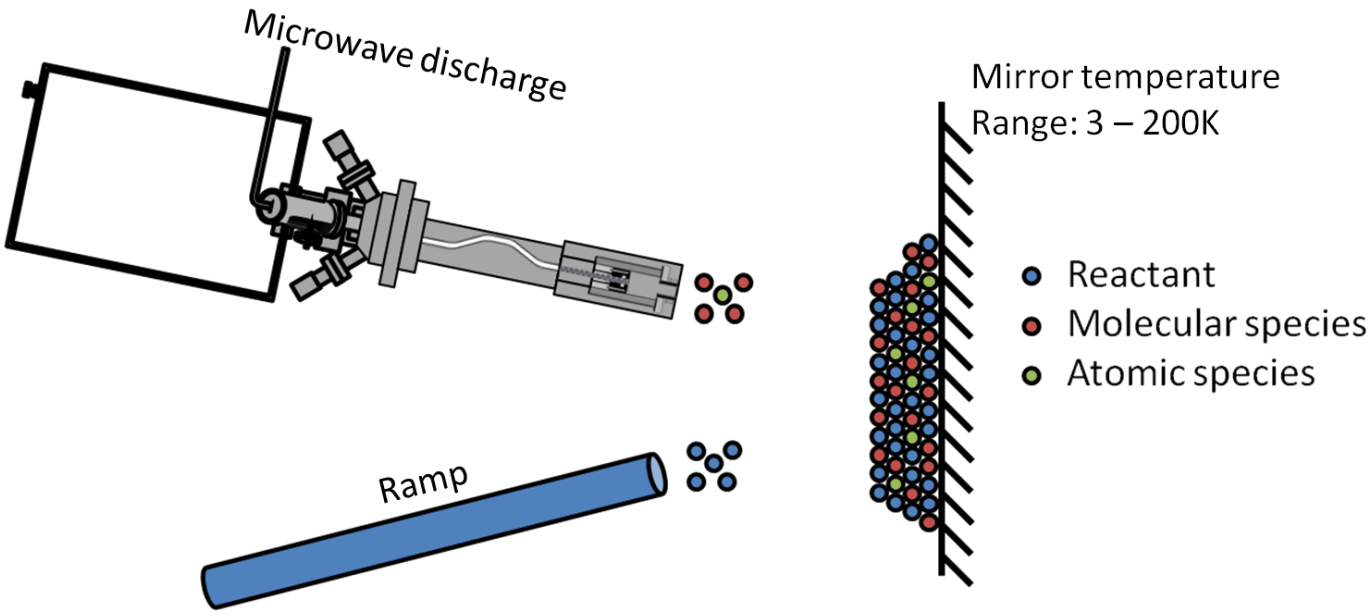

Figure II-25. Radical-molecule co-deposition method

II.6.1. Ramp volume and gas composition

According to a ramping diagram (figure II-15, II.4.4, page 39) the only measurable value is the pressure of the gases in the ramp. According to ideal gas law to obtain the amount of gases in a system can be possible through:

$$n = \frac{pV}{RT} \qquad \text{(II-7)}$$

where **n** is the amount of gas (number of moles), **p** is the pressure of the gas, **V** is the volume of the gas, **R** is the ideal gas constant, equal to the product of the Boltzmann constant and the Avogadro constant (8.3144598(48) $J \cdot mol^{-1} \cdot K^{-1}$) and **T** is the absolute temperature of the gas.

So to calculate the total amount, the R, T (room temperature) and ramp Volume are constants. In other words pressure is directly proportional to the molecular amount: $p \sim n$. But still for correct calculations an accurate volume of the ramps should be known. Due to its complexity it cannot be easily calculated using geometrical methods, therefore the measurement

with gases is done. The volume can be easily estimated using an external bottle of the known volume V_B. The bottle is connected to the ramp and the system is vacuumed. Then a known amount of the injected gas is introduced in the ramp for a given pressure p_B, measured with an accuracy of 0.1 mbar. A connection between the bottle and the rest of the ramp is closed and the ramp with the volume V_S is vacuumed again. The amount of the gas left in the bottle, after the opening the bottle, equally distributes in the system with V_S + V_B volume under a new value of pressure p_S. According to the ideal gas law a link between p_B, p_S, V_B and V_S can be expressed as:

$$p_B V_B = nRT = p_S(V_S + V_B) \quad \text{(II-8)}$$

p_B and V_B are the pressure and volume of injected gas enclosed in the bottle, p_S and V_S are pressure and volume of the gas in the ramp. Equation (II-8) can be further simplified to express the volume of the ramping system:

$$V_S = V_B\left(\frac{p_B}{p_S} - 1\right) \quad \text{(II-9)}$$

Such calculations for Ramp #1 in the MASSIR setup give the volume V_S = 200 cm^3. The amount of material leaving does not necessary mean the same amount is deposited on the cold mirror. This depends on several factors like: temperature of the mirror and the flow speed of gases to the mirror. Obviously due to the temperature the sticking of the molecules also changes. The lower the temperature the more molecules are condensed on the window. Even small temperature increments can decrease condensation amount depending on the molecules. And the other parameter is the flow speed of the gases. Evidently if huge flow is used then there will be a higher spread of molecules coming from the nozzle. With higher spread it is possible that some of the molecules will not be reaching the mirror at all. Lower flow speed also allows molecules to condense on the mirror homogeneously forming distortionless ice crystals. Undoubtedly doing a deposition in lower flux increases the deposition time.

II.6.2. Thickness of the ices

As previously said the thickness of a sample can greatly impact the outcome of the experiments. Knowing the ice thickness is also a great way understanding the chemistry of ices. The exact calculation of ice thickness can be quite challenging. The thickness **d** can be obtained by counting the number of fringes in the interference pattern, created by a visible light by the ice, as a function of the deposition time.[59] Usually a He-Ne laser for emission and a photo diode for reflection as system is used. Photo diode obtained signal through time varies due to interference created by ice. The number of fringes (**k**) can then be converted into a thickness **d** using the following equation:

$$d = k\frac{\lambda}{2n\sqrt{1-\left(\frac{\sin(\theta)}{n}\right)^2}}, \quad \text{(II-10)}$$

where **λ** is the wavelength of the He–Ne laser (λ = 632.8 nm), **n** the refractive index of the studied ice at the laser wavelength and ***θ*** the angle of incidence of the laser beam on the surface sample.

For this calculation there is a need to know of the refractive indices **n** in the visible wavelength domain. This is usually know for a simple ices (NH_3, CH_4, H_2O), but for the more complex molecules (multicomposition samples) more analysis is need. Considering we do not have this type equipment present in this study other means are necessary.

The other method to estimate the approximate ice thickness can be through the column density **n** (molecules/cm^2):

$$n = \frac{d\rho N_a}{M} \qquad \text{(II-11)}$$

where **ρ** is the density of the considered pure ice (in cm^3/g), **M** is the molecular mass (g/mol), $\mathbf{N_a}$ is the Avogadro constant (molecules/mol) and **d** is the ice thickness (cm).

Also the same column density **n** can be obtained from the recorded infrared spectra of the pure ice with the formula which derives from the Beer–Lambert–Bouguer law:

$$\mathrm{n} = \frac{ln10 \int I(v)dv}{A} \qquad \text{(II-12)}$$

where $\int I(v)\,dv$ is the integrated intensity in the IR spectrum (cm^{-1}), **A** is a band strength of the molecule in the same region (cm/molecule). From here also comes a requirement of knowing **ρ** the density of the considered ice and **A** band strength which are known to some molecules. If not additional estimations need to be done.

The correction value of $\frac{\cos(8°)}{2}$ has to be taken into account also. This system is build so that IR beam hits the mirror at a slight angle of 8^o and not directly (figure II-26). The light travel path is increased. Considering that the system is working in the reflection mode the IR beam passes the sample twice thus a ½ constitent.

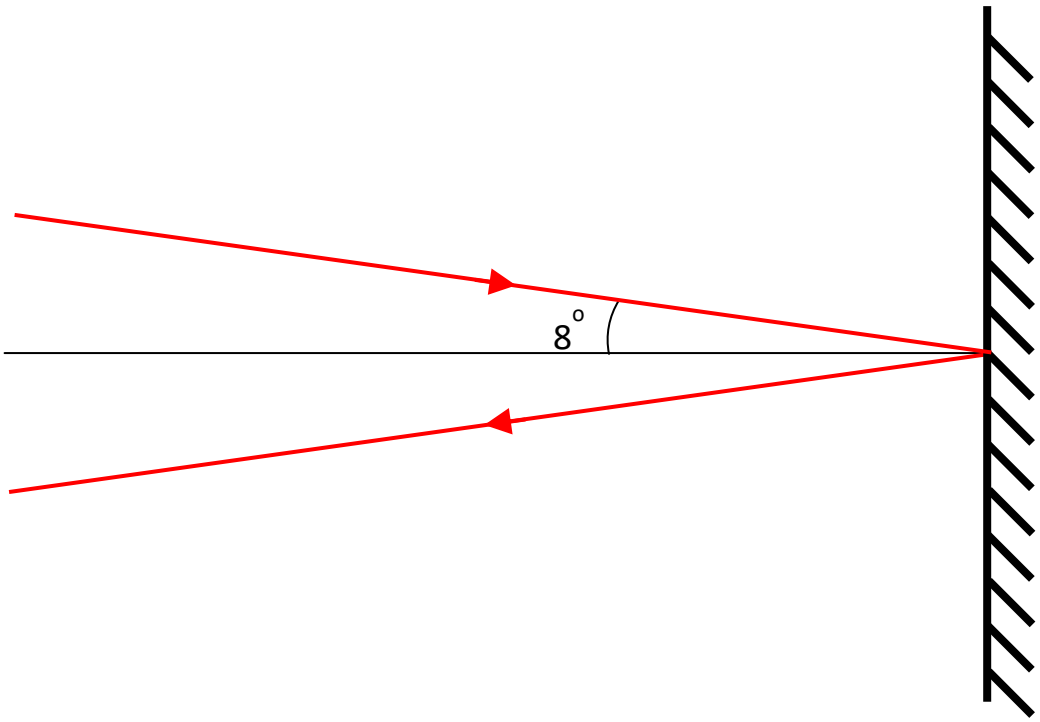

Figure II-26. IR beam pathing on the mirror

In the end the final column density formula can be expressed like this:

$$n = \frac{ln10 \int I(\nu) d\nu}{A} \frac{\cos(8°)}{2} \quad \text{(II-13)}$$

By combining equations II-13 and II-11 we can easily deduce the thickness of the sample:

$$d = \frac{M\ ln10 \int I(\nu) d\nu}{A\ \rho N_a} \frac{\cos(8°)}{2} \quad \text{(II-14)}$$

The thickness of the studied ices can be deduced knowing the density of the ice, the band strength of the measured vibrational mode and the mass of the molecules forming the ice. Under our experimental conditions the thickness range from 0.1 to 5 µm depending on the nature of the experiments carried out.

II.6.3. Chemicals used

Table II-1. Chemical species used in the experiments

Species	Purity, %	Company	Vapor pressure, mbar
Neon, Ne	99.9995	Air liquide	Gas
Oxygen, O_2	99.9995	Air liquide	Gas
Nitrogen, N_2	99.9999	Messer	Gas
Hydrogen, H_2	99.9995	Messer	Gas
Ammonia, NH_3	99.998	Messer	85
Methane, CH_4	99.9995	Messer	Gas
Hydroxylamine, NH_2OH	95	Sigma-Aldrich	Hydroxylamine phosphate salt, $(NH_2OH)_3H_3PO_4$
Propargyl alcohol, $HC{\equiv}CCH_2OH$	99	Sigma-Aldrich	16
Allyl alcohol, $H_2C{=}CHCH_2OH$	98.5	Sigma-Aldrich	28
Propanol, $H_3CCH_2CH_2OH$	99.7	Sigma-Aldrich	20
Propynal, $HC{\equiv}CCHO$	-	Synthesized by oxidation of propargyl alcohol	260
Propenal, $H_2C{=}CH\text{-}CHO$	99	Sigma-Aldrich	290
Propanal, CH_3CH_2CHO	98	Sigma-Aldrich	422

Water (H_2O) – demineralized and degassed.

Bibliography

1 Hollas J. M., Modern spectroscopy. John Wiley & Sons Ltd, England, 2004.
2 Light: Electromagnetic waves, the electromagnetic spectrum and photons. www.khanacademy.org, Retrieved 2017-11-20.
3 Zaarur E., Peleg Y., Pnini R., Theory and problems of Quantum mechanics, Schaum's Oulines, McGraw Hill (USA), 1998
4 Skoog D. A., Holler F. J., Crouch S. R., Principles of instrumental analysis. Thomson Brooks, USA, 2007.
5 Purcell E. M., Morin D. J., Electricity and Magnetism (3rd ed.). Cambridge University Press, Harvard University, USA, 2013.
6 "What Is Electromagnetic Radiation?" www.livescience.com, Retrieved 2017-11-20.
7 Mobley C., Absorption: Physics of absorption. www.oceanopticsbook.info, Retrieved 2017-11-20.
8 Stuart B., Infrared spectroscopy: fundamentals and application. John Wiley & Sons, Inc. USA. 2004.
9 Atkins P., de Paula J., Elements of physicals chemistry (5th ed.). Oxford: Oxford U.P, 2009.
10 Molecular vibrations and rotations, notes of Prof. dr. Ad van der Avoird, January 28, 2010
11 Struve W.S., Fundamentals of Molecular Spectroscopy. John Wiley & Sons, Inc. USA, 1989.
12 Baykara S.Z., 2004. IJHE, 29, 1451.
13 Ekkekakis P., 2009. Journal of Sport & Exercise Psychology, 31, 4, 505.
14 Lambert J.H., Photometria sive de mensura et gradibus luminis, colorum et umbrae. 1760. Augsburg ("Augusta Vindelicorum", Germany: Eberhardt Klett.)
15 Butler L. R. P., Laqua K., "Nomenclature, symbols, units and their usage in spectrochemical analysis-IX. Instrumentation for the spectral dispersion and isolation of optical radiation (IUPAC Recommendations 1995)". Pure Appl. Chem. 1995.
16 Michelson A. A., Morley E. W., 1887. American Journal of Science. 34, 203:333.
17 Hariharan P., Basics of Interferometry. Elsevier Inc., USA. 2007.
18 Jordan C. "Cours d'Analyse de l'École Polytechnique, Vol. II, Calcul Intégral: Intégrales définies et indéfinies" (2nd ed.). Paris, 1883.
19 Perkins W. D., Fourier Transform Infrared Spectroscopy Part II. Advantages of FT-IR. Topics in chemical instrumentation. 1987, 64, 11.
20 Wilbur D., Why Run a Background Spectrum? Department of Chemistry, Tufts University, 2000.
21 Ashcroft A.E., An Introduction to Mass Spectrometry. www.astbury.leeds.ac.uk, Retrieved 2017-11-20.
22 de Hoffman E., Stroobant V., Mass spectrometry, Principles and Application (3rd ed.). John Wiley & Sons Ltd, England, 2007.
23 Li H. J., Deinzer M. L., 2007. Anal. Chem, 79, 1739.
24 Gross J.H., Mass Spectrometry. Springer, 2011.
25 McLafferty F. W., Tureček F., Interpretation of Mass Spectra. University Science Books, 1993.
26 Radebaugh R., 2009. J. Phys.: Condens. Matter, 21, 164219.
27 www.lesker.com/
28 www.prevac.eu
29 O'Hanlon J. F., A User's Guide to Vacuum Technology (3rd ed). John Wiley & Sons, USA, 2003.
30 Operating Instructions, Pascal series. Pfeiffer Vacuum GmbH, Germany, 2015. www.pfeiffer-vacuum.com.
31 http://www.idealvac.com
32 STP-603/1003 Series turbomolecular pump instruction manual. BOC Edwards, Japan, 2003.
33 Shi cryocooler specification, Model: SRP-082B-F70H. Sumitomo Heavy Industries, Ltd. 2009.
34 Biwa T., Tashiro Y., Yazaki T., 2008. Journal of Power and Energy Systems, 2, 1254.
35 de Waele A.T.A.M., 2011. J. Low. Temp. Phys., 164:179.
36 www.lakeshore.com
37 Bally T., Reactive Intermediate Chemistry: Chapter 17, Matrix Isolation. 2004, John Wiley & Sons, Inc. USA.
38 S2D2 VUV light source unit L10706 series. Hamamatsu photonics K.K., 2004. www.hamamatsu.com
39 Brodie K., Neate S., Features and Operation of Hollow Cathode Lamps and Deuterium Lamps. Agilent Technologies, Inc., 2010, USA.
40 Microwave Plasma Source PCS-ECR, SPECS GmbH - Surface Analysis and Computer Technology, Germany, www.specs.de.
41 Scrivens R., Classification of Ion Sources. CERN, Geneva, Switzerland

[42] Abolmasov S. N., 2012. Plasma Sources Sci. Technol., 21, 035006.
[43] Bruker Vertex 80v user manual. 2006, Bruker Optik GmbH, www.brukeroptics.com
[44] Perez-Guaita D., Kuligowski J., Quintás G., Garrigues S., M. de la Guardia., 2013. Appl Spectrosc, 67(11), 1339.
[45] Bentlage M., Sources of Infrared radiation, lecture slides, 2008.
[46] Rogalski A, 2002. Infrared Physics & Technology, 43, 187.
[47] Cazes J., Ewing's Analytical Instrumentation Handbook 3rd ed. CRC Press, Taylor and Francis Group, USA, 2005.
[48] Vermunt L., The helium-neon laser. 2015
[49] Mass Spectrometers for Residual Gas Analysis Applications (RGA). Hiden Analytical Ltd. England, www.HidenAnalytical.com**.**
[50] Babu P., Components of a Mass Spectrometer. Centre for Cellular and Molecular Platforms.
[51] Märk T.D., Dunn G.H., Electron Impact Ionization. Springer Science & Business Media, 2013.
[52] Yost R. A., Enke C. G., 1978. J. Am. Chem. Soc., 100 (7), 2274.
[53] Brown K. L., Tautfest G. W., 1956. Review of Scientific Instruments, 27, 696.
[54] Whittle E., Dows D. A., Pimentel G. C., 1943. The Journal of Chemical Physics, 22, 11.
[55] Růžička K., Fulem M., Růžička V.. Vapor Pressure of Organic Compounds - Measurement and Correlation. 2008.
[56] Holt J. S., Sadoskas D., Pursell C. J., 2004. The Journal of Chemical Physics, 120, 7153.
[57] Jacox M. E., 2002. Chem. Soc. 31, 108.
[58] Pirim C. and Krim L., 2004. RSC Adv., 4, 15419.
[59] Heavens O. S., Optical Properties of Thin Solid Films. Dover Publications, USA, 1965.

Chapter III:

Photochemistry of NH_3-H_2O ice

Most simplistic molecule based on nitrogen atom is ammonia (NH_3). This chapter is divided into several different sections. The study at first started working on the ammonia photolysis in diluted phase, trapped in neon matrix. This helped analyzing the vibrational bands of the products and by heating the sample to analyze the evolution of the reaction from the diluted phase to concentrated ice phase. The coupling between the matrix isolation and pure ice would help the analysis and the description of the mechanism occurring on icy surfaces as it will be discussed in the second section. In the third part of the study we aim to investigate the catalytic role of water molecules in the photodecomposition of ammonia, where we will see that the kinetic of ammonia dissociation at low temperature is water dependent. As the most obvious photofragments from ammonia are H, N, NH and NH_2 which may react to form complex molecules, we have investigated another possibility of their formation. In this way we have analyzed the behavior of H_2-N_2 mixture subjected to a microwave discharge and deposited at low temperature. We show in this last section that many possibilities of nitrogen-hydrogen atomic combination lead to the formation of NH, NH_2 and NH_3, which concentrations depend on both on the temperature of the sample deposition and on the N_2/H_2 mixture ratio.

III.1. Earlier studies and motivation

Ammonia molecule was detected in space almost fifty years ago, back in 1968.[1] Ten years later a deuterated equivalent of ammonia was detected also[2] and soon after that ammonia with isotopic nitrogen $^{15}NH_3$ was detected as well.[3] NH_3 is one of the most important components of icy bodies in the interstellar medium[4]. It may react efficiently with oxygen and carbon-containing species leading to various nitrogen-bearing prebiotic compounds that have been detected in space.

Due to this vast abundance of ammonia in different regions of the universe, many laboratory studies have been focused on reactions involving NH_3. Many of these studies have described the chemical transformations and evolutions of ammonia ices exposed to various energy sources to mimic the behavior of ammonia in interaction with cosmic rays and UV photons in space.[5,6,7,8] Pure ammonia ices and also solid mixtures containing NH_3 have been bombarded by UV photons or energetic particles. The reaction products formed during such studies have been probed using IR spectroscopy in the near and mid infrared region, the spectral region adopted by many astronomers to detect ammonia through many astronomical observations. Under such laboratory experimental conditions, the only resulting signal proving that ammonia undergoes chemical transformations in solid phase is an absorption band around 1500 cm^{-1} which has been assigned to either NH_2 (done by Loeffler& Baragiola[9]) or NH^+_4 (done by Moore et al.[6]) species. These prior studies also suggested that other new reaction products could have been formed in the ice upon irradiation, but could not be revealed using IR spectroscopy as some reaction products have their infrared absorption signals hidden by the broad absorption bands of the reactants making up the ice. In order to circumvent the limitations brought by the single use of IR spectroscopy as a probe for condensed phase reactivity, some

groups have combined IR spectroscopy and mass spectroscopy. They were then able to propose solid-state reaction pathways that would take place in NH_3-ices exposed to external energy sources. In this way, Zheng & Kaiser[10] have shown using mass spectroscopy that new chemical species such as H_2, O_2, H_2O_2, NH_2OH and $(NH_2)_2$ had been produced upon heating of electron-irradiated ammonia-water ice, as these species were released into the gaseous phase between 130 and 200 K. Some other groups have investigated the photo-desorption of ammonia (Martinez et al.[11]) and ammonia-water mixtures (Fernandez-Lima et al.[12]) using fast ion bombardments. The authors do not go into specifics regarding NH_2 and NH_2OH formation but according to their data, it is visible that the NH_2 and NH_2OH mass signals are around one order of magnitude lower than that of NH_3. However, because these species are only detected in the gas phase, it is not possible to draw firm conclusions about whether they were initially formed in the solid phase. In fact they may have been produced during desorption of the irradiated solid samples or even in the mass spectrometer. Consequently, there is still no solid-phase in situ characterization of all the byproducts formed in ammonia-water ice upon irradiation.

Using a combination of bulk ice studies and rare-gas matrix isolation study, this work aims to highlight the influence of H_2O molecules in the photo-induced decomposition of ammonia in the solid phase between 3 and 130 K. Specifically, in order to obtain a clear description of the catalytic role of water in the photochemistry of ammonia. The rare-gas matrix isolation technique has been used where ammonia or ammonia-water systems were isolated within rare-gas matrices (mainly neon for the present study). During the irradiation all photoproducts and reaction intermediates were stabilized and trapped in the neutral Ne-Crystal. Subsequently matrix evaporation allows the recovery of a bulk ice formed mainly by the primary reactants water and ammonia, and the resulting photoproducts stemming from H_2O and NH_3 dissociations. This gives comparison with photolysis of bulk ammonia-rich ice containing only small quantities of water.

III.2. NH_3 photolysis in diluted phase

The neon matrix isolation method allows the trapping, in a neutral cage formed by Ne-atoms, of stable reaction products and also reactive species such as radicals. As all the trapped species are isolated from each other by Ne-atoms and their IR signatures are easily identifiable and close to those measured in the gas phase. The heating of the neon matrix to higher temperatures (above 30 K) enables a total desorption of Ne-atoms and a release of the reactive radical species which can undergo a radical-radical or radical-molecular reactions on the surface of the substrate sampler, processes similar to those involved on the surface of interstellar grains. The evaporation of the irradiated neon matrix allows also recovering an NH_3-H_2O ice formed by stable photoproducts generated in diluted phase and the remaining ammonia and water molecules.

III.2.1. Sample formation and photolysis

The central nitrogen atom has five outer electrons with an additional electron from each hydrogen atom. This gives a total of eight electrons, or four electron pairs that are arranged tetrahedrally. Three of these electron pairs are used as bond pairs, which leaves one lone pair of electrons. The nitrogen atom in the molecule has a lone electron pair, which makes ammonia a base, a proton acceptor. This shape gives the molecule a dipole moment (1.42D) and makes it polar. There is similar case with water molecule. The oxygen atom also has two lone pairs of electrons. As ammonia, the water molecule is also polar and has a dipole moment (1.85D). Because of this polarity, molecules has the ability to form hydrogen bonds.

To characterize NH_3 + H_2O photoinduced reaction in diluted phase, the neon matrix isolation method has been adopted for better spectral attributions of products and reactants. Reactive intermediates and photoproducts are trapped and stabilized in the neutral Ne-crystal. Due to the hydrogen bonding, it creates more difficulty in the sample preparation, especially for working in matrix isolation. The ramping system is made out of stainless steel and polar molecules, due to hydrogen bonding, has a tendency to adsorb on the metal surfaces. This makes it harder for accurate assumption of ratios in matrix crystal.

The depositions itself are performed in a high vacuum chamber at 10^{-10} mbar on a cold sample mirror. The photolysis experiments last 30 min and are probed by recording an infrared spectra of the samples in transmission – reflection mode. In order to avoid direct recombination between the photoproducts derived from ammonia and water dissociations, all the photolysis experiments have been carried out at the lowest temperature reached with our experimental setup, 3K.

As mentioned in the experimental section the Hamamatsu L10706 UV lamp used for the photolysis has a spectral distribution from 115 to 400 nm with the highest intensities, at 121 and 160 nm with a flux around 10^{15} photons$*$cm$^{-2}{}_*$s^{-1}. It has been shown in photodissociation of ammonia study carried out in gas phase by Leach et al.[13] that NH and NH_2 may be formed in ground and exited states by providing energies ranged between 4.2 and 8.6 eV as follows:

$h\nu + NH_3 \rightarrow NH(X\ ^3\Sigma^-) + H_2$ (>4.2eV) (III-1)

$h\nu + NH_3 \rightarrow NH_2(\tilde{X}\ ^2B_1) + H$ (>4.6eV) (III-2)

$h\nu + NH_3 \rightarrow NH(a\ ^3\Delta) + H_2$ (>5.7eV) (III-3)

$h\nu + NH_3 \rightarrow NH_2(\tilde{A}\ ^2A_1) + H$ (>5.9eV) (III-4)

$h\nu + NH_3 \rightarrow NH(b\ ^1\Sigma^+) + H_2$ (>6.8eV) (III-5)

$h\nu + NH_3 \rightarrow NH(A\ ^3\Pi) + H_2$ (>7.8eV) (III-6)

$h\nu + NH_3 \rightarrow NH(X\ ^3\Sigma^-) + H + H$ (>8.6eV) (III-7)

In such a situation, even if we have to take into consideration the fact that these energy values of NH_3 dissociations are provided from the gas phase data and consequently in solid phase we would probably have an increase between 1 and 1.5 eV, the UV lamp used in our study delivers photons at 121 and 160 nm providing energy sets at 10.3 and 7.7 eV which may dissociate NH_3 into NH_2, NH, H and even N fragments. The N and H atoms do not have vibrational signals while the NH radical has its stretching vibrational mode (~3132 cm^{-1},[14]) in the same spectral region of NH_3 and cannot be measured but it does not mean that it is not present in the irradiated ammonia samples. On the same note the energy needed to dissociate H_2O into OH + H or O + H_2 is around 5 eV for both reactions.[15]

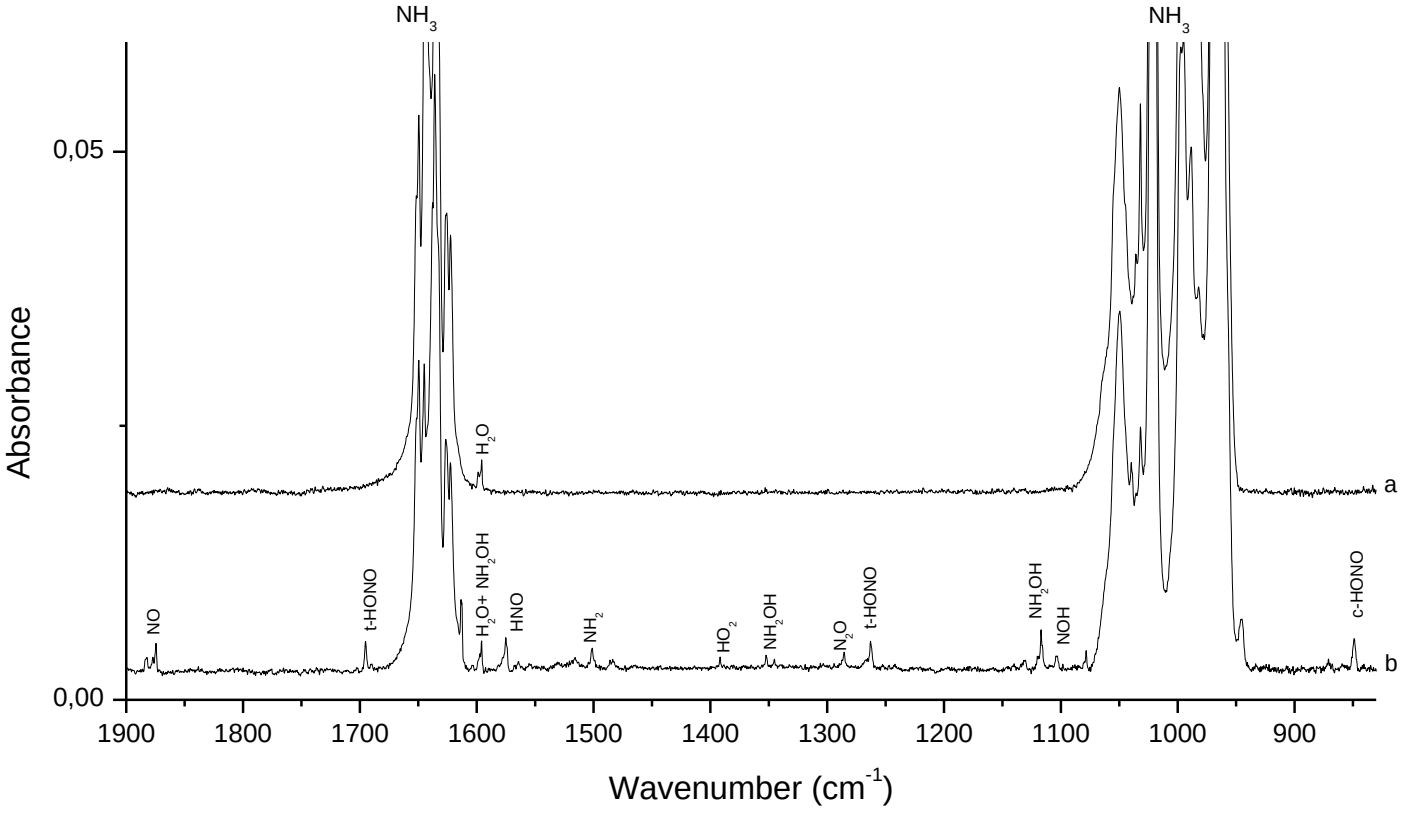

Figure III-1: Isolation of NH_3 + H_2O reaction in a neon matrix at 3K. a) before and b) after UV irradiation

Figures III-1a and III-1b show the isolation of NH_3 +H_2O reaction in neon matrix at 3 K before and after UV irradiation, respectively. The ratio of NH_3:H_2O:Ne sample is 100:1:100000 (estimated though spectral surface integrations). As shown in figure III-1, in diluted phase, many signals have been detected and might be easily assigned to their corresponding chemical species using previous matrix isolation data provided out by different groups.[16-26] Those attributions are shown in table III-1, where in addition of most obvious NH_2 and NH_2OH photo-products, new absorption bands are assigned to newly formed species such as HNO, HON, HO_2, cis and trans HONO, NO, N_2O and NO_2. While matrix isolation gives a great idea about photoproducts, the objective is to mimic the interstellar conditions and working on concentrated samples without

neon. The heating of the matrix to evaporate neon atoms and comparing the data to condensed sample experiments might lead to additional information on formation of some species. This is discussed in section III.6.

Table III-1. Chemical species formed during the photolysis of $NH_3 + H_2O$ in neon matrix at 3K

Species	Spectral position (cm^{-1})	Reference
NH_3	956, 960, 967, 1622, 1636, 1645	Jacox et al.[16]
NH_3-H_2O	1032	Jacox et al.[16]
$(NH_3)_n$	989, 997, 1020	Jacox et al.[16]
NH_2	1500	Milligan et al.[17]
H_2O	1595	Forney et al.[18]
HNO	1563	Ruzi et al.[19]
NOH	1098	Ruzi et al.[19]
NH_2OH	1352, 1117, 1598	Withnall et al.[20]
t-HONO	1689, 1263	Talik et al.[21]
c-HONO	850	Khriachtchev et al.[22]
NH_3-HONO	945	Mielke et al.[23]
NO	1875	Legay et al.[24]
NO_2	1612	Legay et al.[24]
N_2O	1285	Lawrence et al.[25]
HO_2	1103, 1391	Milligan et al.[26]

III.3. Photolysis in concentrated phase of NH_3 ice

Figure III-2 illustrates the IR spectra between 500 and 4000 cm^{-1} of pure ammonia ice at 3K before and after UV irradiation, where the only measurable signal, due to the interaction between NH_3 molecules and UV photons, is detected around 1500 cm^{-1} and assigned to NH_2 radical trapped in solid ammonia. This result is in good agreement with all the previous studies related to the photolysis of ammonia containing ices.[9,10,27]

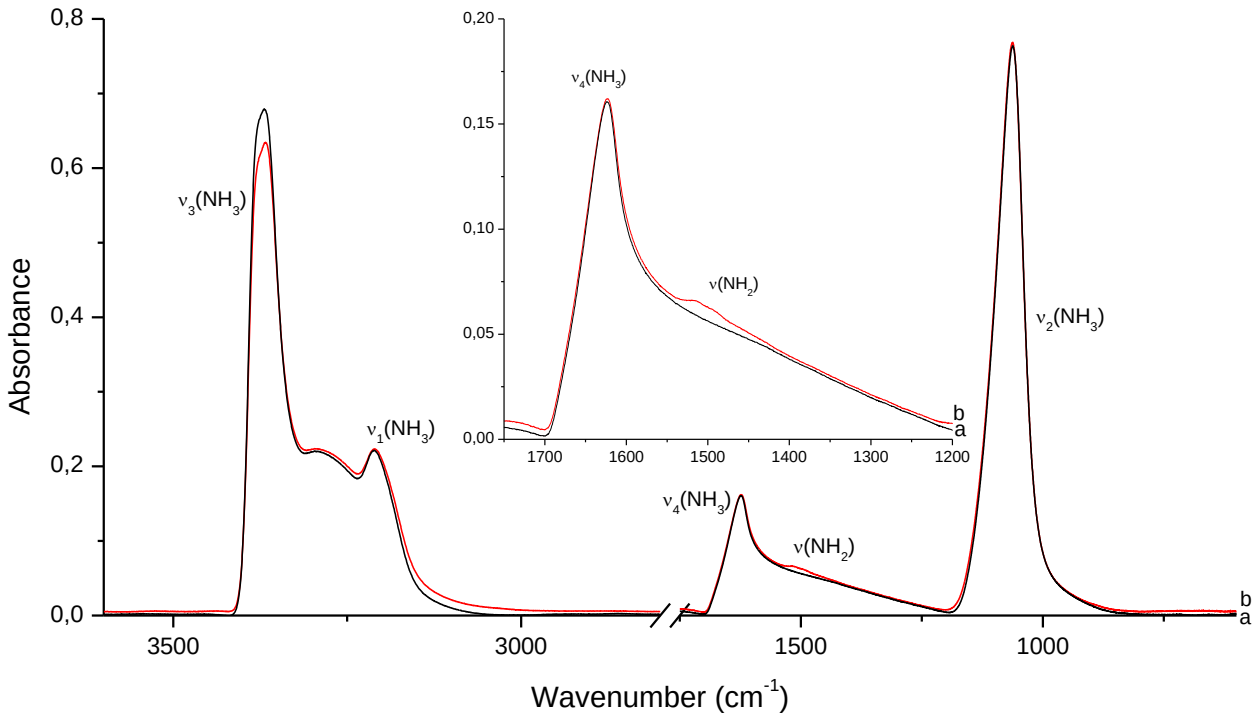

Figure III-2: Photolysis of solid ammonia ice at 3K before and after 30 min of UV irradiation.

Considering the same as for the matrix isolation experiment the irradiation of solid ammonia has been carried out at 3K and all the photo-fragments are trapped in the ice, frozen with no mobility and surrounded by NH_3 molecules. The heating of the sample at higher temperatures would induce trapped species motilities, promoting radical-radical reactions and formations of stable species. Figure III-3 shows the behavior of NH_2 signal when the irradiated ammonia ice is heated gradually between 3 and 130 K. By heating the sample progressively between 3 and 20 K, the signal of NH_2 radical increases slightly, starts decreasing afterwards between 20 and 60 K, to completely disappear at 70 K.

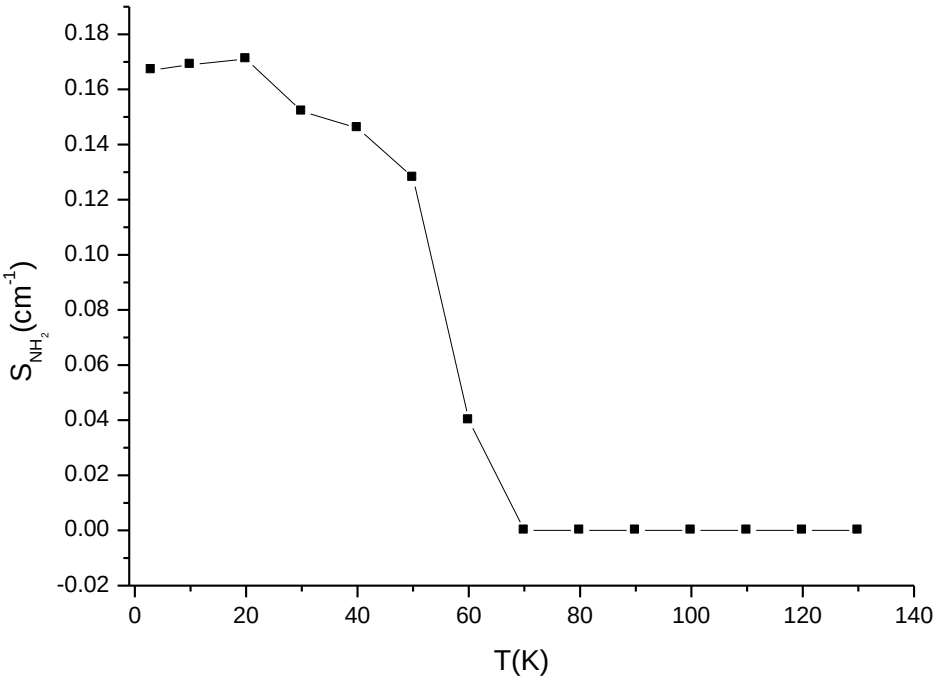

Figure III-3: The behavior of the NH_2 radical signal during the heating of the irradiated ammonia ice between 3 and 130 K.

In parallel of the NH_2 radical signal decrease during the sample heating, no new signal has been detected, except one at 2333 cm^{-1} which can be assigned to N_2 molecules (Figure III-4). The N_2 signal appears when the irradiated sample is heated at 70 K, it starts decreasing at 100 K, to disappear at temperatures higher than 110 K.

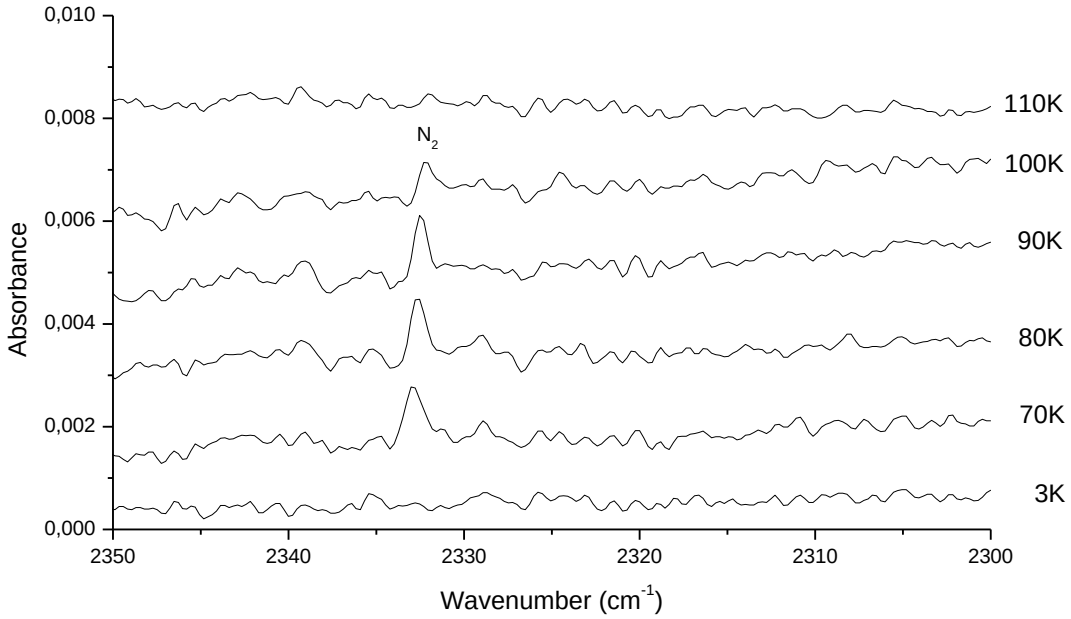

Figure III-4: Formation of N_2 molecules as reaction product during the heating of irradiated ammonia ice.

Considering that during the sample heating, we do not observe species such as N_2H_4, N_2H_3, N_2H_2 which might be formed through radical-radical reactions, the N_2 formation would be due to their thermal decomposition in the irradiated NH_3 ice, as similarly suggested by Loeffler & Baragiola[9], who detected N_2 and H_2 as main products during the proton-irradiation of ammonia ices between 20 and 120 K:

$$NH_2 + NH_2 \rightarrow (NH_2)_2 \rightarrow N_2 + 2H_2 \quad \text{(III-8)}$$

$$NH + NH_2 \rightarrow (NH_2)(NH) \rightarrow N_2 + H_2 + H \quad \text{(III-9)}$$

$$NH + NH \rightarrow (NH)_2 \rightarrow N_2 + H_2 \quad \text{(III-10)}$$

These reaction steps involve NH_3 photofragments namely NH and NH_2. The dimerization of NH and NH_2 leads to the formation $(NH)_2$ and $(NH_2)_2$, respectively. While the interaction between NH and NH_2 leads to the formation of $(NH)(NH_2)$ complex. All these complexes are hydrogen bound and are formed at temperatures ranged between 40 and 60K. As shown in figure III-3 in this temperature range, NH_2 radical signal starts decreasing and consequently start reacting. As we did not see any traces related to the formation of hydrogen bound complexes involving NH_2, such as $(NH)(NH_2)$ and $(NH_2)_2$, we think that energy released during the dimerization processes would be enough to dissociate those hydrogen bound complexes into $N_2 + H_2$. As these reactions occur only at relatively high temperature we only detect the N_2 formed and trapped in ammonia ice, while lighter H_2 molecules would desorb during its formation process.

III.4. Photolysis in concentrated phase of NH_3-H_2O ice

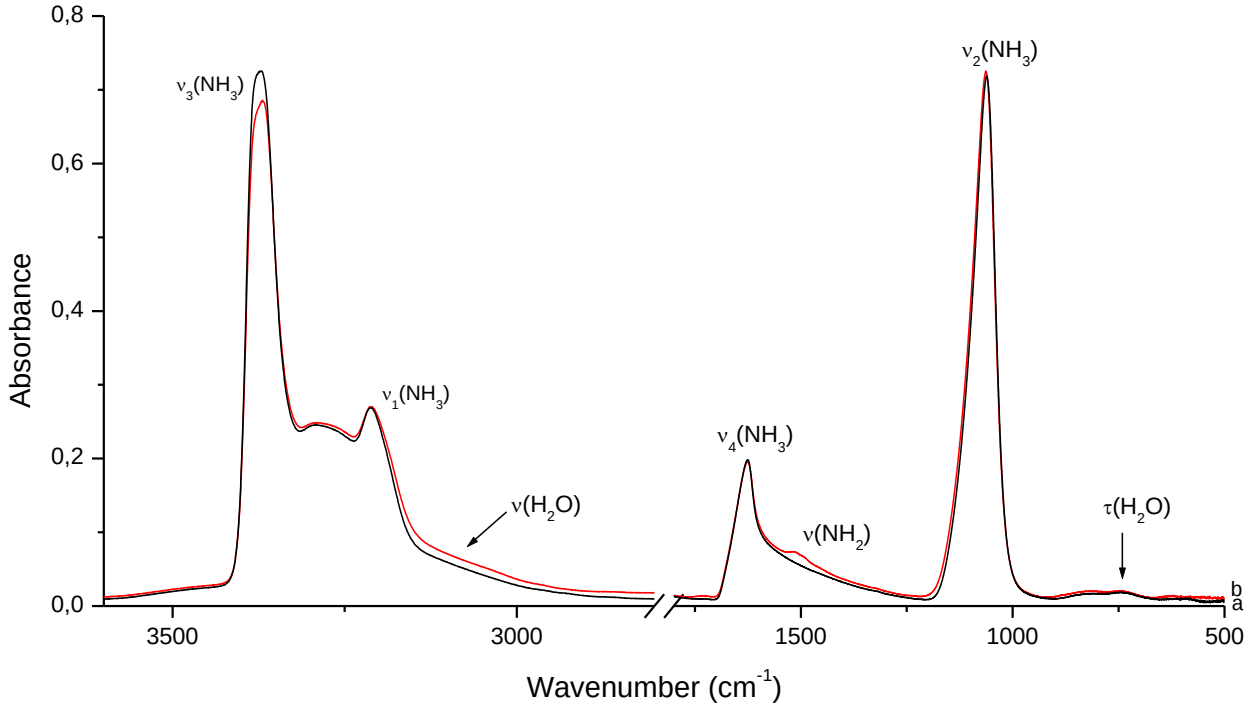

Figure III-5: Photolysis of solid ammonia-water at 3K ice before and after 30 min of UV irradiation.

In order to study the influence of H_2O molecules in the photo-induced decomposition of ammonia in the solid phase, similar experiments have been carried out by adding a small amount of water (2%) into ammonia ice. Figure III-5 shows the IR spectra of ammonia-water ice at 3K before and after UV irradiation, where we detect a relative huge signal around 1500 cm^{-1} (integrated absorption band about 0.33 cm^{-1}) due to NH_2 radical trapped in solid ammonia and a very tiny signal at 1235 cm^{-1} (integrated absorption band about 0.004 cm^{-1}) which was attributed to NH_2OH and will be discussed separately. Figure III-6 compares the amounts of NH_2 radical formed in pure ammonia ice and in ammonia-water ice. It has to be noted that the adding of only 2 % of H_2O in ammonia ice is sufficient to enhance the yield of NH_2 formation, and consequently to accelerate the NH_3 destruction process. As shown in figure III-6, by substituting 2% of ammonia by water molecules, we show that the amount of NH_2 ($S(NH_2)$ = 0.326 cm^{-1}) produced in irradiated ammonia-water ice is increased by 95% in comparison with measurements carried out under the same experimental conditions in pure irradiated ammonia ice ($S(NH_2)$ = 0.167 cm^{-1}), where S is integrated absorption intensity.

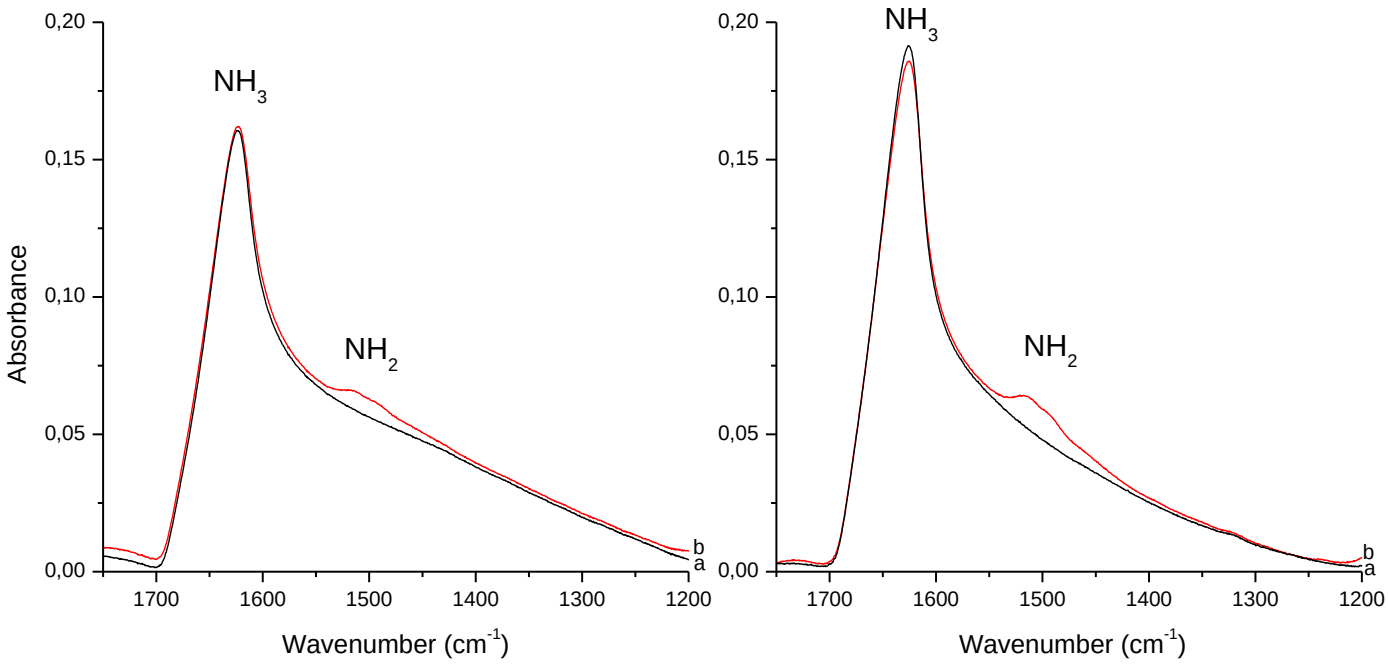

Figure III-6: Spectra a) before and b) after UV irradiation of ammonia containing ices at 3K. The yield of NH_2 formation in pure ammonia ice (left) and in ammonia-water ice (right).

Yet again all the irradiation experiments have been carried out at 3 K. NH_2 yield enhancement in the ammonia-water ice is certainly due to reactions of ammonia molecules forming the hosting ice with excited and dissociated water molecules. We know that the only radicals possible to be produced from photolysis of water molecule are OH, H and O.[15] Numerous investigations on the photolysis of pure water ices show the formation of HO_2, O_2, H_2O_2 and O_3 as main photoproducts due to the radical-radical recombination reactions. However, all those radical reactions would take place efficiently in pure water ice but not when a very small amount of water is diluted in ammonia ice. This might be the reason why none of these species have been detected during the photolysis of ammonia-water ice under our experimental conditions. Therefore, the most probable reactions taking place to enhance the yield of NH_2 formation are those involving NH_3, O and OH radicals. In the case of reactions involving NH_3 and OH, we notice that for each dissociated water molecule into H and OH fragments, NH_2 radical and water molecule can be formed from NH_3 reservoir, forming the hosting ice, as follows:

$$H_2O + h\nu \rightarrow OH + H \qquad \text{(III-11)}$$

$$NH_3 + OH \rightarrow NH_2 + H_2O \qquad \text{(III-12)}$$

The NH_3 + OH reaction, the source of NH_2 and H_2O species, is exothermic with a very low activation energy,[28] and consequently the two reactions mentioned above, may take place during the irradiation of ammonia-water ice. The regeneration of a water molecule during its

photolysis proves the catalytic role played by H_2O into the formation of NH_2 species and then into the destruction of NH_3 molecules.

The catalytic role of water, in reactions involving NH_3 molecules and atomic oxygen, is less evident to be proven as the reaction pathways engaged into the process include the NH radical, a species which cannot be directly monitored in solid phase, as it is not the case for NH_2. In fact, the dissociation of water into O and H_2 fragments may be the source of formation of NH and H_2O species through a catalytic process:

$$H_2O + h\nu \rightarrow O^* + H_2 \quad \text{(III-13)}$$

$$NH_3 + O^* \rightarrow NH_2OH \text{ or } NH_2OH^* \quad \text{(III-14)}$$

$$NH_2OH^* \rightarrow NH + H_2O \quad \text{(III-15)}$$

$$NH_2OH + h\nu \rightarrow NH + H_2O \quad \text{(III-16)}$$

The oxygen insertion reaction in ammonia molecule would take place only with excited atomic oxygen.[28,29] This reaction would form NH_2OH either in excited or ground states. Due to the high exothermicity of the $NH_3 + O^*$ reaction, the excited NH_2OH^* would dissociate during its energy dissipation into NH and H_2O moieties.[28,30] NH_2OH would also dissociate during the photolysis of the ammonia-water ice. Low stability of NH_2OH during the photolysis process shows the catalytic role of H_2O, in the enhancement of the NH radical formation. Under these experimental conditions, the detected amount of NH_2OH during the photolysis of ammonia-water ice was very small, and this might be due to the competition between the formation ($NH_3 + O^*$) and the dissociation of NH_2OH into NH and H_2O. In fact, the fragmentation of NH_2OH may occur to form either $NH_2 + OH$ or $NH + H_2O$, where the former pathway needs an additional energy about 2.6 eV while the latter one needs an additional energy about 3.5 eV, and consequently, both reactions may take place throughout the UV photolysis of ammonia-water ice. Nevertheless it should be noticed that, under these experimental conditions, the dissociation of NH_2OH into $NH_2 + OH$, leads to the formation of two radicals which at 3K and due to the low mobility of the reactants, might recombine back to form NH_2OH, while the dissociation of NH_2OH into NH and H_2O species leads to the formation of a stable NH-H_2O complex. Although NH-H_2O absorbs in the same spectral region as ammonia ice (NH radical at 3132 cm^{-1})[14] and then it cannot be characterized experimentally from the IR spectra of the irradiated ammonia-water ice. We should then not exclude its presence. Accordingly, as we have shown the catalytic character of water to enhance the NH_2 radical formation and then the NH_3 destruction, during the photolysis process, water molecules may also improve the NH radical formation where for each H_2O dissociation into $O^* + H_2$, NH and H_2O may be formed from ammonia ice reservoir.

III.5. Formation of NH_2OH from thermal processing of irradiated NH_3-H_2O ices

The tiny amount of NH_2OH, detected during the photolysis of ammonia-water ice, might be due to the trapping of OH and NH_2 radicals into water and ammonia clusters, respectively. The formation of those complexes OH-$(H_2O)_n$, NH_2-$(NH_3)_n$ at 3K, a temperature at which the mobility of the reactants in the hosting ice is nonexistent, hinders the OH-NH_2 radical recombination. Such a recombination would become possible by heating the sample at temperatures higher than 3K. Therefore, the irradiated ammonia-water ice had been heated in order to increase the mobility of the reactants. Figure III-7 presents the behavior of the infrared absorption spectra of the sample heated at 70 and 90 K, in the 700-1700 cm^{-1} spectral region. The NH_2 signal decreases at 70 K and disappears completely at 90 K while the signal at 1235 cm^{-1}, assigned to NH_2OH, appears more clearly at 70 K than at 3 K and keeps increasing at 90 K. In contrast of the heating of the irradiated pure ammonia ice where the NH_2 radical signal decrease might be linked to the formation of N_2 molecules in solid phase between 3 and 70 K, the decrease of NH_2 radical in the irradiated ammonia-water ice might be only linked to the NH_2OH formation as no signal at 2333 cm^{-1} corresponding to nitrogen molecules has been detected with the heating of the irradiated ammonia-water ice.

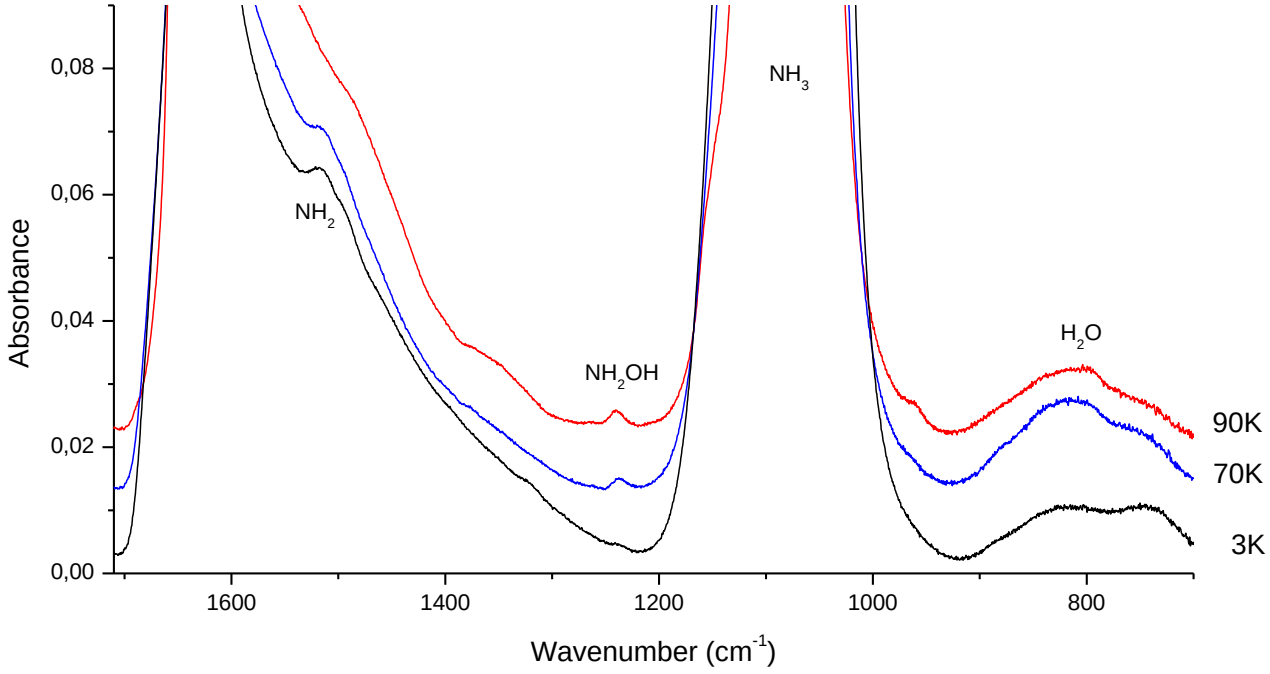

Figure III-7: Behavior of NH_2 and NH_2OH signals at, 3, 70 and 90 K.

Figures III-8 and III-9 show the evolutions of the integrated absorption bands of NH_2 and NH_2OH, respectively, as functions of temperature. From Figure III-8, we notice the NH_2 signal decreases slowly between 3 and 60 K, where only 10 % of NH_2 is consumed in the ammonia-water ice at 60 K, a temperature at which NH_2 is almost consumed in pure ammonia ice (figure

III-3). This slow decrease of NH_2 between 3 and 60K shows that there is equilibrium between the formation of NH_2 radical through $NH_3 + OH \rightarrow NH_2 + H_2O$ reaction and its transformation into NH_2OH from $NH_2 + OH$ reaction. The NH_2 radical signal disappears at temperatures higher than 90K.

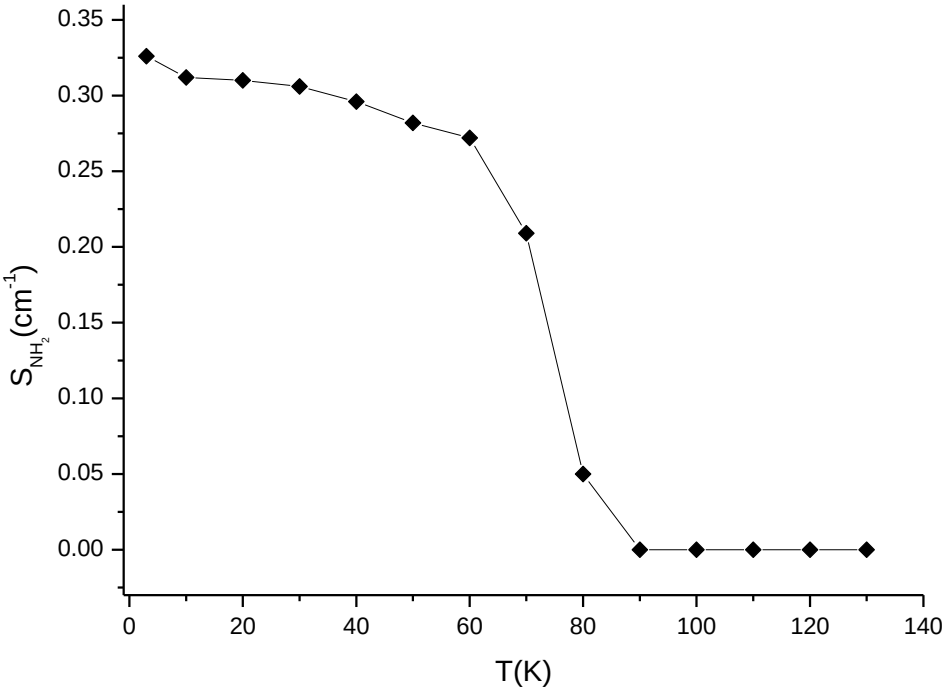

Figure III-8: Evolution of the integrated absorption band of NH_2 *vs* temperature.

From Figure III-9, we notice that the signal of NH_2OH increases slowly between 3 and 60 K and reaches a maximum around 100 K. The highest and then the total NH_2OH amount is reached at 100 K while only 15 % and 50 % of the total amount is formed at 20 K and 65 K, respectively. Comparisons between figures III-8 and III-9 show that the behavior of the signal assigned to NH_2OH might be linked to that of NH_2.

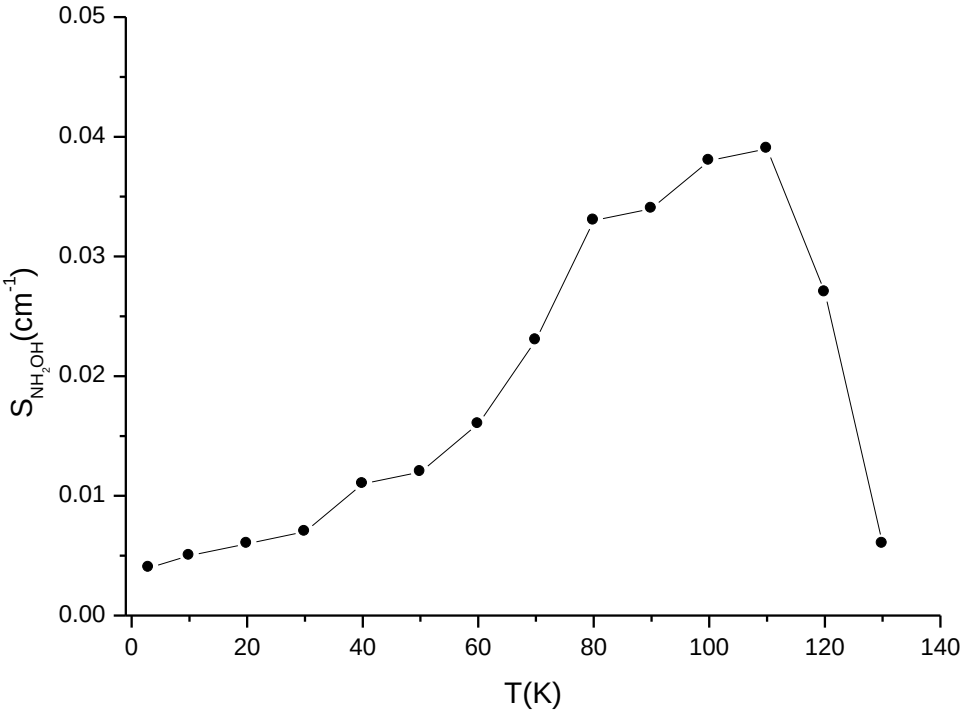

Figure III-9: Evolution of the integrated absorption band of NH_2OH as a function of temperature.

Comparison between the two experiments presented in this chapter show that probing the irradiated ices containing ammonia at temperatures ranged between 3 and 100 K lead to the formation of two photoproducts. In the irradiated NH_3-ice the two products detectable in the solid phase are NH_2 between 3 and 70 K and N_2 between 70 and 100 K. Species such as N_2H_4, N_2H_3 or N_2H_2 due to the recombination of NH and NH_2 radicals have not been detected. Just by a small addition of 2 % of water into NH_3-ice the catalytic role played by water molecules were induced by enhancing the dissociation of NH_3 leading to the additional formation of radical species NH and NH_2. These radical species derived from ammonia dissociation would react with O and OH radicals to form NH_2OH, NHOH, NH_2O, HNO through NH_2 + OH, NH + OH, NH_2 + O and NH + O reactions. In contrast with the measurements carried out in neon matrix where many species have been detected such as HNO, HON, HONO, NH_2OH, the results obtained from irradiated NH_3-H_2O ices show only the formation of NH_2OH and no evidence for other reaction products which may derive from the reactions between NH and OH to from NHOH or between NH and O to form HNO. The nondetection of those species such as NHOH and HNO or even N_2H_4, N_2H_3, N_2H_2 might be due to the huge absorption signal of ammonia ice which probably also hides many other reaction products formed during the photolysis and detected with the neon matrix isolation method.

III.5.1. NH_2OH formation pathways

In this study it was showed that the photolysis of NH_3-H_2O mixture in solid phase leads to the formation of NH_2OH species as the main photoproduct. Such a reaction depends strongly on

the temperature of the sample and on the environment where the primary reactants NH_3 and H_2O are trapped. In an ammonia-water ice, H_2O molecules have a catalytic role in enhancing the amount of NH_2 radical produced during the photolysis. Since the photolysis has been carried out at 3 K, the mobility of all the photofragments derived from the dissociation of ammonia and water is reduced and then radical recombination reactions become very infrequent. The only probable reactions at 3K are those occurring between the photofragments and the molecules forming the hosting ice. For example, the OH radical formed in enriched water environment would mainly form $OH\text{-}H_2O$ complex[31] and the NH_2 radical formed in enriched water environments would only form the very stable complex $NH_2\text{-}H_2O$.[32,33] The reactions leading to the formation of these two hydrated complexes are exothermic:

$$OH + H_2O \rightarrow OH\text{-}H_2O \qquad \Delta H = -23.6 \text{ kJ/mol} \qquad \text{(III-17)}$$

$$NH_2 + H_2O \rightarrow NH_2\text{-}H_2O \qquad \Delta H = -15.1 \text{ kJ/mol} \qquad \text{(III-18)}$$

These two complexes have been already detected in neon matrix. However, in ammonia enriched environment, we do not detect NH_3-OH complex even in diluted neon matrix. The OH radical would then react with ammonia to form NH_2 radical through a hydrogen abstraction reaction. We have already shown experimentally that adding 2% of water increases the formation of NH_2 radical. Figure III-10 shows the reaction pathways involving NH_3, H_2O, OH and NH_2 species.[32,33]

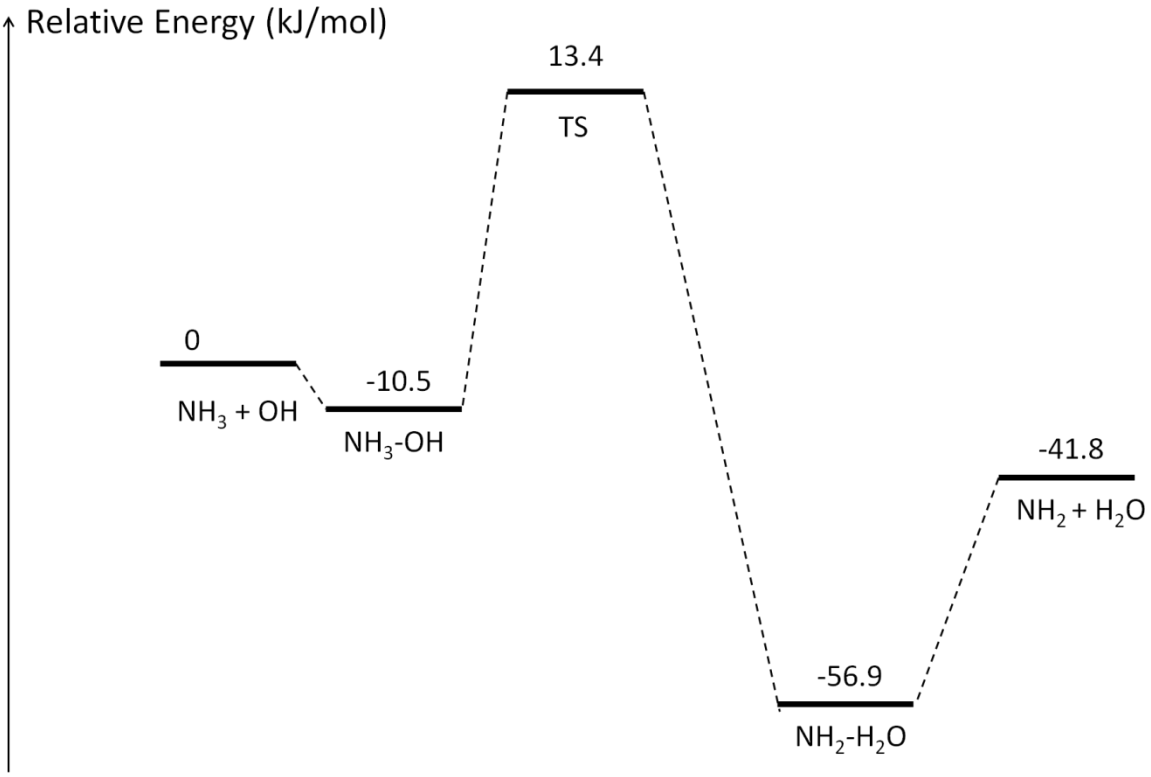

Figure III-10: Reaction pathways involving NH_3, H_2O, OH and NH_2 species[33]

The $NH_3 + OH \rightarrow NH_2 + H_2O$ reaction shows a low energy barrier (13.4 kJ/mol) and could take place under our experimental conditions, however the reaction between NH_2 and H_2O to form OH radical and NH_3 molecule needs an additional energy higher than 55.2 kJ/mol. This is in good agreement with our results obtained at 3 K where we observe an enhancement of NH_2 radical formation by adding 2 % of H_2O in an ammonia ice. Considering the composition of our samples, the reaction of $NH_2 + OH$ is less probable in a sample containing 98 % of NH_3 and 2 % of H_2O. At 3 K, the probability of interactions between OH and NH_3 to form NH_2 and H_2O is by far greater than between OH and NH_2 to form NH_2OH. Consequently, the photolysis process carried out at 3 K would mainly transform $NH_3 + OH$ into NH_2 and H_2O species. We also show that in the irradiated ammonia-water ice, NH_2OH molecule has been formed efficiently during the heating of the sample, in absence of UV photons and its formation is directly linked to the decrease of NH_2 signal which proves that NH_2OH is mainly derived from reactions involving NH_2 and certainly OH radicals:

$$NH_3 + OH \rightarrow NH_2 + H_2O \qquad \text{(III-19)}$$

$$NH_2 + OH \rightarrow NH_2OH \qquad \text{(III-20)}$$

These two reactions are competing, where $NH_3 + OH \rightarrow NH_2 + H_2O$ would arise the amount of NH_2 radical but it could also reduce that of OH species in the sample and then that of NH_2OH, while $NH_2 + OH \rightarrow NH_2OH$ reaction would increase the amount of NH_2OH and reduce that of NH_2 radical. From our experimental results, it has been noticed that the amount of NH_2 radical is almost constant between 3 and 60 K and starts decreasing sharply at temperatures higher that than 60 K. Correspondingly, the amount of NH_2OH increases progressively between 3 and 60 K and exceedingly at temperatures higher than 60 K. In addition to the fact that at higher temperatures the mobility of the radical species such as OH and NH_2 becomes important and increases the $OH \leftrightarrow NH_2$ interaction probability, $NH_3 + OH \rightarrow NH_2 + H_2O$ reaction seems to be efficient only between 3 and 60 K and this may be linked to the energy diagram of figure III-10. The formation of $NH_2 + H_2O$ through $NH_3 + OH$ reaction shows an energy barrier of 13.4 kJ/mol and it should take place via tunneling process. To be efficient, such a tunneling process would need to thermally stabilize the reaction intermediate $OH\text{-}NH_3$ complex. The heating of the sample at temperatures higher than 60 K would dissociate the $OH\text{-}NH_3$ complex, the source of NH_2 formation and OH destruction, and consequently, at higher temperatures, the only reaction kinetically favored is $NH_2 + OH$ to form NH_2OH.

While NH_2OH formation mechanism as a result is obvious, the photolysis of $NH_3 + H_2O$ depends strongly on the temperature of the hosting ice and also on the environment where reactants are trapped. These results might explain the previous astronomy observations carried out by different groups aiming to report the abundances of NH_2 and NH_3 in molecular clouds where it has been shown that NH_2/NH_3 ratio depends strongly on the conditions of the interstellar medium. Hily-Blant et al.[34] and van Dishoeck et al.[35] have reported the NH_2/NH_3 ratios at 0.003

and 0.5, respectively. By monitoring an irradiated ammonia-water ice as a function of temperature, it was shown that the NH_2 amount is almost constant at temperatures lower than 60 and is highly reduced at 70 K. This behavior was attributed to a competition between the formation of NH_2 from NH_3 + OH reaction favored between 3 and 60 K and its consumption from NH_2 + OH reaction which becomes efficient between 70 and 100K. In such situation, for the observations of the interstellar medium, NH_2/NH_3 ratio should grow with the decrease of the temperature of molecular clouds.

III.6 From diluted (NH_3-Ne-H_2O) to concentrated phase (NH_3-H_2O ice)

As mentioned earlier, the photolysis of NH_3-H_2O mixture diluted in the neon matrix would form other species not detected in irradiated condensed phase, such as HONO, HNO and NO. By heating the sample towards 50 K to evaporate the neon atoms and to favor the radical-radical reactions, we obtain the spectrum shown in figure III-11a which is compared to the spectrum of the irradiated NH_3-H_2O ice heated at 50K (figure III-11b). Comparisons between figures III-11a and III-11b, show that in addition to the signal at 1235 cm^{-1} due to NH_2OH, a new signal appears in figure III-11a at 1517 cm^{-1} which could not be assigned to NH_2 radical since the ice corresponding to this figure has been obtained by releasing neon atoms from the solid sample and consequently all the radical species are supposed to react to form stable molecules. This additional new signal shifted by 17 cm^{-1} from that of NH_2 radical is certainly due to a reaction photoproduct derived from H_2O and NH_3 dissociation. It is completely hidden by the absorption signals of water and ammonia in the irradiated H_2O-NH_3 ice (figure III-11b).

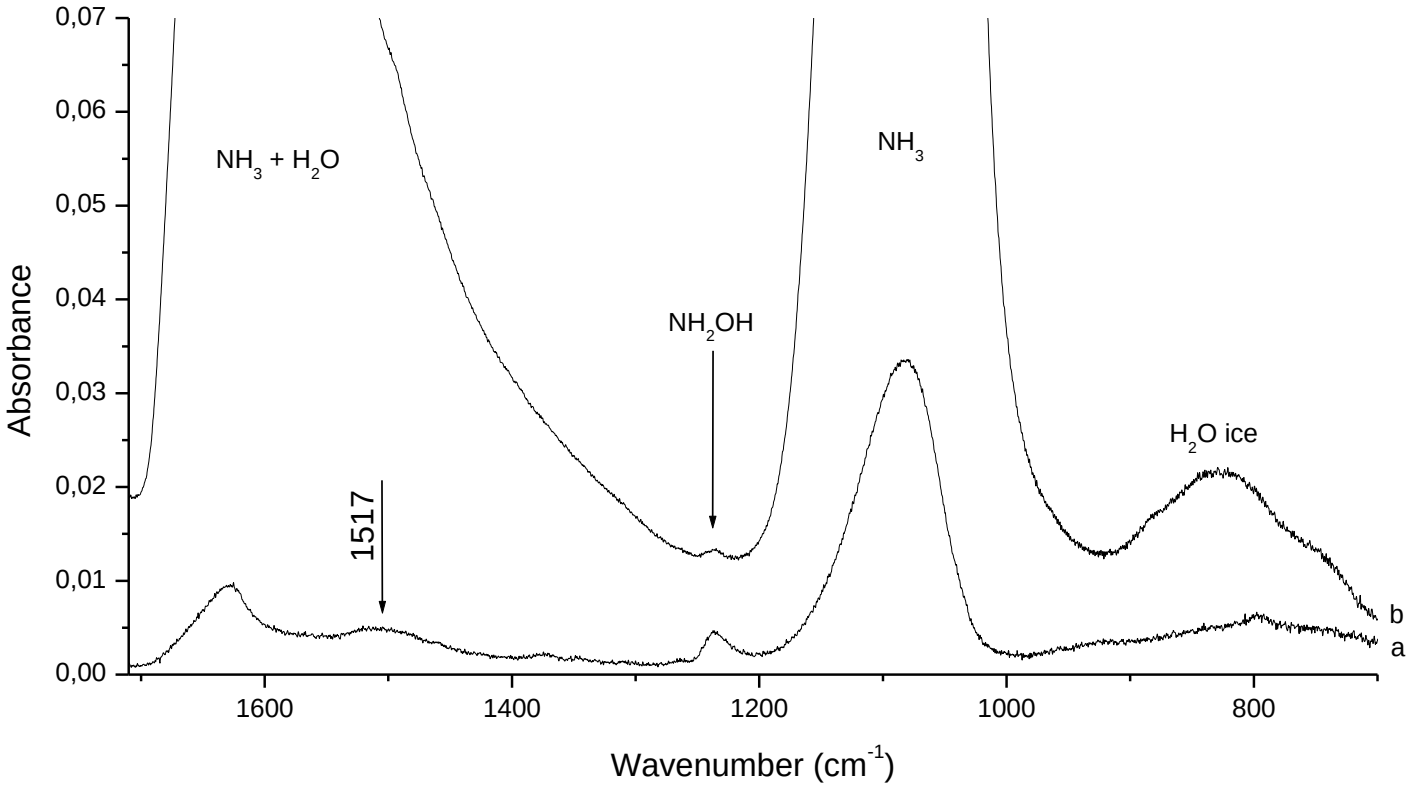

Figure III-11: a) Heating of the irradiated neon matrix at 50 K. b) Irradiated NH_3-H_2O ice heated at 50 K.

In order to better characterize the new signal obtained by heating at 50 K the irradiated neon matrix which contains NH_3, H_2O and the resulting photoproducts obtained in diluted phase, figure III-12 shows the comparison between two reference spectra corresponding to NH_2OH (figure III-12a, the obtainment of NH_2OH spectrum will be explained in following chapter) and NH_3 (figure III-12b) ices and the spectrum of the irradiated (NH_3-H_2O)-neon matrix heated at 50 K (figure III-12c).

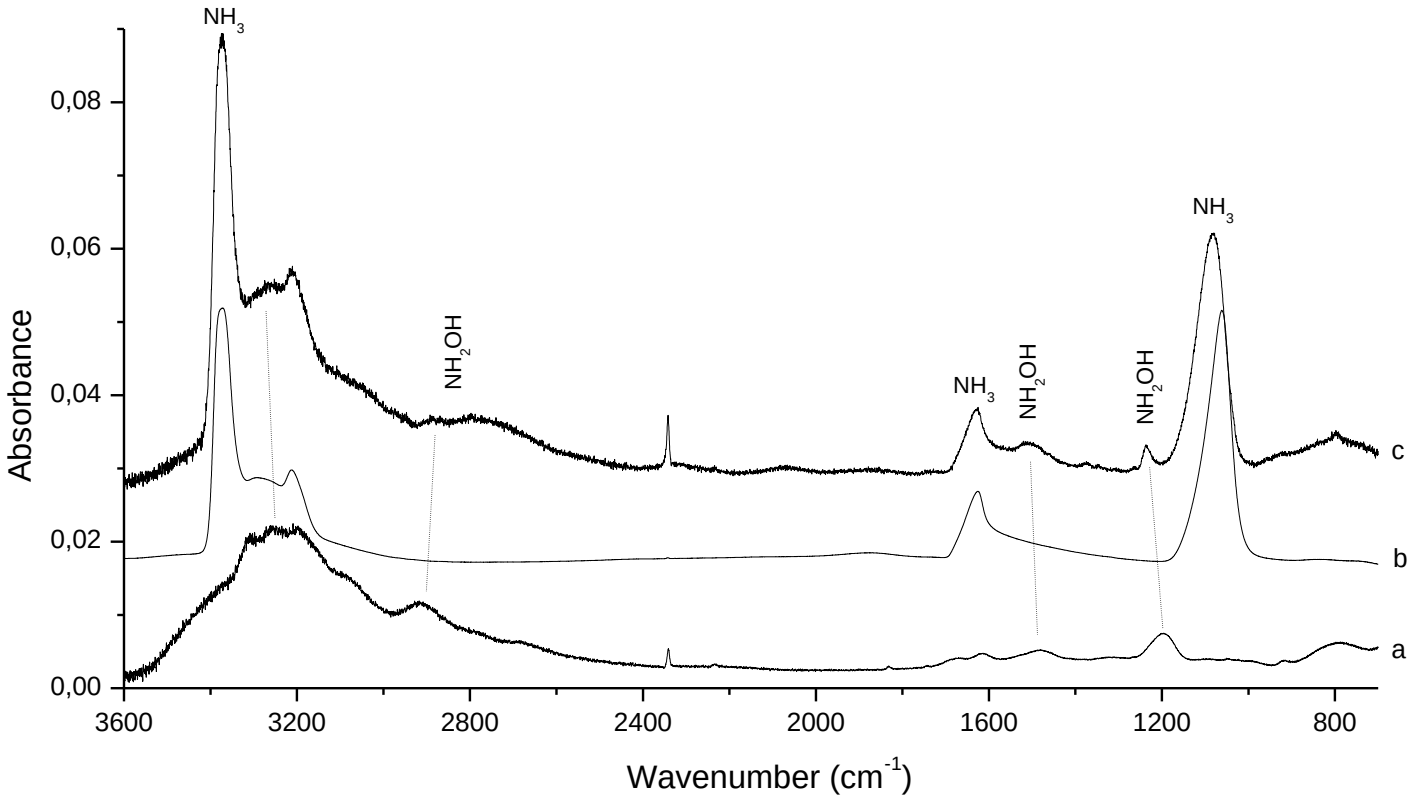

Figure III-12: a) IR spectrum of NH_2OH ice, b) IR spectrum of NH_3 ice, c) Irradiated (NH_3-H_2O)-neon matrix heated at 50 K.

We notice that the spectra of the irradiated NH_3-H_2O mixture from diluted to concentrated phase seem to be exactly equivalent to the sum of the two reference spectra III-12a and III-12b, corresponding to NH_2OH and NH_3 ices, respectively. We also notice, from figure III-12c, that any of the signals due to the stable species such as NO, NO_2, HONO, HO_2 and HNO produced in diluted phase do not remain after the evaporation of the neon matrix. Those species are formed only in diluted phase and probably released into the gas phase with the evaporation of neon atoms or they formed in small amounts to be observable in the IR spectrum of figure III-12c.

III.7. NH and NH_2 radical formation: photochemistry of NH_3 versus N/N_2+H/H_2 radical addition reactions

As discussed in previous paragraphs the great interest in ammonia is due to the amino radical NH_2. This group is present in hydroxylamine, we discussed earlier, and also in glycine, the simplest possible amino acid. It was shown that amino radical can be formed through the interaction with UV photons and its production increased further with addition with water. While it is very plausible formation pathway in the interstellar medium, but this requires already

ammonia NH_3 as a precursor. Ammonia like amino radical is formed though the obvious hydrogenation of nitrogen atom:

$$N \xrightarrow{+H} NH \xrightarrow{+H} NH_2 \xrightarrow{+H} NH_3 \qquad \text{(III-21)}$$

In paragraph II.1 we discussed that using our experimental equipment it is possible to form atoms from molecular gases with the help of the microwave discharge source. Thus it is possible to mimic the conditions of interstellar medium having the right reactants. As shown in the same chapter this experimental equipment has two microwave discharge sources, opening different possibilities in achieving the required conditions. Ideally we want to form ice only with atomic nitrogen and later on bombard the ice by hydrogen atoms, but this cannot be achieved because the molecular dissociation ratios are not a fully 100%. Thus forming nitrogen based ice, we would have a mixture of N/N_2 and after the same would be with H/H_2. Using hydrogen for bombardment of samples is possible at slightly higher temperatures (~8K), to avoid the condensation of H_2 molecules, but the surface reaction with atomic H can still occur.

On the one hand it looks possible, but on the other hand the negative aspect that N_2 gases are non-reactive and works like a matrix cage for nitrogen atoms. This would not be an issue with other molecules, but at hydrogenation temperature (~8K) nitrogen molecules have enough mobility to induce the reaction between atomic and molecular nitrogen.[36] Another possibility was adopted in starting the discharge with a N_2/H_2 gas mixture, by doing this we form atomic nitrogen and hydrogen in the plasma chamber and instantly have a deposition of them. This also greatly increases the possibility of their interaction. Meanwhile only very small H_2 can be entrapped in the ice during the deposition, so we create a mixture of $N/H/N_2$. Having N_2 also at this point is a good benefit, as mentioned earlier the molecular nitrogen works as a neutral matrix cage trapping the reaction products: NH, NH_2 and NH_3.

III.7.1. Determining the optimal N_2/H_2 ratio for formation of nitrogen hydrates

As established before the deposition of N/H atoms it is possible to induce a reaction III-21, but this reaction depends strongly on the amount of the hydrogen. Considering that the dissociation ratios are not 100% using a microwave discharge, the ratio for creating the nitrogen hydrates also had to be determined. The same amount of material was deposited at five different N_2-H_2 ratios, varying from 10 to 90% of H_2. The region between 2500 and 900 cm^{-1} of recorded IR absorption spectra are shown in figure III-13 and vibrational attributions in table III-2. From the acquired data we can see the varying range of products. The products like CO_2, CO and H_2O are unavoidable impurities that come from the plasma chamber. Starting with the mixture having 10% of hydrogen the main products found are: NH_3, N_2O and N_3. N_2O and N_3 are understandable due to the lack of excess hydrogen and thus promoting the reactions of N with other species.

Table III-2. Chemical species formed by depositing the discharged N_2-H_2 mixture

Species	Spectral position (cm^{-1})	Reference
NH_3	969, 1630, 3330, 3435	Jacox et al.[16]
NH_2	1500, 3220	Milligan et al.[17]
NH	3132	Rosengren et al.[14]
H_2O	1598	Forney et al.[18]
N_3	1653, 1659	Mencos et al.[36]
CO	2141	Jamieson et al.[39]
N_2O	2235	Lawrence et al.[25]
N_2	2328	Bernstein et al.[37]
CO_2	2348	Jamieson et al.[39]

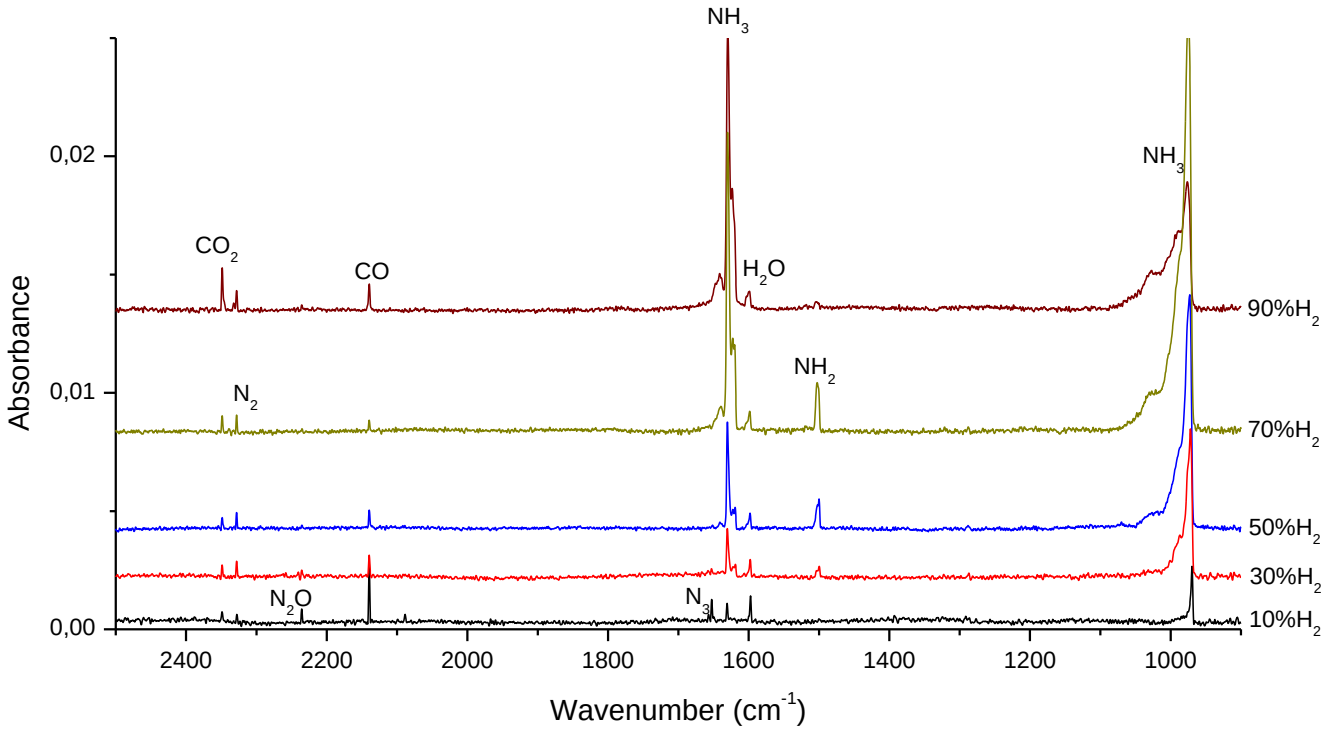

Figure III-13. Recorded IR spectra of N_2-H_2 discharged species with a different hydrogen ratio in the region between 2500 and 900 cm^{-1}

Interestingly almost no NH_2 is observed in 10% H_2 sample while, NH_3 is observed meaning the all hydrogen is used in formation of NH_3 without entrapping the intermediate NH_2. With higher hydrogen amount (30% up to 70% of H_2) the amount of detected NH_2 increases. However, at 90% of H_2, the formation of NH_2 becomes inefficient in contrast with that of NH_3. Obviously by increasing the hydrogen amount in the samples and then by decreasing of N_2 molecules, NH_3 the saturated species become predominant in the sample. These concentration behaviors of NH_2 and NH_3 are shown in figure III-13. As noted before ammonia being a polar molecule it is very susceptible to the formation of stable hydrogen bound aggregates easily observable in the N-H stretching region from 3500 to 3100 cm^{-1} (figure III-14). One of the N-H stretching region is the possibility to probe simultaneously the formation of NH_3, NH_2 and NH.

Figure III-14 show the spectral position of NH_2 and NH stretching vibrations at 3220 and 3132 cm^{-1}, respectively. Additionally we can distinguish the signals from the $(NH_3)_n$ aggregates.

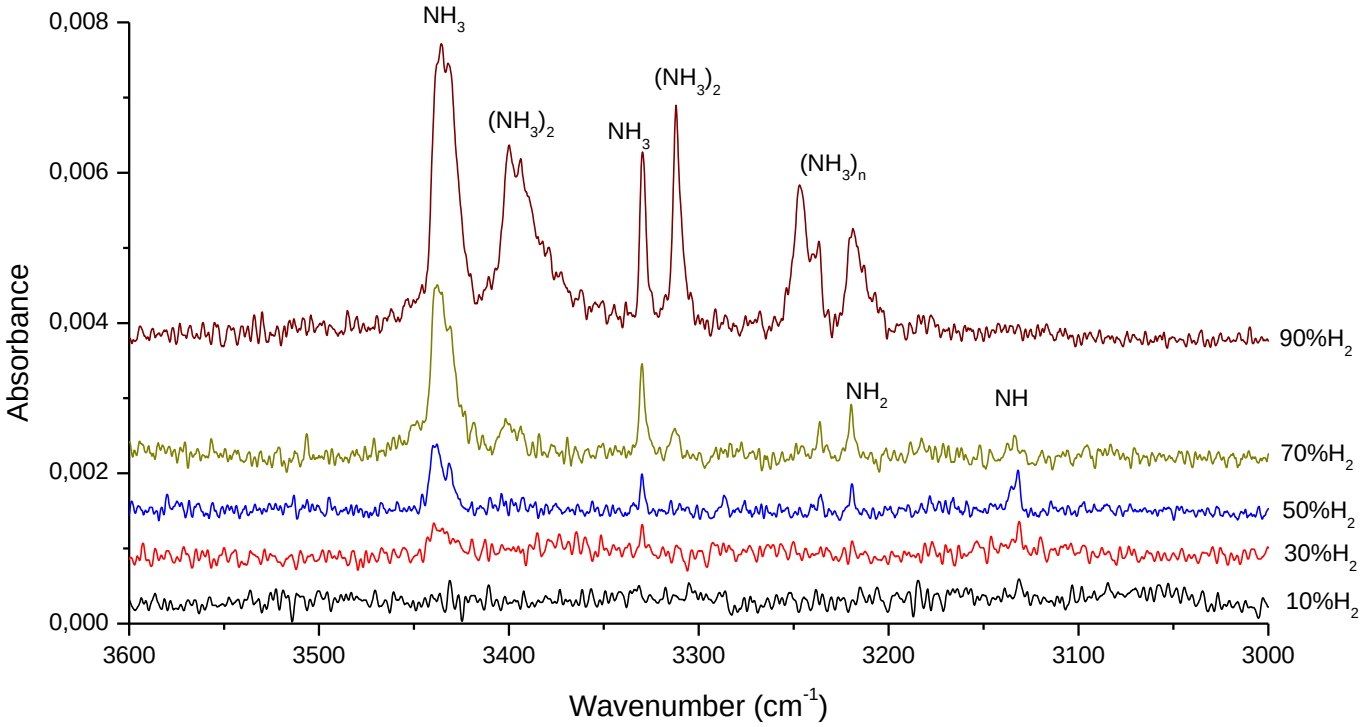

Figure III-14. Recorded IR spectra of N_2-H_2 discharged species with a different hydrogen ratio in the region between 3600 and 3000 cm^{-1}

The challenge was to determine the best conditions to form NH_2 radical, the most important intermediate for the NH_2OH synthesis. In order to do that the integrated intensities of NH_3 band at 1630 and NH_2 at 1500 cm^{-1} are provided in the table III-3. The band of NH_3 at 1630 cm^{-1} was chosen as it is the least affected by the aggregation of ammonia. The highest amount of NH_2 was observed in the sample having 70% of H_2. However this sample shows also a huge amount of ammonia and the ratio of $S_{(NH_2)}/S_{(NH_3)}$ = 0,18. This ratio becomes higher ($S_{(NH_2)}/S_{(NH_3)}$ = 0,33) in the sample with 50% of H_2. Table III-3 provides the integrated intensities of NH_2 and NH_3 and their corresponding ratio for the different concentrations of N_2 and H_2. Another negative aspect with the 70% of H_2 sample is that the NH_3 aggregates start forming while the detection of NH radical becomes less efficient as shown in figure III-14. Consequently, the experimental conditions using a mixture of 50%-50% of N_2-H_2 in a microwave discharge, allow producing adequate amounts of NH, NH_2 and NH_3. Once we have characterized the formation of NH and NH_2 through N/N_2-H/H_2 radical recombination, subsequent experiments involving water have been carried out.

Table III-3. The amount of ammonia and amine radical observed the discharged N_2-H_2 mixtures

Sample (% of H_2)	$S(NH_2)$, cm^{-1}	$S(NH_3)$, cm^{-1}	$S(NH_2)/S(NH_3)$
10	0,00006	0,00248	0,02
30	0,00204	0,0083	0,25
50	0,00579	0,01776	0,33
70	0,01116	0,06145	0,18
90	0,00126	0,06387	0,02

III.7.2. Influence of water molecules on N/N_2+H/H_2 radical addition reactions

Discharging a mixture of N_2-H_2 to the surface of water ice we can see the induced interactions of radical species in contact with water molecules. First a small portion of water was deposited on the mirror, so the bending region (~1680 cm^{-1}) would not be too intense and the NH_2 band would be observable. Later on, the mixture of N_2-H_2 was discharged on top of the water ice. Figure III-15a and III-15b shows the recorded spectra of the discharged mixture on a clean mirror cooled down at 8K and on the mirror covered by water ice, respectively. Apart of the wide water band around ~1680 cm^{-1} there is no difference in spectral bands of NH_3 and NH_2. This fact might be understandable, because as explained earlier the discharged mixture contains molecular nitrogen (N/N_2 = 10/100), which may efficiently stick on the top of the sample at 8K. Bombarding water ice with a mixture of N/N_2 and H/H_2 would form layers of N_2 molecules which limits the interaction of NH, NH_2 and NH_3 with the surface water ice. This behavior is presented in figure III-16.

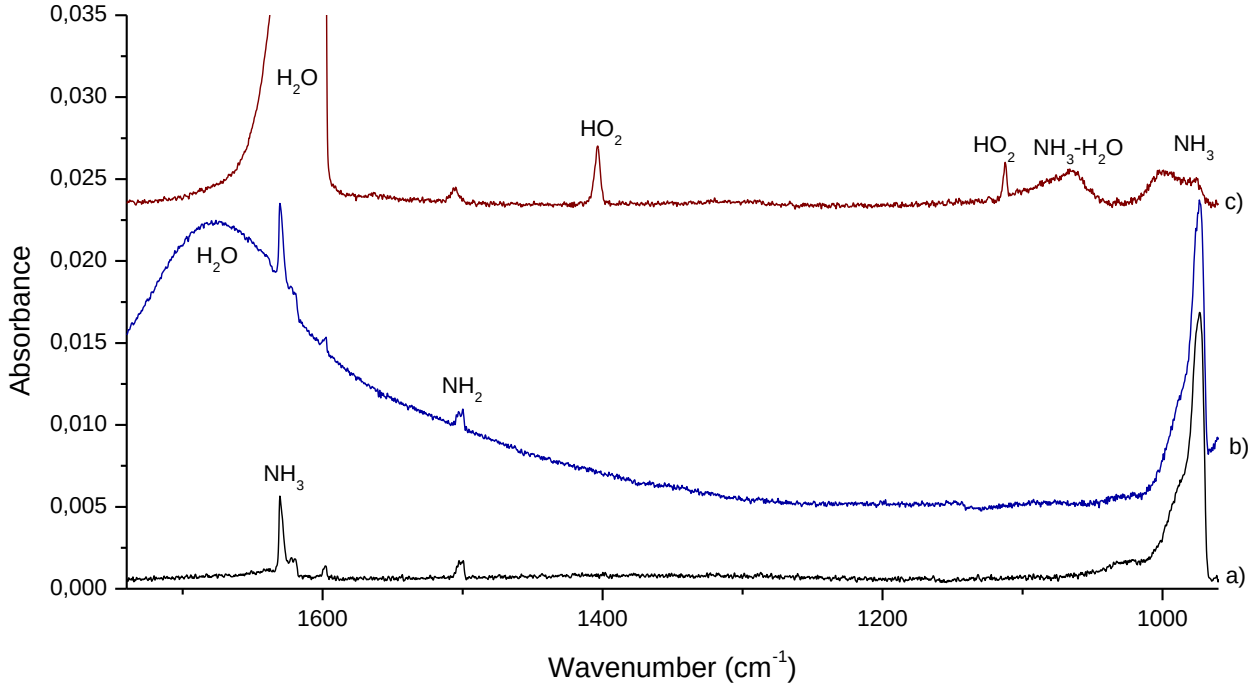

Figure III-15. Comparison of the species formed in a discharge of N_2-H_2 mixture a) on empty mirror, b) on the water ice, c) co-deposited with water molecules

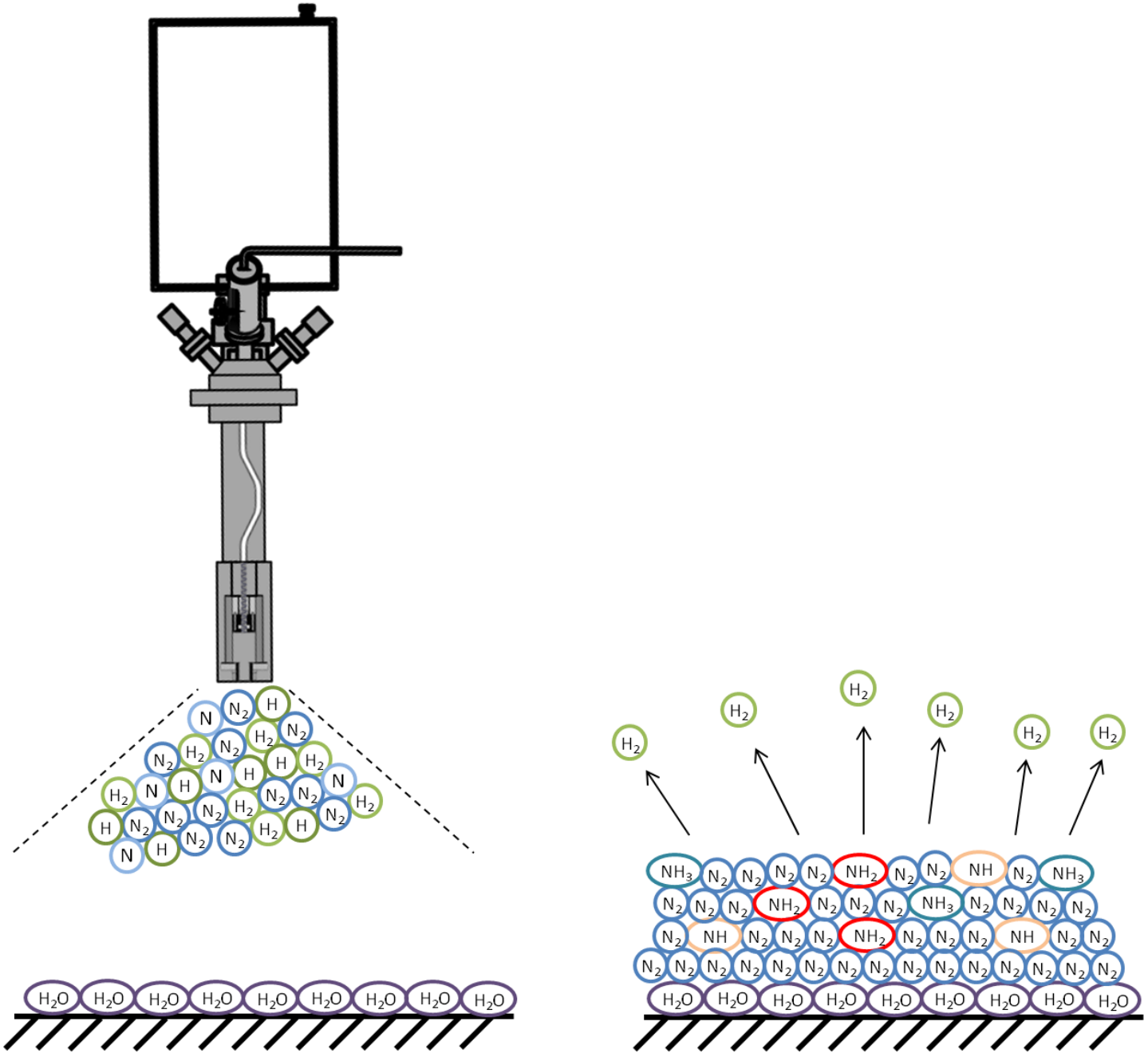

Figure III-16. Water surface bombarded with $N/N_2/H/H_2$ forming NH, NH_2 and NH_3 trapped in N_2 with H_2 leaving the sample

In order to overcome such a problem and also to increase the interaction probability between the water ice and NH and NH_2 formed though N/N_2 + H/H_2 radical recombination, we have preferred to carry out the co-injection experiment by co-depositing simultaneously H_2O and (N/N_2 + H/H_2) on the surface of the sampler maintained at 8K. During the deposition of N_2-H_2

discharged species, water molecules were introduced through side deposition line. The flux was set to very possible limits, not even detectable by the equipment, so the amount of water would not be greater than the amount of discharged species. This has been done to avoid the huge absorption of water ice which may hide all the IR signals of the other reaction products. The H_2O - (N/N_2 + H/H_2) co-deposition at 8K, favors the formation of molecular N_2 matrix where reactants, including water molecules, intermediates and products are trapped. The result of this experiment is shown in figure III-15c.

Firstly a big wide water band entrapped in N_2 matrix is observable around the ~1620 cm^{-1} region masking the NH_3 band, but a small amount is at around 990 cm^{-1} and also aggregated with water molecules at 1064 cm^{-1}. Two new sharp bands are observed at 1403 and 1112 cm^{-1} attributed to HO_2.[38] Comparing the band of NH_2 formed during the clean surface (N/N_2 + H/H_2) bombardments, water ice (N/N_2 + H/H_2) bombardments and H_2O - (N/N_2 + H/H_2) co-deposition experiments, it appears that the same amount of NH_2 is formed and there is no influence of water into formation and transformation of NH and NH_2. This is understandable and in good agreement with theoretical calculations mentioned above. In fact, we have already remarked that the reaction between water molecules and NH_2 radicals has a huge activation barrier and then NH_2-H_2O is a stable and non-reactive system. The zoom in the spectra corresponding to water ice (N/N_2 + H/H_2) bombardments and H_2O - (N/N_2 + H/H_2) co-deposition experiments is shown in figure III-17 where the spectral shift of NH_2 band allow the differentiation between the NH_2 radical and NH_2-H_2O complex.

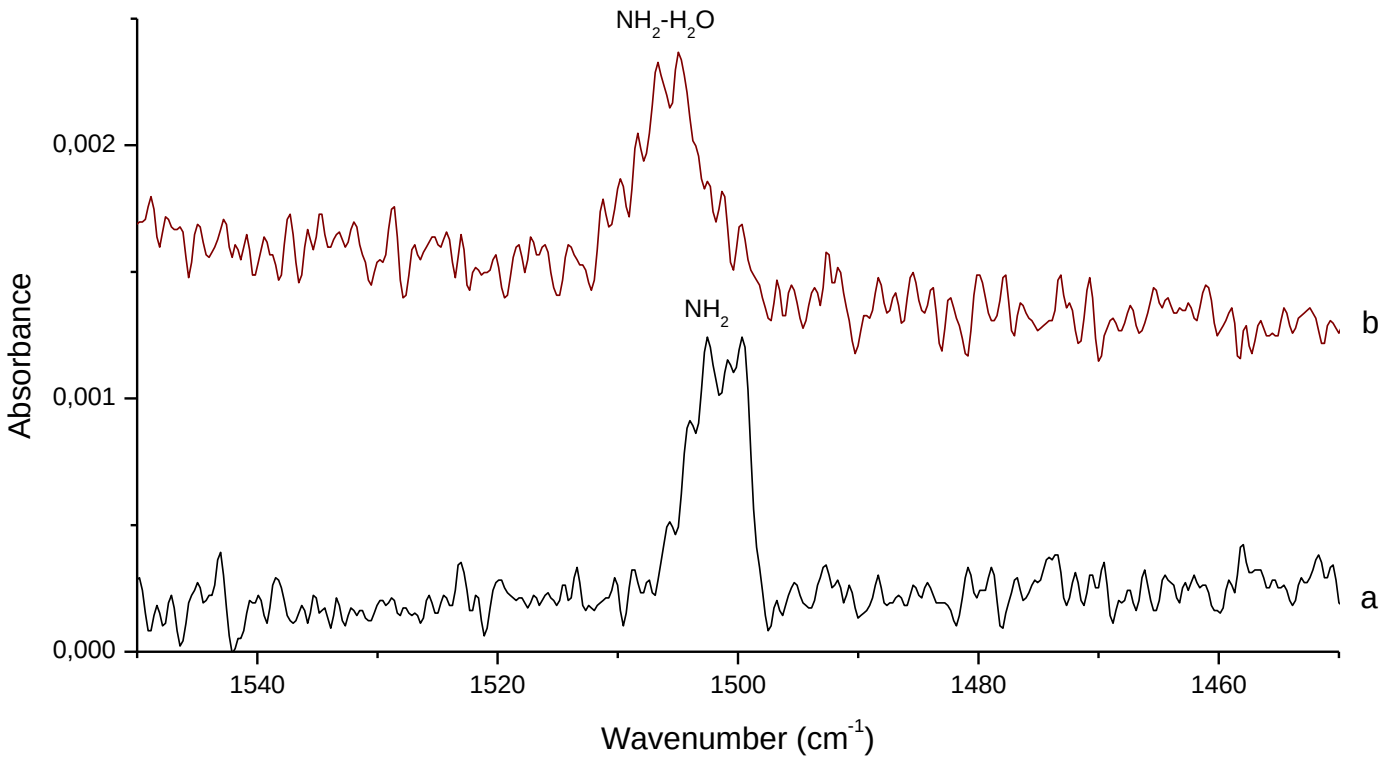

Figure III-17. Comparison of NH_2 formed in a discharge of N_2-H_2 mixture on the a) water ice and b) co-deposited with water molecules

III.8. Conclusions

In this study an in situ infrared spectroscopy was used to monitor reactions occurring in the solid phase on interstellar ice, reflect mechanisms taking place at the surface of icy interstellar grains. The photolysis of NH_3-H_2O in a neon matrix diluted phase leads to several photoproducts such as NH_2, NH_2OH, cis and trans HONO, HO_2, HON, HNO, NO, N_2O and NO_2, while in the condensed bulk phase the only products detected are N_2, NH_2 and NH_2OH. Bulk ice NH_3 + H_2O photo-induced reaction greatly depends on the temperature of the sample and also on the environment where the reactants are trapped. The addition of 2 % of water in ammonia ice makes possible the NH_3 + OH → NH_2 + H_2O reaction to occur at low temperature and induces a 95% increase of NH_2 formation. Monitoring an irradiated ammonia-water ice as a function of temperature, it was observed that the NH_2 amount, almost constant at temperatures lower than 60 K, but is greatly decreased when the temperature is increased to 70 K. Such a behavior is attributed to the competition between NH_2 formation via the NH_3 + OH reaction pathway and its consumption via the NH_2 + OH reaction pathway that leads to the production of hydroxylamine. The catalytic role played by H_2O molecules in enhancing NH_2 formation during photolysis along with those two competing reactions might explain the variation of NH_2/NH_3 ratios reported in astronomical observations of the interstellar medium. Similarly, a different approach was used to produce the amino NH_2 radical using hydrogenation of the atomic nitrogen. Using the different

N_2-H_2 gas ratios in the microwave discharge, it was determined that the ratio of equal parts of nitrogen and hydrogen produces the best distribution of the NH, NH_2 and NH_3 species. Using the same ratio, these species where co-deposited with water molecules and formation of NH_2-H_2O complex was observed shifted from NH_2 band, proving the formation of more stable complex. From these results we can say there is no obvious catalytic role of water into formation of reactivity of NH and NH_2. The catalytic role of water remains only in the photochemical processing through the formation of OH radical which involves in the kinetic of dissociation of NH_3 and in the formation of NH_2OH as shown in figure III-18:

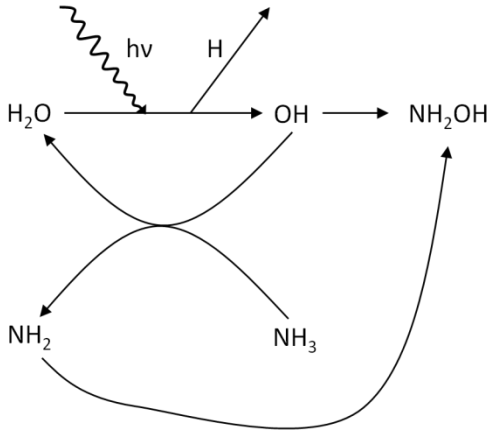

Figure III-18. Catalytic role of water in the formation of NH_2 radical

Bibliography

1 Cheung A. C., Rank D. M., Townes C. H., Thornton D. D., Welch W. J., 1968. Phys. Rev. Lett. 21, 1701.
2 Rodriguez Kuiper E. N., Zuckerman B., Kuiper T. B. H., 1978. Astrophys. J. 219, L49.
3 Wilson T. L., Pauls T., 1979. Astron. Astrophys. 73, L10.
4 Oberg K. I., Boogert A. C. A., Pontoppidan K. M., van den Broek S., van Dishoeck E. F., Bottinelli S., Blake G. A., Evans N. J., 2011. ApJ, 740, 109.
5 Sandford S. A., Allamandola L. J., 1993. Astrophys. J., 409, L65.
6 Moore M. H., Ferrante R. F., Hudson R. L., Stone J. N., 2007. Icarus, 190, 260.
7 Loeffler M. J., Raut U., Baragiola R. A., 2010. J. Chem. Phys., 132, 054508.
8 Zheng W., Jewitt D., Kaiser R. I., 2009. ApJS, 181, 53.
9 Loeffler M. J., Baragiola R. A., 2010. J. Chem. Phys., 133, 214506.
10 Zheng W., Kaiser R. I., 2010. J. Phys. Chem. A, 114, 5251.
11 Martinez R., Ponciano C.R., Farenzena L.S., Iza P., Homem M.G.P., Naves de Brito A., Wien, K. da Silveira E.F., 2006. Int. J. Mass Spectrom., 253, 112.
12 Fernandez-Lima F. A., Cardozo T. M., da Silveira, E. F., Chaer Nascimento M. A., 2009. Chem. Phys. Letters, 474, 185.
13 Leach S., Jochims H. W., Baumgartel H., 2005. Phys . Chem. Chem. Phys., 7, 900.
14 Rosengren K., Pimentel G. C, 1965. J. Chem. Phys., 43, 507.
15 Johnson R. E., Quickenden T. I., 1997. J. Geophys. Res., 102, 10985.
16 Jacox M. E., Thompson W. E., 2004. J. Mol. Spectrosc., 228,414.
17 Milligan D. E., Jacox M. E., 1965. J. Chem. Phys., 43, 4487.
18 Forney D., Jacox M. E., Thompson W. E., 1993. J. Mol. Spectrosc., 157, 479.
19 Ruzi M., Anderson D. T., 2015. J. Phys. Chem. A, 119, 12270.
20 Withnall R., Andrews L., 1988. J. Phys. Chem., 92, 2155.
21 Talik T., Tokhadze K. G., Mielke Z., 2000. Phys. Chem. Chem. Phys., 2, 3957.
22 Khriachtchev L., Lundell J., Isoniemi E., Räsänen M., 2000. J. Chem. Phys., 113, 4265.
23 Mielke Z., Tokhadze K. G., Latajka Z., 1996. J. Phys. Chem., 100, 539.
24 Legay F., Legay-Sommaire N., 1995. J. Chem. Phys., 102, 7798.
25 Lawrence W. G., Apkarian V. A., 1992. J. Chem. Phys., 97, 2224.
26 Milligan D. E., Jacox M. E., 1963. J. Chem. Phys., 38, 2627.
27 Zins E. L., Krim L., 2013. RSC Adv, 3, 10285.
28 Mousavipour S. H., Pirhadi F., HabibAgahi A., 2009. J. Phys. Chem. A, 113, 12961.
29 Troya D., Mosch M., O'Neill K. A., J. Phys. Chem. A, 2009. 113, 13863.
30 Klippenstein S. J., Harding L. B., Ruscic B., Sivaramakrishnan R., Srinivasan N. K., Su M. C., Michael J. V., 2009. J. Phys. Chem., 113, 10241.
31 Gao A., Li G., Peng B., Xie Y., Schaefer H. F., 2016. J. Phys. Chem. A, 120, 10223.
32 Ennis C. P., Lane J. R., Kjaergaard H. G., McKinley A. J., 2009. J. Am. Chem. Soc.,131, 1358.
33 Monge-Palacios M., Corchado J. C., Espinosa-Garcia J., 2013. J. Chem. Phys., 138, 214306.
34 Hily-Blant P., Maret S., Bacmann A., Bottinelli S., Parise B., Caux E., Faure A., Bergin E. A., Blake G. A., Castets A., Ceccarelli C., Cernicharo J., Coutens A., Crimier N., Demyk K., Dominik C., Gerin M., HennebelleP., HenningT., Kahane C., Klotz A., Melnick G., Pagani L., SchilkeP., Vastel C., Wakelam V., Walters A., Baudry A., Bell T., Benedettini M., Boogert A., Cabrit S., Caselli P., Codella C., Comito C., Encrenaz P., Falgarone E., Fuente A., Goldsmith P. F., Helmich F., Herbst E., Jacq T., Kama M., Langer W., Lefloch B., Lis D., Lord S., Lorenzani A., Neufeld D., Nisini B., Pacheco S., Phillips T., Salez M., Saraceno P., Schuster K., Tielens X., van der Tak F., van der Wiel M. H. D., Viti S., Wyrowski F., Yorke, 2010. A&A, 521, 52.
35 Van Dishoeck E. F., Jansen D. J., Schilke P., Phillips T. G., 1993. ApJ, 416, L83. 385.
36 Mencos A., Nourry S., Krim L., 2017. MNRAS 467, 2150.
37 Bernstein M. P., Sandford S. A., 1999. Spectrochim. Acta. Mol. Biomol. Spectrosc., 55, 2455.
38 Joshi P. R., Zins E. L., Krim L., 2012. MNRAS, 419, 1713.
39 Jamieson C. S., Bennett C. J., Mebel A. M., Kaiser R. I., 2005. ApJ, 624:436.

Chapter IV:

Behavior of NH_2OH in interstellar ice analogs

IV.1. Earlier studies and motivation

In the previous chapter it was shown that the photolysis of ammonia-water ices leads to the formation of the hydroxylamine NH_2OH. This observation is interesting in the matter that the presence of NH_2OH on dust grain mantles may be the most probable source for large prebiotic molecules and a precursor molecule in the formation of amino-acids. Many laboratory investigations have focused their theoretical[6-8] as well as experimental[1-5] studies into the formation of NH_2OH under extreme conditions similar to those found in the interstellar medium. From an experimental point of view, most of the studies have been devoted into the synthesis processes of hydroxylamine in solid phase at cryogenic temperatures. Many laboratory experimental studies simulating the icy grain space chemistry, found that NH_2OH molecules may be easily formed in solid phase with high abundances. We have shown that the UV irradiation of ammonia containing ices may be one of the efficient reaction pathways to produce hydroxylamine through radical recombination involving, NH_2, H, OH and H_2O:

$$NH_2 + OH \rightarrow NH_2OH \qquad \text{(IV-1)}$$

Using electron irradiations of ammonia-water ices between 10 and 50K, Zheng and Kaiser[2] have also investigated the NH_2OH formation, where the synthesis of molecular hydroxylamine has been accompanied by many secondary reaction products such as H_2, H_2O_2 and N_2H_4. Strazzulla[3] proposed such similar studies, suggesting that the irradiated NH_3–H_2O–CH_4 mixture on Saturnian satellite surfaces can be partially converted into pre-biotic molecules. In recent years various experiments involving atom or radical bombardment of interstellar ice analogs have been proposed to justify the formation of complex organic molecules in space. Within this context, Congiu et al.[4] illustrated the NH_2OH formation on interstellar ice analogs might arise from successive hydrogenation of solid nitric oxide at 10K, while He et al.[5] reported another hydroxylamine synthesis on an amorphous silicate surface through the oxidation of ammonia at 70K. Concurrently with these experimental studies, many theoretical investigations have been devoted to diverse mechanisms of reactions leading to the formation of NH_2OH as an intermediate or a final reaction product. The radical recombination NH_2 + OH reaction has been theoretically investigated on the lowest singlet and triplet surfaces by Mousavipour et al.[6,7] They underline the formation of two hydroxylamine isomers NH_2OH and NH_3O which may decompose into smaller fragments such as HON + H_2, HNO + H_2 and NH_3 + O. Similar study has been also proposed by Wang et al.[8] by investigating the branching product for O + NH_3 reaction which was found to be occurring through an insertion mechanism leading to a long-lived chemically activated NH_2OH as an intermediate before it dissociated into NH_2 and OH to dissipate its internal energy derived from the exothermicity of the O insertion reaction.

Even though all those laboratory investigations suggest the efficient way to form hydroxylamine under conditions similar to those found in the interstellar medium and some planetary atmospheres, but there is one big problem to all of this: the NH_2OH molecule remains still undetected. Many deep searches of hydroxylamine toward several astronomical sources

carried out by McGuire et al. and Pulliam et al. result in a non-detection of this simple molecule.[9,10] An obvious and possible explanation might be that the NH_2OH abundances in different regions in space might be lower than estimated from the laboratory studies and the astrophysical models. The laboratory experimental studies showed several reaction pathways to form NH_2OH in solid phase while all the space observations conclude that NH_2OH is not detected, meaning that some kind of chemical transformation of NH_2OH in solid phase during the desorption processes of interstellar grains containing hydroxylamine could result in its very low abundance in space. Such a contradiction between laboratory experimental simulations and spatial observations leads to the investigation towards this experimental study to see if there is any chemical transformations of NH_2OH occurring in the solid phase before the desorption processes of hydroxylamine from the mantle of interstellar icy grains. Strangely hydroxylamine being a stable and commercially available molecule, all the laboratory investigations have focused on the formation of NH_2OH in 'cold-solid-phase' interstellar medium conditions, but no experiments have ever been performed to simulate the desorption of NH_2OH trapped in water ices to monitor the hydroxylamine evolution during the solid–gas transitions.

In this chapter we try to have a link between the efficiency of NH_2OH solid phase formation and its evolution into the gas phase. To do this we have formed NH_2OH containing ices by considering two different methods by heating the $[NH_2OH]_3[H_3PO_4]$ salt at 40°C to release NH_2OH in gas phase:

- The first method consists on the formation of NH_2OH–H_2O ices though a direct deposition of NH_2OH and H_2O at 10K.
- The second method consists on Ne matrix isolation carried out by coinjecting the NH_2OH, H_2O and Ne at 3K. Following the matrix isolation, the sample has been heated to remove neon atoms and cooled down to 10K in order to have the same temperature ices with both methods.

The matrix isolation experiment also allowed to make vibrational attributions and to assess the purity of the sample. The heating and desorbing progressively the neon atoms to reach NH_2OH-H_2O ice would also help to get the right vibrational attributions in bulk ice. Having characterized spectroscopically the NH_2OH-H_2O ice by two methods, the temperature programmed desorption have been carried out between 10 and 300K in order to characterize the thermal desorption of NH_2OH and also its evolution during at solid-gas interface.

IV.2. Sample preparation: evaporation of NH_2OH from the $[NH_2OH]_3[H_3PO_4]$ salt

Pure hydroxylamine is highly toxic. It is an irritant to the respiratory tract, skin, eyes and it may be adsorbed through the skin. It is also very harmful if swallowed. Hydroxylamine may explode upon heating. The nature of the explosive hazard is not well understood, but it is related to the high exothermic decomposition. Some incidents have occurred leading to some serious

damage and casualties, like at a re-distillation unit of a hydroxylamine manufacturing plant in Ojima, Japan in 2000. Detonation of a highly concentrated hydroxylamine aqueous solution led to the explosion that destroyed several building and 4 deaths (hopefully it occurred on weekend), plus many injuries.[11]

Due to the dangers of hydroxylamine, it is almost always provided and used as an aqueous solution in 1-1 ratio with water. This would make the experiment much more complex due to the high amount of water in the samples and introduction of other impurities. Another possibility is using hydroxylamine in the form of salts, where it can be more safely handled. Hydroxylamine forms salts in ratio to: 1-1 with hydrogen chloride (HCl), 2-1 with sulfuric acid (H_2SO_4) and 3-1 with phosphoric acid (H_3PO_4). Salts at room temperature are solid with very low vapor pressure. To increase the vapor pressure and luckily, to dissociate the salt into their counterparts without the total destruction of the molecules, the salt has to be heated. For selecting the optimal salt, the melting and boiling points of pure molecules, consisting in these salts, where assessed from the PubChem open chemistry database.[12] Looking at the data provided in table IV-1, it is visible that the phosphoric acid has the higher melting point than hydroxylamine. Heating the hydroxylamine phosphate salt between the temperatures of 33 and 43 °C it is possible to dissociate the salt and create vapor pressure of hydroxylamine without phosphate impurities.

Table IV-1. Physical properties of the molecular counter parts found in hydroxylamine salts

Molecule	Melting point, °C	Boiling point, °C
Hydroxylamine, NH_2OH	33	70
Hydrogen chloride, HCl	-114	-85
Sulfuric acid, H_2SO_4	10	337
Phosphoric acid, H_3PO_4	43	407

In this experiment, hydroxylamine was produced from a hydroxylamine phosphate $[NH_2OH]_3[H_3PO_4]$ salt. Considering that this salt, at room temperature, is solid with low vapor pressure, the equipment system had to be redesigned for this experiment. It was done by changing the injection system. The glass tube with hydroxylamine phosphate salt was introduced next to injection port to the vacuum chamber and overall volume reduced to promote having more hydroxylamine molecules reaching the cold mirror. The glass tube was equipped with a controlled heating system. Taking into consideration the melting points for pure hydroxylamine (~34°C) and phosphate (43°C) the best determined temperature for heating the mixture salt was around 40°C, by trying not to introduce any of the phosphate molecules.

As for the confirmation that we are obtaining pure NH_2OH in gas phase before its deposition at low temperature, the mass spectrum of hydroxylamine injected into the experimental chamber has been recorded and is shown in figure IV-1. The main mass signal situated at m/z = 33 is due to NH_2OH molecules in addition to some low signals at m/z = 32, 31

and 30 due to the fragmentation patterns of hydroxylamine in the mass spectrometer. This spectrum is in agreement with a reference spectrum of hydroxylamine from NIST Chemistry WebBook.[13] Other signals at m/z = 28 and 18 are also detected, that can be attributed to N_2 and water H_2O. These are obvious impurities, because this salt is hygroscopic. For the formation of the samples no additional water was needed, due to its presence in the sample. From this spectrum we estimate the lowest amount of water we can have in our samples. This amount can also be increased by injecting water during the deposition of NH_2OH.

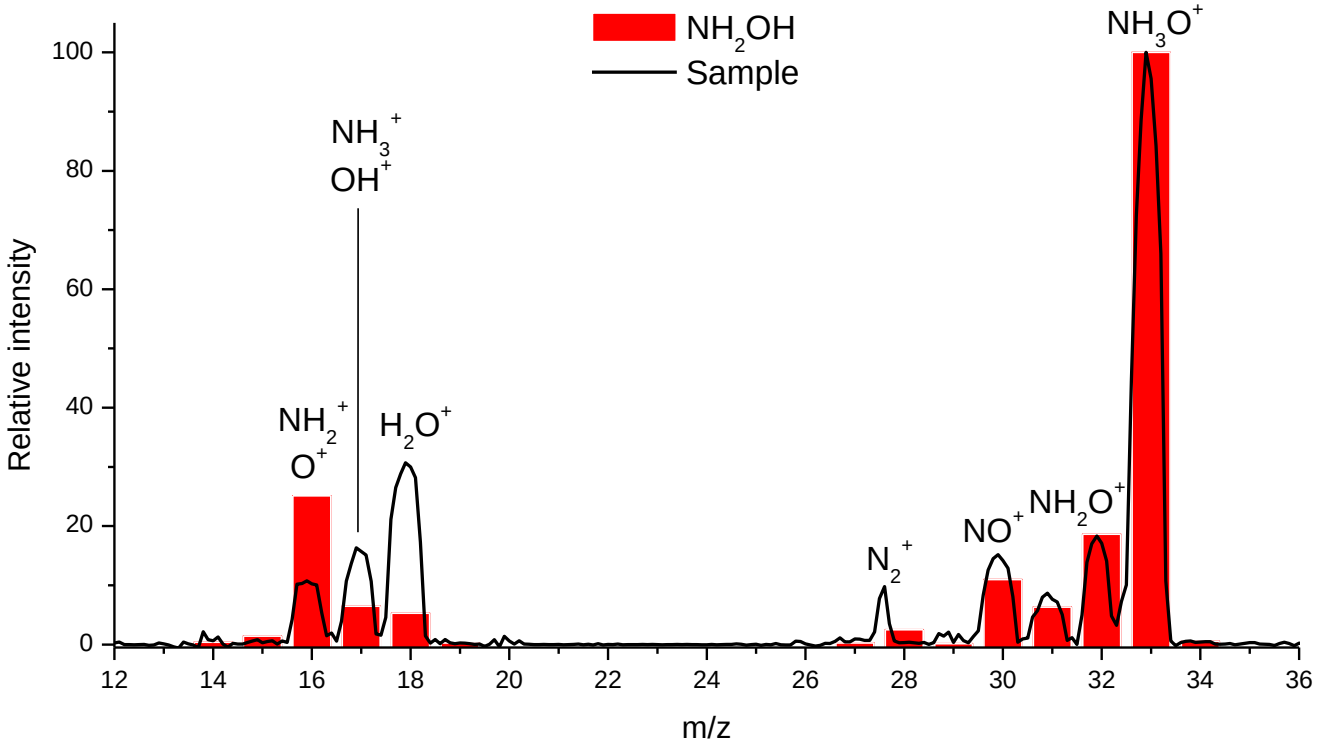

Figure IV-1. Mass spectrum recorded during the sample deposition and fragmentation pattern of NH_2OH in the mass spectrometer.

IV.3. NH_2OH-H_2O matrix isolation

In order to make the specific vibrational mode assignments of NH_2OH, the condensation experiment of the thermal decomposition of $[NH_2OH]_3[H_3PO_4]$ salt through a neon matrix isolation technique was needed to be performed. In this context, an experiment was run using neon as carrier gas at constant flux for 30 min. The results of this experiment is shown in the infrared spectrum of figure IV-2, where most of the detected absorption peaks for NH_2OH trapped in neon matrix are found to be similar to those investigated by other groups.[14,15] To compare our results to earlier hydroxylamine investigations, table IV-2 gathers the vibrational mode frequencies of NH_2OH measured in our experiments and those given by previous studies. Through this neon matrix isolation experimental method, all the specific vibrational modes of NH_2OH molecule isolated in the rare gas matrix were assigned as shown in figure IV-2. This

also helps to better characterize, through the IR spectroscopy, the purity of our hydroxylamine arising from the thermal decomposition of the salt. The detection of H_2O vibrational modes in our IR spectrum as shown in Figure IV-2, at 3744, 3651 and 1595 cm^{-1}, prove that NH_2OH is found to be mixed with water molecules and also some other impurities like NO (1875 cm^{-1}), N_2O (2225, 1285 cm^{-1}), N_2 (2330 cm^{-1}) and CO_2 (2347 cm^{-1}). Impurities like N_2, CO_2 and H_2O is adsorbed from air, as noted before the salt is hydroscopic. On the other hand species like N_2O and NO_x could only be products formed during the decomposition of the salt due to the dissociation of NH_2OH. Altogether the majority of the species trapped in neon matrix is still NH_2OH, allowing further investigation and formation of NH_2OH-H_2O ices.

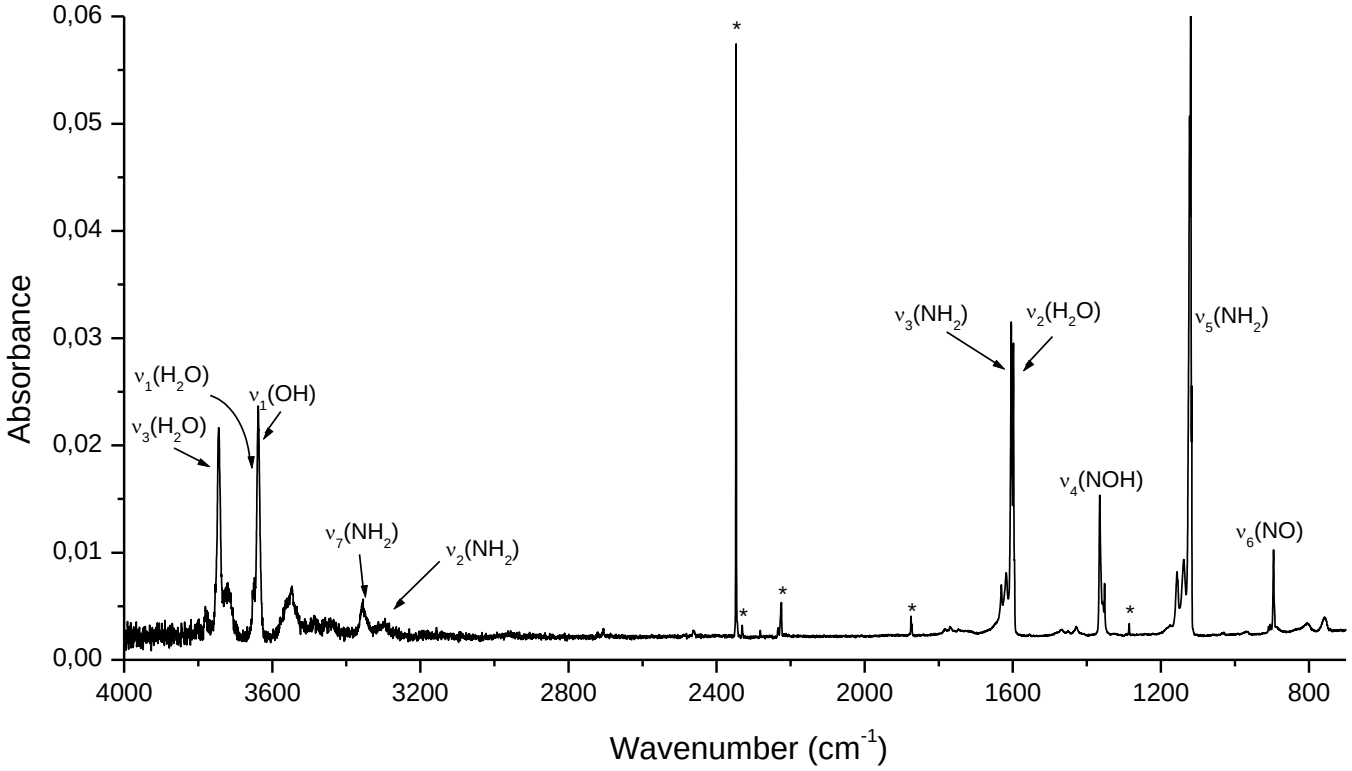

Figure IV-2: Infrared spectrum of neon matrix isolation of the products from the thermal decomposition of $[NH_2OH]_3[H_3PO_4]$ salt deposited at 3K temperature. Impurities NO, N_2O, N_2, and CO_2 are marked with *

Table IV-2. Assignments of NH_2OH molecule's vibrational modes in Ne matrix.

Vibrational mode	This exp	Withnall et al.[14]	Luckhaus et al.[15]
ν_1(OH)-stretch	3637.9	3634.7	3649.89
ν_2(NH_2)-sym. stretch	3297.1	3289.7	3294.25
ν_3(NH_2)-scissoring(HNH)	1598.4	1598.9	1604.52
ν_4(NOH)-bend	1351.7	1350.7	1353.3
ν_5(NH_2)-wagging	1117	1117	1115.47
ν_6(NO)-stretch	895.7	895.9	895.21
ν_7(NH_2)-antisym. stretch	3346.5	3353.3	3358.76
ν_8(NH_2)-rocking	-	-	1294.5
ν_9(OH)-torsion	-	375.9	385.96

IV.4. Formation of NH_2OH-H_2O ice

IV.4.1. Ice formation through a direct NH_2OH-H_2O deposition

One of the ways to form the NH_2OH-H_2O ice is through the deposition of the species derived from the thermal evaporation of the $[NH_2OH]_3[H_3PO_4]$ salt. To form solid NH_2OH-H_2O ice samples, the same conditions were used as in the previous experiment, just without Ne gas. It has to be considered that during the thermal evaporation of the $[NH_2OH]_3[H_3PO_4]$ salt, no pressure increase was noticed in the ramping system. Due to this fact the deposition time was extended to two hours. The infrared spectrum recorded after the two hour deposition of the species derived from the thermal evaporation of the salt is shown in figure IV-3. Hydroxylamine similarly like ammonia and water is also a polar molecule (0.68 D). Due to this fact, as water and ammonia, NH_2OH also produces wide vibrational bands in solid state. The recorded spectrum can be divided into two groups: the NH and OH stretching region (between 3600 and 2600 cm^{-1}) that shows similarities to water vibrational bands and NH bending region (between 1800 and 800 cm^{-1}). There are three noticeable bands in NH bending region at 1620, 1475 and 1195 cm^{-1}. The band at 800 cm^{-1} has to be noted, that is easily attributed to water ice torsion. From this we can conclude that the ice formed from the thermal evaporation of the $[NH_2OH]_3[H_3PO_4]$ salt is a mixture of NH_2OH-H_2O.

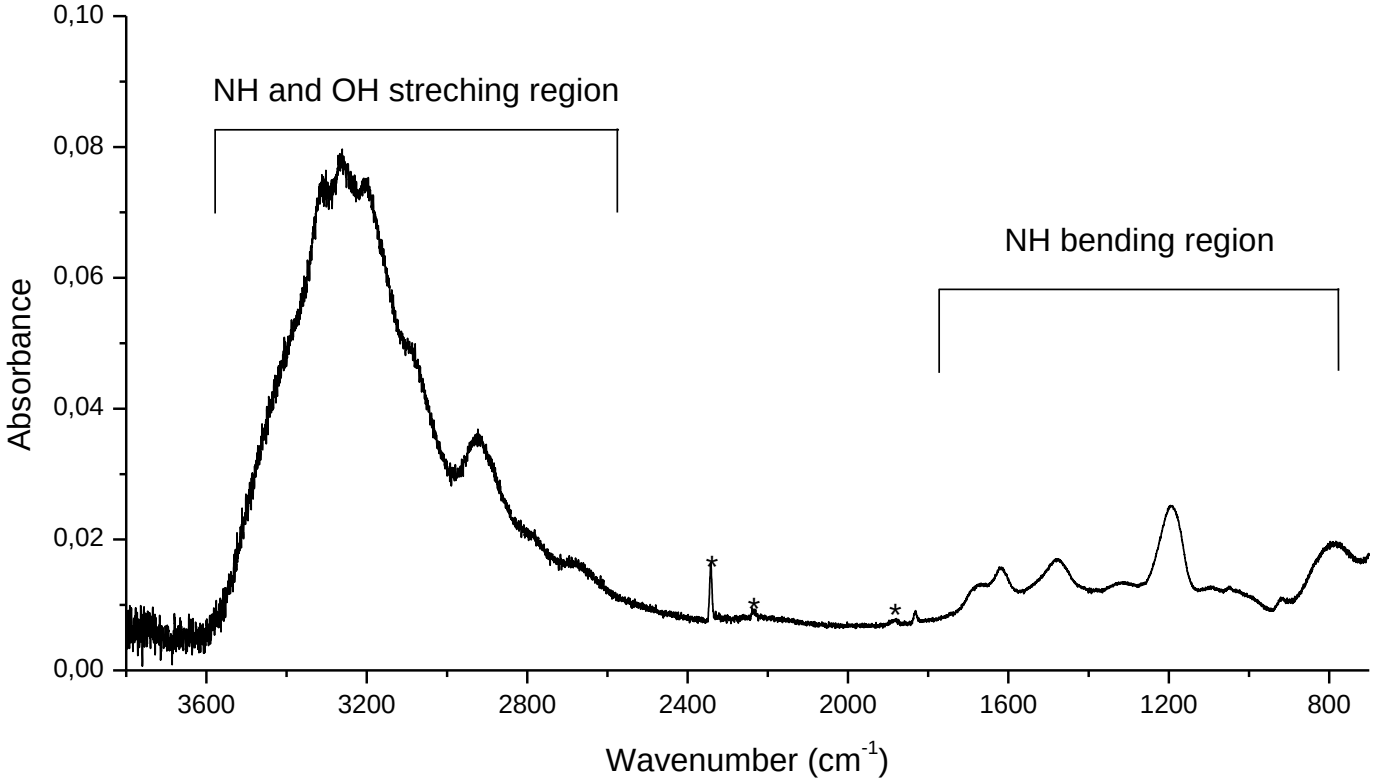

Figure IV-3: A sample formed by thermal decomposition of $[NH_2OH]_3[H_3PO_4]$ salt on the cold 10K mirror. Impurities are marked with an asterisk * (CO_2 at 2342; N_2O – 2233; NO - 1875 cm^{-1})

IV.4.2. Ice formation from matrix isolated NH_2OH-H_2O

As noted before, another way of ice formation is by heating the species trapped in neon matrix at higher temperatures so all the neon atoms released from the sample leading to the formation of a neon-free solid NH_2OH. In order to connect the infrared spectrum of NH_2OH ice recorded after a direct condensation during 2h at 10K of hydroxylamine arising from the thermal evaporation of $[NH_2OH]_3[H_3PO_4]$ salt and those recorded using rare gas matrix isolation experiments, the neon matrix samples formed at 3K have been heated progressively between 3 and 20 K to completely release the neon atoms from the sample. The results of the heating of the neon matrix between 3 and 20K are shown in figures IV-4b, IV-4c and IV-4d. As shown in figure IV-4c, at 15 K almost all the neon atoms leave the solid sample while at 20K NH_2OH-H_2O ice can be clearly formed. The ice is characterized by wide absorption bands related to solid H_2O and NH_2OH similar to those observed by direct NH_2OH-H_2O deposition. The sample may be cooled down at 10K after the total sublimation of neon atoms at 20K in order to compare at the same temperature the two sample deposition methods for the formation of NH_2OH-H_2O ice.

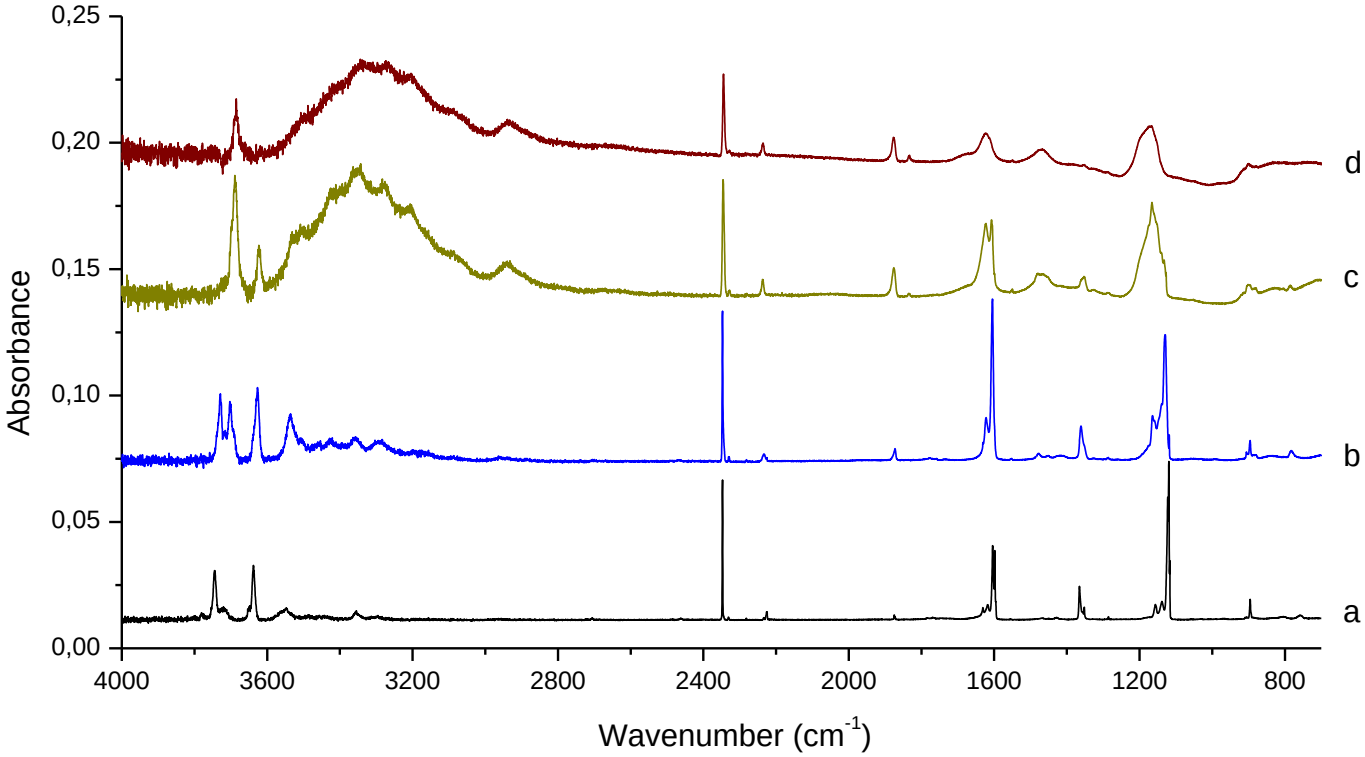

Figure IV-4: Neon matrix isolation of the products from the thermal evaporation of $[NH_2OH]_3[H_3PO_4]$ salt. Infrared spectrum of NH_2OH and H_2O trapped in neon matrix a) deposition at 3K temperature. b) Heating of the sample at 10K. c) Heating of the sample at 15K d) Heating of the sample at 20K.

Figure IV-5 shows the evolution of the vibrational modes of NH_2OH and H_2O at 10K from a NH_2OH-H_2O-Ne matrix to NH_2OH-H_2O ice. Figure IV-5a shows the absorption bands of the trapped species in neon matrix at 10K, while figure IV-5b shows the evolution of those bands after heating of the sample at 20K for a while (1-2h) to remove all the neon atoms (checked by

mass spectrometry), followed by a cooling down of the sample to 10K. The similarity between the spectrum of figure IV-5b and that of NH_2OH-H_2O ice at 10K in figure IV-5c, shows that even though the two experimental methods are different but they lead to the formation of the same NH_2OH-H_2O ices. Additionally as mentioned before we took advantage by coupling these two experimental methods to have the right vibrational assignments of the IR signals of NH_2OH-H_2O ice. Moreover, these two methods allowed us the attributions of the IR signals of the products detected during the NH_3-H_2O ice photolysis, as discussed in the previous chapter.

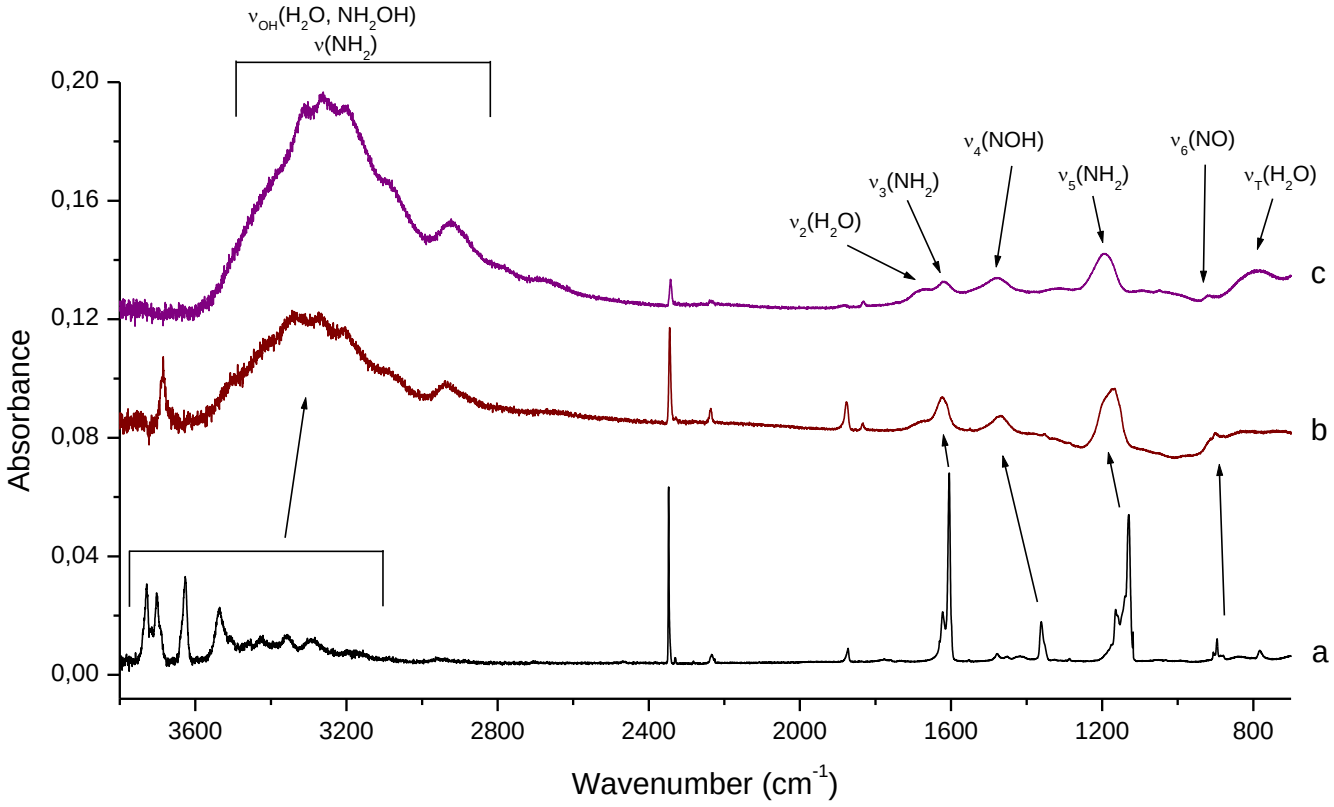

Figure IV-5: Infrared spectra in 750-3700cm^{-1} region of NH_2OH. a) NH_2OH trapped in neon matrix heated at 10K temperature. b) NH_2OH trapped in neon matrix heated at 20K temperature and cooled down to 10K. c) NH_2OH-H_2O ice deposited directly at 10K.

IV.5. Thermal processing of NH_2OH-H_2O interstellar ice analog

After the vibrational characterization of NH_2OH-H_2O ices at 10K, our main interest was to study the thermal processing of NH_2OH in contact with water molecules at low temperatures. A scenario that might be used, to characterize the NH_2OH molecule evolution during the sublimation of icy grains in the interstellar medium. The sublimation of icy grains is one of the sources of the many chemical species detected in gas phase. In this context, NH_2OH-H_2O ices formed at 10K have been gradually heated at higher temperatures until a total desorption of the sample. Solid phase evolution have been investigated by IR spectroscopy. By increasing the

temperature from 10 to 100K we noticed no visible changes in the infrared spectra of the heated ices, figures IV-6a and IV-6b. This phenomenon was not very surprising as most of the many previous experimental works related the chemistry of solid NH_2OH show that the desorption temperature of NH_2OH is much higher. As exposed in figures IV-6c – IV-6g, in temperatures higher than 100K, the IR spectra show the decrease of NH_2OH IR signals and the appearance of new IR features in different spectra regions. The most isolated and intense IR signal appearing during the ice heating is clearly shown at 980 cm^{-1} in figures IV-6c – IV-6g. On the other side the mass spectra have been recorded during the heating of the sample to characterize the species released into the gas phase. The appearance of the species in the gas phase depend on their concentrations in the solid phase and also on their desorption temperatures. In this context the recorded mass spectra during the heating of the sample between 100 and 160K (figure IV-9, page 104) show a very low peak at m/z = 33 (NH_2OH) proving that the decrease of the NH_2OH IR signals in this range of temperatures is mainly due to the NH_2OH chemical transformations in solid phase rather than hydroxylamine desorption. It should be underlined that the very low amount of NH_2OH desorbing in gas phase between 100 and 160K, associated to the appearance of new IR features which may be due to thermal reaction products formed in NH_2OH-H_2O ice, show that the NH_2OH desorption from the NH_2OH-H_2O ice would be very limited while most of NH_2OH molecules trapped in water ice would undergo chemical transformations.

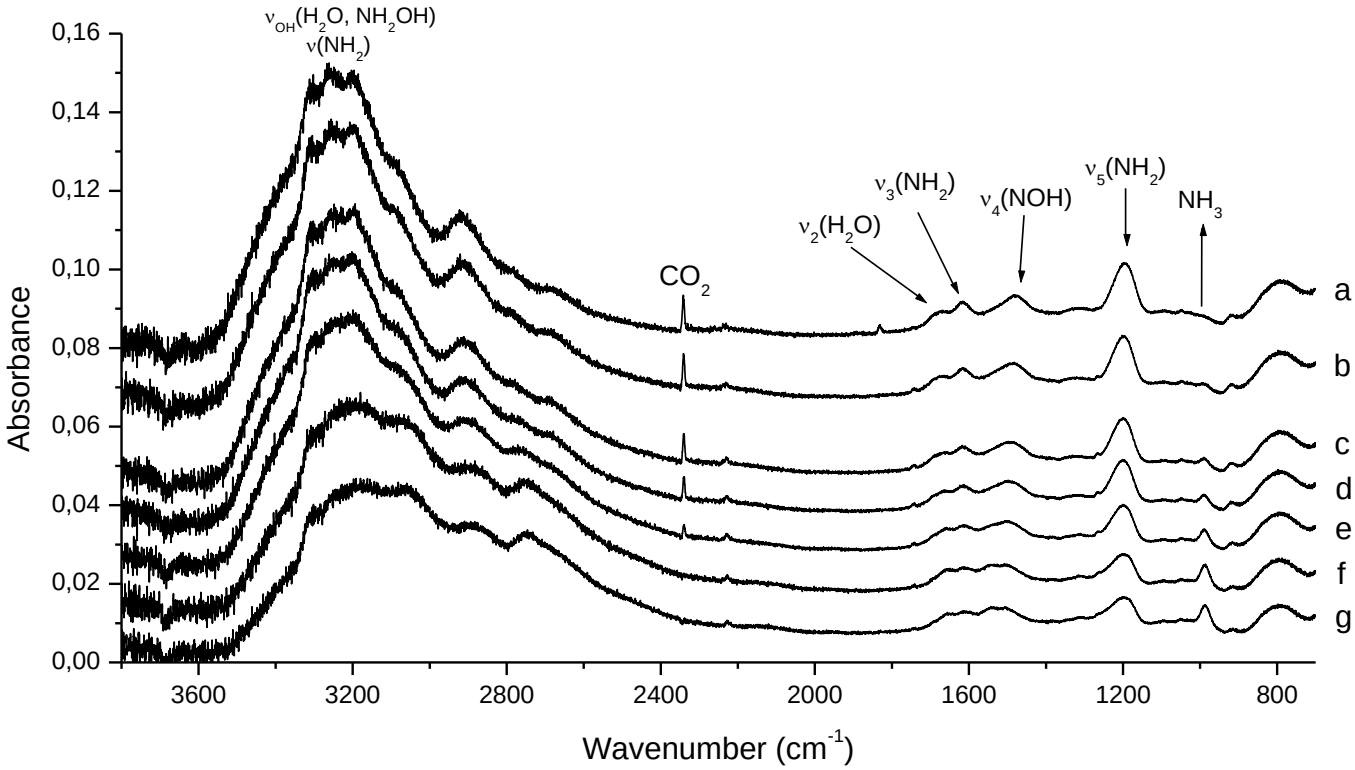

Figure IV-6: Infrared spectra in the 800-1400cm^{-1} region of NH_2OH ice. a) Deposition at 10K. b) At 100K temperature. c) At 130K temperature. d) At 140K temperature. e) At 150K temperature. f) At 160K temperature. g) At 170K temperature.

To quantify such a thermal chemical transformation, instead of NH_2OH desorption, figure IV-7 shows a zoom of two distinguishing IR absorption bands at 1200 cm^{-1} and 980 cm^{-1}, corresponding to NH_2OH and one of the thermal reaction products from NH_2OH decomposition in water ice, respectively.

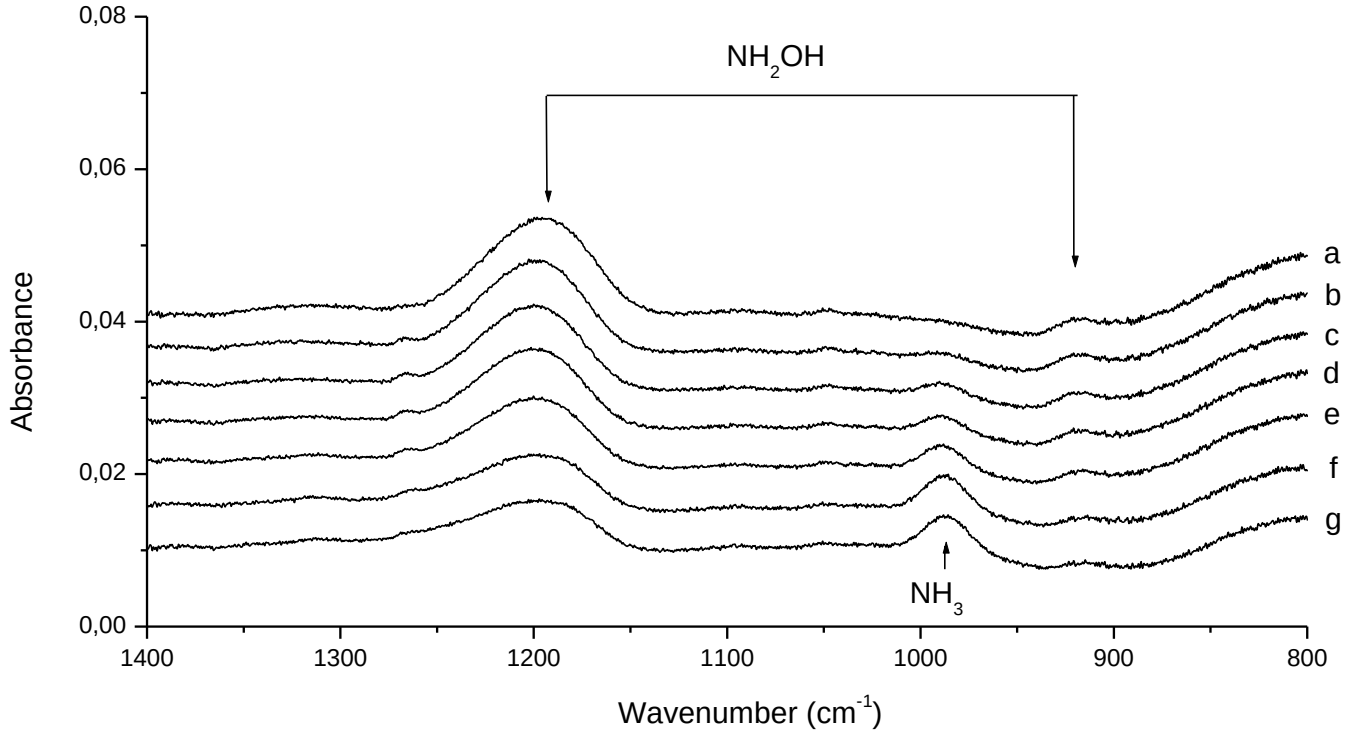

Figure IV-7: Infrared spectra in the 800-1400cm^{-1} region of NH_2OH ice. a) Deposition at 10K. b) At 100K temperature. c) At 130K temperature. d) At 140K temperature. e) At 150K temperature. f) At 160K temperature. g) At 170K temperature.

The 980 cm^{-1} band appears in the NH_3 vibration spectral region and it may be easily attributed to NH_3 molecules, linked to the surface of our solid sample, or coupled to other chemical species. Fedoseev et al.[16] have already reported the absorption band signal of ammonia in solid phase at 975 cm^{-1}. The appearance in our infrared spectra of a band at 980 cm^{-1} is consistent with the presence of NH_3 diluted in ice, and not as pure ammonia ice which has a characteristic band at 1070 cm^{-1}.[29] In fact, when ammonia is present in solid phase as a minor species trapped in ice, its spectral position is shifted to lower frequency, which is also reliable with Fedoseev's work who detected ammonia as a minor reaction product in solid phase, around 975 cm^{-1}.

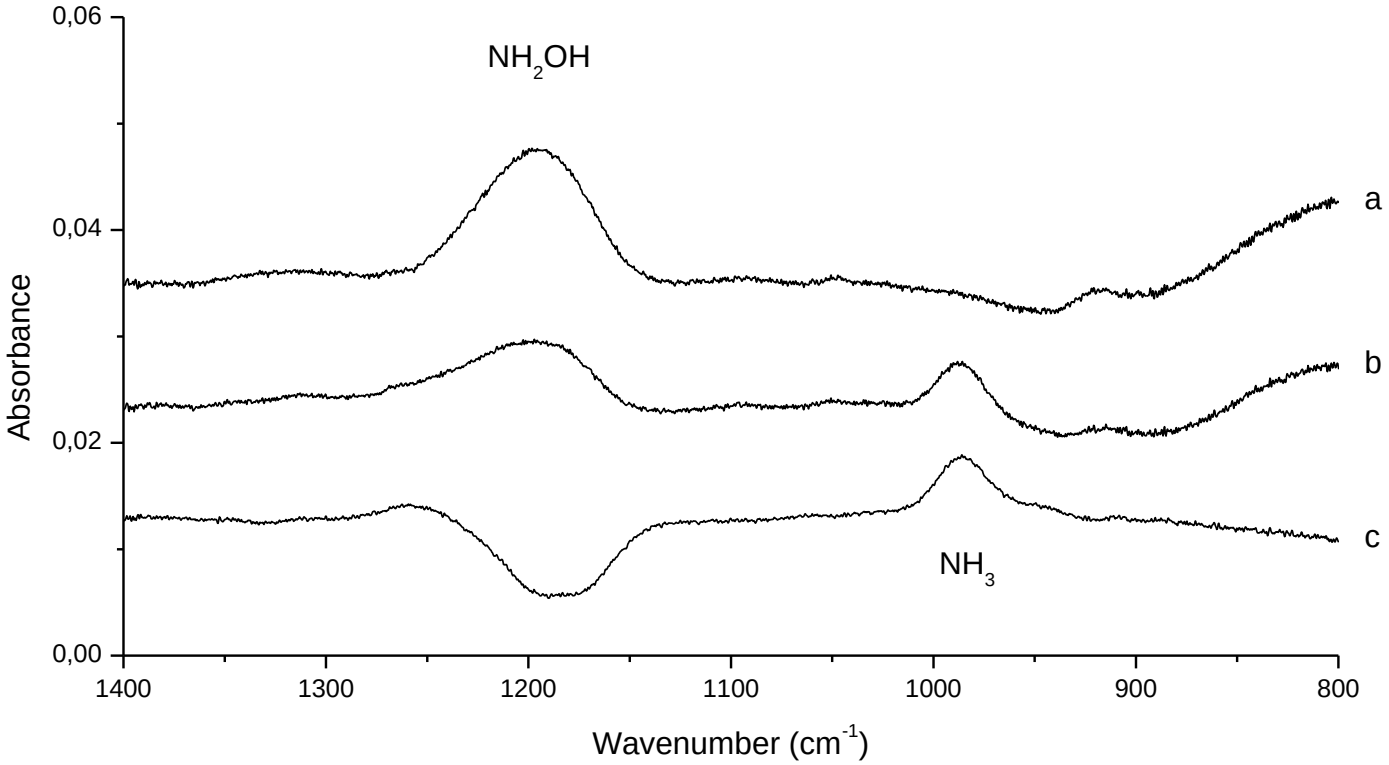

Figure IV-8. Infrared spectra in the 800-1400 cm^{-1} region of NH_2OH ice. a) after deposition at 10K. b) at 170K temperature. c) subtraction spectrum

The detection of ammonia under our experimental conditions by inducing a thermal reaction between water and hydroxylamine proves that NH_2OH molecules desorbing from the surface of NH_2OH-H_2O ice undergoes a decomposition leading to the formation of NH_3 molecules linked to the surface of the solid sample. The close up spectra and subtraction spectrum for two extreme temperatures, 10 and 170K, are shown in figure IV-8.

The detection of ammonia under our experimental conditions, just by inducing a thermal reaction between water and hydroxylamine, proves that NH_2OH molecules desorbing from NH_2OH–H_2O ice undergoes a decomposition leading to the formation of new chemical species which may be formed and trapped into the NH_2OH–H_2O ice host between 100 and 170 K without any desorption.[17,18,19,20]

From the results exposed in figure IV-8 we can determine the column densities of our reactants and products **N** (molec cm^{-2}), using the band strengths **A** (cm $molec^{-1}$) of the detected species, in order to get an order of magnitude of the composition of our samples before and after the reaction occurs at 10 and 170 K, respectively. Table IV-3 gathers the characteristic vibrational frequencies, the band strengths and the column densities of the three detected species which show specifically characteristic isolated band absorptions, namely, H_2O, NH_3 and NH_2OH.

Table IV-3. Vibrational frequencies, band strengths and column densities of H_2O, NH_3 and NH_2OH.

Characteristic vibrational frequency (cm^{-1})	Molecule	Band strength[21,22]	Vibrational mode	Column densities (molec·cm^{-2}), at 10 K	Column densities (molec·cm^{-2}), at 170 K
760	H_2O	3.1×10^{-17}	torsion	0.18×10^{17}	0.14×10^{17}
980	NH_3	1.2×10^{-17}	NH wag	0	0.12×10^{17}
1194	NH_2OH	1.2×10^{-17}*	NH wag	0.59×10^{17}	0.26×10^{17}

*Adopted from the value of NH_3.

Through these column density calculations it is shown, that just after the deposition of the sample, the amount of NH_2OH is 3 times higher than that of H_2O, and while the concentration of H_2O decreases by only 20%, approximately 60% of NH_2OH have been decomposed from 10 to 170 K to form new reaction products. Among others reaction products, NH_3, which may be simply identified in our IR spectra, could be associated to the formation of O_2, a species, easier to distinguish with mass spectroscopy detection. In fact, although the nature of all the formed species in the NH_2OH thermal transformation will be argued in the discussion part, from the mass spectroscopy point of view, the observation of a very low mass signal of the desorbed NH_2OH at 180 K, in comparison with other desorbed species such as NH_3, HNO, H_2O and O_2, might also be a proof of hydroxylamine decomposition instead of its simple desorption.

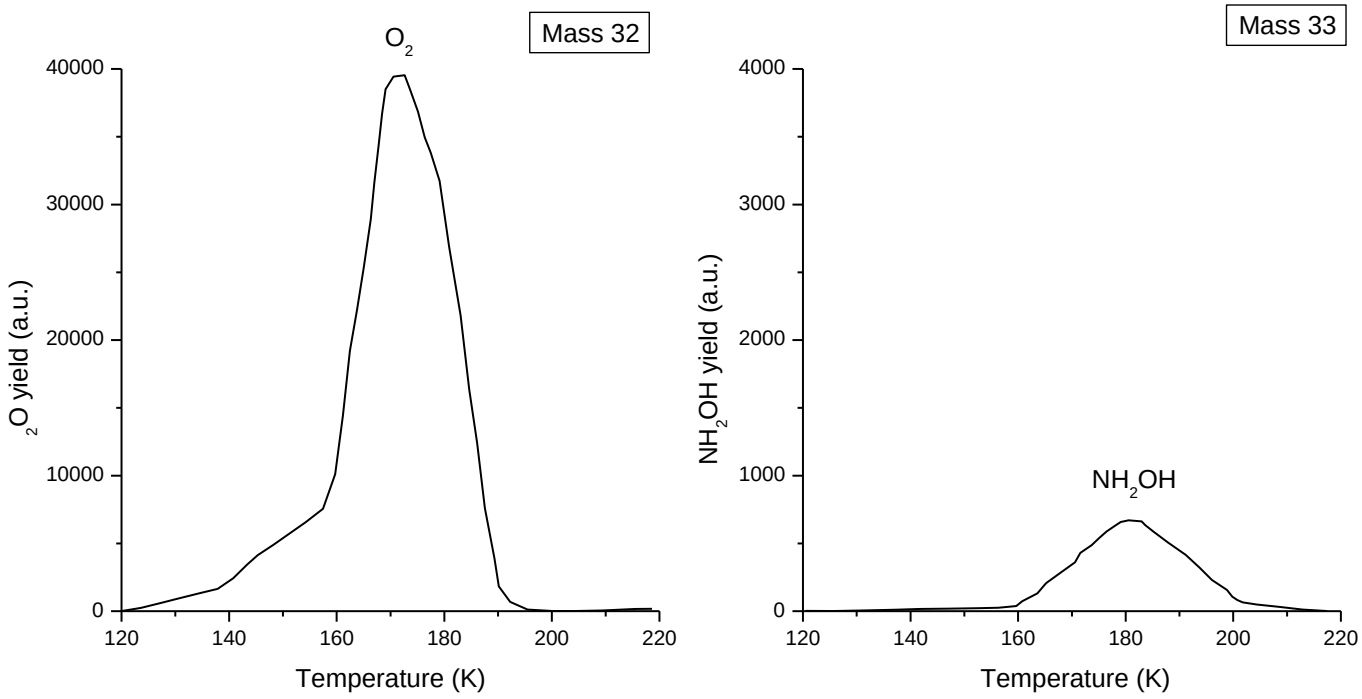

Figure IV-9. Mass evolution of desorbed O_2 and NH_2OH during the heating of NH_2OH–H_2O ice. Desorbed O_2 signal reaches a maximum at 170 K while that of NH2OH at 180 K.

As an example, figure IV-9 shows the evolution of desorbed NH_2OH versus O_2 abundances. NH_2OH and O_2 species start desorbing from the NH_2OH–H_2O refractory ice and reach highest desorption signals at 180 and 170 K, respectively. We show through this mass spectrum evolution that the signal due to the desorbed O_2 starts increasing at low temperature but not lower than 120 K which is consistent with the infrared measurements exposed in figure IV-6. The analysis of the hydroxylamine IR absorption bands illustrates that 15% of NH_2OH is transformed between 100 and 130 K and a clear IR signature of NH_3, one of the reaction products in the alteration of NH_2OH during the heating of the NH_2OH-H_2O ice, is obviously detected only at temperatures above 130 K. Similarly, the mass spectrum evolution of desorbed O_2 reveals that oxygen may be another reaction product in the thermal transformation of NH_2OH. It is important to note that, the mass signal of desorbed O_2 shown in figure IV-9 is almost 60 times higher than that of NH_2OH, while the NH_2OH–H_2O solid sample formed at 10 K contained simply NH_2OH and H_2O as primary reactants, with an amount of NH_2OH, 3 times higher than that of H_2O as seen in figure IV-1 where, for sure, there were no traces of O_2 during the sample deposition.

IV.6. Analysis of NH_2OH thermal transformation in H_2O ice

We show that even before reaching the desorption temperature of NH_2OH, hydroxylamine undergoes the chemical transformations leading to the formation of species such as NH_3 in addition to other species which may be only characterized by mass spectroscopy such as O_2. However some of the new detected absorption signals during the heating processing overlap with those of NH_2OH, as shown in figure IV-6 around 2800 and 1600 cm^{-1}, and this makes it impossible to separate the reactants, namely water and hydroxylamine from the new products. Thankfully, one of these new chemical products shows a strong and isolated spectral absorption band around 980 cm^{-1}, in the NH_3 vibration spectral region. To have a clear description of NH_2OH-H_2O reaction in solid phase at cryogenic temperatures lower than that of NH_2OH desorption, we try to explain the reaction pathways leading to a decomposition of hydroxylamine. Regarding such a molecule with N-H, N-O and O-H bounds, NH_2OH may decompose into several fragments depending on implemented reaction mechanisms and on the nature of the chemical bounds involved in such decomposition. Several theoretical investigations have been interested in the formation and decomposition reactions of hydroxylamine. According to Feller et al.[23] NH_2OH may react with water to form NH_3 and H_2O_2:

$$H_2O + NH_2OH \rightarrow NH_3 + H_2O_2 \qquad \text{(IV-2)}$$

The reaction is found to be exothermic, showing a heat of formation $\Delta H = -11\ kcal/mol$. Such a reaction may happen under our experimental conditions, as we have detected a very specific signal characteristic of ammonia, and then it might explain the low stability of hydroxylamine in contact with water at temperatures lower than that of hydroxylamine desorption. In this situation H_2O_2 may be considered as the other reaction product formed during the thermal decomposition of NH_2OH-H_2O ices. However, an accurate analysis of our infrared spectra show no characteristic signals related to H_2O_2. The absence H_2O_2 signals from our infrared spectra can be

understandable, as many investigations have already shown that H_2O_2 may decompose into H_2O + O.[24] The association of our experimental results and Feller's group calculations allows asserting that the thermal decomposition of NH_2OH-H_2O ices leads to the formation of ammonia and atomic oxygen as new reaction products. As, the reaction is occurring in solid phase at cryogenic temperatures, those oxygen atoms may complex with ammonia molecules or recombine to form molecular oxygen. In this case NH_2OH-H_2O heated system decompose into NH_3 + O_2 + H_2O, instead of desorption into NH_2OH + H_2O. The detection of NH_3 and O_2 under our experimental conditions would prove that H_2O + NH_2OH →NH_3 + H_2O_2 is one of the possible reaction mechanisms into the degradation of NH_2OH in contact with H_2O at cryogenic temperatures.

Similar calculations have been carried out to study the decomposition of NH_2OH aggregates and NH_2OH interacting with H_2O. Wang et al.[26] investigated a thermal decomposition of NH_2OH more deeply by varying the amount of reactants, namely NH_2OH and H_2O. They proposed a decomposition mechanism involving dimmers or aggregates of hydroxylamine. The association of two hydroxylamine lead to the formation of NH_3 and HNO as reaction products.

$$2NH_2OH \rightarrow H_2O + NH_3 + HNO \qquad \text{(IV-3)}$$

HNO molecule is characterized by three absorption signals at 2685, 1565 and 1500 cm^{-1} corresponding to NH stretching, NO stretching and HNO bending vibrational modes.[25] The formation of HNO as a new reaction product, in addition to ammonia, in the thermal decomposition of NH_2OH-H_2O may be possible as the analysis of our infrared spectra, exposed in figure IV-6, shows an increase of a signal around 2700 which may due to the NH stretching mode of HNO molecules, while that of NH_2OH is decreasing. However, contrary to ammonia molecules which can be easily characterized by a strong and isolated absorption band around 980 cm^{-1}, located far away from the NH_2OH absorption signals. In the spectral region between 1500 and 1600 cm^{-1}, even though the new appearing signal may be due to the two other vibrational modes of HNO, they overlap with NH_2OH signals and this makes it impossible to separate the reactants, namely water and hydroxylamine from the new probable product HNO.

Wang's group calculations show that NH_2OH dimmer lead to a decomposition of NH_2OH to form ammonia as one of reaction products. A decomposition of NH_2OH dimmer is consistent with our experimental condition where our solid samples were prepared using a direct condensation of pure NH_2OH favoring the formation of NH_2OH aggregates and also NH_2OH–H_2O clusters. However, our solid samples are ice mixtures of NH_2OH and H_2O as it is probably the case on the icy interstellar grains. In this situation what is the role of water molecules in those decomposition processes of NH_2OH? To answer this question, we should analyze in more detail the reaction of NH_2OH decomposition from formation and activation energies point of view. First hydroxylamine molecule undergoes isomerization into ammonia oxide:

$$NH_2OH \xrightarrow{50kcal/mol} NH_3O,\ \Delta H = +25\ kcal/mol \qquad \text{(IV-4)}$$

This reaction is highly endothermic, showing very high activation energy and it probably needs an initiating energy to convert NH_2OH into NH_3O. However by passing from monomolecular mechanism to bimolecular mechanism, more favorable in solid phase, the energy barrier decreases from 50 kcal/mol to 25 kcal/mol! and the energy formation of the conversion reaction from NH_2OH into NH_3O decreases from 25 kcal/mol to 15 kcal/mol. The decrease of both activation and formation energies shows that the reaction is more favorable with bimolecular mechanism.

$$2NH_2OH \xrightarrow{25kcal/mol} NH_3O + NH_2OH,\ \Delta H = +15kcal/mol \qquad \text{(IV-5)}$$

Wang et al limited its calculations to the isomeric conversion reaction for only one, two and three NH_2OH molecules.

$$2NH_2OH + NH_2OH \xrightarrow{20kcal/mol} NH_3O + 2NH_2OH,\ \Delta H = +10kcal/mol \qquad \text{(IV-6)}$$

Similarly, with three NH_2OH molecules the conversion mechanism leading to the formation of NH_3O confirms a decrease of both activation and formation energies showing that the reaction is more favorable in solid phase by increasing the NH_2OH aggregate size. From these calculations, we can imagine that by increasing the number of NH_2OH molecules, the activation energy might decrease to zero and the NH_2OH conversion reaction would become probably exothermic and then feasible. In such a context, calculations are highly needed to validate or invalidate conclusion like this.

As under our experimental conditions we showed a transformation of NH_2OH into ammonia molecules or ammonia complexed with other species, it is important to analyze the role played by water molecules in those decomposition or transformations processes of NH_2OH. In fact it was shown in the Table IV-3, that when 60% of NH_2OH decompose between 10 and 170 K to form new reaction products, concentration of H_2O also decreases by 20%, showing that water molecules may also play a role in NH_2OH transformations. In this context Wang et al.[26] investigated the influence of the number of water molecules into the NH_2OH transformation reaction:

$$2NH_2OH + H_2O \xrightarrow{21kcal/mol} NH_3O + NH_2OH + H_2O,\ \Delta H = +13kcal/mol \qquad \text{(IV-7)}$$

By comparing reactions involving three NH_2OH molecules to that obtained by substituting one of three NH_2OH molecules by one H_2O molecule, we see that the NH_2OH conversion into NH_3O occurs slightly under the same energetic condition. Both of the reactions are endothermic with almost the same activation energy, around 20 kcal/mol. However by

increasing the number of water molecules the NH_2OH conversion into NH_3O become more favorable showing a considerable decrease of the energy barrier.

$$2NH_2OH + 2H_2O \xrightarrow{18kcal/mol} NH_3O + NH_2OH + 2H_2O,\ \Delta H = +7kcal/mol \quad \text{(IV-8)}$$

$$2NH_2OH + 3H_2O \xrightarrow{16kcal/mol} NH_3O + NH_2OH + 3H_2O,\ \Delta H = +4kcal/mol \quad \text{(IV-9)}$$

Wang et al limited these calculations to three water molecules and two hydroxylamine molecules. They showed that the NH_2OH isomeric conversion into NH_3O show a high energy barrier, around 50 kcal/mol and a high energy reaction, around 25 kcal/mol. Such a situation is more probable in a gas phase, or in a diluted water-free environment where NH_2OH molecule should be stable. By solvating a NH_2OH molecules into spherical solvation NH_3OH-$(H_2O)_3$, NH_2OH isomeric conversion into NH_3O shows a considerable decrease of both energy barrier, going from 50 to 16 kcal/mol, and energy formation going from 25 to 4 kcal/mol. In this way the increasing of water molecules will increase the spherical solvation NH_3OH-$(H_2O)_n$ and would probably transform the NH_2OH isomeric conversion into NH_3O reaction into a barrierless exothermic process.

NH_2OH conversion into NH_3O, is very consistent with our results showing a transformation of NH_2OH-H_2O ices before we reach the NH_2OH desorption temperature, in solid samples where aggregates $(NH_2OH)_m$-$(H_2O)_n$ are easily formed during the deposition and the heating of NH_2OH-H_2O ices. Wang et al.[26] show that, since ammonia oxide is less stable than hydroxylamine further reactions may occur, leading to a decomposition of NH_3O into HNO and H_2.

$$NH_3O \rightarrow HNO + H_2 \quad \text{(IV-10)}$$

Also, Wang et al.[27] show that ammonia oxide NH_3O may decompose in contact with water or hydrogen leading to the formation of ammonia and hydrogen peroxide as new reaction products in the transformation of NH_2OH. However, some studies have shown that hydrogen peroxide is not stable[24] and this could be the reason, why no traces of H_2O_2 have been detected under our experimental conditions.

$$NH_3O + H_2O \rightarrow H_2O_2 + NH_3 \quad \text{(IV-11)}$$

$$NH_3O + H_2 \rightarrow H_2O + NH_3 \quad \text{(IV-12)}$$

$$2H_2O_2 \rightarrow 2H_2O + O_2 \quad \text{(IV-13)}$$

The association of our experimental results and those calculations allows affirming that the heating of NH_2OH-H_2O ices lead to a decomposition of NH_2OH before reaching it's desorption temperature. From a theoretical point of view the decomposition of NH_2OH reaction pathway passes through an isomerisation process leading to the formation of a less stable

ammonia oxide NH_3O, which may decompose and lead to several final reaction products, namely, HNO, NH_3, O_2 and H_2. Those NH_2OH transformations are more favorable with in the presence of aggregates of water. A situation, similar to our experimental condition, where the heating of NH_2OH-H_2O ices leads to a decrease of NH_2OH signal and an increase new signals. As mentioned earlier, among those new signals, the most important one is that strong and isolated signal located at 980 cm^{-1} in the NH_3 vibration spectral region and it may be due to NH_3 molecules as well as to NH_3O. The latter species has never been detected experimentally. However even though the other new signals overlap with the NH_2OH absorption bands and we are able to associate the final reaction products predicted with the theory and those detected experimentally, namely, HNO, O_2 and H_2. For the HNO molecules, as mentioned above the increase of an absorption band near the NH spectral region may be a confirmation of the HNO formation through a heating of NH_2OH-H_2O ices. The two other vibrational modes of HNO as well as O_2 vibration absorb in the spectral region between 1500 and 1600 cm^{-1},[28] where we clearly see the appearance of new signals overlapping with the decreasing NH_2OH signals and this may show the good agreement between our experimental results and these two theoretical investigations.

IV.7. Conclusions

NH_2OH a simple chemical species which probably plays an important role in the molecular complexity of the universe and it can still be considered as a main precursor of amino acids even if NH_2OH is not yet detected in space. This experimental study was carried out to form samples of NH_2OH ices similar to that of found in interstellar medium. The non-detection of hydroxylamine in gas phase within any of the explored astronomical sources could mainly be due to its high reactivity in solid phase on the icy interstellar grains. The experimental results show clearly that the chemical transformation of NH_2OH occurring in the solid phase at relatively lower temperatures before the desorption processes of NH_2OH from the mantle of interstellar icy grains might be the main cause of the very low abundance of hydroxylamine in space and then it might explain its non-detection. The evolution of NH_2OH molecule, via a thermal chemistry during the desorption of NH_2OH-H_2O ices in the temperature range of 10-200K, allow the characterization of NH_2OH stability using infrared spectroscopic analysis and the temperature-programmed desorption. Knowing that the NH_2OH desorption temperatures range from 160 to 190K, it was showed, through this study, there is a competition between NH_2OH desorption into the gas phase and its chemical transformation in the solid sample, occurring at relatively lower temperature and leading to the formation of HNO, NH_3 and O_2. This is the first infrared spectroscopic experimental study probing at different temperatures an ice formed directly condensing NH_2OH molecules. From these experimental results, it was proved that the chemical transformation of NH_2OH starts occurring in solid phase at 130K, a temperature far lower than that of NH_2OH desorption and this may reduce considerably the abundance of NH_2OH molecules releasing in the gas phase. We also show that this NH_2OH chemical transformation is due mainly

to the presence of high amount H_2O and NH_2OH aggregates. Finally, these results might be the primary reasons to the non-detectability of hydroxylamine in space.

Bibliography

1 Nishi N., Shinohara H., Okuyama T., 1984. J. Chem. Phys., 80, 3898.
2 Zheng W., Kaiser R. I., 2010. J. Phys. Chem. A, 114, 5251.
3 Strazzulla G., Palumbo M. E., 1998. Planet. Space Sci., 46, 1339.
4 Congiu E. et al., 2012. ApJ, 750, L12.
5 He J., Vidali G., Lemaire J. L., Garrod R. T., 2015. ApJ, 799, 49.
6 Mousavipour S. H., Pirhadi F., HabibAgahi A., 2009. J. Phys. Chem. A, 113, 12961.
7 Mousavipour S. H., Pirhadi F., Ramazani S., 2014. Phys. Chem. Res., 2, 53.
8 Wang L., Mebel A. M., Yang X., Wang X., 2004. J. Phys. Chem. A, 108, 11644.
9 Pulliam R. L., McGuire B. A., Remijan A. J., 2012. ApJ, 751, 1.
10 McGuire B. A. et al., 2015. ApJ, 812, 76
11 H. Koseki, M. Tamura. Explosion and fire of highly-concentrated hydroxylamine at a re-distillation unit, 2010. Japan Science and Technology Agency.
12 https://pubchem.ncbi.nlm.nih.gov
13 http://webbook.nist.gov
14 R. Withnall, L. Andrews, 1988. J. Phys. Chem., 92, 2155.
15 D. Luckhaus, 1997. J. Chem. Phys., 106, 8409.
16 Fedoseev G., Ioppolo S., Zhao D., Lamberts T., Linnartz H., 2015. MNRAS, 446, 439.
17 Collings M. P., Anderson M. A., Chen R., Dever J. W., Viti S., Williams D. A., McCoustra M. R. S., 2004. MNRAS, 354, 1133.
18 Zheng W., Jewitt D., Kaiser R. I., 2006. ApJ,639, 534.
19 Brown W. A., Bolina A. S., 2007. MNRAS, 374, 1006.
20 Martín-Doménech R., Muñoz Caro G. M., Bueno J., Goesmann F., 2014. A&A, 564, A8.
21 Gerakines P. A., Schutte W. A., Greenberg J. M., van Dishoeck E. F., 1995. A&A, 296, 810.
22 Richey C. R., Gerakines P. A., 2012. ApJ, 759, 74.
23 Feller D., Dixon D. A., 2003. J. Phys. Chem. A, 107, 10419.
24 Giguère P. A., Liu I. D., 1957. Can. J. Chem., 35, 283.
25 Clough P. N., Thrush B. A., Ramsey D. A., Stamper J. G., 1973. Chem. Phys. Lett., 23, 155.
26 Wang Q., Wei C., P´erez L. M., Rogers W. J., Hall M. B., Mannan M. S., 2010. J. Phys. Chem. A, 114, 9262.
27 Wang Q., Mannan M. S., 2010. J. Chem. Eng. Data, 55, 5128.
28 Bennett C. J., Kaiser R. I., 2005. ApJ, 635, 1362.
29 Richey C. R., Gerakines P. A., 2012. ApJ, 759, 74.

Chapter V:

Photochemistry of CH_4-H_2O ice

Similar experiments to those performed for the chemistry of the ammonia-water ices we have investigated the photochemistry of solid methane. This chapter is devoted to the photodecompositions of the most simplistic saturated molecule of carbon – methane (CH_4) and also to determine the catalytic effect of water in such processes. The study starts by showing the difference between the photolysis of methane trapped in neon matrix and a photolysis of tiny pure CH_4 ices vs bulk methane ices. Methane ices have been formed by including different amounts of water molecules in order to investigate the nature and yields of the photoproducts as a function of [H_2O]. We will expose through this study the difficulties of detecting large complex molecules both by IR and mass spectroscopy observations and how we managed their characterizations.

V.1. Earlier studies and motivation

Following the work already done with ammonia, the similar experiments were carried out with methane. Even though methane is most simplistic saturated molecule based on carbon it is not that much abundant in space (ranging around 1-5% in CO environments and 0.5-2% in H_2O rich ices).[1,2] This means that CO is the most abundant molecule in space based on the carbon atom and not the saturated equivalent – methane. Similarly to the highly abundant CO molecules which can form large variety of species (Chapter I.4.2, Figure I-4, page 14) through interactions involving C, N and H atoms,[3] methane molecules might be the origin of large complex molecules in space such as C_2H_6, C_2H_4, C_2H_2 and also CH_3OH, CH_3CH_2CHO... In this context many laboratory studies have been focused on energetic and non-energetic processing of methane ices in order to determine the molecular complexity induced by reactions involving CH_4. Many of these laboratory studies[5-9] have already shown that bombardments of interstellar ice analogs containing water/methane mixtures by ionizing radiation involving either photons or charged particles lead mainly to the same reaction products: carbon monoxide (CO), carbon dioxide (CO_2), formaldehyde (H_2CO), methanol (CH_3OH), ethane (C_2H_6), ethanol (C_2H_5OH)... Very recently Bergantini et al.[10] have suggested the formation of two C_2H_6O isomers: ethanol (C_2H_5OH) and dimethyl ether (CH_3OCH_3). All of these molecules are detected in the interstellar medium suggesting the reactions between methane and water even at a low abundance of methane. All of these molecules can be included to form more complex molecules detected in the ISM, such as isomers of methyl acetate (CH_3COOCH_3) and ethyl formate (C_2H_5OCHO)[11] or glycolaldehyde ($HOCH_2CHO$).[12] The more complex molecules are found around the hot cores comprising of temperatures higher than 150K. Even though, it is suggested that such species are formed on interstellar grains in cold clouds with ranging temperatures around 10K followed by UV or thermal gas phase injections in star forming regions.[12]

While these laboratory studies provide significant data correlating to observations, all these experiments were performed in samples dominated with high quantity of water. Strangely no groups have performed any experiments related to irradiation of methane with addition of low water abundance to study the impact of formation of water photofragments on methane-water ices. The suggested scheme should be similar to what has been discussed in Chapter III.

Interaction of methane with hydroxyl radical should in term increase the production of methyl radical: $CH_4 + OH \rightarrow CH_3 + H_2O$. Unlike with ammonia with nitrogen atoms, the creation of CH_3 radicals can be the key in the creation of larger carbonic chains. Wu et al.[13] have studied photolysis of methane dispersed in solid neon and showed the possible formation of carbonic chains up to five carbon atoms using a vacuum-ultraviolet light from a synchrotron. Later on following the same work Lin et al.[14] performed similar work showing the formation of carbon chains up to 20 carbon atoms and other various hydrocarbon radicals.

All things considered this study focuses on the laboratory ice analogs of methane-water ices to highlight the influence of water molecules in photo-induced reactions in solid phase at cryogenic temperatures. The rare gas matrix isolation technique was performed to express the difference between low concentration and bulk methane-water ice compositions. Later on the samples were heated to observe the desorption of different formed species though infrared and mass spectroscopy.

V.2. Sample formation and identification of photoproducts

Methane is a tetrahedral molecule with four equivalent C–H bonds. Its electronic structure is described by four bonding molecular orbitals resulting from the overlap of the valence orbitals on C and H. Since methane consists of 5 atoms, this would give methane 3 * 5 – 6 = 9 fundamental modes of vibration. Due to the symmetry of methane molecule, 5 modes are degenerate. Of those 4 fundamental modes only ν_4 and ν_3 are IR active. Also methane does not have a dipole moment (0 D), making it non-polar molecule unlike ammonia and water. Because of this fact, the registered IR spectra of CH_4 matrix isolated and solid methane should be very similar.

Similarly as in the experiment with ammonia, the neon matrix isolation experiment can help to trap and stabilize the reactive intermediates and photoproducts. To assure the statement that the IR spectra of CH_4 matrix isolated and solid methane samples should be similar, two experiments were carried out. As previously the depositions were performed in a high vacuum chamber at 10^{-10} mbar on a cold sample mirror. The infrared spectra of the samples were recorded in transmission – reflection mode and all the experiments have been carried out at the lowest temperature reached with our experimental setup, 3K. The CH_4:Ne matrix was formed with a ratio of 2:1000 (total amount of CH_4:Ne deposited, during 30min, is 140mbar which include only 0.28mbar of CH_4), while solid CH_4 sample consists of a deposition of 2mbar of methane gas, during 20s. Both recoded IR spectra are shown in figure V-1 and both spectra are very alike. They consist of two main methane bands ν_4 at 1301 cm^{-1} and ν_3 at 3012 cm^{-1}. Also both spectra consist of several overtone bands, all the vibrational assignments are found in table V-1. Due to the high concentration in methane ice (10 times more) in comparison with the amount of CH_4 isolated in neon matrix many bands are detected exclusively in the methane ice IR spectra. Some of these observed bands are even IR inactive such as the absorption bands located at 1530 and 2906 cm^{-1} and attributed to ν_2 and ν_1 vibrational modes. While the other detected bands are only

due to the combination and overtone modes absorbing at 2593, 3845 and 4529 cm^{-1}. The assignments of CH_4 IR signals detected under our experimental conditions have been carried out, based on Ulenikov et al.[15] methane gas phase investigations.

Table V-1. Vibrational assignments of methane.

Assignment of CH_4	Position (cm^{-1})
ν_4	1301
ν_2	1530
$2\nu_4$	2593
$\nu_2 + \nu_4$	2816
ν_1	2906
ν_3	3012
$3\nu_4$	3845
$\nu_2 + 2\nu_4$	4114
$\nu_1 + \nu_4$	4201
$\nu_3 + \nu_4$	4301
$\nu_2 + \nu_3$	4529

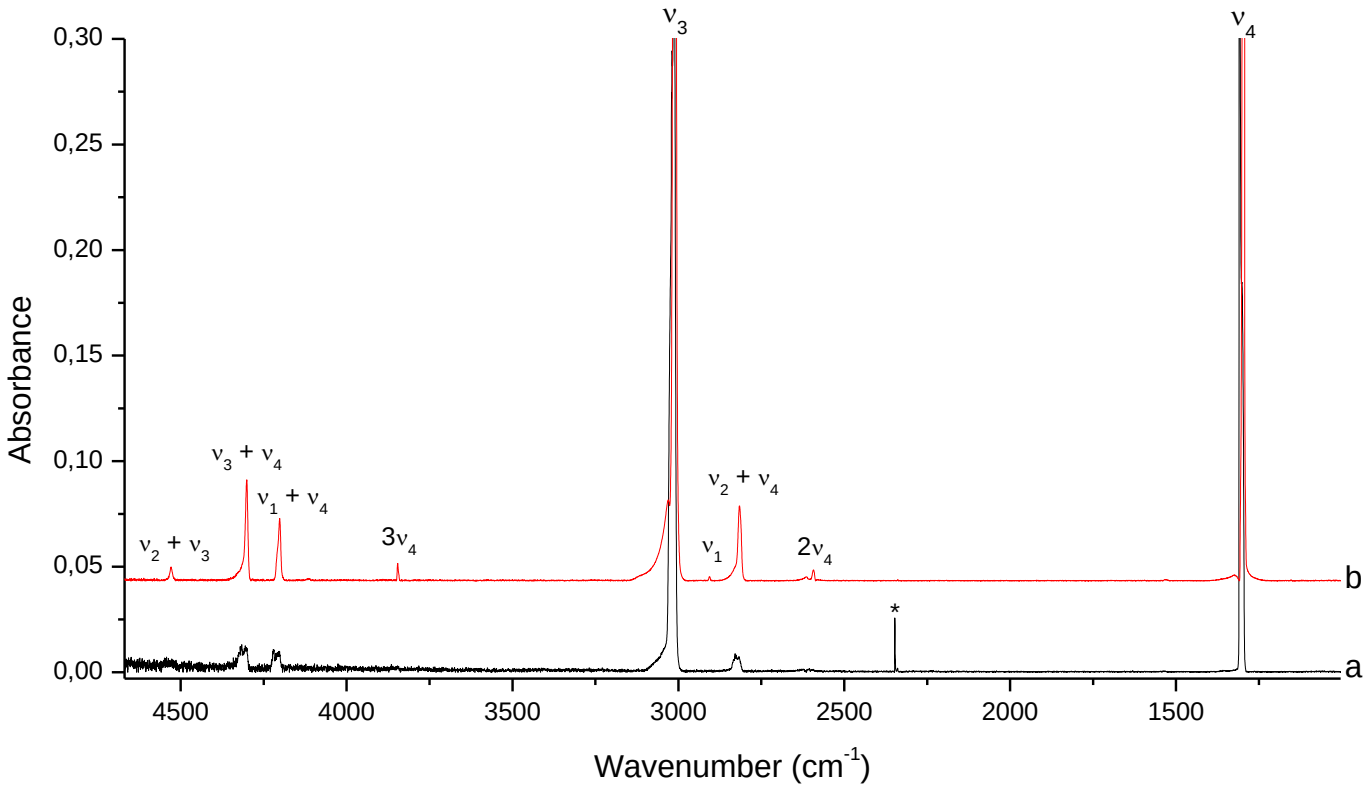

Figure V-1. IR spectra of a) CH_4 isolated in neon matrix and b) solid CH_4. * - band of CO_2 in neon matrix

As mentioned in the chapter III the photolysis of our samples have been investigated using the VUV lamp (outputs of 30% at 121 nm ~10.3 eV and 100% at 160 nm ~7.7 eV). In order to assist the different photofragments from methane decomposition we have used the experimental results of Gans et al.[16] who studied the photolysis of CH_4 in gas phase at 121 nm and listed different dissociation channels:

$h\nu + CH_4 \rightarrow CH_3(X^2 A_2'') + H$ $\Delta H = 4.47eV$ (V-1)

$h\nu + CH_4 \rightarrow CH_2(a^1 A_1) + H_2$ $\Delta H = 5.01eV$ (V-2)

$h\nu + CH_4 \rightarrow CH_2(b^1 B_1) + H_2$ $\Delta H = 6.04eV$ (V-3)

$h\nu + CH_4 \rightarrow CH_2(X^3 B_1) + 2H$ $\Delta H = 9.14eV$ (V-4)

$h\nu + CH_4 \rightarrow CH_2(a^1 A_1) + 2H$ $\Delta H = 9.53eV$ (V-5)

$h\nu + CH_4 \rightarrow CH(X^2 \Pi) + H + H_2$ $\Delta H = 9.06eV$ (V-6)

$h\nu + CH_4 \rightarrow C(^1D)$ $\Delta H = 9.27eV$ (V-7)

From this gas phase study it has been shown that the highest quantum yields are due mainly to the formation of CH_3 (42%) and CH_2 (48%) derived directly from the first 2 reactions. All these thermodynamic thresholds are provided in the gas phase, so the binding energy might be higher in a low temperature solid phase of CH_4. Even taken into consideration a rough increase of energies about ~1.5eV, we can see that the first three reactions leading to the formation of CH_3 and CH_2 are still very probable under our experimental conditions.

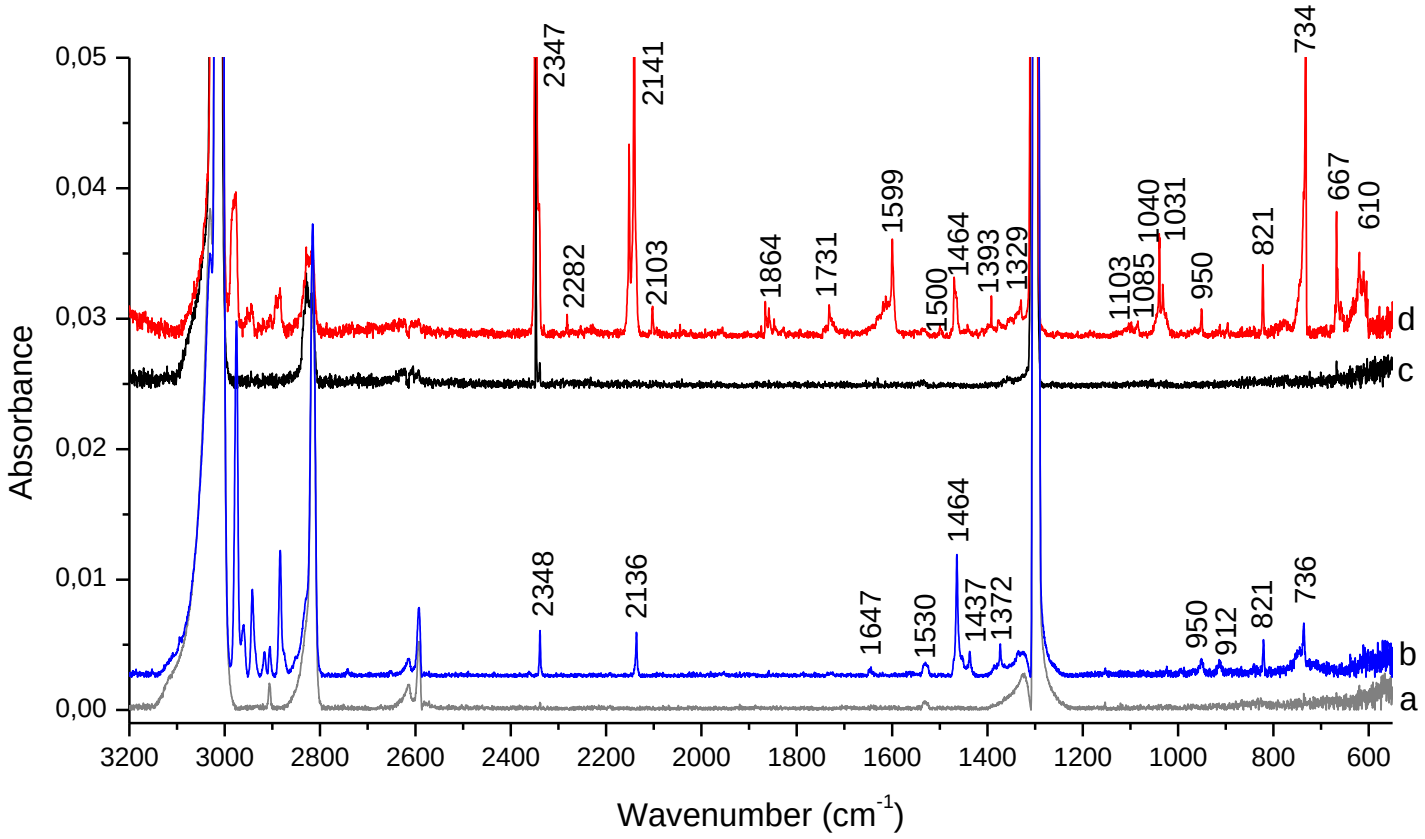

Figure V-2. IR spectra of: a) Solid CH_4 ice before photolysis; b) Solid CH_4 ice after photolysis; c) matrix isolated CH_4 before photolysis; d) matrix isolated CH_4 after photolysis

Figure V-2 shows the comparison of photoproducts formed in CH_4 ice and in neon matrix containing CH_4. The assignments of the observed photoproducts are listed in table V-2. The most obvious direct photoproducts observed are CH_3, C_2H_2, C_2H_4 and C_2H_6, which are derived from the direct recombination of the reaction products. Even if the concentration of methane is very high in the methane ice in comparison with the amount of CH_4 trapped in neon matrix, many chemical species have been detected only in neon matrix showing the efficiency of the photochemistry of methane molecules embedded in solid neon in comparison with that occurring in pure methane ice. This can be also due to the thickness of the sample. In fact, with the matrix isolation, 140mbar of Ne/CH_4 have been deposited while the methane ice sample has been formed by a deposition of only 2mbar of methane gas. Consequently the methane ice is not bulky enough to trap efficiently radical species, which is not the case for the neon matrix where many products and reaction intermediates can be formed and stabilized in a neutral cage formed by neon atoms. CO and CO_2 are current impurities in photochemistry experiments. These two species can be the source of much oxygen bearing species which concentrations depend strongly on [CO] and [CO_2] in the sample. From figure V-2d we notice that photolysis in neon matrix lead to the formation and efficient trapping of huge amounts of CO and CO_2. Consequently species such as HCO, H2CO, H2O, HO2 and CH3OH are clearly detectable in neon matrix in comparison with experiment carried in methane ice where small amount of CO and CO_2 have been detected. Table V-2 lists the spectral positions of all the photo reaction products obtained in neon matrix and in methane ice. We notice that 14 photoproducts have been detected in neon matrix where 10 of them are oxygen bearing molecules. While, in methane ice, only 7 photoproducts including 4 oxygen bearing chemical species have been observed: CO, CO_2, H_2O and CH_3OH.

Table V-2. Vibrational assignments of methane photoproducts in CH_4 ice and CH_4/Ne matrix samples.

Assignment	Matrix	Ice	References
CH_3	610	-	Lin et al.[14]
CO_2	667	-	Nxumalo et al.[18]
C_2H_2	732	736	Lin et al.[14]
C_2H_6	822	821	Lin et al.[14]
C_2H_4	950	950	Lin et al.[14]
Alcs :	1031	1024	Han et al.[19] Coussan et al.[20]
CH_3OH	1040	-	
CH_3CH_2OH	1085	-	
HO_2	1103	-	Milligan et al. [21]
?	1329	-	
HO_2	1391	-	Milligan et al. [21]
C_2H_6	-	1373	Lin et al.[14]
C_2H_4	-	1437	Lin et al.[14]
C_2H_6/Alcs	1469	1464	Lin et al.[14]
H_2CO	1499	-	Khoshkhoo et al.[22]
H_2O	1599	1644	Forney et al.[24]
H_2CO	1731	-	Khoshkhoo et al.[22]
HCO	1858	-	Ewing et al.[23]
^{13}CO	2103	-	Leroi et al.[17]
CO	2141	2136	Leroi et al.[17]
$^{13}CO_2$	2282	-	Nxumalo et al.[18]
CO_2	2347	2338	Nxumalo et al.[18]

Ethane C_2H_6 is the most expected molecule to be observed due to the recombination of methyl radical: $CH_3 + CH_3 \rightarrow C_2H_6$. Unsaturated equivalents of ethane: ethylene C_2H_4 and acetylene C_2H_2 can be formed in at least two ways. They can be formed though the subsequent irradiation with photons:

$$C_2H_6 + h\nu \rightarrow C_2H_4 + H_2; \quad \text{(V-8)}$$

$$C_2H_6 + h\nu \rightarrow C_2H_2 + 2H_2; \quad \text{(V-9)}$$

$$C_2H_4 + h\nu \rightarrow C_2H_2 + H_2, \quad \text{(V-10)}$$

or they can be formed though the recombination of their respective radicals:

$$CH_2 + CH_2 \rightarrow C_2H_4; \quad \text{(V-11)}$$

$$CH + CH \rightarrow C_2H_2. \quad \text{(V-12)}$$

It is hard to validate the recombination pathway, due to the fact that the radicals CH_2 and CH are hardly detectable in IR spectra and not observed in this case, even though it cannot be discarded. While on the other hand, the photo-irradiation pathway is more probable and would also explain the low quantities of C_2H_4 found in solid sample, due to the fact that is was converted into acetylene C_2H_2 which was found in similar quantities as C_2H_6.

Another more interesting spectral region is the CH stretching region between 3100 and 2800 cm^{-1}. The zoom of this region is shown in figure V-3 for both matrix and ice samples before and after the irradiation. While matrix isolation is good to trap radical species, the solid sample in this case shows more information specifically for the CH IR signal which may be due to not only to the species discussed earlier, namely C_2H_2, C_2H_4 and C_2H_6.

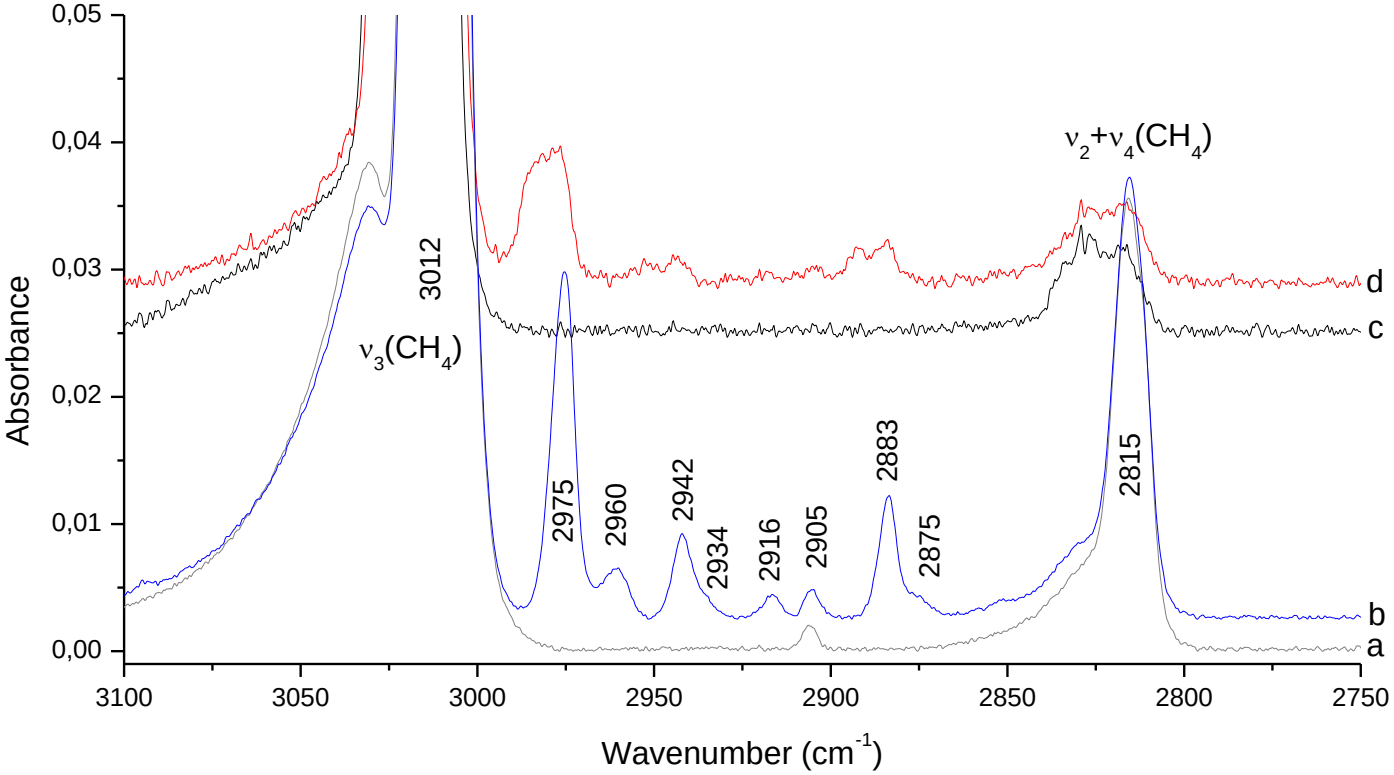

Figure V-3. IR spectra of CH stretching region between 3100 and 2800 cm^{-1}: a) Solid CH_4 ice before photolysis; b) Solid CH_4 ice after photolysis; c) matrix isolated CH_4 before photolysis; d) matrix isolated CH_4 after photolysis

In fact, many signals appearing after the UV bombardments of pure methane ice and shown in figure V-3 correspond to CH stretching of many saturated alkanes. The CH signal due to CH_4 is detected at 2905 cm^{-1} and observed both before and after the photolysis of the sample. Three signals at 2975, 2942 and 2883 cm^{-1} can be easily assigned to C_2H_6 as they have the same behavior as the IR signals attributed to C_2H_6, measured in the bending region lower than 1500 cm-1 and listed in table V-2. In order to assign the other new signals, the IR spectrum of methane ice after photolysis is compared to the IR signatures of three saturated alkanes, CH_4, C_2H_6, C_3H_8 and shown in figure V-4.

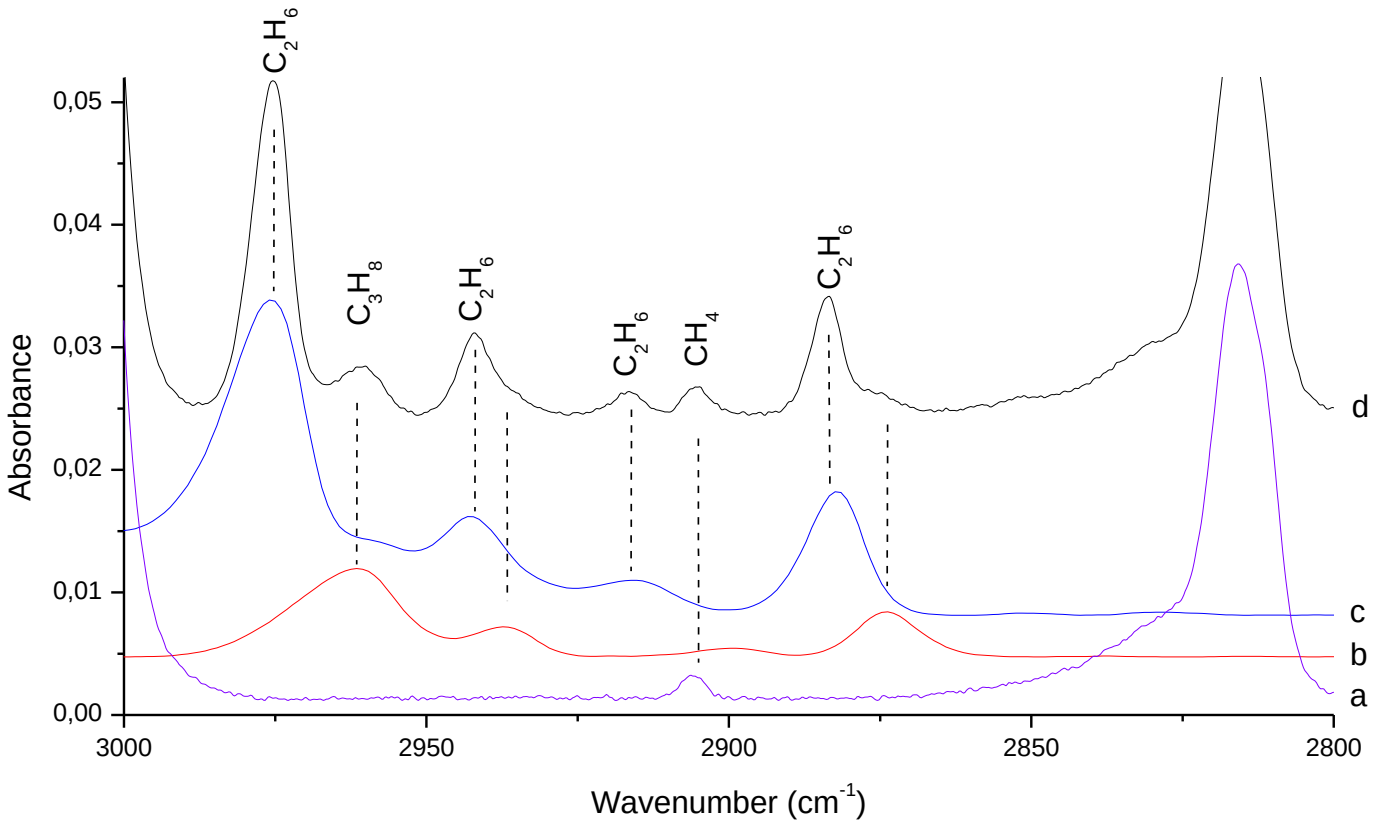

Figure V-4. IR spectra comparison in CH stretching region between 3100 and 2800 cm^{-1}: a) CH_4 ice; b) C_3H_8 ice; c) C_2H_6 ice; d) CH_4 ice after photolysis

From figure V-4 we notice that in addition to the formation of C_2H_6 which has already been confirmed by analyzing the CH bending region of irradiated methane ice, at least another a new reaction product is also formed and correspond to the C_3H_8 photoproduct, characterized by 3 absorption bands at 2960, 2934 and 2875 cm^{-1}. It should be underlined that all saturated alkanes larger than C_2H_6 such as C_3H_8 and C_4H_{10} have the same absorption bands with very close spectral positions. The UV lamp used in this experimental setup is efficient enough to form at least the propane C_3H_8 molecule and probably other alkanes larger C_3H_8 which infrared signals may be hidden by absorption signals of C_2H_6 and C_3H_8. Table V-3 compare the new infrared signals obtained after the methane photolysis to the IR signals of 4 alkanes, namely CH_4, C_2H_6, C_3H_8 and C_4H_{10}. The spectrum of the formed species in the solid sample is compared to a three basic solid alkanes spectra (figure V-4).

Table V-3. Vibrational assignments of alkanes.

Detected bands, cm^{-1}	CH_4	C_2H_6	C_3H_8	C_4H_{10}
3012	3012	-	-	-
2975	-	2975	-	-
2960	-	-	2961	2961
2942	-	2942	-	-
2934	-	-	2934	2927
2916	-	2914	-	-
2905	2905	-	2898	-
2883	-	2882	-	-
2875	-	-	2873	2873, 2860
2815	2815	-	-	-

We show in this section that the photolysis of methane lead mainly to the formation of saturated and unsaturated alkanes: CH_4, CH_3, C_2H_6, C_3H_8, C_2H_4 and C_2H_2. The formation of oxygen bearing species is due to the impurities and amplified in neon matrix. In the case of methane ice photolysis very small amounts of CH_3OH and H_2O have been detected. We think that CH_3OH could be mainly due to the presence of traces of water not even detectable in the spectra of pure methane ice. In order to investigate the influence of water molecule on the photolysis of methane ice we have preferred to add small amount of H_2O into methane ice sample and analyze the photoreaction products.

V.3. Photolysis of methane-water ice

As noted before the CH_4 is a non-polar molecule. Because of this, there is a possibility to trap the reactive species in ice similarly like neon matrix using a bulk CH_4 ice. Having this in mind another series of experiments was performed with increased deposited amount of methane increased by 10 times and adding water. Figure V-5 shows the deposited CH_4 ice (~19.4mbar) before and after photolysis with the ice containing the additional 0.1% of water.

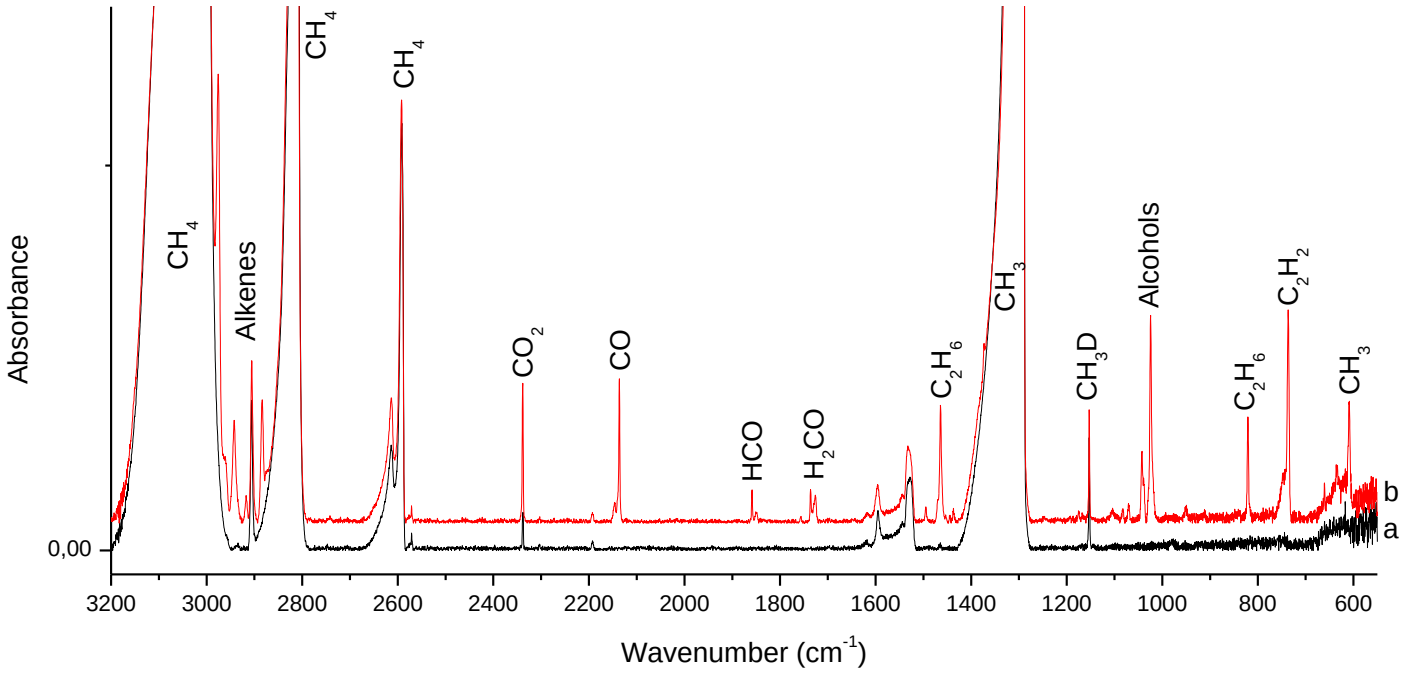

Figure V-5. IR spectra of bulk CH_4 ice a) before and b) after photolysis

Apart the widening of the main methane bands due to the higher concentration, detected formed species in the photolysis spectrum are the same found trapped in neon matrix, such as formaldehyde, alcohols and radical species like CH_3 and HCO. This proves that all the oxygen bearing species derive from methane are really due to the presence of water in the sample. To confirm this hypothesis we have investigated the photolysis of two different ices containing the same amount of methane with different amount of water.

V.3.1. Photolysis of methane-water ice: effect of water concentrations

While this study is to see the impact of the water in the photolysis of CH_4 ices, another sample was created with additional water and the same amount of methane. In this sample methane molecules form a crystal where water molecules are entrapped in it. Through this methane matrix isolation we can distinguish the formation of many hydrated complexes such as $(H_2O)_x$ where x = 1-6. All these complexes absorb in the same spectra region for the bending mode around 1600 cm^{-1}, but they have their characteristic spectral positions in the OH stretching region. Figure V-6 shows the spectral positions of these complexes ranging from 3800 to 3100 cm^{-1}. The formation of water clusters in CH_4 matrix is in good agreement with the studies carried out by Yamakawa et al.[25] We notice that adding 0.1% of water in the methane matrix allows the isolation of only water monomers and by increasing the amount of water to by only 2% we favor the formation of water aggregates as shown in figure V-6. In addition to the formation of the water complexes, the increasing of water in the methane matrix lead to an increase of IR intensities of the two inactive vibrational modes located at 2906 and 1530 cm^{-1} while all the other absorption bands of methane have the same IR intensities, as shown in figure V-6. The IR

spectrum containing high amount of water can also be characterized by a huge and wide signal in the 800 – 600 cm^{-1} region which correspond to the water aggregate libration.

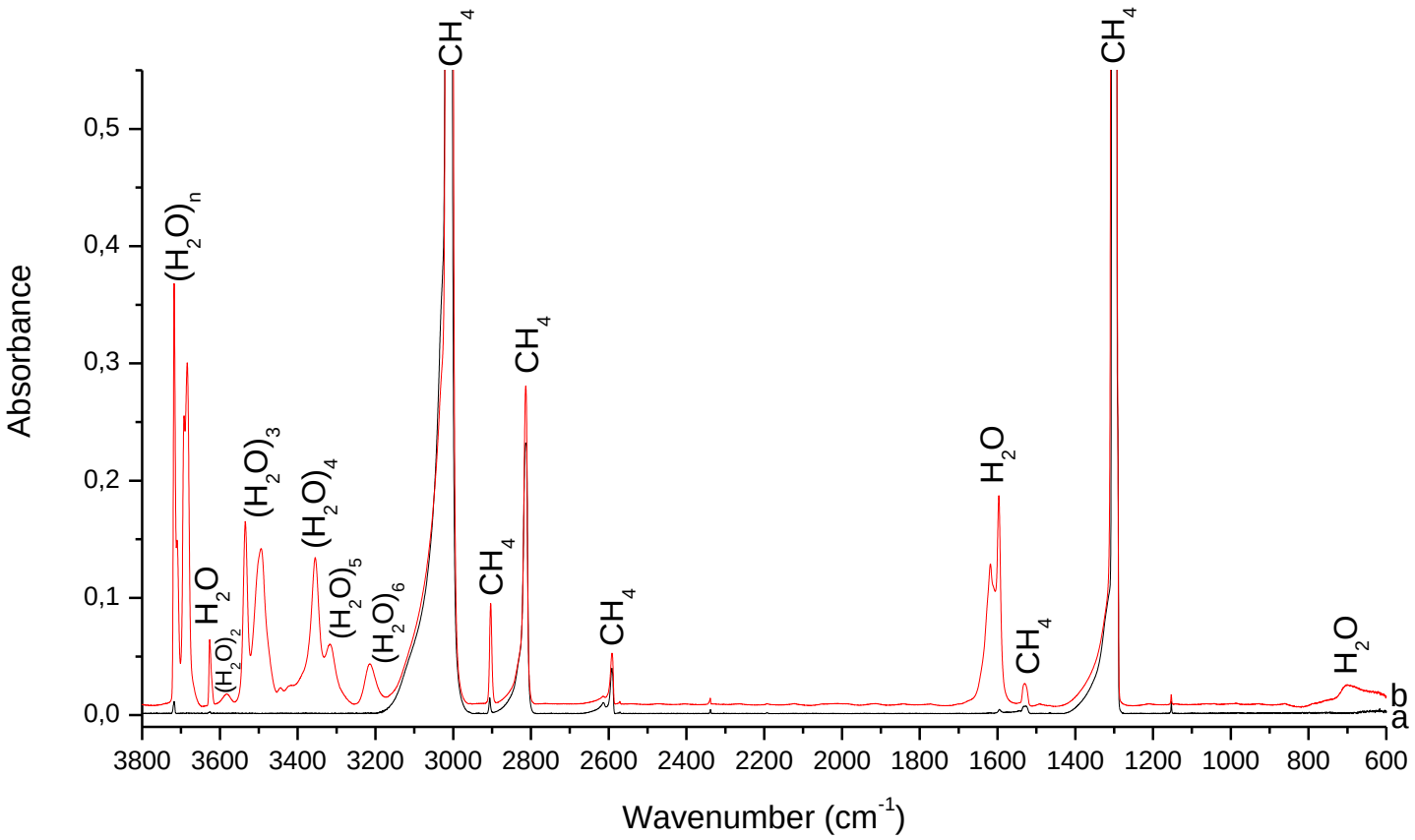

Figure V-6. IR spectra of CH_4 ice with a) additional 0.1% and b) 2% of water

The influence of water in the photolysis of methane ice is shown in figure V-7 where it is exposed the IR spectra of methane ice containing 0.1% of water before and after the photolysis in addition to the spectrum of the irradiated water-methane ice with 2% of water.

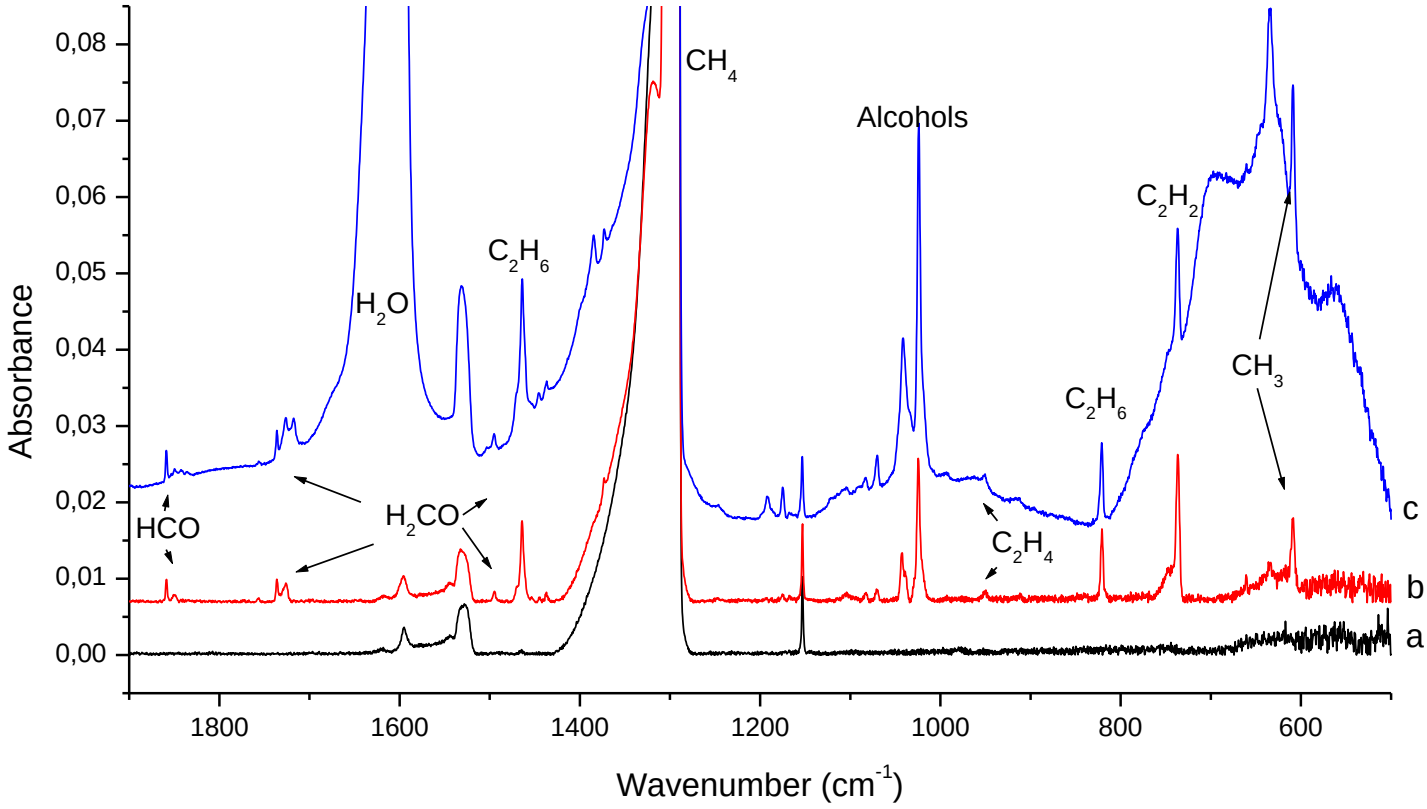

Figure V-7. IR spectra of CH_4 ice: a) with additional 0.1% before photolysis; b) after photolysis; c) after photolysis with additional 2% of water

From figure V-7c we notice that the appearance of the bulk water ice libration mode in the 800 – 600 cm^{-1} region makes comparison of the methane photoproducts much more difficult when the amount of water is varying. However, it is possible to admit that C_2H_6 and C_2H_2 are slightly formed with the same efficiency whatever is the concentration of water. On the other side, the amount of CH_3 (610 cm^{-1}) radical and alcohols (1025 cm^{-1}) depend strongly on the amount of water in the sample and they seem to be formed efficiently in water rich samples.

For samples containing the same amount of methane the CH_3 formation is more efficient when the amount of water increases from 0.1% to 2%. This shows that water molecules may play a kinetic role into decomposition of methane, the behavior similar to that observed for the photodecomposition of ammonia through $NH_3 + OH \rightarrow NH_2 + H_2O$. Consequently the formation of CH_3 radical during the photolysis of methane-water ices can be due to either $CH_4 + h\nu \rightarrow CH_3 + H$ or $CH_4 + OH \rightarrow CH_3 + H_2O$ where OH derive from the photodecomposition of water. The simultaneous presence of OH and CH_3 radicals in the irradiated sample may also contribute into the formation of alcoholic species through radical recombination at least for methanol: $CH_3 + OH \rightarrow CH_3OH$. It is important to note as the amount of water is very low in comparison with that of methane in our samples, the photofragments from water, O, H and OH are involved in reactions with methane and photoproducts derived from methane. In this context, we did not detect species such as O_2, O_3, HO_2 or H_2O_2 usual photoproducts formed in irradiated water ices. Additionally 4 new bands

appear when the amount of water is increased in the sample (figures V-7b and V-7c). These bands are located at 1385, 1192, 1175 and 630 cm^{-1} may be due species related to the formation of CH_3 radical or alcohol species, the only reaction photoproducts which amounts increase by increasing the concentration of water in the sample. In order to better characterize these new IR signal we have investigated the thermal processing of irradiated water-methane ices.

V.4. Thermal processing of irradiated water-methane ices

By heating the sample it is possible to monitor the behavior of radical recombination and formation of more stable species (figure V-8). The difference starts to appear going from 10K temperature to 20K. First of all the radical CH_3 signal at 609 cm^{-1} and that species at 1385 cm^{-1} decrease significantly while the non-assigned band at 630 is almost constant. Since the band at 1385 cm^{-1} behaves similarly as a CH_3, that suggest that this band can be also attributed radical species; in fact, Chettur and Snelson[26] suggest that this region can be possibly linked to C_2H_5. The signal due to C_2H_2 at 737 cm^{-1} slightly decreases while that due to the C_2H_6 at 822 cm^{-1} increases by 0.1%. The two peaks absorbing in the region between 1050 and 1010 cm^{-1} have been assigned to methanol and ethanol. The methanol band is at 1025 cm^{-1} and decreases by 37% while the ethanol band at 1043 cm^{-1} increase by 3%. The two signals at 1192 and 1175 have different behavior when the temperature of the sample increases from 10 to 20K. The signal at 1175 cm^{-1} remains constant and that at 1192 cm^{-1} increase by 47%. Previous experimental studies for UV irradiated CH_3OH rich ices have detected infrared signal at 1195 cm^{-1} which has been attributed to the CH_2OH radical species.[27] Due to the high decrease of CH_3 many reaction mechanisms are probable and will be discussed later. The increase of C_2H_6 could be firstly linked to the decrease of CH_3 through the reaction:

$$CH_3 + CH_3 \rightarrow C_2H_6 \qquad \text{(V-13)}$$

On the other hand, the increase of the band attributed to CH_2OH can be also linked to the decrease CH_3 and CH_3OH signals:

$$CH_3 + CH_3OH \rightarrow CH_2OH + CH_4 \qquad \text{(V-14)}$$

The increase of CH_3CH_2OH could be due to the radical recombination between CH_3 and CH_2OH.

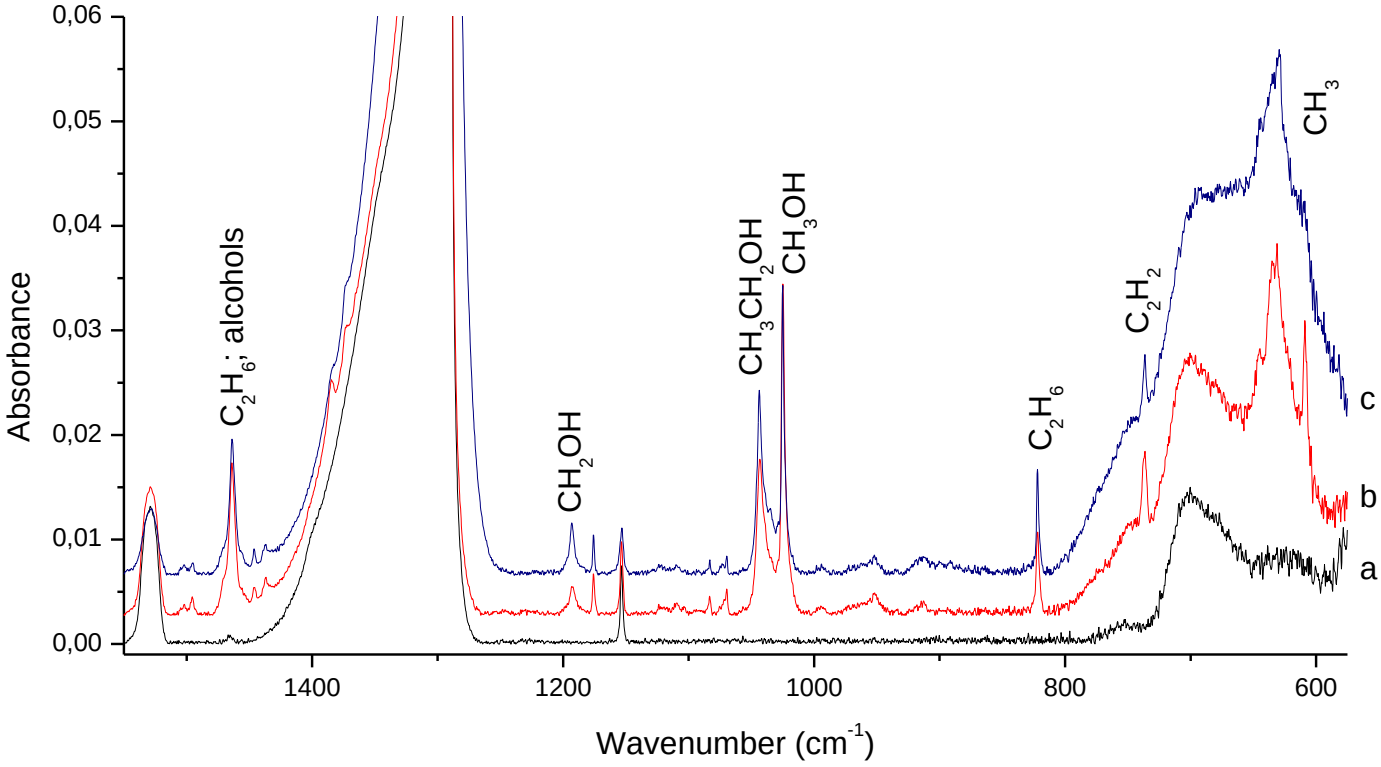

Figure V-8. The IR spectra of photolyzed CH_4-H_2O ice at different temperatures a) before photolysis 3K; b) 10K; c) 20K

By heating the sample at higher temperature around 40K, many of the absorption bands have their shapes changed mainly due the methane desorption from the solid sample. The absorption bands in alcohol region (~1050 cm^{-1}) become wider and are spectrally shifted, as shown in figure V-9 which compare the heating of the sample from 20 to 40K. The band attributed to CH_2OH at 1192 cm^{-1} which is consistent with a radical species disappears during the heating. The bands of C_2H_6 and CH_3CH_2OH have their spectral positions unchanged in contrast with the band due to CH_3OH which is blue shifted by 10 cm^{-1}. At this analysis level we reach the limit of IR spectroscopy in the characterization of the reaction products trapped in solid phase at low temperature. However, using high thermal processing we are able to control selectively the desorption of the species trapped in irradiated methane-water ice. Table V-4 shows the desorption temperatures of the different species formed in irradiated CH_4-H_2O ice samples.

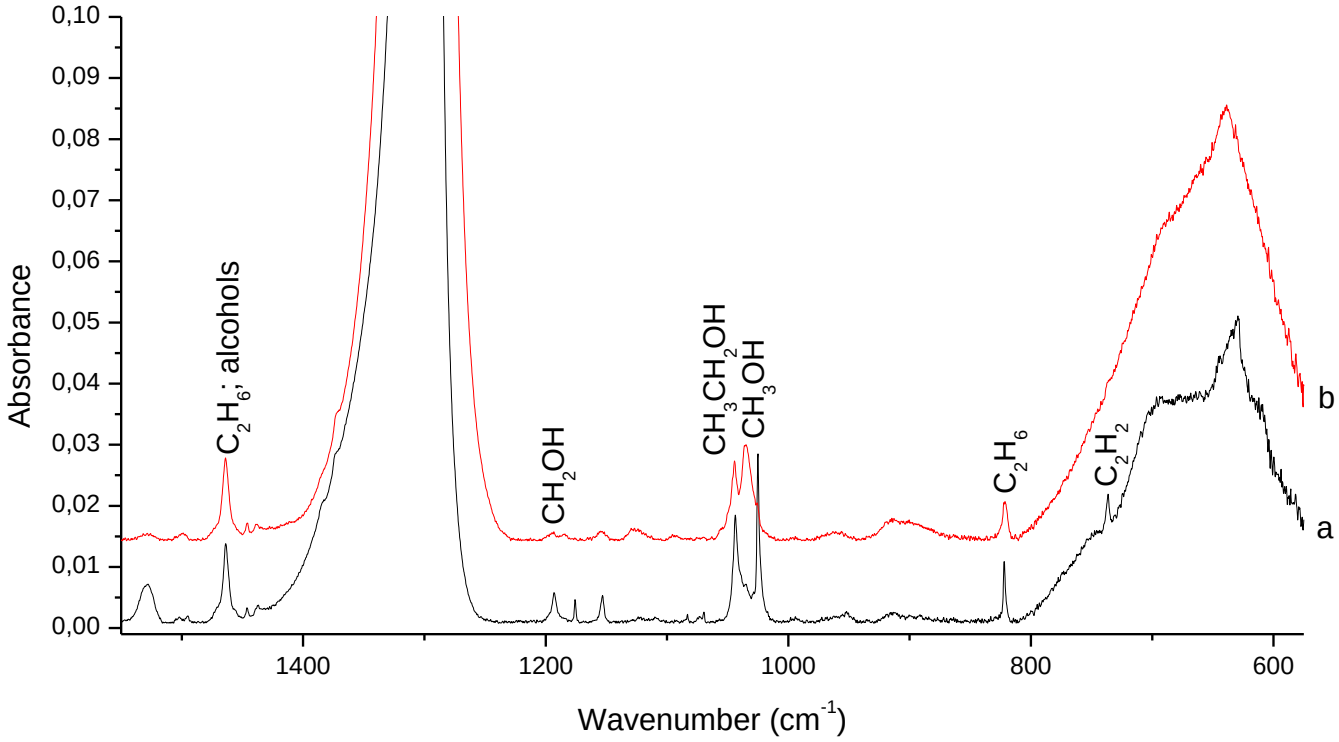

Figure V-9. The IR spectra of photolyzed CH_4-H_2O ice at different temperatures a) 20K; b) 40K

Table V-4. Desorption temperatures of the formed species

Species	Desorption temperature, K
CH_4	50
C_2H_2	65
C_2H_4	65
C_2H_6	70
C_3H_8	85
CH_3OH	130
CH_3CH_2OH	150

From table V-4 we notice that all alka[e]nes desorb at temperatures lower than 100K while the alcohol species desorb at temperatures higher than 100K. In order to be certain that the irradiated methane water would contain only alcohol species we have analyzed the IR spectra recorded at temperatures close to the alcohol desorption temperatures.

V.4.1. Thermal processing of irradiated water-methane ices: alcohol identification

As noted before the irradiation of methane-water ices have already shown that at least two alcohol species have been formed and attributed to methanol and ethanol. The rest of the formed species left in the sample should be based on alcohols after the heating of the irradiated CH_4-H_2O ice, with 2% of additional water. However, we have noticed that the heating of the sample at temperatures higher than 100K to alka[e]ne species (C_2H_2, C_2H_4, C_2H_6 and C_3H_8) suggests that more than two alcoholic species might be formed as shown in figure V-10. The figure V-10

shows the two characteristic spectral regions of many alcohol species when the sample is heated to 130K (the starting desorption temperature of many alcohols). The spectrum recorded at 130K is compared to the 4 alcohol ices mixed with water: methanol, ethanol, propanol and methoxymethanol as shown in figure V-10. The 4 alcohols have their most intense IR signals in the spectral region around ~1000 cm^{-1} corresponding to C-O stretching mode and also in the C-H stretching region around 3000 cm^{-1}.

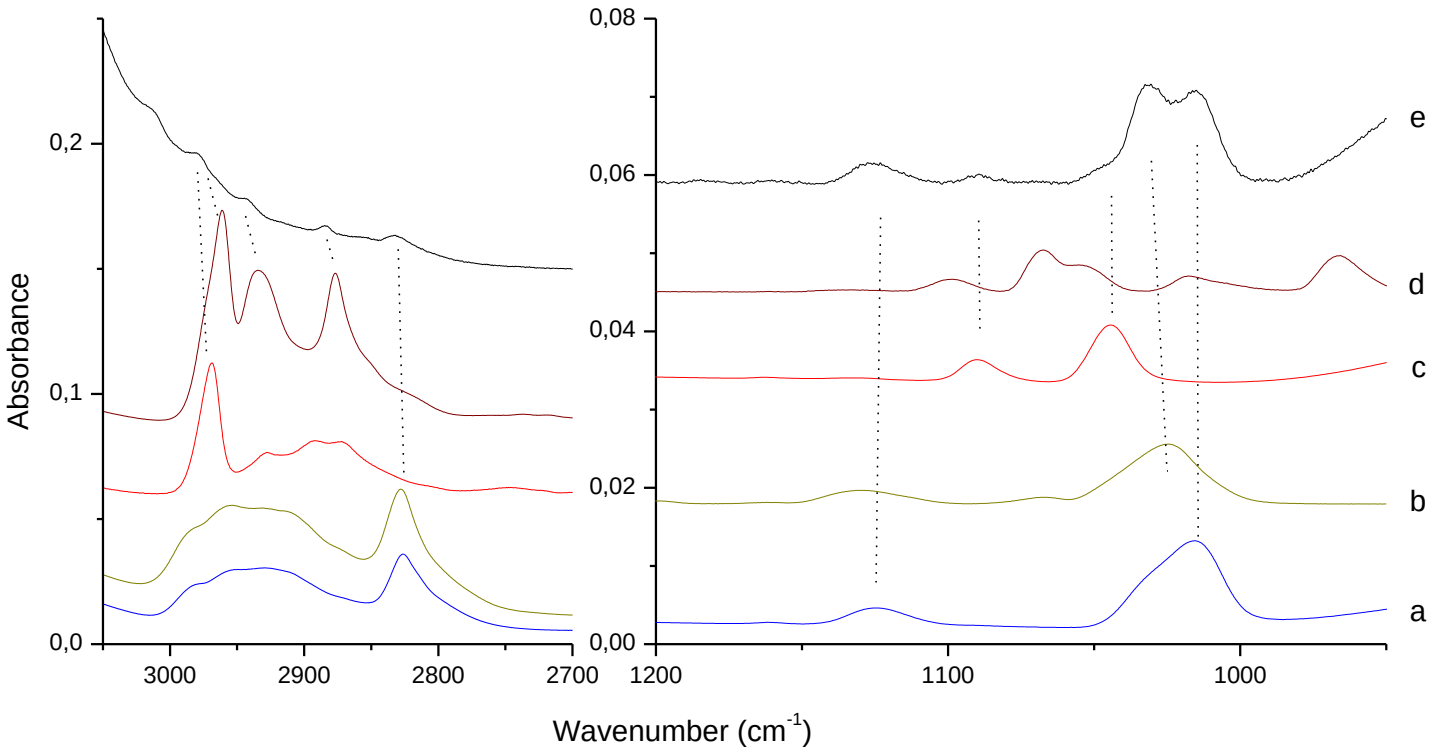

Figure V-10. Comparison of IR spectra of: a) CH_3OH ice; b) CH_3OCH_2OH ice; c) C_2H_5OH ice; d) C_3H_7OH ice; e) photolysed CH_4-H_2O ice at 130K

Photolyzed CH_4-H_2O ice heated to 130K show an IR signal made of at least 6 peaks in the region around ~1000 cm^{-1}. Two of these absorption peaks can be attributed to methanol (1015 cm^{-1}) and ethanol (1048 cm^{-1}). However, all other peaks are visible and can be consistent with more complex alcohols such as propanol ($CH_3CH_2CH_2OH$) and metoxymethanol (CH_3OCH_2OH). Propanol may be formed through the radical recombination between CH_3CH_2 and CH_2OH, while metoxymethanol can be formed through the interactions between CH_3O and CH_2OH. All these radical species are easily formed in the irradiated CH_4-H_2O ices. From figure V-10 metoxymethanol has characteristic band which can be reliable to one of the IR peaks we measure in the spectrum of photolyzed CH_4-H_2O ice heated to 130K. The identification of alcohols may also be carried out in the C-H stretching region. From figure V-10 we notice that both methanol and metoxymethanol have two specific IR absorption signals, one narrow signal on the right side and one broad band on the left side. While the IR spectrum of ethanol shows the reverse. Propanol and many other large alcohols have a very specific structure made of 3 wide

peaks. The comparison between all these reference spectra and the IR spectrum of the photolyzed CH_4-H_2O ice heated to 130K shows that in addition to methanol and ethanol, that have been already observed during the photolysis of the sample, at least two larger alcohol species can be formed during the heating of the sample through radical recombination. To further confirm the formation of these large alcohol species, we have already completed our investigations using mass spectroscopy and probing all the chemical species released in the gas phase during the sublimation of the irradiated methane-water sample.

V.4.2. Alcohol identification: from solid to gas phase

As it is seen in the previous section, the IR spectroscopy gives us a nice overview on the formation of the species, even though it is not sufficient enough to fully identify the reaction products. In this case, mass spectroscopy comes to help. By reaching the desorption temperatures of the species it is possible to identify them in gas phase. While we already have a great overview to look for alcoholic species, it needs to be taken into consideration other species of the same masses. Larger molecules also have the isomers - the same amount of atoms with different configuration, which results in a different fragmentation patterns. The fragmentation patterns of different alcohol species and their isomers are shown in figure V-11. Methanol M=32 does not have any other stable isomers, while C_2H_6O, M=46 and C_3H_8O, M=60 does have 2 and 3 isomers, respectively. The ether isomers of the ethanol and propanol possess a strong C-O stretching absorption band in the 1300 – 1100 cm^{-1} region, which was not detected both for dimethyl ether and methyl ethyl ether. Also other molecules with the same molecular masses should be noted like formic acid (CH_2O_2, M=46), methyl formate and acetic acid ($C_2H_4O_2$, M=60). Even though these molecules carry the same molecular mass they are not considered in this experimental study because of the complexity and again showing no traces of existence in the recorded IR spectra. All things considered the only alcoholic species of interest left are already confirmed methanol, ethanol and two isomers of propanol and probably as it has been suggested through the IR analysis – metoxymethanol.

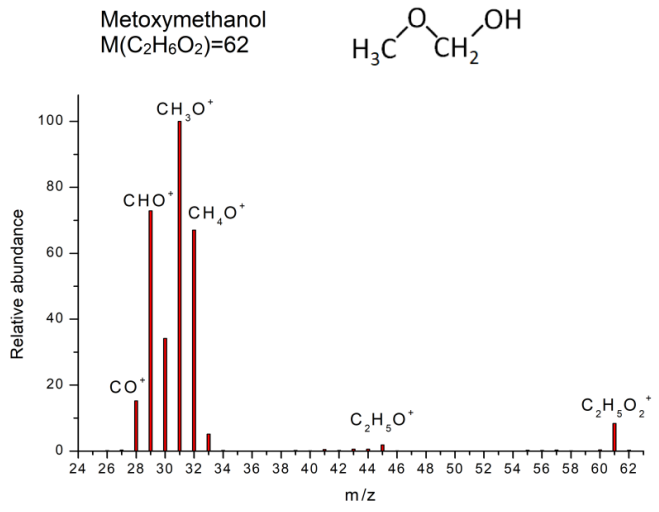

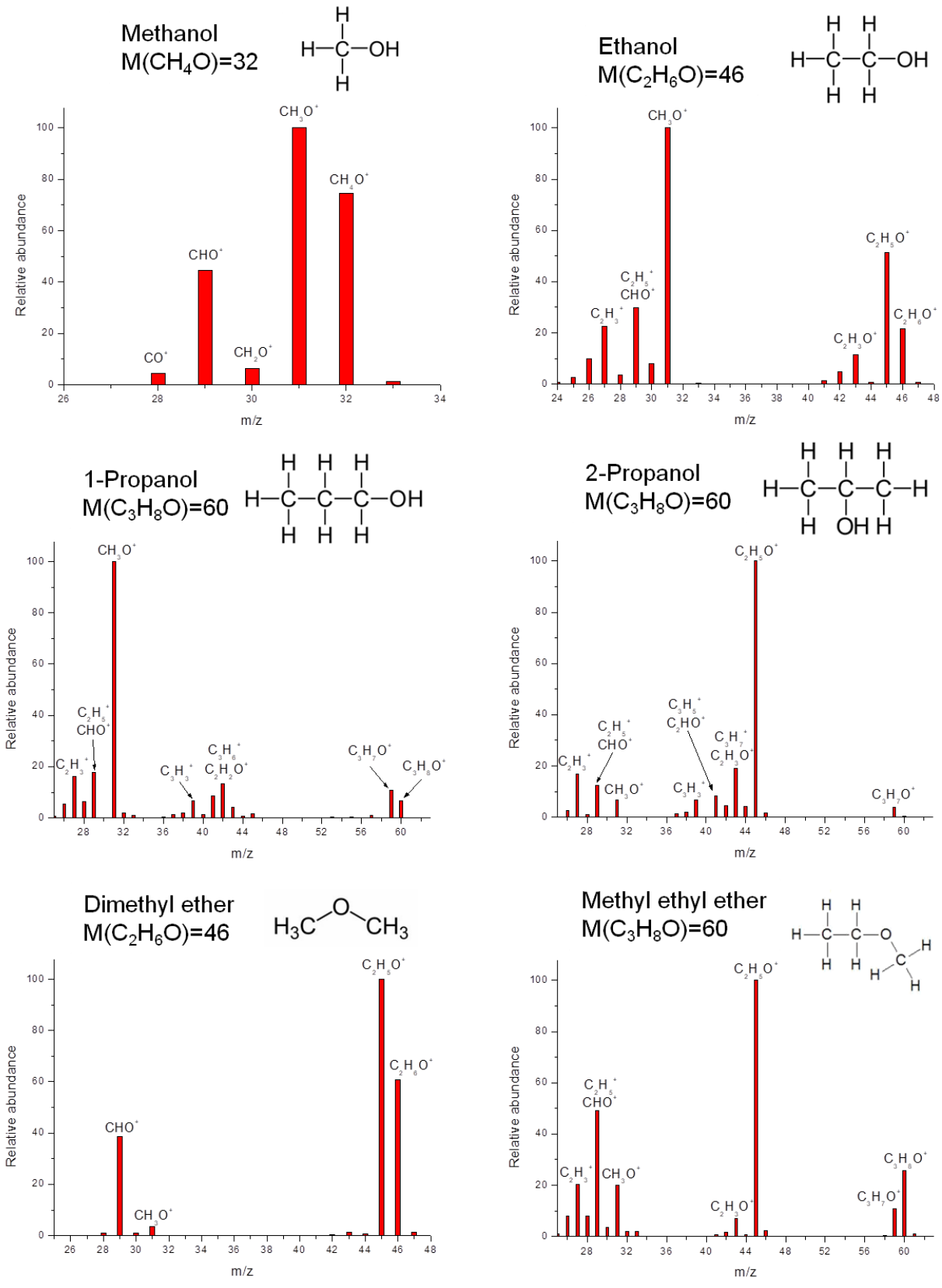

Figure V-11. Mass fragmentation patterns of alcohols and their isomers

Upon closer inspection of the figure V-11 it is visible that for ethanol and 1-propanol the highest abundance fragment is at M=31, the same as methanol. Even so ethanol and 1-propanol carries higher mass fragments (M=45, 46, 59 and 60). Looking at the mass spectrum of 2-propanol it is visible that the main fragment is M=45. Comparing 2-propanol and ethanol it is clear that it would be hard to distinguish both of them from the fragmentation patterns. It has to be taken into consideration that both propanols can be identified by 59 and 60 masses and these where the masses chosen upon their identification. As for metoxymethanol, most abundant mass fragment is also M=31, but it also possess the heavier fragment at M=61, but strangely no fragment at M=62. Metoxymethanol also has quite high yield of M=32 fragment and in turn can be easily mixed with methanol. Even so, as shown in all the alcohols, the M=31 should always have the highest yield during the recording of the mass spectrum. For methanol detection, a fragment used is M=32, for ethanol M=45 and 46, for propanol M=59 and 60 and M=61 for metoxymethanol.

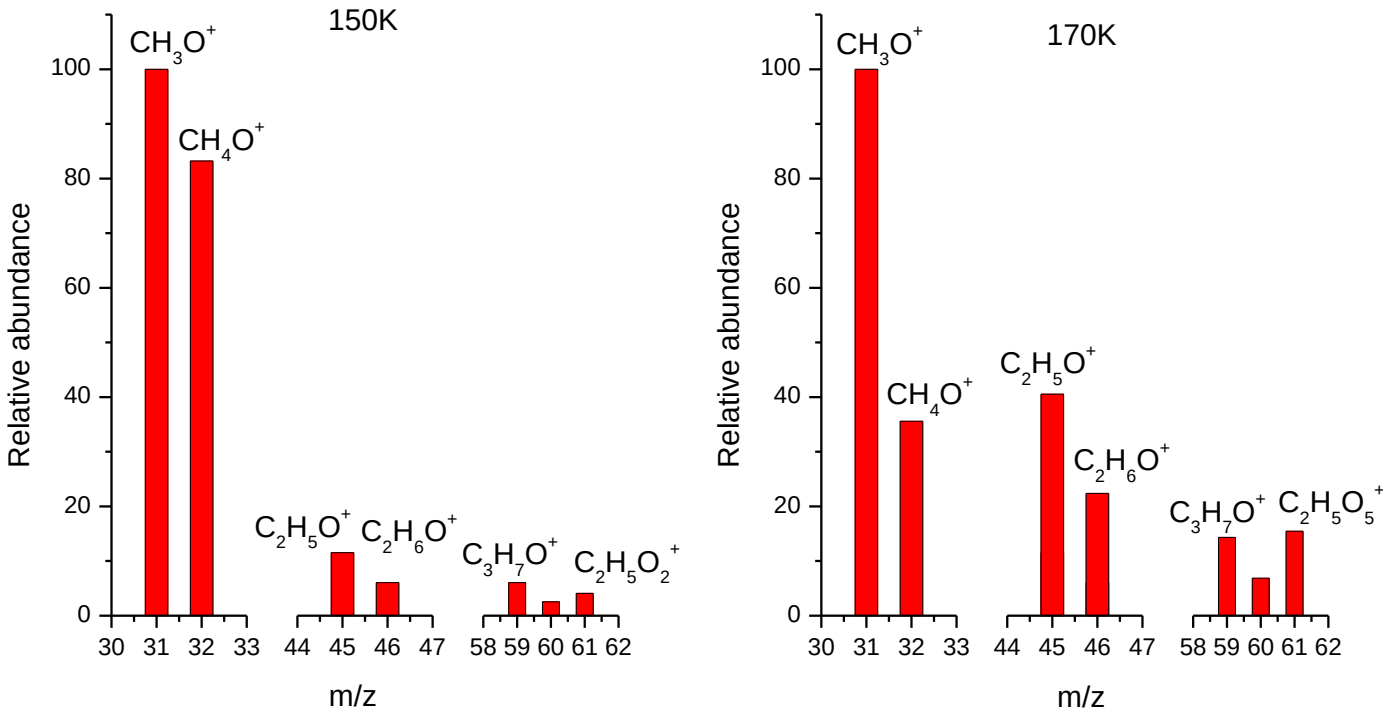

Figure V-12. Recorded mass fragments during the heating cycle at 150 and 170K

The two recorded mass fragmentation spectra during two heating cycles from 140 to 150K and from 160K to170K are shown in figure V-12. The heating period was set for 2K per minute to give enough time to record the mass spectra. As seen in the spectra towards 150K the main component is methanol due to the higher yield of the M=32, while towards the 170K we see decrease of M=32 and increase in other components leading to the desorption of the heavier alcohols.

The exact same experiment was carried out again, but at this time instead of recoding the fragmentation mass spectra, the desorption was monitored through temperature programmed

desorption (TPD) using a set up specific masses. The selected masses are M=31 for a global alcohol monitoring, and 32, 45 and 59 for methanol, ethanol and propanol, respectively, including mass 61 for metoxymethanol. The recorded TPD profiles over the temperature range from the 120K to 190K are pictured in the figure V-13.The TPD profiles shows a similar behavior as already noted with the fragmentation patterns: first the desorption of methanol peaking at 150K and later in higher temperatures those of heavier alcohols.

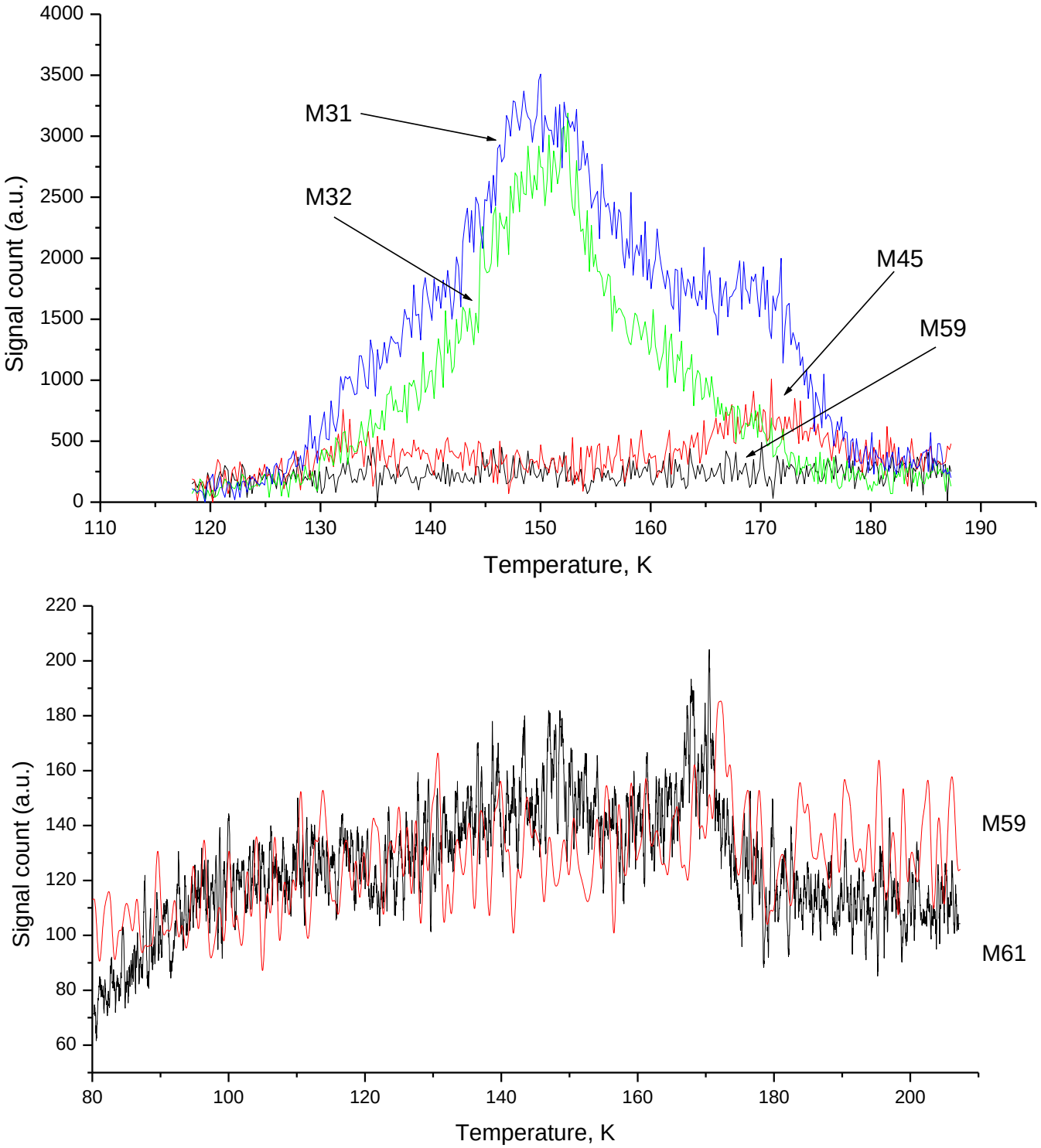

Figure V-13. Recorded TPD profiles in the 100 to 190K temperature range for masses: 31, 32, 45, 59, 61.

While there is no visible huge signal increase in the TPD profile related to propanol and metoxymethanol it has to be noted that the signal still increases in intensity at 170K mark in comparison to lower temperatures. The signal of heavier species keeps steadily increasing until reaching the room temperature. This can be explained that the species desorbing from the sample

mirror adsorb on the shield surrounding the sample holder. Sample holder has no heating element attached to it so during the heating cycle the temperature of the shield is lower than the sample holder itself and is heated much slower. This was confirmed by recording the mass signals through time after reaching the room temperature. After 2 hours the same signal patterns are recorded again but in much higher intensity, the signals decrease to their background level after several hours.

V.5. Formation pathways of alcohols

This experiment was performed to study the catalytic effect of water, similarly of what was seen in the experiments with ammonia, where the reaction of $NH_3 + OH \rightarrow NH_2 + H_2O$ took place increasing the amount of the formed amino radical. Even if the results are skewed to perform conclusive quantitative analysis, it is possible to state that increasing the water amount in the methane ice samples the production of the radical CH_3 also increases, thus consequently increasing the species attributed to alcohols. It means that the similar reaction occurs during the photolysis of the methane-water ices allowing the abstraction of hydrogen from methane with hydroxyl radical $CH_4 + OH \rightarrow CH_3 + H_2O$, consequently, leading to the formation of additional radical species and to the formation of more alcoholic species.

By heating the sample, the species attributed to ethanol increased while the band attributed to methanol decreased (figure V-8). This shows further occurring radical-molecular and radical-radical reactions in formation of larger molecules. Even though propanol and metoxymethanol could not be identified at lower temperatures, but based on these experiments and the data acquired from FTIR and mass spectra analysis, it is possible to confirm the detection of the larger alcoholic species than ethanol as a result of the exposure of methane-water ices to the UV radiation.

In section V.2. it was shown that through the photolysis of CH_4 ice it is possible to form the methyl CH_3 radical. Not only this but in the following paragraph it was shown that the addition of water increases the production of methyl radical, meaning two possible reactions are occurring:

$$CH_4 + h\nu \rightarrow CH_3 + H \qquad \text{(V-15)}$$

$$CH_4 + OH \rightarrow CH_3 + H_2O \qquad \text{(V-16)}$$

According to Tsiouris et al.[28] theoretical and experimental data the reaction $CH_4 + OH \rightarrow CH_3 + H_2O$ is exothermic with energy of formation ΔH=56.1 kJ/mol. They state that similarly like with ammonia the OH and CH_4 forms a stable complex and after overcoming a barrier it can form $CH_3 + H_2O$. This reaction pathway is shown in figure V-14. Even though they do not provide any data about the weakly bound H_2O-CH_3 complex, it should exist as confirmed experimentally by Rudić et al.[29] While the reaction of $CH_4 + OH$ to form $CH_3 + H_2O$ has higher barrier predicted theoretically (22.37 kJ/mol) than the one involving ammonia (13.4 kJ/mol,

Chapter III.5.1, figure III-10), some experimental kinetic rate measurements suggest much lower (~15kJ/mol) energy barrier.[30] Due to the possible tunneling effect, in lower temperatures, this reaction can easily take place under our experimental conditions. On the other hand the opposite reaction ($CH_3 + H_2O \rightarrow CH_4 + OH$) is definitely impossible due the energetic restrictions.

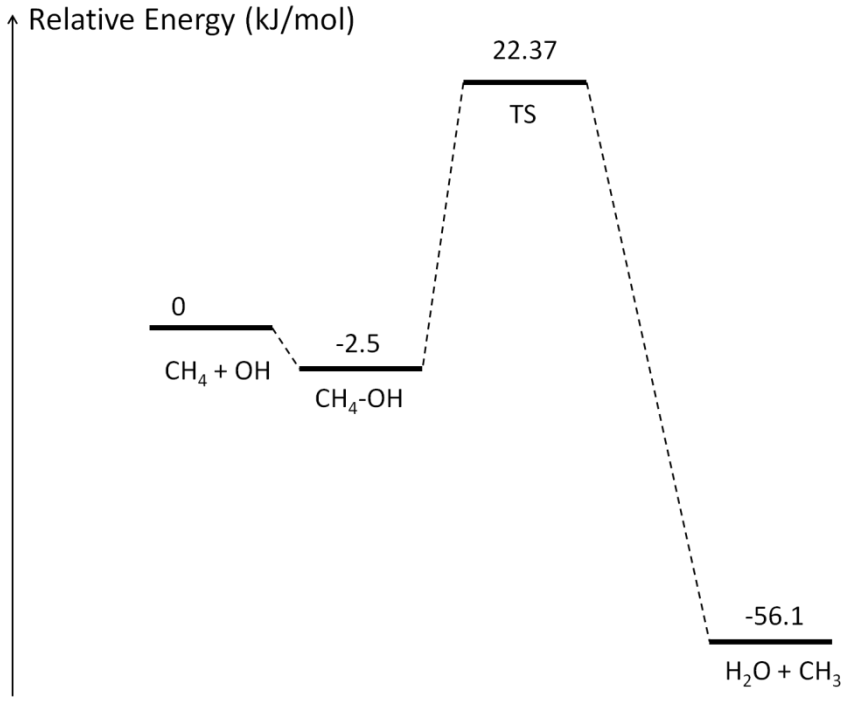

Figure V-14. Reaction pathways involving CH_4, H_2O, OH and CH_3 species

As was seen from the figure V-8 by further heating the sample after the photolysis the increase in ethane and ethanol was noticed while on the same time a decrease of methanol. For the further analysis there is no sufficient data like barrier heights, only the formation energies that are taken from the compilation data collected by Baulch et al.[31] for some of the reactions. It has to be taken into consideration that the provided energies are for room temperature gasses and these values should be much lower in our experiments, but it gives an overview for creation of reaction pathways.

Starting from the beginning the two main obvious photo-products that can be formed due to the radical-radical recombination is ethane and methanol:

$CH_3 + CH_3 \rightarrow C_2H_6$ $\Delta H = -376$ kJ/mol (V-17)

$CH_3 + OH \rightarrow CH_3OH$ $\Delta H = -385$ kJ/mol (V-18)

Another larger than ethane product, propane, can also be formed through the radical-radical interaction:

$C_2H_5 + CH_3 \rightarrow C_3H_8$ $\Delta H = -372.0$ kJ/mol (V-19)

But in this case it would require a radical C_2H_5 that can be also created thought the photolysis of the ethane:

$$C_2H_6 + h\nu \rightarrow C_2H_5 + H \qquad \text{(V-20)}$$

Similarly to the creation of CH_3, the C_2H_5 radical can be formed though hydrogen abstraction in the radical-molecular reaction:

$$C_2H_6 + OH \rightarrow C_2H_5 + H_2O \qquad \Delta H = -74.1 \text{ kJ/mol} \qquad \text{(V-21)}$$

$$C_2H_6 + CH_3 \rightarrow C_2H_5 + CH_4 \qquad \Delta H = -16.0 \text{ kJ/mol} \qquad \text{(V-22)}$$

It is visible that reaction with CH_3 radical can increase the production of C_2H_5 which should be also quite viable in irradiated CH_4-H_2O ice. While the interaction with CH_3 can lead to the formation of C_2H_5, the more energetically favorable reaction is with OH radical. The further interaction of C_2H_5 and CH_3 can lead to the formation of propane:

$$C_2H_5 + CH_3 \rightarrow C_3H_8 \qquad \text{(V-23)}$$

While it is quite simplistic pathway for creation of carbon chain, it is visible that the addition of water plays a role for increasing the possible amount of products during the photolysis process.

Another detected product, ethanol, can be obtained with a reaction between C_2H_5 and OH radicals:

$$C_2H_5 + OH \rightarrow C_2H_5OH \qquad \text{(V-24)}$$

While ethanol is another detected photolysis product, a possible creation of propanol was also observed through the combination of IR and mass spectroscopies. The creation pathway of propanol is similar that to ethanol, through a radical recombination between C_3H_7 and OH:

$$C_3H_7 + OH \rightarrow C_3H_7OH \qquad \text{(V-25)}$$

For this reaction to occur the radical C_3H_7 is required, that can be obtained again either though photolysis or the hydrogen abstraction with OH and CH_3:

$$C_3H_8 + h\nu \rightarrow C_3H_7 + H \qquad \text{(V-26)}$$

$$C_3H_8 + OH \rightarrow C_3H_7 + H_2O \qquad \text{(V-27)}$$

$$C_3H_8 + CH_3 \rightarrow C_3H_7 + CH_4 \qquad \text{(V-28)}$$

While there is no data supplied for the hydrogen abstraction of propane, but it is plausible to assume that the reaction formation energies would be similar to the reaction of ethane with OH and CH_3 radicals. It has to be noted that there are two possible isomers of C_3H_7: $CH_3CH^*CH_3$

and $CH_3CH_2CH_2^*$. Both of these radicals interacting with hydroxyl radical OH would lead to the formation of propanol (both isomers 1-propanol and 2-propanol).

While the pathway of radical-radical recombination between C_3H_7 and OH radicals to form propanol is the most obvious, there is also another possible way, by forming additional radical species from methanol and ethanol. Methanol similarly like methane and ethane can interact with photons during the photolysis process or CH_3 and OH radicals. Two radical species can be formed by removing a hydrogen atom though such reactions:

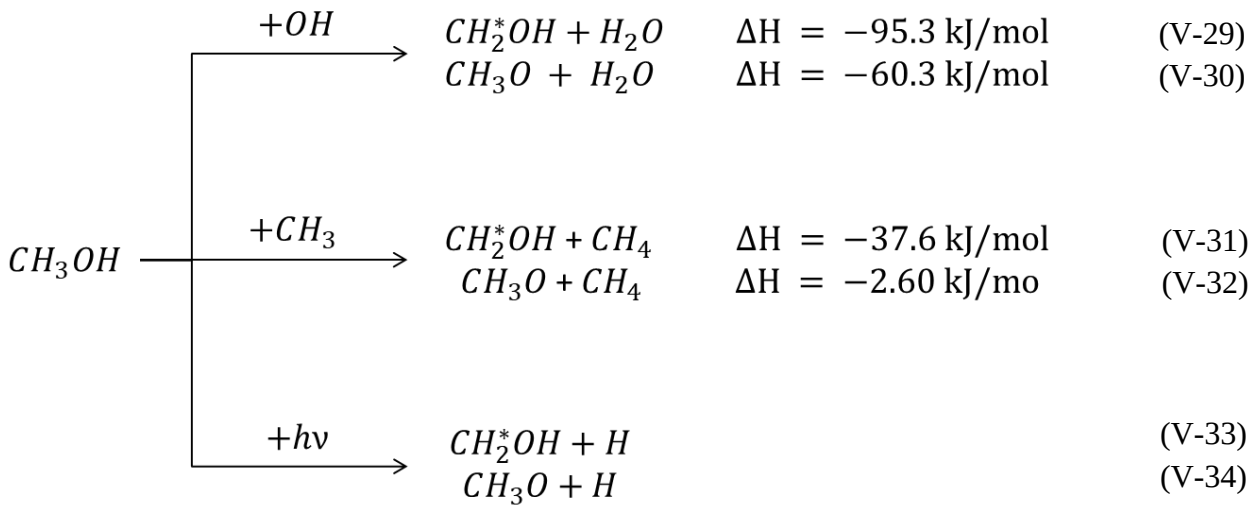

While the interaction with photons is only available during the photolysis, the interaction with radical species can take place after the photolysis. This can be confirmed by noticing the small decrease in the intensity of the band corresponding to the methanol by increasing the temperature of the sample from 10 to 20K (figure V-8). Another point has to be noted, that those reactions are energetically favorable more with the OH radical than to the CH_3 that would lead to the depletion OH after the photolysis is finished. The formed hydroxymethyl and methoxy radicals can interact with methyl and ethyl radicals. Methyl and ethyl radical interaction with hydroxymethyl radical can form larger alcohols:

$$CH_2OH + CH_3 \rightarrow C_2H_5OH \quad \text{(V-35)}$$

$$CH_2OH + C_2H_5 \rightarrow C_3H_7OH \quad \text{(V-36)}$$

While interaction with methoxy radical can form dimethyl ether and methyl ethyl ether:

$$CH_3O + CH_3 \rightarrow CH_3OCH_3 \quad \text{(V-37)}$$

$$CH_3O + C_2H_5 \rightarrow CH_3OC_2H_5 \quad \text{(V-38)}$$

Radical recombination CH_3O and CH_2OH, the two intermediates in the formation of methanol, may also lead to the formation of metoxymethanol:

$$CH_3O + CH_2OH \rightarrow CH_3OCH_2OH \quad \text{(V-39)}$$

Similar processes we proposed above can be applied in reactions involving ethanol instead or methanol. There can be three radicals (1-hydroxyethyl, 2-hydroxyethyl and ethoxy radical) formed from the hydrogen abstraction of ethanol:

$$C_2H_5OH \xrightarrow{+OH} \begin{cases} CH_2^*CH_2OH + H_2O & \Delta H = -59.2\ \text{kJ/mol} \quad \text{(V-40)} \\ CH_3CH^*OH + H_2O & \Delta H = -95.6\ \text{kJ/mol} \quad \text{(V-41)} \\ CH_3CH_2O^* + H_2O & \Delta H = -80.0\ \text{kJ/mol} \quad \text{(V-42)} \end{cases}$$

$$C_2H_5OH \xrightarrow{+CH_3} \begin{cases} CH_2^*CH_2OH + CH_4 & \Delta H = -22.4\ \text{kJ/mol} \quad \text{(V-43)} \\ CH_3CH^*OH + CH_4 & \Delta H = -37.9\ \text{kJ/mol} \quad \text{(V-44)} \\ CH_3CH_2O^* + CH_4 & \Delta H = -1.60\ \text{kJ/mol} \quad \text{(V-45)} \end{cases}$$

$$C_2H_5OH \xrightarrow{+h\nu} \begin{cases} CH_2^*CH_2OH + H & \text{(V-46)} \\ CH_3CH^*OH + H & \text{(V-47)} \\ CH_3CH_2O^* + H & \text{(V-48)} \end{cases}$$

The interaction of 1-hydroxyethyl, 2-hydroxyethyl and ethoxy radicals with methyl radical can lead to the formation of 2-propanol, 1-propanol and methyl ethyl ether, respectively:

$$CH_3CH^*OH + CH_3 \rightarrow CH_3CHOHCH_3 \quad \text{(V-49)}$$

$$CH_2^*CH_2OH + CH_3 \rightarrow CH_3CH_2CH_2OH \quad \text{(V-50)}$$

$$CH_3CH_2O^* + CH_3 \rightarrow CH_3CH_2OCH_3 \quad \text{(V-51)}$$

All the reaction processes proposed with methanol fragments (CH_3O and CH_2OH) can be used with ethanol fragments (1-hydroxyethyl, 2-hydroxyethyl and ethoxy radical) to form larger complex molecules. These are only the fraction of possible interactions in the performed experiments. Other interactions involving unsaturated larger species are not taken into consideration, while their existence was not observed in these experiments. All the discussed reactions are presented in the pathway formation map in figure V-15.

`

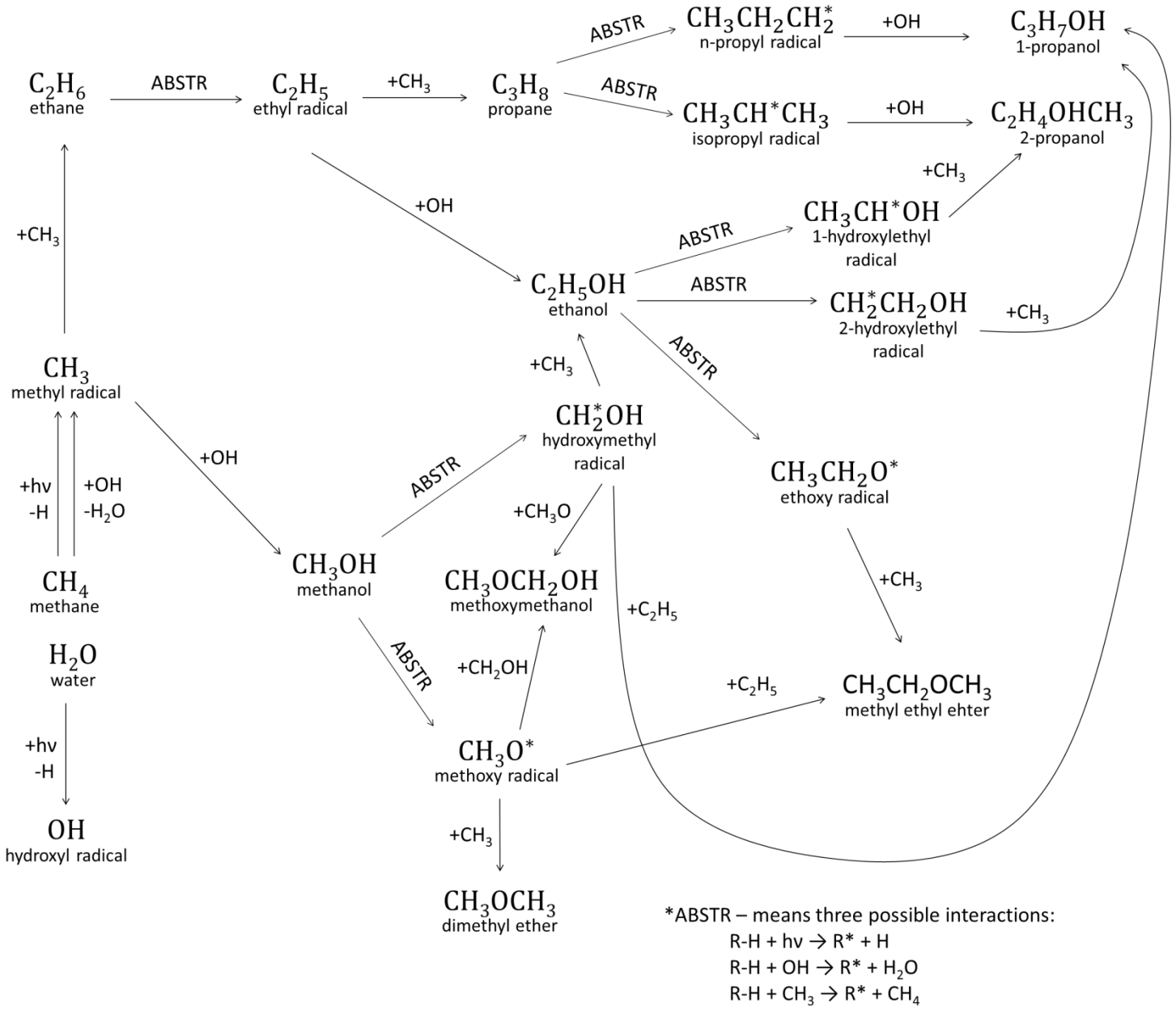

Figure V-15. Reaction pathways involving CH_4, H_2O, OH and CH_3 species

V.6. Conclusions

In this study the infrared spectroscopy was used to monitor the reactions taking place in the solid phase on interstellar ice grain analogs. It was shown that the similar catalytic behavior takes place in methane-water ice during the photolysis process as observed in ammonia-water ices. The increase of 2% of water shows the increase in production of methyl radical though the additional reaction $CH_4 + OH \rightarrow CH_3 + H_2O$ taking place. On the other side, we notice that the analysis of the irradiated ammonia and ammonia-water ices is by far easier than that of irradiated

methane and methane-water ices. While during the photolysis of NH_3 and NH_3-H_2O ices lead to the formation of a very few reaction products, NH_2, N_2 and NH_2OH, the UV irradiation of CH_4 and CH_4-H_2O is a source of many large carbon chains. This should be taken into account for the photolysis of mixed NH_3-CH_4 and NH_3-CH_4-H_2O interstellar ice analogs. We show that the simultaneous presence of CH_3 and OH radicals in the same sample leads to more complex reactions during the sample heating. The heat treatment further on revealed the formation of larger alcoholic species – propanol and metoxymethanol, while metoxymethanol has been observed quite recently (2017) unlike propanol which is not observed in space as of today. One can notice that complex species may be formed through photofragmentation of small molecules such as methane and water which are one of the major components of the ISM. However, the non-detection of large alcohols like propanol or allyl alcohol in the ISM would suggest that other reactions are involved in these regions more important than photochemistry. In fact, it is well known that the H addition reaction in many dense molecular clouds would be more important than photo-induced reactions and this could be one of the reasons of the non-detections of large alcohols. As many aldehydes have been already detected in the ISM, the H addition reaction on these species would lead to the formation of different alcohols just like the most studied reaction corresponding to the conversion of H_2CO into CH_3OH through successive hydrogenation. Before going further in this thesis work and presenting the results of the photolysis of CH_4-NH_3 and CH_4-NH_3-H_2O interstellar ice analogs, we have preferred to investigate the possible formation of large alcohols such as propanol and allyl alcohol through H addition reactions on aldehydes more complex than H_2CO.

Bibliography

[1] Lacy, J. H., Carr, J. S., Evans, N. J. I., et al. 1991, ApJ, 376, 556
[2] Boogert, A. C. A., Schutte, W. A., Tielens, A. G. G. M., et al. 1996, A&A, 315, L377
[3] Charnley S. B. (2001b) Interstellar organic chemistry. In The Bridge Between the Big Bang and Biology (F. Giovannelli, ed.), pp. 139–149. Consiglio Nazionale delle Ricerche President Bureau Special Volume, Rome, Italy
[4] Gerakines P. A., Moore M. H., Hudson R. L., 2001. J. Geophys. Res., 106(E12), 33381
[5] Stief, L. J., Decarlo, V. J., & Hillman, J. J. 1965, J.Chem.Phys., 43, 2490
[6] Hodyss, R., Johnson, P. V., Stern, J. V., et al. 2009, Icar, 200, 338
[7] Öberg, K. I., van Dishoeck, E. F., Linnartz, H., et al. 2010, ApJ, 718, 832
[8] Weber, A. S., Hodyss, R., Johnson, P. V., et al. 2009, ApJ, 703, 1030
[9] Moore, M. H., & Hudson, R. L. 1998, Icar, 135, 518
[10] Bergantini A., Maksyutenko P., Kaiser R.I., 2017. ApJ, 841, 96.
[11] Tercero B.,Kleiner I.,Cernicharo J.,Nguyen H.V.L., López A., Muñoz Caro G. M., 2013. ApJL, 770:L13.
[12] Brouillet, N., Despois, D., Baudry, A., et al. 2013, A&A, 550, A46
[13] Wu Y.J., Chen H.F., Camacho C., Witek H.A., Hsu S.C., Lin M.Y., Chou S.L., Ogilvie J. F., Cheng B.M., 2009. ApJ, 701:8.
[14] Lin M.Y., Lo J.I., Lu H.C., Chou S.L., Peng Y.C., Cheng B.M., Ogilvie J. F., 2014. J. Phys. Chem. A, 118, 3438.
[15] Ulenikov O.N., Bekhtereva E.S., Albert S., Bauerecker S., Niederer H. M., Quack M., 2014. J. Chem. Phys., 141, 234302.
[16] Gans B., Boyé-Péronne S., Broquier M., Delsaut M., Douin S., Fellows C.E., Halvick P., Loison J.C., Lucchese R. R., Gauyacq D., 2011. Phys. Chem. Chem. Phys., 13, 8140.
[17] Leroi G. E., Ewing G. E., Pimentel G. C., 1964. J.Chem.Phys., 40, 2298.
[18] Nxumalo L.M., Ford T.A., 1994. J.Mol.Struc., 327, 145.
[19] Han S. W., Kim K., 1996. J. Phys. Chem.,100, 17124.
[20] Coussan S., Bouteiller Y., Perchard J. P., Zheng W. Q., 1998. J.Phys.Chem.A, 102, 5789.
[21] Milligan D. E., Jacox M. E., 1963, J. Chem. Phys., 38, 2627
[22] Khoshkhoo H., Nixon E.R., 1973. Spectrochimica Acta Part A: Molecular Spectroscopy, 29, 4, 603.
[23] Ewing G.E., Thompson W.E., Pimentel G.C., 1960. J.Chem.Phys. 32, 927.
[24] Forney D., Jacox M. E., Thompson W. E., 1993, J. Mol. Spectrosc., 157, 479
[25] Yamakawa K., Ehara N., Ozawa N., Arakawa I., 2016. AIP Advances 6, 075302.
[26] Chettur G., Snelson A., 1987. J. Phys. Chem. , 91, 3483.
[27] Öberg K. I., Garrod R. T., van Dishoeck E. F., Linnartz H., 2009. A&A 504, 891.
[28] Tsiouris M., Wheeler M. D., Lester M. I., 1999. Chem. Phys. Let., 302, 192.
[29] Rudić S., Merritta J. M., Millera R. E., 2009. Phys. Chem. Chem. Phys., 11, 5345.
[30] Gierczak T., Talukdar R. K., Herndon S. C., Vaghjiani G. L., Ravishankara A. R., 1997. J. Phys. Chem. A, 101, 3125.
[31] Baulch D. L. , Bowman C. T. , Cobos C. J. , Cox R. A. , Just Th. , Kerr J. A. , Pilling M. J. , Stocker D., Troe J., Tsang W., Walker R. W., Warnatz J., 2005. J. Phys. Chem. Ref. Data, 34(3), 757.

Chapter VI:

Formation of large alcohols under ISM conditions:

Photolysis vs hydrogenation

As we showed in the previous chapter, the photolysis of CH4 and CH4-H2O ices lead to the formation of several carbon chain species. Propanol was one of the reaction products we have detected in our irradiated samples, however, it is still not observed in the ISM. In this section we have investigated other possibilities of formation of propanol and other large alcohols: H addition reaction on unsaturated species, the most predominant processing in the ISM. Looking back at the diagram in figure I-4 (Chapter I.4.2, page 95)[1] we notice that more complex organic molecules can be formed thought the atomic addition starting with CO molecule. While it was already shown in the previous chapter one possible formation of propanol, another one is through hydrogenation of C_3O. But still arises the question, why different aldehydes like methanal, ethanal, propynal and propanal are present in dense molecular clouds while the only alcohol detected in those cold regions is methanol? In addition, ethanol and metoxymethanol have only been detected in hot cores. Are those saturated and unsaturated aldehyde and alcohol species chemically linked in molecular clouds through solid phase H-addition surface reactions or are they formed only through energetic routes as we showed in Chapter V? To answer such a query, it was decided to investigate a hydrogenation of such saturated and unsaturated aldehydes and alcohols at 10 K, the temperature the most evoked in dense molecular clouds.

VI.1. Earlier studies and motivation

Reactions involving hydrogen atoms reacting with different astrochemicaly relevant species on the icy interstellar grains at temperatures around 10 K have been often proposed to have a crucial role in the production of some of those detected molecules.[2,3,4,5,6] However, at very low temperatures, hydrogen atoms could not react with compounds bearing an unsaturated functional group to lead to the corresponding more saturated derivatives when the activation barriers of the reactions cannot be passed over. Unfortunately, all the calculated energy barriers for many reactions are given in the gas phase and then we are not able to predict if a given reaction show similar activation energies from gas to solid phase. Consequently, an important part of the understanding of solid phase chemistry occurring on the icy surfaces of the interstellar dust grains could be given by a better knowledge of what is reduced and what is not reduced in lab simulations concerning unsaturated compounds already observed in the ISM. Some detected molecules could thus find a possible way for their formation while the lack of reactions with hydrogen for some other species could demonstrate that another chemical pathway has to be found to explain their presence in this medium. Many studies have been devoted to the reaction of hydrogen atoms with carbon monoxide or formaldehyde in the aim to form methanol or its both radical precursors (CH_3O and CH_2OH).[7,8,9,10] Unambiguously hydrogen atoms react with formaldehyde, the simplest aldehyde. Is this reduction reaction of a carbonyl group still occurring with substituted derivatives? For derivatives with a carbon-carbon double or triple bond, is this unsaturated group more or less easily reduced than the carbonyl group? Both questions pushed us to study the hydrogenation of unsaturated aldehydes to know if the H-addition reactions could propose an origin to the observation of saturated aldehydes[11,12,13] or saturated alcohols[14,15,16] or, at the opposite, could demonstrate that they cannot be formed through those reaction pathways.

From astronomy observations, propynal has been observed in the ISM[17] while propenal has been tentatively detected.[12] The synthesis of propynal[17] in the ISM would start from C_3O and the chemoselective hydrogenation of this latter, proposed by Hollis et al.[12] would form propenal and propanal. In fact, among the partially saturated compounds, propanal has been detected[12]while neither allyl- nor propargyl alcohols have been found. On the other hand, although methanol and ethanol are abundant in the interstellar medium,[18] propanol ($CH_3CH_2CH_2OH$) is still missing in the list of detected molecules. In this context, reactions of hydrogen radicals with the unsaturated derivatives under ISM conditions are the keys for a better understanding of their chemistry. As mentioned earlier, the H addition reactions in solid phase have been investigated by different groups on simple astrochemical relevant species to quantify the formation of saturated species such as CH_3OH, CH_3NH_2 from hydrogenation of simple molecules like CO, H_2CO and HCN.[19,20] However, in some of those studies the reaction products are probed and quantified only in gas phase by mass spectroscopy from the temperature programmed desorption (TPD). This gas phase detection method has been adopted as the IR signals of the reaction products formed and trapped in solid phase might either be under the limit of detection or overlap with the IR signals of the reactants. Nevertheless, the characterization of reaction products from the TPD makes it impossible to confirm whether the products detected by mass spectroscopy are actually formed in solid phase through a hydrogenation process or during the temperature programmed desorption of the solid samples. Consequently, only, an accurate IR analysis of the reactant ices before and after H-bombardment remains the single possibility to show if an H-addition reaction would take place in solid phase at very low temperature mimicking the surface reactions of the icy interstellar grains.

In this study it is reported the solid phase H-addition reactions of propynal (HC≡CCHO), propenal (H_2C=CH-CHO, acroleine), propanal (CH_3CH_2CHO) and also on unsaturated alcohols such as propargyl ($HC{\equiv}CCH_2OH$) and allyl alcohol (H_2C=$CHCH_2OH$). Figure VI-1 shows the possible reaction pathways for successive H addition reactions of unsaturated compounds. Also it has to be noted that proposed pathways shows all the possible steps, while on the contrary the hydrogenation can be very reactive and skip the formation of molecule instantly being reduced from C≡C to C-C bonds.

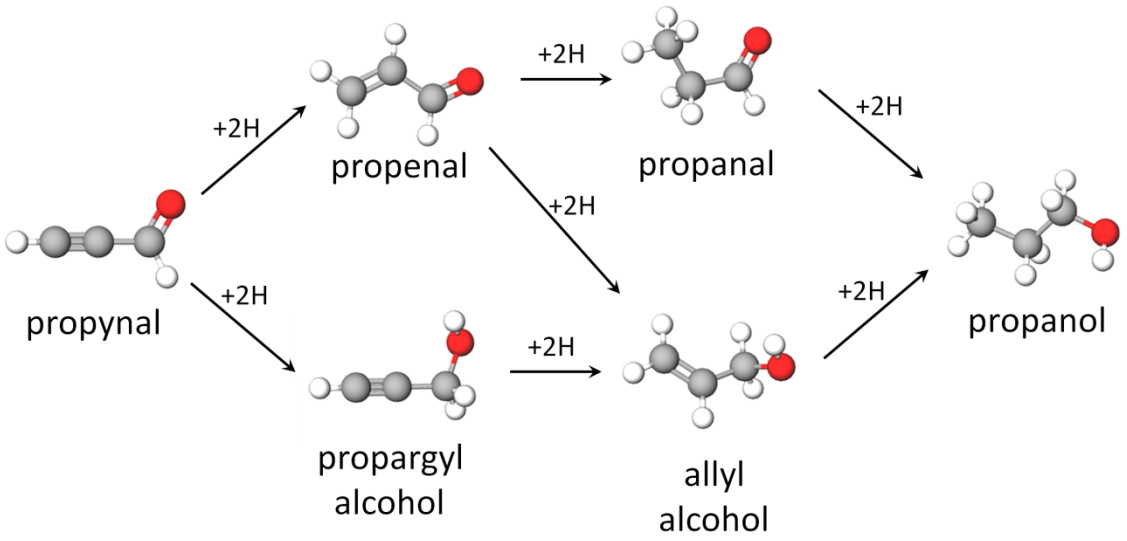

Figure VI-1: Possible reaction pathways for the hydrogenation processes of unsaturated compounds: HC≡CCHO, H_2C=CH-CHO, CH_3CH_2CHO, HC≡CCH_2OH, H_2C=$CHCH_2OH$

VI.2. Sample formation

Propargyl alcohol, allyl alcohol, propanol, propenal and propanal were purchased from the Aldrich company. Propynal was synthesized by oxidation of propargyl alcohol following the procedure of Sauer.[21] Similarly like in the previous experiments, the solid samples have been prepared under ultrahigh vacuum in a chamber maintained at 10^{-10} mbar, where pure alcohol and aldehyde ices have been formed by condensing the saturated or unsaturated corresponding alcohol or aldehyde vapor on a highly polished, Rh-plated copper mirror maintained at 10 K using a closed-cycle helium cryogenerator.

At room temperature, the vapour pressures of aldehydes are approximately a few hundred mbars (propanal 422 mbar, propenal 290 mbar)[22] while those of alcohols are one order of magnitude lower (propanol 20 mbars, allyl alcohol 28 mbars). The glass flasks containing the pure organic compounds were kept in cooling baths formed by a mixture of liquid nitrogen and methanol, to maintain the temperature of the aldehydes or the alcohols as low as -50 °C, in order to control the amount of deposited material. Afterwards, the frozen compounds are partially evaporated by increasing the temperature of the cooling bath between -50°C and 5°C to introduce them into the injection ramp. A pressure of less than 10 mbars of vapor gas was subsequently injected into the high vacuum chamber to form the organic ices by condensation onto the mirror sampler.

Working with only single pure molecule and knowing the volume of the injection ramp, the amount of deposited material is evaluated from the decrease of the pressure in the ramp during the deposition of the sample (formula II-7, Chapter II.6.1, page 48). Pure organic ices have been formed at 10 K and characterized by infrared spectroscopy. The amounts of the organic species deposited have been chosen to obtain thick ices (few tens of micrometers) for a better vibrational mode characterization and also in order to increase the yield of H-addition

reaction and thus to have the upper limit of the reaction products.[19] Table VI-1 lists the amounts of deposited organic species.

Table VI-1: The amounts of deposited species (μmol).

propargyl alcohol	($HC{\equiv}CCH_2OH$)	0.30	± 0.08
allyl alcohol	($H_2C{=}CHCH_2OH$)	1.0	± 0.2
propanol	($H_3CCH_2CH_2OH$)	0.20	± 0.05
propynal	($HC{\equiv}CCHO$)	3.1	± 0.5
propenal	($H_2C{=}CH\text{-}CHO$)	10	± 1
propanal	(CH_3CH_2CHO)	4.0	± 0.6

Looking back at the figure VI-1 the final formation product should result in propanol, so the experiments were started with alcoholic species to evaluate the reduction C≡C and C=C functional groups using the hydrogen addition.

VI.3. Hydrogen addition reactions of unsaturated alcohols

VI.3.1. Hydrogenation of allyl alcohol ($H_2C{=}CHCH_2OH$):

Figure VI-2a shows the infrared spectrum of pure allyl alcohol ($H_2C{=}CHCH_2OH$) ice formed on a mirror maintained at 10 K, with OH and CH stretching modes located in 3600-2500 cm^{-1} spectral region, C=C and C-O vibrations at 1644 and 1110 cm^{-1}, respectively and CH_2, OH and $CH{=}CH_2$ deformations at 1430, 1240 and 994 cm^{-1}, respectively.[23] After IR-analysis, the allyl alcohol ice has been bombarded during 45 min by H atoms. The result of the H-bombardment is shown in figure VI-2b where new signals appear clearly at 2965, 2932 and 2877 cm^{-1}, illustrating a clear transformation of allyl alcohol ice under H exposure. To better characterize such a transformation, Figure VI-2c shows the difference spectrum before and after H bombardment. The difference spectrum can be compared to a reference spectrum of propanol ice (figure VI-2d) obtained by condensing 0.2 μmol of pure propanol. Comparison between figures VI-2c and VI-2d shows that the hydrogenation of allyl alcohol ice leads mainly to the reduction of the C=C double bond to form the saturated propanol ($H_3C{-}CH_2CH_2OH$). If we suppose that for a given species deposited at 10K, the sticking probability on the 1 cm^2 cold mirror of our sampler is 1, we can then deduce the amount of propanol formed in solid phase through:

$$H_2C{=}CHCH_2OH + 2H \rightarrow H_3C{-}CH_2CH_2OH \qquad \text{(VI-1)}$$

In fact, the infrared intensity of the signal of the 0.20 ± 0.05 μmol deposited propanol is almost 1.5 times higher than that of the prapanol ice formed by hydrogenation of $H_2C{=}CHCH_2OH$. Thus we estimate that less than 0.13 μmol of $H_3C{-}CH_2CH_2OH$ could be formed by bombarding a thick ice of allyl alcohol during 45 min with H atoms. Nevertheless the decrease of $H_2C{=}CHCH_2OH$ signal could not be quantified due to the overlapping absorption bands of the reactant and product. However, in some spectral regions as those at 1200-1000 cm^{-1} and 800-500 cm^{-1} (figure

VI-2c), the signal of the bombarded allyl alcohol ice decreases by almost 15 %. From these first results, we can conclude that even though propanol is not yet detected in the interstellar medium, its abundance and astronomical detection could be linked with the unsaturated allyl alcohol ($H_2C=CHCH_2OH$) though such reaction:

$$H_2C=CHCH_2OH + 2H \rightarrow H_3C{-}CH_2CH_2OH \qquad \text{(VI-2)}$$

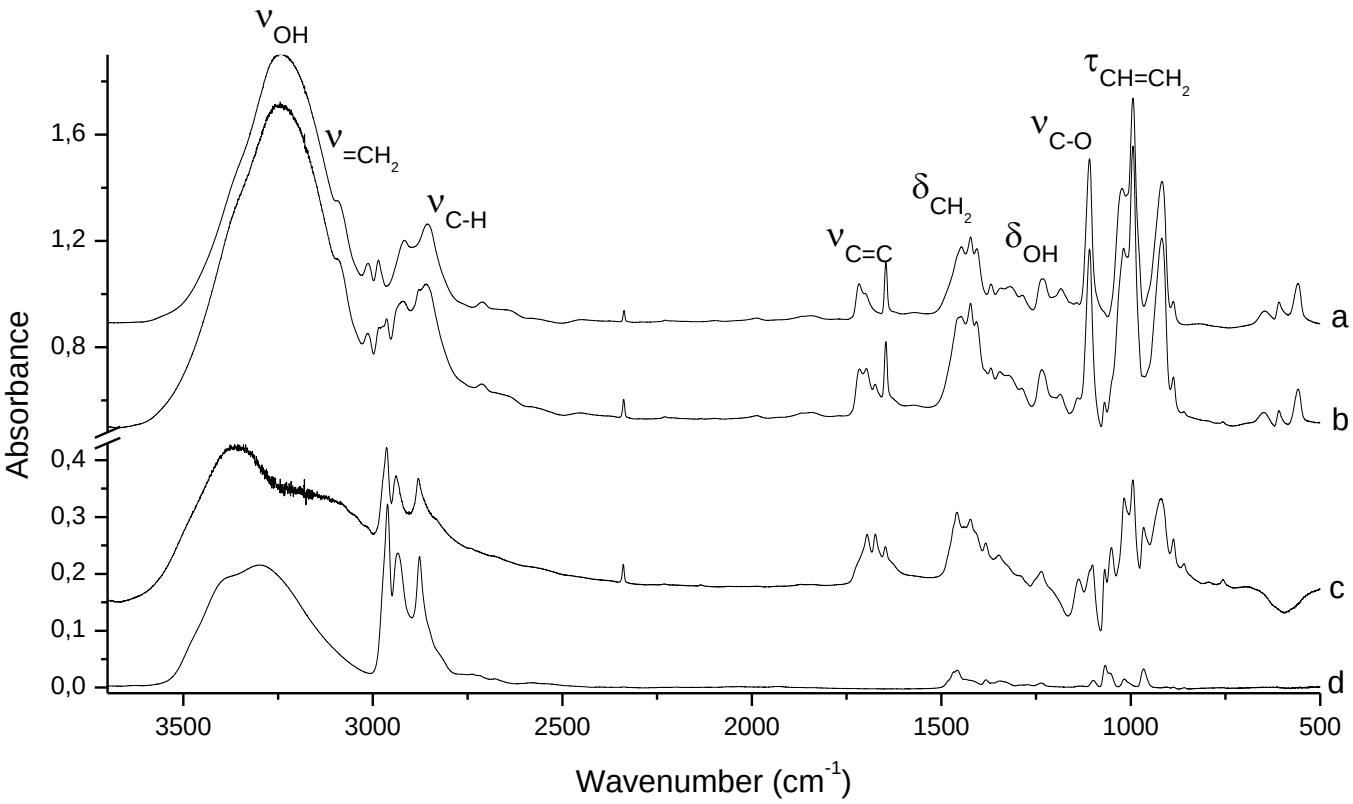

Figure VI-2: IR spectra of:
a) Deposition of 1.0 µmol of allyl alcohol ($H_2C=CHCH_2OH$) on a mirror maintained at 10K.
b) Hydrogenation of solid allyl alcohol ($H_2C=CHCH_2OH$) at 10K.
c) Difference spectrum: Spectrum (b) - spectrum (a).
d) Deposition of 0.2 µmol of pure propanol ($H_3C{-}CH_2CH_2OH$) on a mirror maintained at 10 K.

VI.3.2. Hydrogenation of propargyl alcohol ($HC{\equiv}CCH_2OH$)

Similar experiment have been carried out with the unsaturated propargyl alcohol ($HC{\equiv}CCH_2OH$) to highlight the triple CC bond reduction by H addition in solid phase at 10 K. Figures VI-3a and VI-3b show the infrared spectra of the propargyl alcohol ice before and after H bombardments, respectively, while figure VI-3c shows the resulting difference spectrum. To analyze the consequences of the H-bombardment on propargyl alcohol ice, two reference spectra have been added, in figures VI-3d and VI3e, corresponding to unsaturated allyl alcohol ($H_2C=CHCH_2OH$) and saturated propanol ($CH_3CH_2CH_2OH$) ices, respectively.

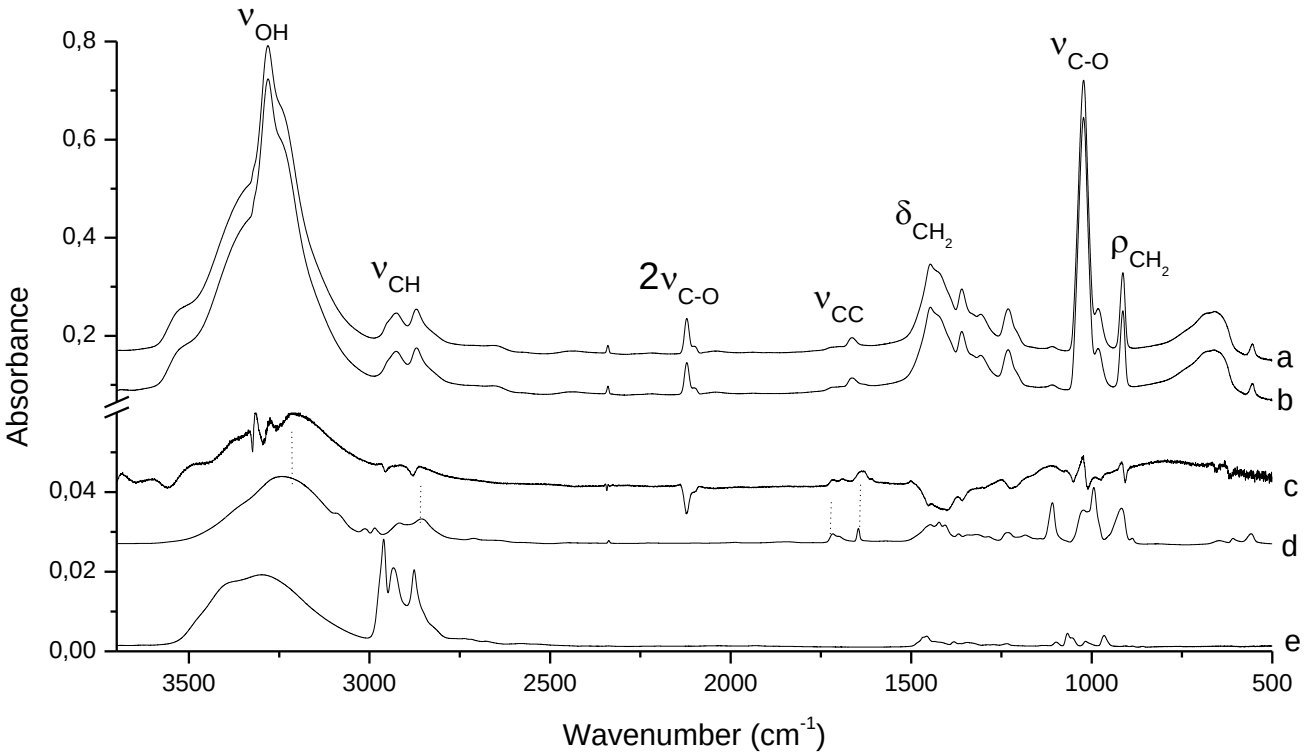

Figure VI-3: IR spectra of:
a) Deposition of 0.30 μmol of propargyl alcohol ($HC{\equiv}CCH_2OH$) alcohol on a mirror maintained at 10K.
b) Hydrogenation of solid propargyl alcohol at 10K.
c) Difference spectrum: Spectrum (b) - spectrum (a).
d) Deposition of pure allyl alcohol ($H_2C{=}CHCH_2OH$) on a mirror maintained at 10K (signal divided by approximately 60 in comparison with that of figure VI-2a).
e) Deposition of 0.20 μmol of pure propanol ($H_3C{-}CH_2CH_2OH$) on a mirror maintained at 10 K (signal divided by approximately 10 in comparison with that in figure VI-2d).

In order to see whether the H-reduction of the triple CC bond in propargyl alcohol ($HC{\equiv}CCH_2OH$) would lead to the formation of a double or a single CC bond, the difference spectrum (figure VI-3c) is compared to the two reference spectra (figures VI-3d and VI-3e). We notice that the difference spectrum, derived from the hydrogenation process of solid propargyl alcohol, is more consistent with the IR signatures of solid allyl alcohol (VI-3d) rather than with those of solid propanol (VI-3e). This can be noted from the spectral region between 3600 and 2500 cm^{-1}, where the shapes of the absorption bands corresponding to OH and CH stretching modes, in the difference spectrum (figure VI-3c) and in that of solid allyl alcohol (Figure VI-3d), are almost similar. However, they differ from those observed in the spectrum of solid propanol (figure VI-3e) which shows three specific structured absorption signals at 2965, 2932 and 2877 cm^{-1}. On the other hand, analysis in the spectral region ranged between 2000 and 1200 cm^{-1} confirm such a point, where the signals shown in the difference spectrum (VI-3c) are more comparable to those corresponding to solid allyl alcohol (figure VI-3d) rather than to those of solid propanol (figure VI-3e).

Here, we can also estimate the amount of allyl alcohol formed through:

$$HC{\equiv}CCH_2OH + 2H \rightarrow CH_2{=}CHCH_2OH \qquad \text{(VI-3)}$$

In fact, by comparing the intensity of the signals in the difference spectrum (VI-3c) to those of solid allyl alcohol obtained by condensing 1.0 ± 0.2 μmol of $H_2C{=}CHCH_2OH$ at 10K. In figure VI-3d, the signal of solid allyl alcohol is divided by 60 in comparison with that of figure VI-2a. Thus, approximately less than 1/60 μmol of $H_2C{=}CHCH_2OH$ could be formed by H-addition on a thick ice of propargyl alcohol. We estimate from the decreasing IR signals in figure VI-3c, that only 5 % of $HC{\equiv}CCH_2OH$ molecules are consumed during the hydrogenation process. From this experiment it can be noted, that the hydrogenation of solid propargyl alcohol ($HC{\equiv}CCH_2OH$) would lead mainly to the formation of allyl alcohol $CH_2{=}CHCH_2OH$.

As a first conclusion we show that the detection of large alcohol species such as propanol is directly associated to the detection of its unsaturated derivatives and there is a chemical link between unsaturated, partially unsaturated and fully saturated large alcohols through H addition reactions occurring under ISM conditions. We managed to improve, experimentally, the bottom formation pathway shown in figure VI-1. Now the question which remains: is there a link between saturated and unsaturated aldehydes on one hand and between aldehydes and their corresponding alcohols on the other hand?

VI.4. H addition reactions of unsaturated aldehydes

Similarly as with alcoholic species in this part the study was extended on aldehydes also. After the hydrogenation of species containing a single, double or triple CC bonds and a CO double bonds it will be visible whether the H atom attack takes place preferably on the multiple CC bonds as observed earlier in the case of the hydrogenation of unsaturated alcohols or on the CO function which it would correspond to the reaction pathway to transform aldehydes into alcohols.

VI.4.1. Hydrogenation of propanal (CH_3CH_2CHO)

As mentioned earlier, propanal (CH_3CH_2CHO) has been detected in the ISM since 2004.[12] In such a situation, this aldehyde could be the source of propanol ($H_3C{-}CH_2CH_2OH$) through CH_3CH_2CHO + 2 H reaction. Figures VI-4a and VI-4b show the infrared spectra of solid propanal before and after H bombardments, respectively. The two spectra are similar showing structured signals between 3000 and 2750 cm^{-1} corresponding to CH stretching modes, a very huge absorption band at 1730 cm^{-1} characteristic of the CO functional group and three sets of signals between 1500 and 750 cm^{-1} corresponding to CH_3 bending and rocking modes.[23] Figure VI-4c shows the resulting difference spectrum and as a reference, the spectrum of solid propanol is presented in figure VI-4d, since the obvious reaction product for a hydrogenation reaction of propanal should be propanol. However, as shown in figures VI-4c and VI-4d, the hydrogenation of propanal does not lead to the formation of propanol. The difference spectrum (figure VI-4c) does not show any slight similarity with that of solid propanol (figure VI-4d). In fact, in the

difference spectrum of figure VI-4d characterizing the H bombardment of solid propanal, we notice that the CO absorption band remains unchanged and simultaneously, while the CH stretching signals slightly decrease those corresponding to the CH_3 bending and rocking modes increase. Such behaviors could be attributed to a transformation of the structure of solid propanal under H atom exposure.[24] However, we do not detect any new signals which could be attributed to a new reaction product such as propanol or even propanal fragments. These results show that CH_3CH_2CHO + 2 H reaction could not be a source of transformation of propanal (CH_3CH_2CHO) into propanol ($CH_3CH_2CH_2OH$), and propanal seems to be stable under H attacks. This may be one of the reasons why propanal is highly abundant in some molecular clouds where one of the predominant reactions are the surface H-addition.

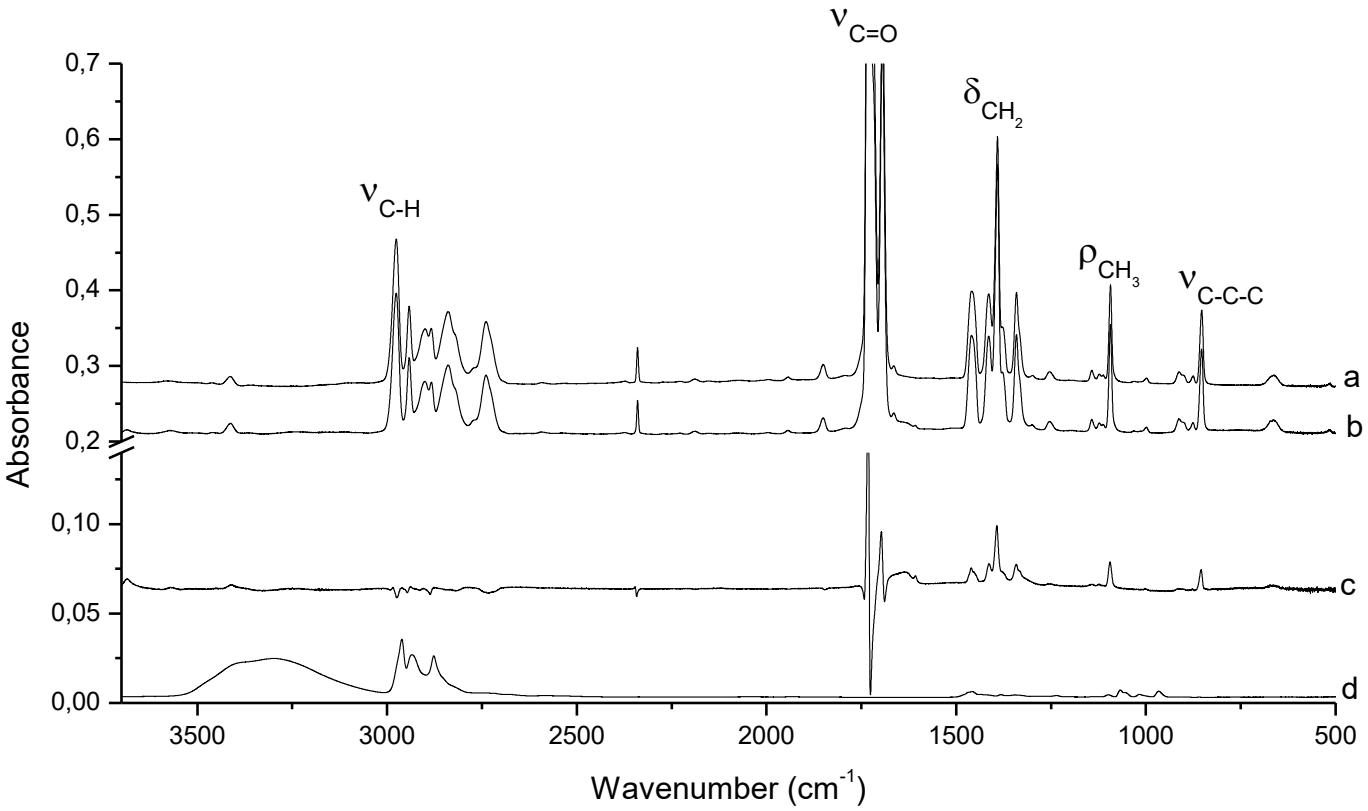

Figure VI-4: IR spectra of:
a) Deposition of 4 µmol of propanal (CH_3CH_2CHO) on a mirror maintained at 10K.
b) Hydrogenation of solid propanal at 10K.
c) Difference spectrum: Spectrum (b) - spectrum (a).
d) Deposition of 0.2 µmol of pure propanol ($H_3C{-}CH_2CH_2OH$) on a mirror maintained at 10 K (signal divided by approximately 10 in comparison with that of figure VI-2d).

VI.4.2. Hydrogenation of propenal (H_2C=CHCHO)

Similarly to the previous hydrogenation experiments, propenal ice has been bombarded for 45 min with H atoms. Figure VI-5a shows the infrared signatures of solid propenal characterized by two sets of signals around 3000 cm^{-1} corresponding to CH stretching modes, two signals around 1700 cm^{-1}, features of C=O and C=C stretching modes, and three sets of signals

between 1500 and 500 cm^{-1} corresponding to CH_2 bending modes, in addition to the C-C stretching signal at 1161 cm^{-1}.[23] Figure VI-5b illustrates the results of the hydrogenation of solid propenal and figure VI-5c shows the corresponding difference spectrum after and before H bombardment. In these latter figures, new signals appear at 2975, 2938, 2890 cm^{-1} in the CH stretching region, at 1730 cm^{-1} in the C=O stretching region, and at 1458, 1397, 1342, 1092 and 855 cm^{-1} in the bending mode region. Those new signals fit exactly the IR signatures of solid propanal CH_3-CH_2CHO as shown in figure VI-5d. We thus conclude that the hydrogenation of unsaturated propenal CH_2=CHCHO containing a double C=C bond and a CO functional group leads exclusively to the reduction of the double C=C into C-C single bond to form propanal CH_3-CH_2CHO and consequently, this reaction cannot be a source of formation of alcohol species:

$$H_2C{=}CHCHO + 2\ H \rightarrow CH_3CH_2CHO \qquad \text{(VI-4)}$$

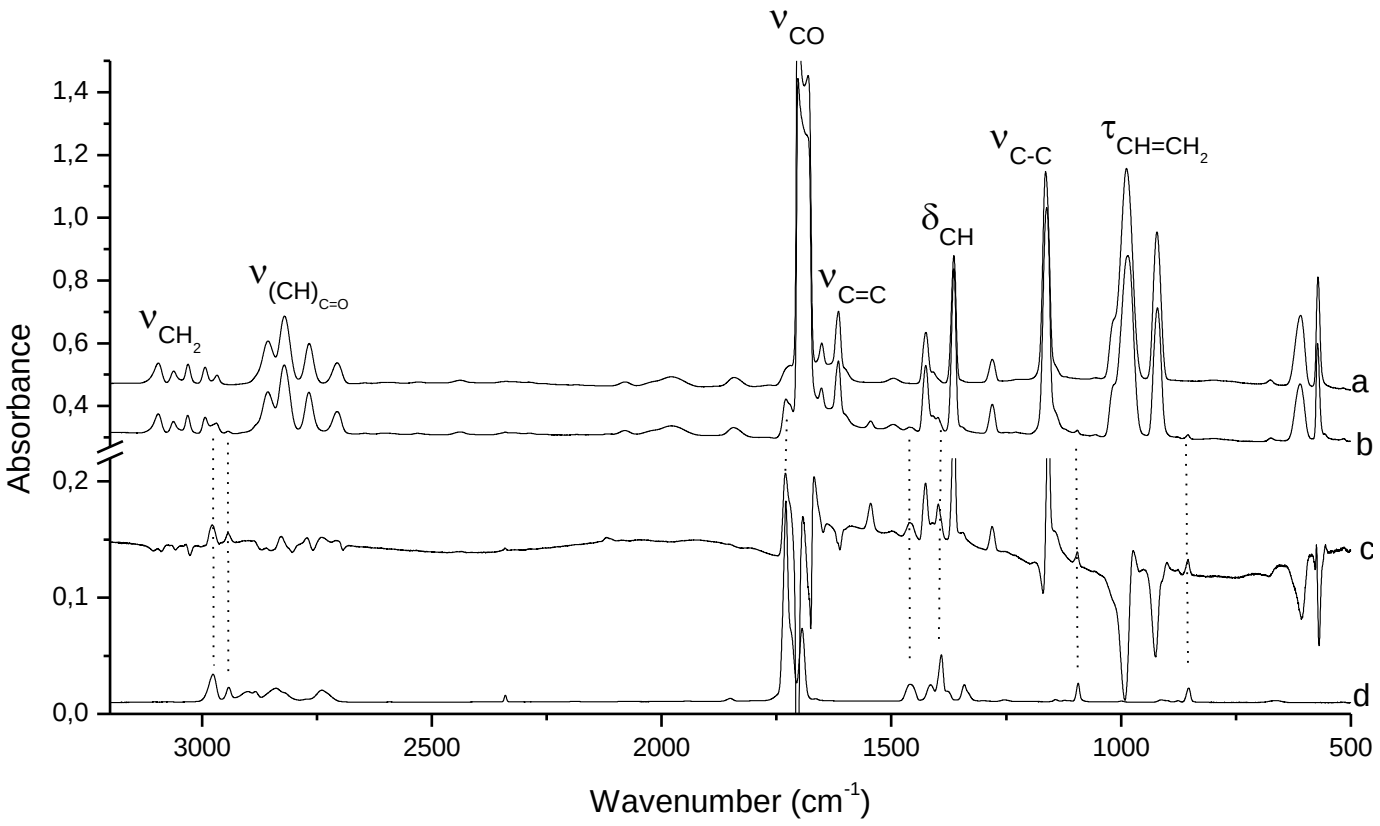

Figure VI-5: IR spectra of:
a) Deposition of 10 µmol of propenal (H_2C=CHCHO) on a mirror maintained at 10K.
b) Hydrogenation of solid propenal at 10K.
c) Difference spectrum: Spectrum (b) - spectrum (a).
d) Deposition of 4 µmol of propanal CH_3-CH_2CHO on a mirror maintained at 10K (signal divided by approximately 10 in comparison with that of figure VI-4a).

In addition to the signals appearing after H-bombardments of solid propenal which are easily assignable to propanal CH_3-CH_2CHO (CH and CO signals around 3000 and 1700 cm^{-1},

respectively, figures VI-5b and VI-5c), figure VI-6 compare the difference spectrum before and after H bombardment, to the IR signatures of solid propanal in two different spectral regions: 3200-2500 cm^{-1} and 1100-800 cm^{-1}. From this figure, we notice a decrease of propenal signal, estimated around 8 % and due to the C=C bond reduction through to $H_2C{=}CHCHO + 2\ H \rightarrow CH_3CH_2CHO$ reaction. More specifically, while signals involving C=C vibrational modes such as ν_{CH2} and $\tau_{CH=CH2}$ disappear, those involving C−C vibrational modes such as ρ_{CH3} and $\nu_{C\text{-}C\text{-}C}$ appear and can be attributed to solid propanal. Comparison between the IR intensities in the difference spectrum (VI-5c and VI-6c) and those of solid propanal obtained by condensing of 4 .0 ± 0.6 µmol of CH_3CH_2CHO at 10K (in figures VI-5d and VI-6d, the signal of solid propanal is divided by 10 in comparison with that of figure VI-4a) shows that approximately 4/10 µmol of CH_3CH_2CHO could be formed by H-addition on a thick ice of $H_2C{=}CHCHO$.

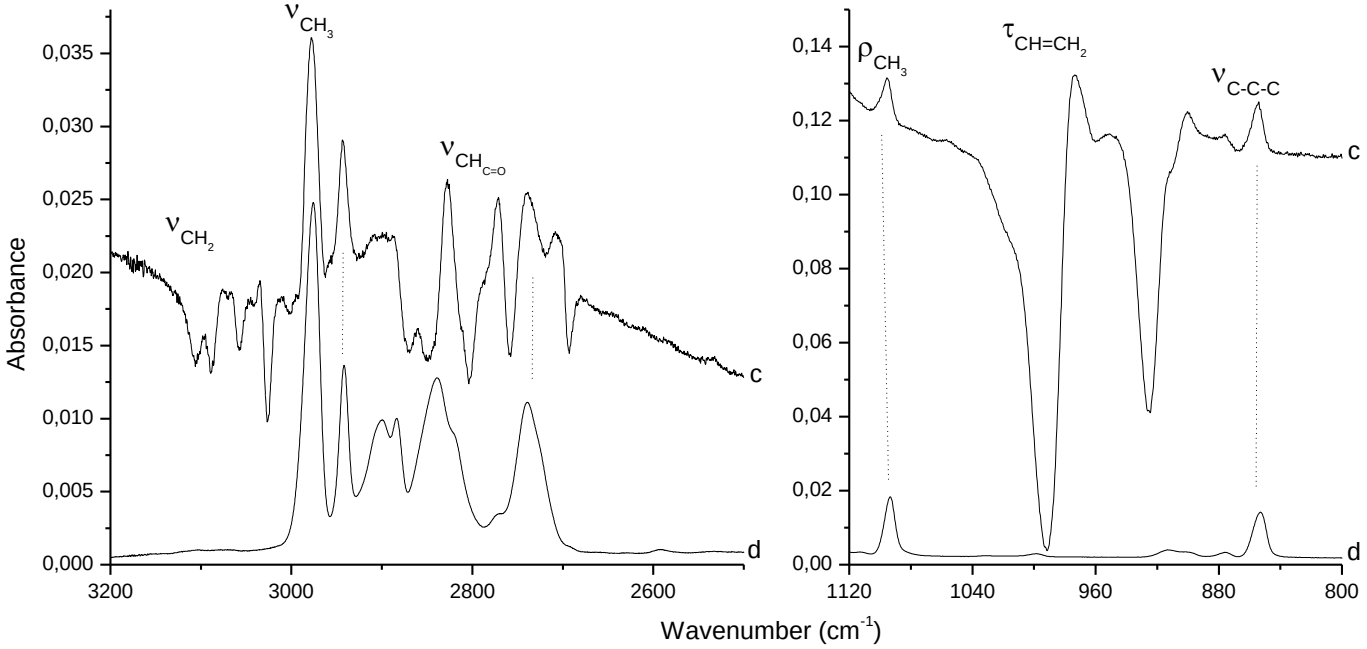

Figure VI-6: Zoom of IR spectra in figures VI-5c and VI-5d, in two spectral regions, 3200-2500 cm^{-1} (left) and 1100-800 cm^{-1} (right):
c) Difference spectrum: Spectrum-figure VI-5b - spectrum-figure VI-5a.
d) Deposition of propanal CH_3-CH_2CHO on a mirror maintained at 10K (signal divided by approximately 10 in comparison with that of figure VI-4a)

VI.4.3. Hydrogenation of propynal (HC≡CCHO)

Figures VI-7a and VI-7b show the infrared spectra of solid propynal before and after H bombardments, respectively. From figure VI-7a characterizing the solid propynal, we note two sets of signals around 3000 cm^{-1} corresponding to CH stretching modes, three signals at 2100, 1660 and 947 cm^{-1} attributed to C≡C, C=O and C-C stretching modes, respectively and the HCO bending mode, located at 1388 cm^{-1}.[25] Figure VI-7b shows the results of the hydrogenation of solid propynal while figure VI-7c illustrates the difference spectrum after and before H bombardments. As a reference, the spectrum of solid propenal ($H_2C{=}CHCHO$) is presented in

figure VI-7d, supposing that the hydrogenation of a triple C≡C bond might lead to the formation of a C=C double bond, thus the propenal species. Since from the previous observations, it was showed that the hydrogenation of $HC{\equiv}CCH_2OH$ leads to the formation of $CH_2{=}CHCH_2OH$ and that the CO function remains unchanged for the $H_2C{=}CHCHO$ + 2 H reaction.

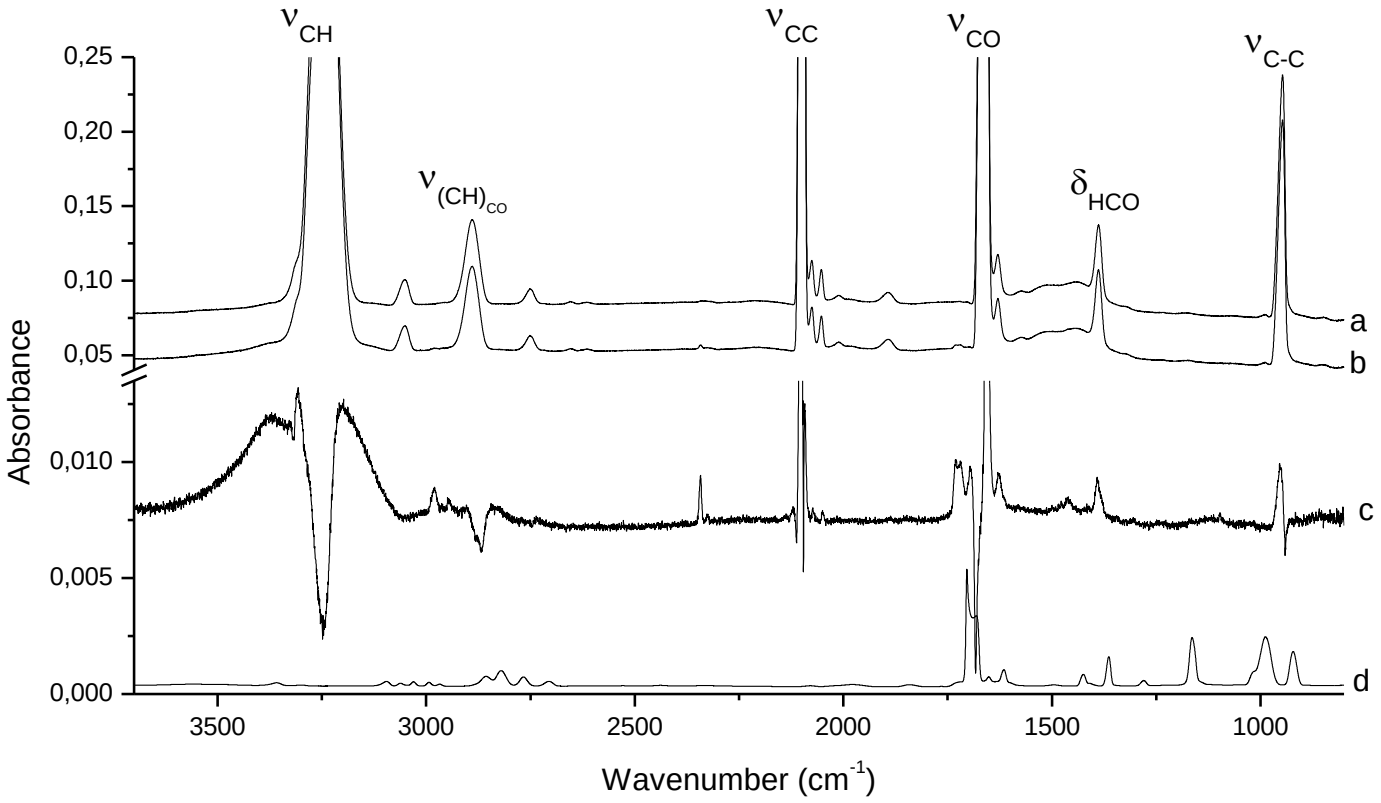

Figure VI-7: IR spectra of:
a) Deposition of 3.1 µmol of pure propynal (HC≡CCHO) on a mirror maintained at 10K.
b) Hydrogenation of solid propynal at 10K.
c) Difference spectrum: Spectrum (b) - spectrum (a).
d) Deposition of 10 µmol of pure propenal ($H_2C{=}CHCHO$) on a mirror maintained at 10 K (signal divided by approximately 600 in comparison with that of figure VI-5a).

Although the difference spectrum (figure VI-7c) shows a small decrease of propynal (HC≡CCHO) signal estimated around 1.5 %, due to HC≡CCHO + 2 H reaction, the new signals appearing at 2975, 1730 1458, 1397 cm^{-1} do not show any similarity with the IR absorption signals of solid $H_2C{=}CHCHO$ (figure VI-7d), suggesting that the hydrogenation of propynal may lead to the formation of another chemical species rather than propenal. In fact, the new species formed during the hydrogenation process is propanal resulting from a direct transformation of the triple C≡C bond into single C−C bond.

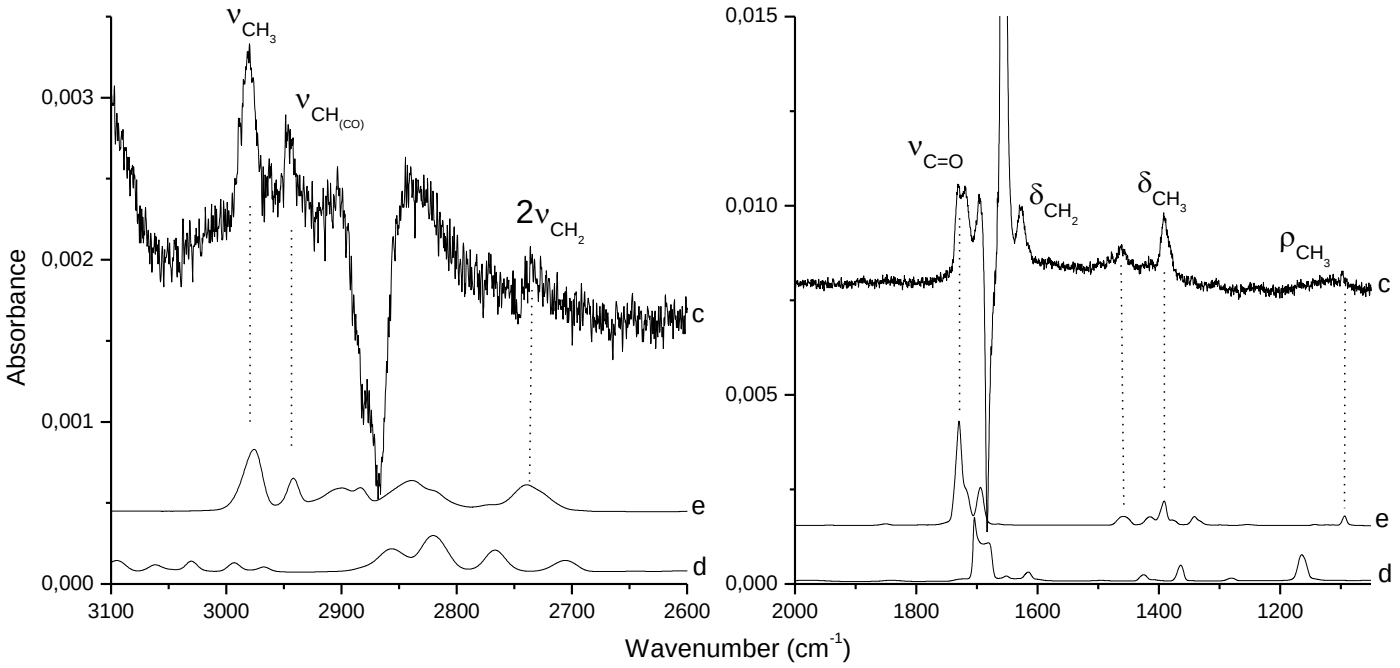

Figure VI-8: Zoom of IR spectra in figures VI-7c and VI-7d, in two spectral regions, 3200-2500 cm^{-1} (left) and 2000-1000 cm^{-1} (right): c) Difference spectrum: Spectrum-figure VI-7b - spectrum-figure VI-7a
d) Spectrum of solid propenal formed at 10K (signal divided by 600 in comparison with that of figure VI-5a)
e) Spectrum of solid propanal CH_3-CH_2CHO formed at 10K (signal divided by approximately 400 in comparison with that of figure VI-4a)

To confirm such a suggestion, figures VI-8c and VI-8d show a zoom in the 2000-1000 cm^{-1} and 3100-2600 cm^{-1} spectral regions of figures VI-7c and VI-7d, and figure VI-8e corresponds to solid propanal. We notice, from figure VI-8, that in addition to the decrease of the signal at $\nu_{CH(C=O)}$ and $\nu_{C=O}$ of propynal, the new signals appearing at 2975, 2946, 2738, 1730 1458, 1397 and 1092 cm^{-1}, after H bombardment of propynal ice, are in good agreement with the IR signatures of the solid propanal (figure VI-8e) rather than with those of solid propenal (VI-8d). Comparison between the IR intensities in the difference spectrum (VI-8c) and those of solid propanal from figure VI-8e, where the IR signal due the condensation of 4.0 ± 0.6 µmol of CH_3-CH_2CHO is divided by 400, allows an estimation of the amount of propanal formed by hydrogenation of propynal. In such a situation, approximately less than 4/400 µmol of CH_3CH_2CHO could be formed by H-addition on HC≡CCHO. Such a direct transformation of propynal into propanal without observing propenal as intermediate might be due to the fact that H_2C=CHCHO + 2 H → CH_3CH_2CHO reaction could be kinetically faster than HC≡CCHO + 2H → H_2C=CHCHO.

VI.5. Transformation pathways

The efficiency of a hydrogenation reaction, carried out by bombarding solid samples by H atoms, should depend on the thickness of the ice sample, the energy barrier of the H-addition reaction and the flux of the H atoms.[7,8,9,19] In this study all the ices formed under our experimental conditions are thick and are exposed to the same amount of H-atoms, the yield of the studied hydrogenation reactions would depend more on the energy barriers of a given reaction than on the reactant concentrations. However, the concentration of the reactants and the products can be evaluated from the IR spectrum analysis. The integrated intensities of the absorption bands of the reactants and products can be calculated and corresponding column densities **n** (molecules/cm^2) might be deduced knowing the IR absorption band strength (A cm/molecule) for a given species X trapped in the solid sample using the formula II-12 (page 52) already explained in chapter II:

$$\mathbf{n} = \frac{ln10 \int I(v)dv}{A} \frac{\cos(8°)}{2} \qquad \text{(VI-5)}$$

Still, in order to have an order of magnitude of the concentrations of the species involved in solid phase, the band strength (A) for a given trapped species X should be known. This is the case for simple molecules such as CO, CH_3OH, H_2CO, HCN but not that for relatively larger molecules investigated in the present study. For this reason the band strengths of different absorption bands of $HC{\equiv}CCH_2OH$, $H_2C{=}CHCH_2OH$, $H_3C{-}CH_2CH_2OH$, $HC{\equiv}CCHO$, $H_2C{=}CH{-}CHO$, $CH_3{-}CH_2CHO$ pure ices were estimated, by taking into account the exact amount of the vapor pressures of the deposited species and by supposing that the sticking probability on the cold surface (1cm^2) of our sampler is 1. Table VI-2 lists the calculated band strengths A_{OH}, A_{CH}, $A_{C=O}$, $A_{C=C}$, $A_{C\equiv C}$, corresponding to OH, CH, CO and CC absorption bands for the studied alcohols and aldehydes.

Table VI-2: Calculated band strengths (in cm molecule^{-1}) A_{OH}, A_{CH}, $A_{C=O}$, $A_{C=C}$, $A_{C\equiv C}$

Species X	**n** 10^{17}	A_{OH} 10^{-16}	A_{CH} 10^{-17}	$A_{C=O}$ 10^{-17}	$A_{C=C}$ 10^{-17}	$A_{C\equiv C}$ 10^{-17}
propargyl alcohol ($HC\equiv CCH_2OH$)	1.8 ± 0.5	8 ± 2	4 ± 1			0.5 ± 0.1
allyl alcohol ($H_2C=CHCH_2OH$)	6.0 ± 1	4 ± 1	5 ± 1		1.3 ± 0.3	
Propanol ($H_3CCH_2CH_2OH$)	1.2 ± 0.3	6 ± 2	22 ± 6			
propynal ($HC\equiv CCHO$)	19 ± 3		1.6 ± 0.2	1.0 ± 0.2		0.9 ± 0.1
propenal ($H_2C=CH-CHO$)	60 ± 6		0.4 ± 0.1	0.06 ± 0.01	0.6 ± 0.1	
propanal (CH_3CH_2CHO)	24 ± 4		0.8 ± 0.1	1.4 ± 0.2		

n: column density (molecules/cm^2)

Spectral regions for band strengths calculations:

propargyl alcohol - ν_{OH}: 3700-2995 cm^{-1}, ν_{CH}: 2995-2710 cm^{-1}, ν_{CC}: 1760-1616 cm^{-1}

allyl alcohol - ν_{OH}: 3609-3031cm^{-1}, ν_{CH}: 2966-2738 cm^{-1}, ν_{CC}: 1751-1607cm^{-1}

propanol - ν_{OH}: 3593-3006cm^{-1}, ν_{CH}: 3006-2766 cm^{-1}

propynal - ν_{CH}: 3393-3110cm^{-1}, ν_{CC}: 2135-2030 cm^{-1}, ν_{CO}: 1697-1608cm^{-1}

propenal - ν_{CH}: 3142-2941cm^{-1}, ν_{CC}: 1715-1664 cm^{-1}, ν_{CO}: 1663-1600cm^{-1}

propanal - ν_{CH}: 3026-2680cm^{-1}, ν_{CO}: 1747-1705cm^{-1}

We note, from table VI-2, that CH band strengths of propynal are twice that of propanal and four times that of propenal. On the other hand the CO band strength of CH_3CH_2CHO is 1.4 times higher than that of $HC\equiv CCHO$ but nearly 23 times higher than that of $H_2C=CH-CHO$, which will make it easier to detect species such as propynal and propanal rather than propenal. Furthermore, while the OH band strengths of the three alcohols have the same order of magnitude, the CH band strength of propanol is almost five times higher than that of $H_2C=CHCH_2OH$ and $HC\equiv CCH_2OH$. Knowing the band strengths of those aldehydes and alcohols, we can deduce the column densities (molecules/cm^2) of the different species formed during the hydrogenation processes. Table VI-3 gathers the column densities of a given reaction product Y though X + H $\rightarrow$Y successive H-addition reaction.

Table VI-3: Column densities of Y species formed through X + H→Y reaction

Deposited species X	Nature of Y species formed through X + H→Y reaction	Y Column densities (molecules/cm^2) 10^{17}
$HC{\equiv}CCH_2OH$	$H_2C{=}CHCH_2OH$	0.10 ± 0.02
$H_2C{=}CHCH_2OH$	$H_3CCH_2CH_2OH$	0.8 ± 0.2
$H_3CCH_2CH_2OH$	-	-
$HC{\equiv}CCHO$	CH_3CH_2CHO	0.06 ± 0.01
$H_2C{=}CH\text{-}CHO$	CH_3CH_2CHO	2.3 ± 0.3
CH_3CH_2CHO	-	-

From table VI-3, we notice that even though the hydrogenation reactions of $HC{\equiv}CCH_2OH$ and $H_2C{=}CHCH_2OH$ involve two successive H-additions, the comparison between the amounts of the obtained reaction products shows that the $H_2C{=}CHCH_2OH$ + 2H reaction is 8 times more efficient than the $HC{\equiv}CCH_2OH$ + 2H reaction. We conclude that the reaction $HC{\equiv}CCH_2OH$ + 2H should get an energy barrier relatively higher than that of $H_2C{=}CHCH_2OH$ + 2H and this may explain the low amount of allyl alcohol formed when *$HC{\equiv}CCH_2OH$* ices are exposed to H atoms. Consequently, the low yield of the $HC{\equiv}CCH_2OH$ + 2H → $CH_2{=}CHCH_2OH$ reaction may prevent a complete reduction of the *$C{\equiv}C$* triple bond of propargyl alcohol.

Similarly, the transformation of the $H_2C{=}CH\text{-}CHO$ aldehyde into CH_3CH_2CHO seems to be very efficient as it leads to the formation of a huge amount of propanal ($2.3{\times}10^{17}$ molecules/cm^2). However in the case of $HC{\equiv}CCHO$ hydrogenation, we observed directly a total reduction of the triple C≡C bond and there is no evidence for the detection of $H_2C{=}CH\text{-}CHO$ as a reaction intermediate. We conclude that $H_2C{=}CH\text{-}CHO$ + 2H reaction should not have an energy barrier or at least, it would show an activation energy lower than that of $HC{\equiv}CCHO$ + 2H, and thus as soon as the $H_2C{=}CH\text{-}CHO$ is formed through $HC{\equiv}CCHO$ + 2H reaction, it is transformed into propanal. These results are in good agreement with the interstellar observations where propynal and propanal are abundant in molecular clouds while the detection of propenal has never been confirmed.[11,12] On the other hand, by comparing the results of the CC bond reductions in alcohols and aldehydes, we would point out that the non-detection of propanol from *$HC{\equiv}CCH_2OH$* + 4H reaction would be due to the fact that the energy barrier of $H_2C{=}CHCH_2OH$ + 2H reaction should be higher than that of $H_2C{=}CH\text{-}CHO$ + 2H. In the case of the unsaturated aldehyde species, it also shows that there is no link between large aldehydes and their corresponding reduced alcohols via successive hydrogen additions occurring under ISM conditions.

Even though many studies have proposed the existence of links between aldehydes and their corresponding alcohols in the interstellar grains[16] taking as examples the CO + H and H_2CO + H surface reactions,[2,3,4,6] the solid phase hydrogenation reaction of the simplest aldehyde H_2CO to form CH_3OH would be an exception. It is shown in this study that propanal does not react with

H atoms under interstellar conditions to form propanol and this is consistent with the fact that CH_3CH_2CHO is highly abundant in space while $CH_3CH_2CH_2OH$ is still not detected.

Consequently the presence of aldehydes and their corresponding alcohols, very often not in the same interstellar regions,[16] does not mean that alcohol species are necessarily produced on icy mantles in the ISM via aldehydes + H reaction. In contrast with the photoinduced reaction we have studied in Chapter V corresponding to the photolysis of CH_4-H_2O interstellar ice analogs, which can be proposed as the only pathways to be taken into account to explain the formation of large alcohols detected in hot cores.

In order to understand why formaldehyde is reduced into methanol by H-addition reaction and not larger aldehydes such as propanal and propenal, we have first analyzed, from a theoretical point of view, the key step of CH_3OH formation which is H + H_2CO reaction.[27]

Many theoretical models have already shown that H + H_2CO reaction leads to the formation to H_3CO which is converted by tunneling into a more stable radical H_2COH. Afterwards, the H_2COH or both radicals would react with H atoms to form methanol. Figure VI-9 shows the relative energies of H_2COH and H_3CO and transition states for H + H_2CO reaction. The energy barrier for the $H_2CO + H \rightarrow H_3CO$ reaction is 5.7 kcal/mol while that of $H_2CO + H \rightarrow H_2COH$ is 11.6 kcal/mol. H_2COH radical is 8.4 kcal/mol more stable than H_3CO and this relative stability between the two radicals allows the isomeric conversion $H_3CO \rightarrow H_2COH$. It would play an important role, as we will specify later, in the formation of methanol by successive H addition on H_2CO.

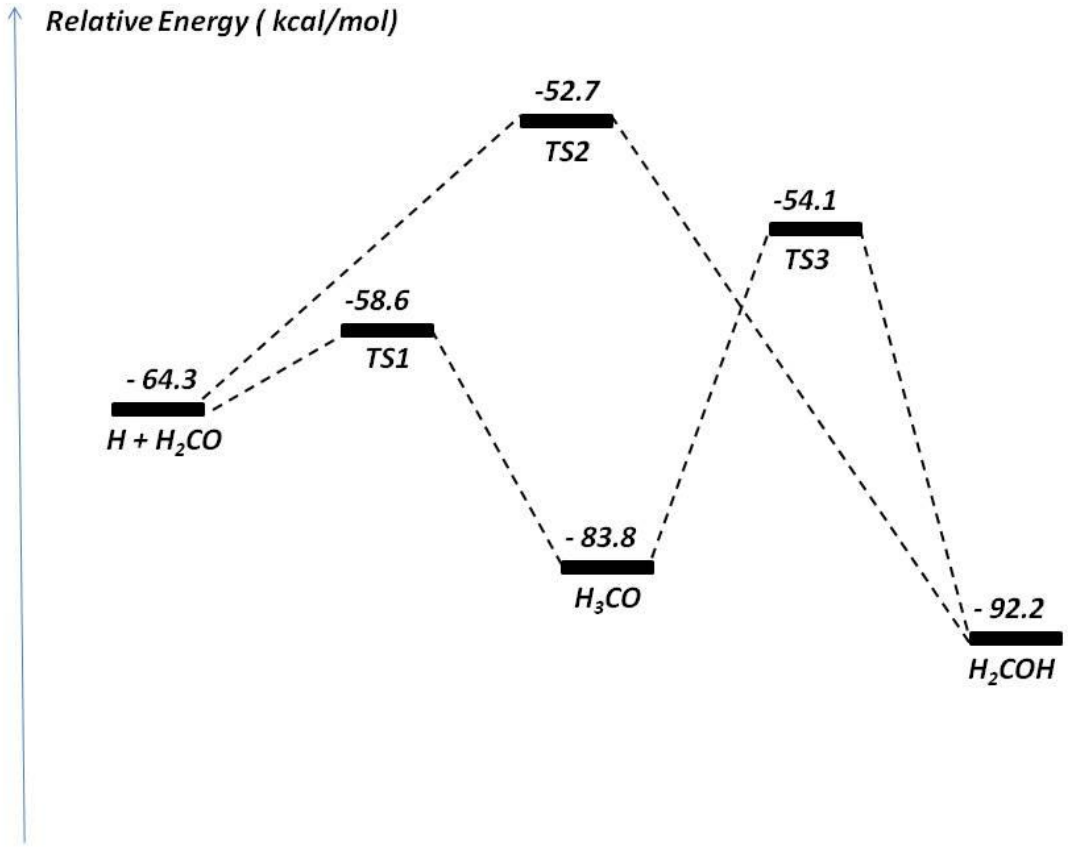

Figure VI-9: Relative energies of H_2COH and H_3CO and transitions states for H + H_2CO reaction according to Xu et al.[27] TS1 and TS2 are the transitions states that lead to the reaction products H_3CO and H_2COH. TS3 is the transition state between the two isomeric forms H_3CO and H_2COH.

Even though there is no theoretical model for the hydrogenation of larger aldehydes such as propanal, propenal and propynal, Kwon et al.[28] investigated the potential energy surface of the $O(^3P)$ + C_3H_5 reaction , where H_2C=CH-CHO was formed and reacted with H atoms to form three radicals H_2C-CH_2-CHO, H_2C=CH-CH_2O and H_2C=C-CH_2OH. The former one is due to the reduction of the C=C bond of propenal while the two latter ones, similar to H_3CO and H_2COH from H_2CO + H reaction, should play the key role for the formation of the allyl alcohol species from H_2C=CH-CHO + H reaction.

Figure VI-10 shows the relative energies of H_2C-CH_2-CHO, H_2C=CH-CH_2O and H_2C=C-CH_2OH. First the reduction of the C=C bond of propenal may take place through H + H_2C=CH-CHO → H_2C-CH_2-CHO reaction which is exothermic by 31.3 kcal/mol and has a low energy barrier of 7.2 kcal/mol. Afterwards the H_2C-CH_2-CHO radical may react with an additional H atom through a hydrogen attack on the carbon atom to form propanal (H_3C-CH_2-CHO), a scenario which has been validated by our experimental results.

The reduction of the C=O function would start by the H + H_2C=CH-CHO reaction which would lead to the formation of H_2C=CH-CH_2O radical, an intermediate of H_2C=CHCH_2OH alcohol. This reaction is exothermic by 12.7 kcal/mol, has a low energy barrier of 4.7 kcal/mol and may easily occur under our experimental conditions.

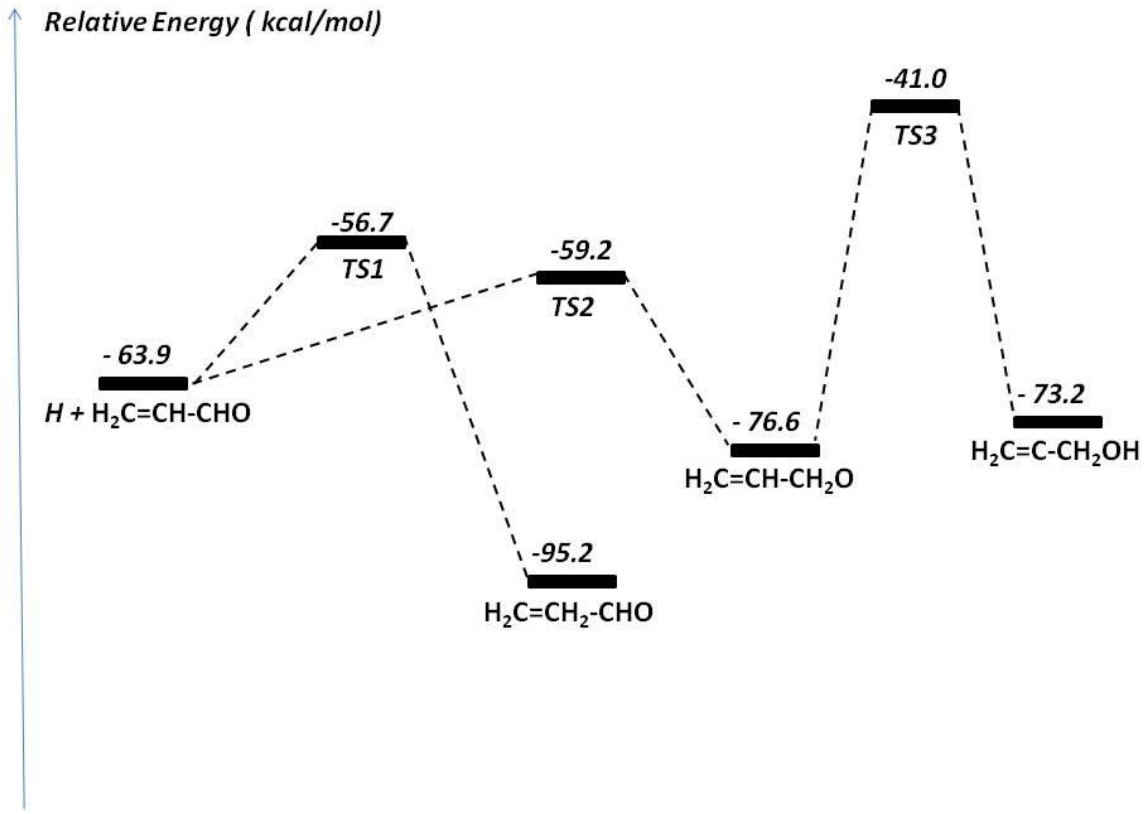

Figure VI-10: Relative energies of H_2C=CH_2-CHO, H_2C=CH-CH_2O and H_2C=C-CH_2OH and transitions states for H + H_2C=CH-CHO reaction according to Kwon et al.[28] TS1 and TS2 are the transitions states that lead to the reaction products H_2C=CH_2-CHO and H_2C=CH-CH_2O. TS3 is the transition state between the two isomeric forms H_2C=CH-CH_2O and H_2C=C-CH_2OH.

Conversely to the formation of H_3CO and its conversion by tunneling $H_3CO \rightarrow H_2COH$ into the corresponding stable isomer CH_2OH which would open two different routes for the formation of methanol though H_3CO + H and CH_2OH + H, the radical H_2C=CH-CH_2O, more stable by 3.4 kcal/mol than its corresponding isomer H_2C=C-CH_2OH, would not be converted into H_2C=C-CH_2OH by tunneling. Thus without providing an external energy to the system, there is only one route for the formation of H_2C=CHCH_2OH alcohol which is H_2C=CH-CH_2O + H reaction where an H atom would attack the oxygen atom of H_2C=CH-CH_2O. It is important to underline all these calculations have been given in the gas phase and then in diluted medium. Solid phase reactions may involve other chemical and physical processes, such as strong hydrogen bonding which may prevent some reaction to take place. In fact, the formation of H_2C=CH-CH_2O as a first reaction intermediate could not lead to a complete hydrogenation

process as the oxygen atom of H_2C=CH-CH_2O would be probably engaged in hydrogen bonds with neighboring molecules. This hydrogen bonding, favorable in solid phase, would prevent the formation of the OH function as proposed in the diagram figure VI-11.

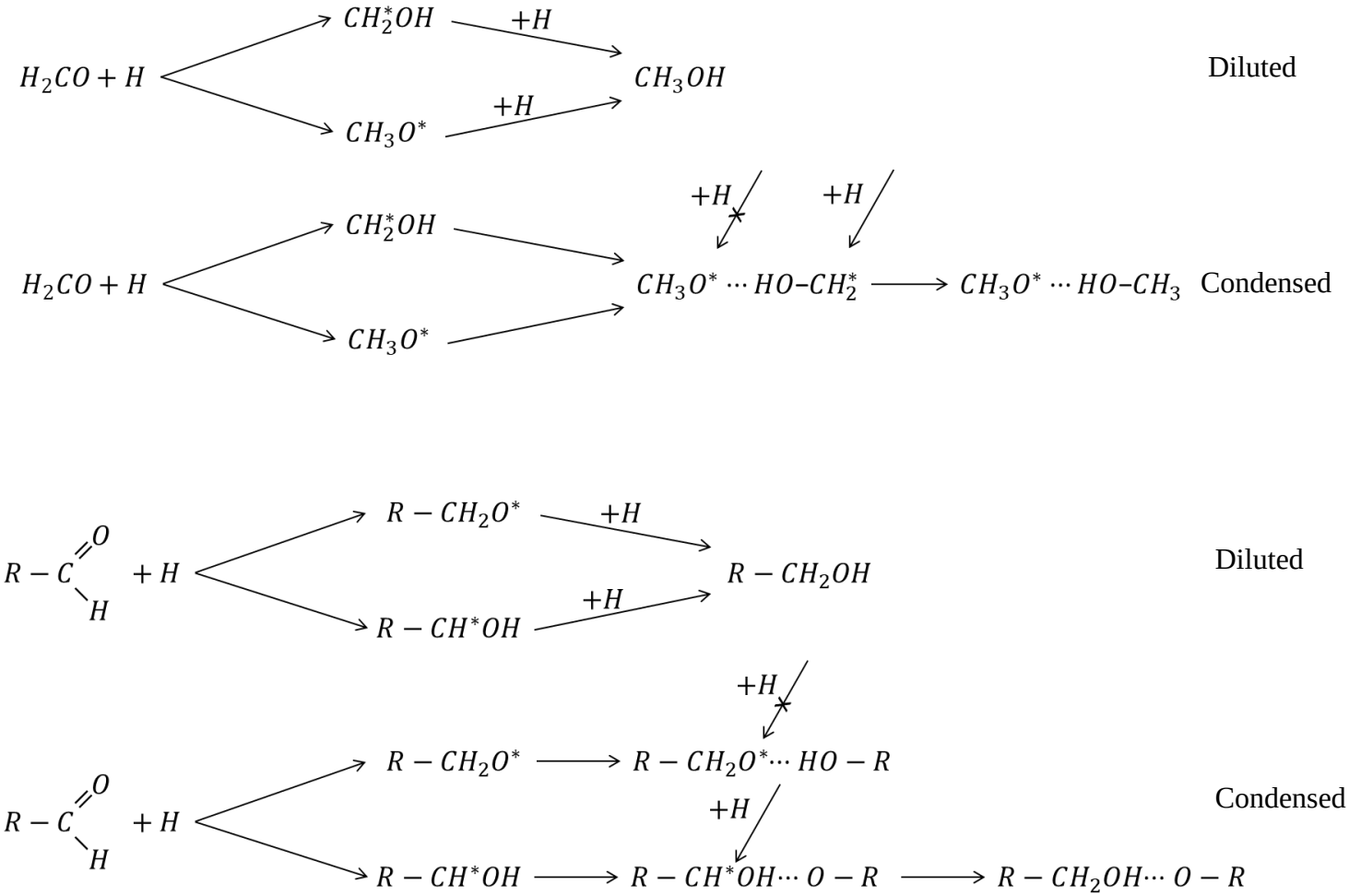

Figure VI-11. Comparison of methanol formation from H_2CO and alcohol formation from larger aldehydes in both diluted and condensed phase due to the hydrogen bonding

From the figures VI-10 and VI-11 we notice that the H_2C=C-CH_2OH + H reaction would be more viable than H_2C=CH-CH_2O + H, as the H attack would occur on the central carbon, free from any intermolecular interactions. We conclude that in order to form H_2C=$CHCH_2OH$ by successive H addition reactions on H_2C=CH-CHO, we should support the H_2C=C-CH_2OH + H reaction rather than H_2C=CH-CH_2O + H. This would occur only by inducing a conversion of the stable radical H_2C=CH-CH_2O into the less stable one H_2C=C-CH_2OH by providing, to the system, an external energy higher than 35.6 kcal/mol. This is consistent with our experimental results proving that the reduction of a CC bond may occur just by H-addition reaction however the transformation of aldehydes species into alcohols cannot take place through aldehydes + H solid phase reaction and it would probably require further energy to occur.

VI.6. Conclusions

The hydrogenation of the simplest aldehyde H_2CO to form CH_3OH would not justify the link between other aldehydic species and their corresponding alcohols in icy mantles on the interstellar grains as proposed in many astrophysical models. Propynal and propanal have been observed in the ISM where H addition reactions are predominant while neither propargyl nor propanol alcohols have been detected. This led to the investigation of the hydrogenation process of alcohols and aldehydes involving triple, double and single CC bonds under the ISM conditions for a better understanding of their chemistry. It should be noted that unsaturated species are firstly detected in the ISM in high abundances. Pure aldehyde and alcohol ices formed at 10 K have been bombarded by H-atoms and the yield of the reactions has been measured in solid phase by infrared spectroscopy. It was showed in this experimental study that unsaturated alcohols can be reduced to fully or partially saturated alcohols while unsaturated aldehydes such as propynal and propenal are exclusively reduced to fully saturated aldehyde, propanal. This study also shows that there is no link between larger aldehydes and their corresponding reduced alcohols via successive H-addition occurring in solid phase at cryogenic temperatures. Most usually the presence of aldehydes and saturated alcohols are often not in the same interstellar regions, implying that alcoholic species are not necessarily produced on icy grains via aldehydes + H reactions. Thus, rather than H thermal reactions, energetic routes such as photolysis or radiolysis of carbon bearing species mixed with water should be more investigated to explain the formation pathways of alcohol species. We have already shown in chapter V that UV irradiation of CH_4-H_2O ices is temperature dependent and leads to the formation of larger alcohols.

Bibliography

[1] Charnley S. B. (2001b) Interstellar organic chemistry. In The Bridge Between the Big Bang and Biology (F. Giovannelli, ed.), pp. 139–149. Consiglio Nazionale delle Ricerche President Bureau Special Volume, Rome, Italy

[2] Hiraoka K., Sato T., Sato S., Sogoshi N., Yokoyama T., Takashima H., Kitagawa S., 2002, ApJ, 577, 265

[3] Watanabe N., Nagaoka A., Shiraki T., Kouchi A., 2004, ApJ, 616, 638

[4] Hidaka, H., Watanabe, N., Shiraki, T., Nagaoka, A., Kouchi, A. 2004, ApJ, 614, 1124

[5] Dulieu F., Amiaud L., Congiu E., Fillion J.-H., Matar E., Momeni A., Pirronello V., Lemaire J.-L., 2010, A&A, 571, A30

[6] Krim L., Laffon C., Parent Ph., Pauzat F., Pilme J., Ellinger Y., 2010, J. Phys. Chem. A, 114, 3320

[7] Hiraoka K., Ohashi N., Kihara Y., Yamamoto K., Sato T., Yamashita A., 1994, Chem. Phys. Lett., 229, 408,

[8] Watanabe N., Kouchi A., 2002, ApJ, 571, L173

[9] Fuchs G. W., Cuppen H. M., Ioppolo S., Romanzin C., Bisschop S. E., Andersson S., van Dishoeck E. F., Linnartz H., 2009, A&A, 505, 629

[10] Pirim C., Krim L., 2011, PCCP, 13, 19454

[11] Turner B. E., ApJ, 1991,76, 617

[12] Hollis J. M., Jewell P. R., Lovas F. J. Remijan A., MØllendal H., 2004, ApJ., 610, L21

[13] Hollis J. M., Lovas F. J., Remijan A. J., Jewell P. R., Ilyushin V. V., Kleiner I., ApJ., 2006, 643, 25

[14] Ball J. A., Gottlieb C. A., Lilley A.E., Radford H. E., 1970, ApJ, 162, L203

[15] Zuckerman B., Turner B. E., Johnson D. R., Lovas F. J., Palmer P., Morris M., Lilley A. E., Ball J. A., Clark F. O., 1975, ApJ, 196, L99

[16] Hollis J. M., Lovas F. J., Jewell P. R., Coudert L. H., 2002, ApJ., 571, L59

[17] Irvine W. M., Brown R. D., Cragg D. M., Friberg P., Godfrey P., Kaifu N., Matthews H. E., Ohishi M., Suzuki H. D., Takeo H., 1988, ApJ, 335, L89

[18] Bisschop S. E., Jørgensen, J. K., van Dishoeck E. F., de Wachter E. B. M., 2007, A&A, 465, 913

[19] Watanabe N., Shiraki T., Kouchi A., 2003, ApJ, 588, 121

[20] Theule P., Borget F., Mispelaer F., Danger G., Duvernay F., Guillemin J. C., Chiavassa T., 2011, A&A 534, A64

[21] Sauer J. C., 1963, Organic Syntheses, Coll. Vol. 4, 813

[22] Stull D. R., Ind. Eng. Chem., 1947, 39, 517

[23] Dostert K.H., O'Brien C.P., Mirabella F., Ivars-Barcelo F., Schauermann S., 2016, PCCP, 18, 13960

[24] Accolla M., Congiu E., Dulieu F., Manico G., Chaabouni H., Matar E., Mokrane H., Lemaire J. L., Pirronello V., 2011, PCCP, 13, 8037

[25] Klarde P., Kremer G., 1977, Spectrochim Acta, 33A, 947.

[26] Moore, M. H., Hudson, R. L. 1998, Icarus, 135, 518

[27] Xu Z. F., Raghunath P., Lin M. C., 2015, J. Phys. Chem. A, 119, 7404

[28] Kwon H., Park J., Lee H., Kim H., Choi Y., Choi J., 2002, J. Chem. Phys., 116, 2675

Chapter VII:

Photochemistry of CH_4-NH_3-H_2O ice

The last chapter tackles the combination of both studies already discussed above: photolysis of methane and ammonia ices containing water in order to have specific role of water of photodecomposition of NH_3 molecules in one hand and CH_4 molecules in the other hand. The combination of both methane and ammonia doubles the hardships of both cases, already discussed in previous chapters: high overlap of IR bands and difficult identifications of possible species. This study will be devoted into the formation of species containing at least N and C and eventually O atoms. We already showed that N_2 and NH_2OH derive from NH_3-H_2O photolysis while alka[e]nes and at least 4 alcohols in addition to H_2CO are formed during the photolysis of CH_4-H_2O ices. The question should be raised now: how photofragments such as NH, NH_2, CH, CH_2, CH_3, OH and H would recombine to form complex organic molecules? As we already showed that all these reactive radical species may be formed in our NH_3-H_2O and CH_4-H_2O irradiated ices, one can suggest that in an irradiated CH_4-NH_3-H_2O mixture, species like CH_3NH_2 or NH_2CH_2OH or even $N_xC_yOH_z$ would be formed. The results shown in this chapter would try to answer such questions.

VII.1. Earlier studies and motivation

Species containing C, N, O and H are considered as biologically pertinent, such as proteins, and play an important role in the foundation of life. It is well known that proteins are large biomolecules, consisting of one or more long chains of amino acids. One of the most simplistic and smallest amino acids is glycine (NH_2CH_2COOH). Tentative observations of glycine was done in the Orion Molecular Cloud and reported by Kuan et al.[1] The number of supposedly positively identified transitions reported by Kuan et al. is fairly large. However, it was brought to attention that there seem to be some inconsistencies in the intensities of the lines. It showed doubt on the derived abundances and possibly even on the interstellar detection itself. This was disputed later on by Snyder et al.[2] In overall, it is recommend to take the detection of glycine very cautiously. Despite this, numerous amino acids were detected in the carbonaceous meteorites,[3,4] including glycine. Also the detection of extraterrestrial glycine was confirmed from the samples returned by Stardust mission from the comet 81P/Wild2,[5] thus creating a possible way of potential delivery and survival of amino acids or other prebiotic molecules to the early Earth by comets. Kaiser et al.[6] studied the formation of dipeptides from irradiated ices and suggested two pathways toward the formation of glycine. Both of them involve radical-radical recombination. The first one is through CH_2NH_2 and HOCO radicals formed from methylamine (CH_3HN_2) and formic acid (HCOOH), while the second one through CH_2COOH and NH_2 radicals formed from acetic acid (CH_3COOH) and ammonia (NH_3). The formation of glycine in ISM is very probable because all of these species (methylamine,[7] formic acid,[8] acetic acid,[9] ammonia[10]) are already detected through several astronomical observations, making the methylamine one of the precursors for the formation of the prebiotic molecules.

Gardner and McNesby were the first ones to show the formation of methylamine in the mixtures of CH_4 and NH_3 gases using ionizing UV radiation. [11] Kim & Kaiser[12] studied the

electron irradiation of an ice analog composed of ammonia and methane, which led to the formation of the cyanide anion (CN^-) and a tentative detection of methylamine using mass spectrometry as detection probes. They also suggested that methylamine is a likely precursor in the formation of the cyanide anion. While Theulé et al.[13] experimentaly observed the formation of methylamine by hydrogenation of solid hydrogen cyanide (HCN) linking the unsaturated C≡N bond with the fully saturated methylamine. Due to the hardships coming both from IR and mass spectrometry, recently in 2017 Förstel et al.[14] confirmed the detection of methylamine in irradiated methane-ammonia ices by using electron impact ionization and high sensitivity reflectron time-of-flight mass spectrometer (PI-ReTOF-MS).

The study towards the formation of methylamine in irradiated NH_3-CH_4 ices is still required due the fact of unambiguous detections in IR spectra. In the previous chapters it was shown the ability to increase the production of NH_2 and CH_3 radicals with introduction of water in the samples. Incorporating what was already analyzed this leads to the similar study on the NH_3-CH_4 mixtures. The hardships of this study come from the selection of the right NH_3-CH_4-H_2O mixture and deposition concentrations, increasing the potential of one reaction over the others. In addition to amplifying the yield of formation of NH_2 and CH_3, and consequently that of methylamine, adding small amount of water in the NH_3-CH_4 ices would help to easily assign photoreaction products which IR signatures would not be hidden by the huge absorption signals of water ice. Additionally fragments from water molecules would lead to the formation of oxide species we will attempt to identify.

VII.2. Sample formation and addition of water

To eliminate the possible causes of concentration effect, the amounts chosen for this study are the same as used in the previous experiments for methane and ammonia. Again as in the previous experiments the mixtures were introduced in the mixing ramp and after that deposited on the cold mirror cooled down to 3K. The depositions itself are performed in a high vacuum chamber at 10^{-10} mbar pressure. The following photolysis experiments lasted for 30 min and the formed samples were probed by recording infrared spectra. In this study we will show the results in two ices containing the same amount of ammonia and methane two different concentrations of water. The ratios of the CH_4/NH_3/H_2O used, estimated from column density calculations in IR spectra, are 250/7/1 for water rich samples and 250/7/0.05 for samples with low water concentration.

Figure VII-1 shows the comparison between the NH_3-H_2O (figure III-2a, page 61), CH_4-H_2O (figure V-5a, page 115) and CH_4-NH_3-H_2O ices with low water concentration. There are obvious similarities between those spectra having the pure ice bands at the same positions as discussed in the previous chapters. There are visible an appearance of 4 additional bands at locations: 985, 1644, 3304, 3237 cm^{-1}. These bands are attributed to NH_3 monomer trapped in the methane matrix cage.

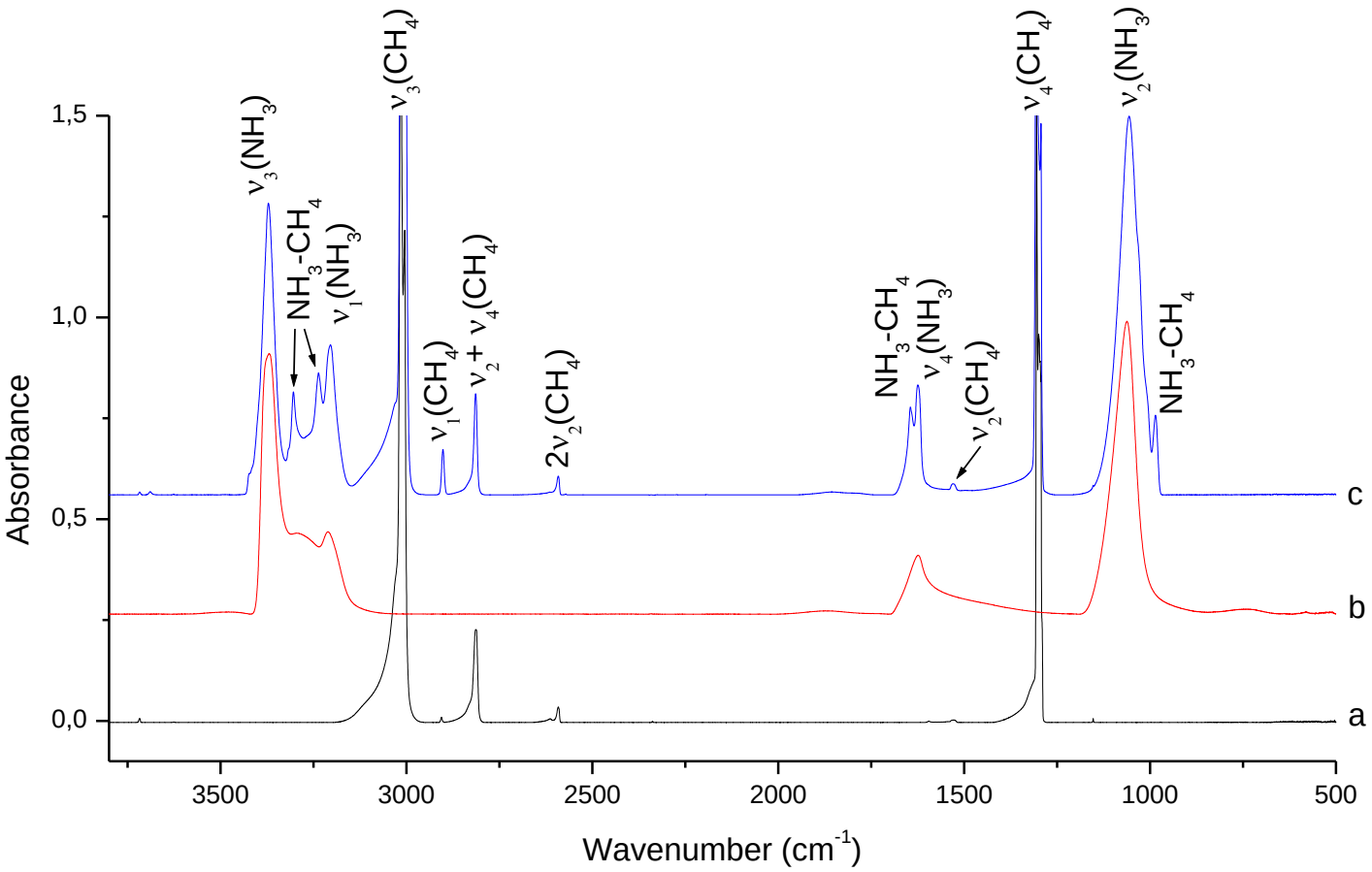

Figure VII-1. IR spectra of: a) CH_4-H_2O ice; b) NH_3-H_2O ice; c) CH_4-NH_3-H_2O ices with a ratio of 250:7:0.05

By increasing the water amount into the sample figure VII-2 shows the IR spectra of CH_4-NH_3-H_2O ices with the two ratios of (250:7:1) and (250:7:0.05). Comparing the both ice samples we have calculated the corresponding water amounts in each sample. By increasing the amount of water, 3717, 3689, 3625 and 1596 cm^{-1} bands clearly appear and are attributed to water molecules being trapped in CH_4 matrix cage. Also similarly like in the CH_4-H_2O research CH_4-$[H_2O]_x$ aggregates are formed with absorption bands hidden by the high intensity signals of ammonia ice.

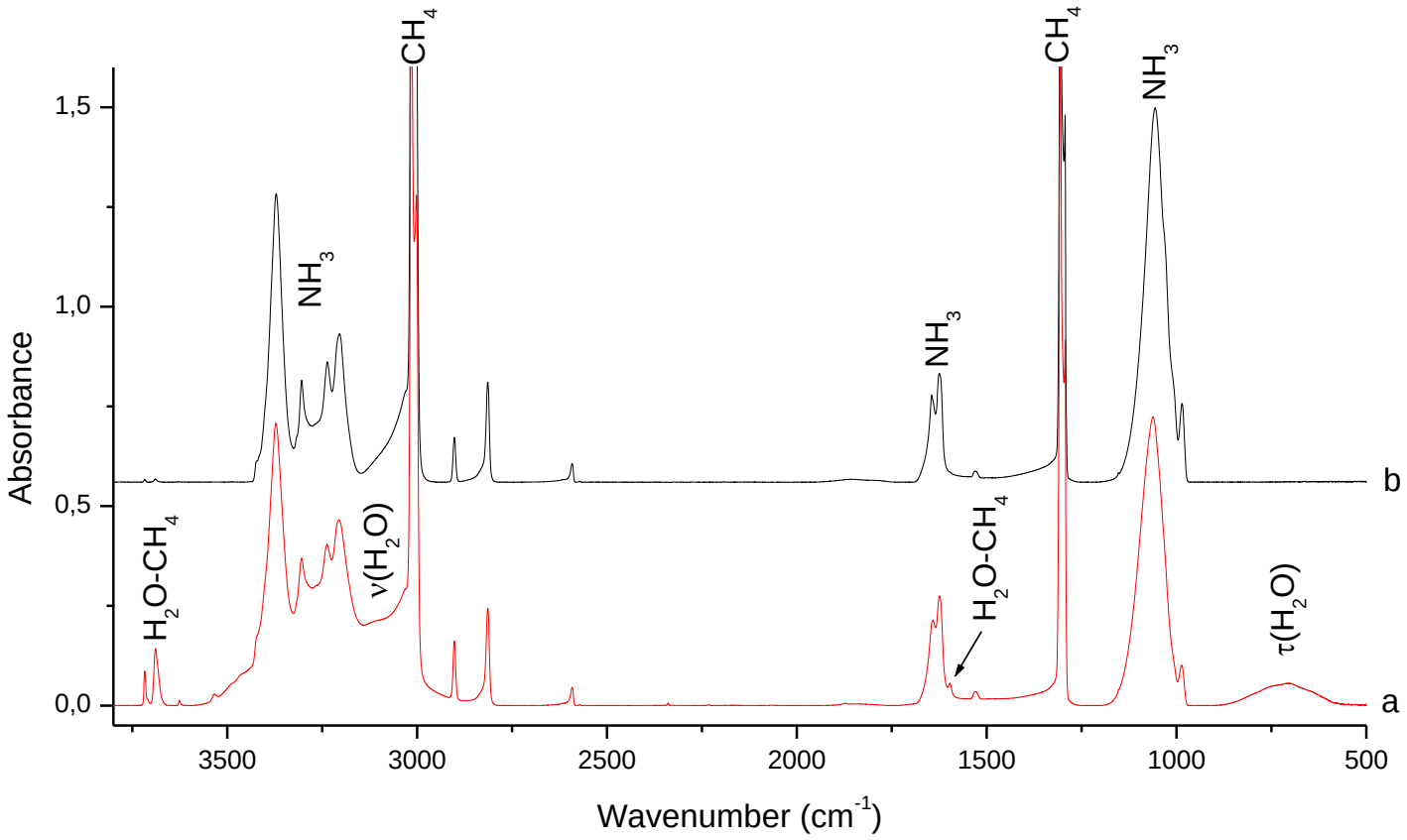

Figure VII-2. IR spectra of: a) CH_4-NH_3-H_2O ice (ratio of 250:7:1); b) CH_4-NH_3-H_2O ice (ratio of 250:7:0.05)

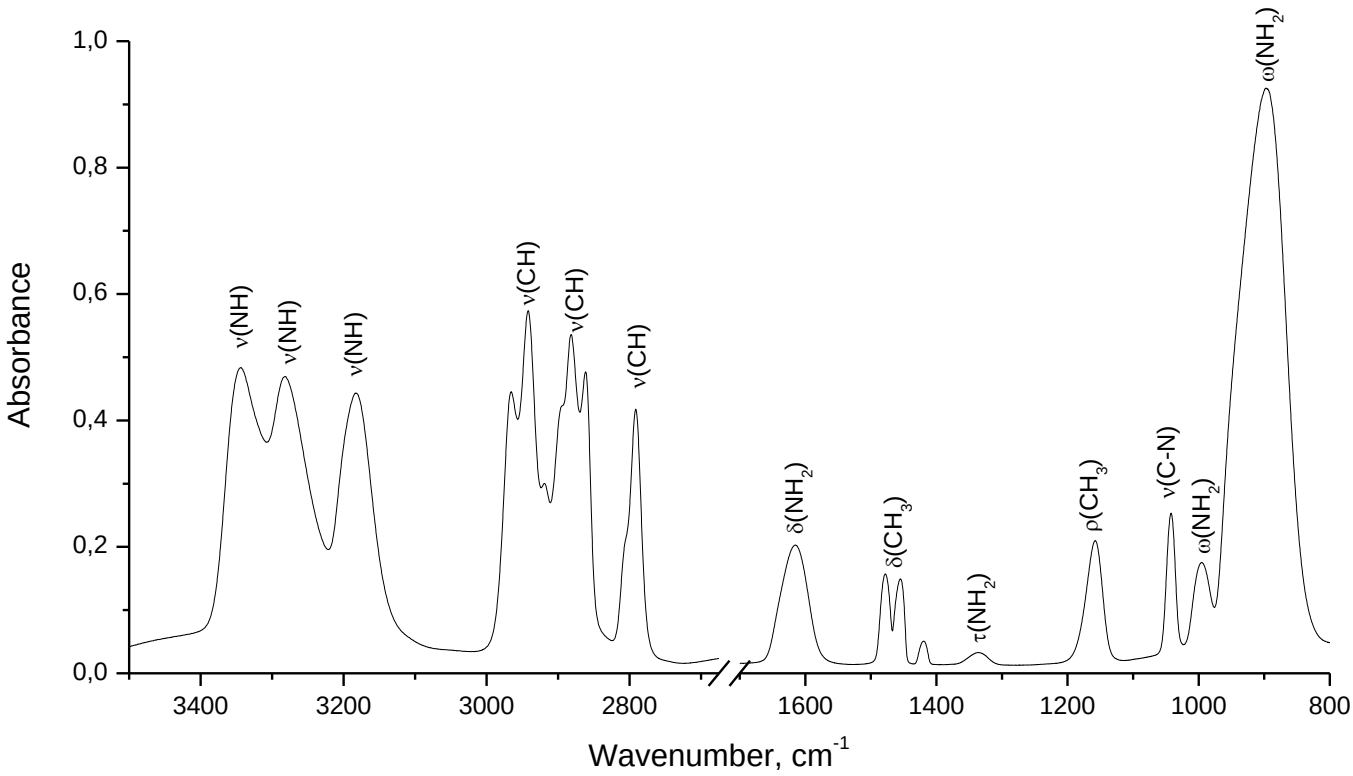

Figure VII-3. Reference IR spectrum of CH_3NH_2 ice

VII.3. Identification of photolysis products in irradiated CH_4-NH_3-H_2O ices

Considering the huge overlapping IR absorption bands of reactants and to more clearly see and identify the appeared bands of the products we prefer to show the difference spectra of CH_4-NH_3-H_2O ices after and before 30 min UV irradiation. The figure VII-4 shows these difference spectra for two different amounts of water ([H_2O]:1 and 1/20) in the spectral region of 1000 – 550 cm^{-1}. Some of the new bands appearing after photolysis have already been identified in IR spectra of CH_4-H_2O irradiated ices: C_2H_4 (951 cm^{-1}), C_2H_6 (822 cm^{-1}), C_2H_2 (737 cm^{-1}), CH_3 (609 cm^{-1}). Also the band at 912 cm^{-1} which has already been observed in irradiated CH_4-H_2O is attributed according to Kim & Kaiser[12] to a double bonded (=CH_2) wagging vibration, which can be probably propylene.[15] The only new bands which are observed in samples containing both NH_3, CH_4 and H_2O and depend on the concentration of water are located at 884, 808 and 729 cm^{-1} and are probably due to new photoproducts involving either ammonia, methane and water species or their fragments. The band at 884 cm^{-1} can be tentatively assigned to the CH_3NH_2 as the most intense signal of CH_3NH_2 ice is located at 888 cm^{-1} as shown in a reference of methylamine ice we have recorded under the same experimental conditions (figure VII-3). Considering this is the most intense band found in CH_3NH_2 ice, the similar band in this region should also be visible in the irradiated CH_4-NH_3-H_2O ice. This is the first IR identification of CH_3NH_2 in irradiated ammonia-methane ices. All the similar studies carried out have identified methylamine one of the formed photoproducts only through mass spectroscopy. This is probably due to the fact that in

irradiated NH_3-CH_4 ices the CH_3NH_2 is formed with a very low amount to be probed though solid phase IR spectroscopy. As we have already shown that the adding of a very small amount of water in NH_3 and CH_4 ices increases the yield formation of NH_2 and CH_3, water molecules in irradiated CH_4-NH_3-H_2O ices also induce additional formation of CH_3NH_2 species which become detectable in solid IR spectra. We have noticed the band assigned to CH_3NH_2 increases slightly during the heating of the irradiated sample from 3 to 10K. The two other bands (808, 729) are still not assigned but we think they are probably due to either molecular complexes or radical species as their IR signals decrease during the heating of the sample as we will discuss later.

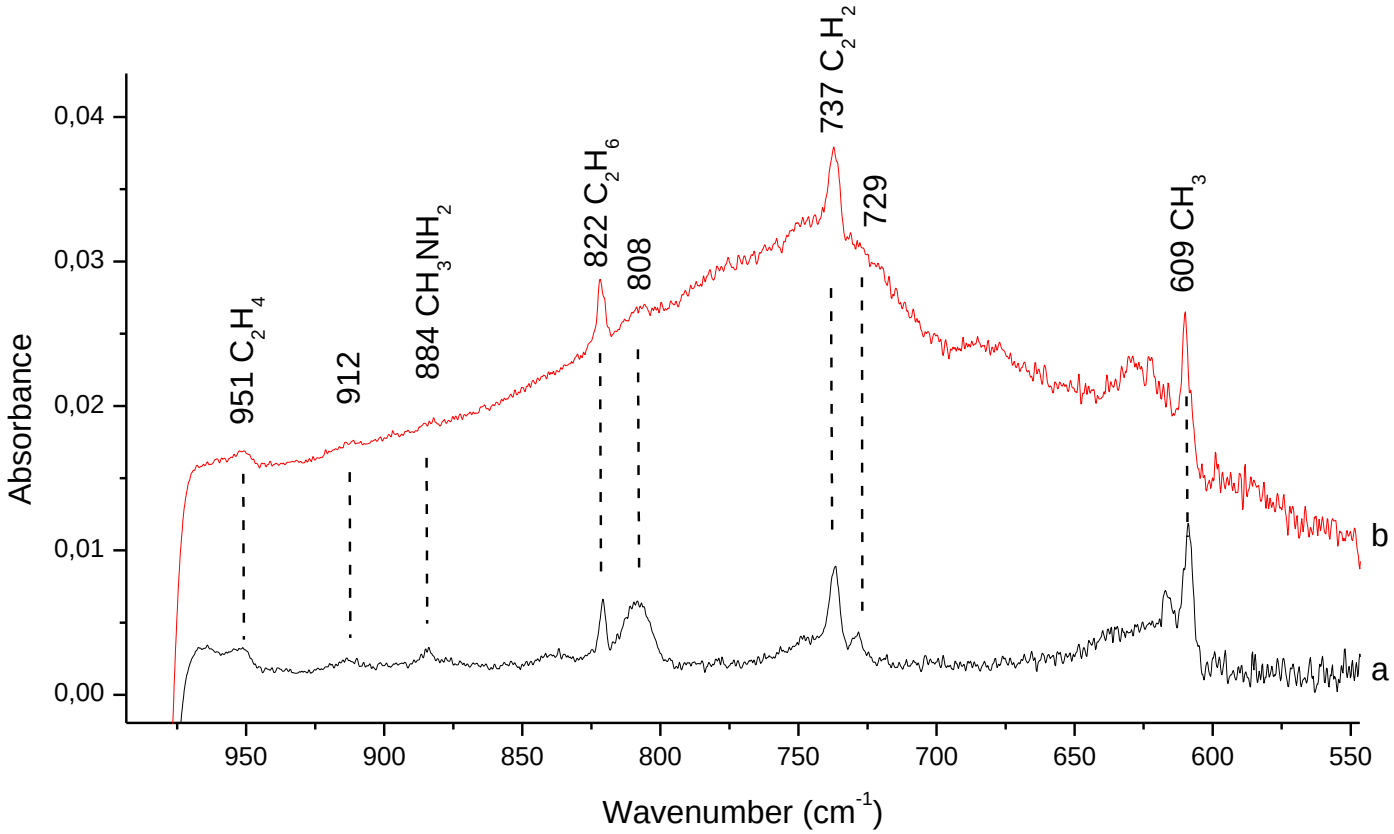

Figure VII-4. Difference IR spectra before and after the photolysis in the region of 1000 – 550 cm^{-1} CH_4-NH_3-H_2O with different ratios: a) 250/7/0.05; b) 250/7/1

The figure VII-5 shows the difference spectra of CH_4-NH_3-H_2O ices after and before 30 min UV irradiation in the region of 1600 – 1300 cm^{-1} a spectral region which is not congested by the IR signals of methane or ammonia ices. All the species absorbing in this spectral region have been already identified during the photolysis of the either CH_4-H_2O or NH_3-H_2O and discussed in the previous chapters.

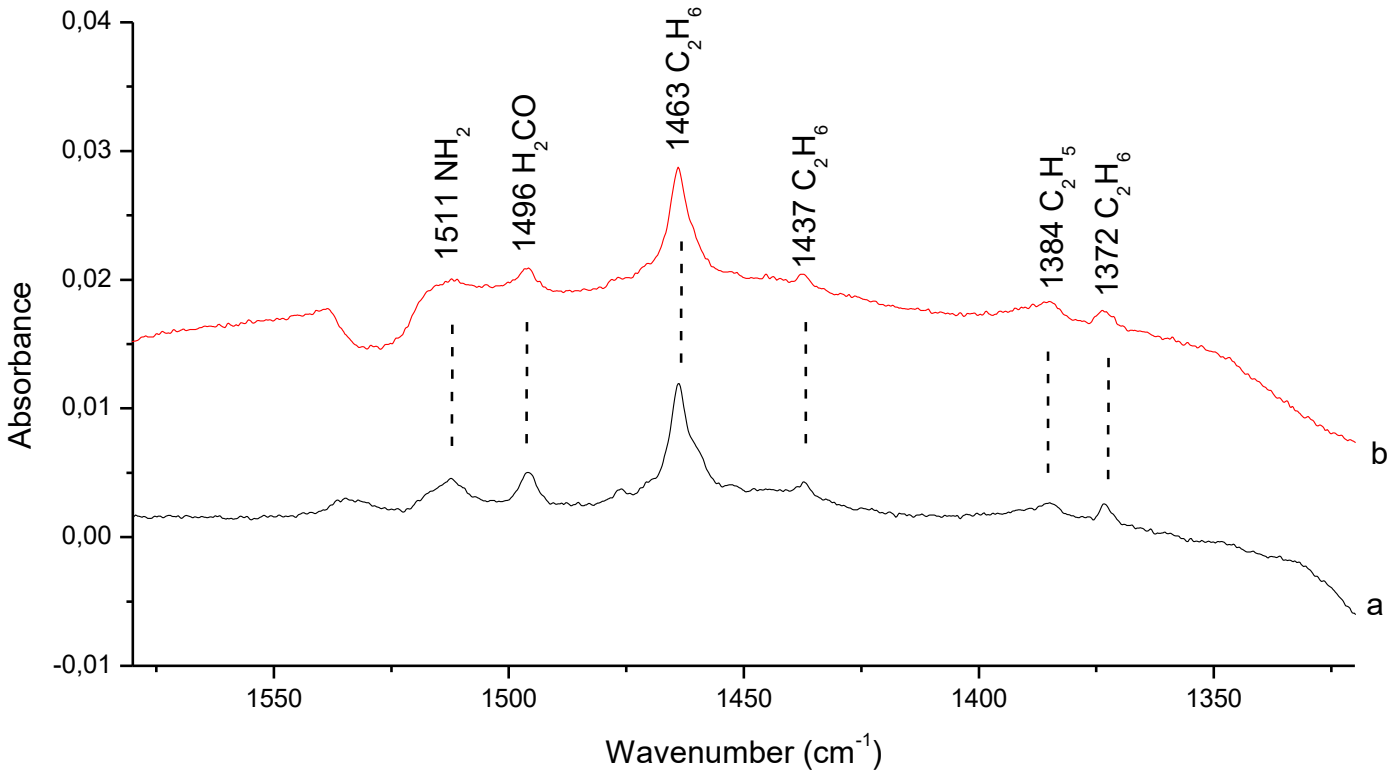

Figure VII-5. Difference IR spectra before and after the photolysis in the region of 1600 – 1300 cm^{-1} CH_4-NH_3-H_2O with different ratios: a) 250/7/0.05; b) 250/7/1

The figure VII-6 shows the difference spectra of CH_4-NH_3-H_2O ices after and before 30 min UV irradiation in one interesting spectral region between 2400 – 1700 cm^{-1} corresponding to the characteristic IR absorptions of CO, CN and NO functional groups. The formation of CO bonding would result from methane and water fragments, that of CN from methane and ammonia fragments and that of NO from ammonia and water fragments. There are 4 clear and easily attributable bands 2339 (CO_2), 2137 (CO), 1858 (HCO) and 1726 cm^{-1} (H_2CO) which IR intensities increase by increasing the water amount in the irradiated samples. The band at 2258 cm^{-1} is more clearly in water rich samples is attributed to HNCO.[16,17] In C≡N spectral region we observe a band at 2072 cm^{-1} which may correspond either to HCN (2100 – 2077 cm^{-1})[18] or CN^- (2086).[19] Bennett et al.[27] have already shown that the presence of NH_3 and HCN may lead to the formation of ionic species NH_4^+ which absorb in the same region as NH_2 (1500 cm^{-1}) and CN^- (2086 cm^{-1}) through the reaction:

$$HCN + NH_3 \rightarrow CN^- + NH_4^+ \qquad \text{(VII-1)}$$

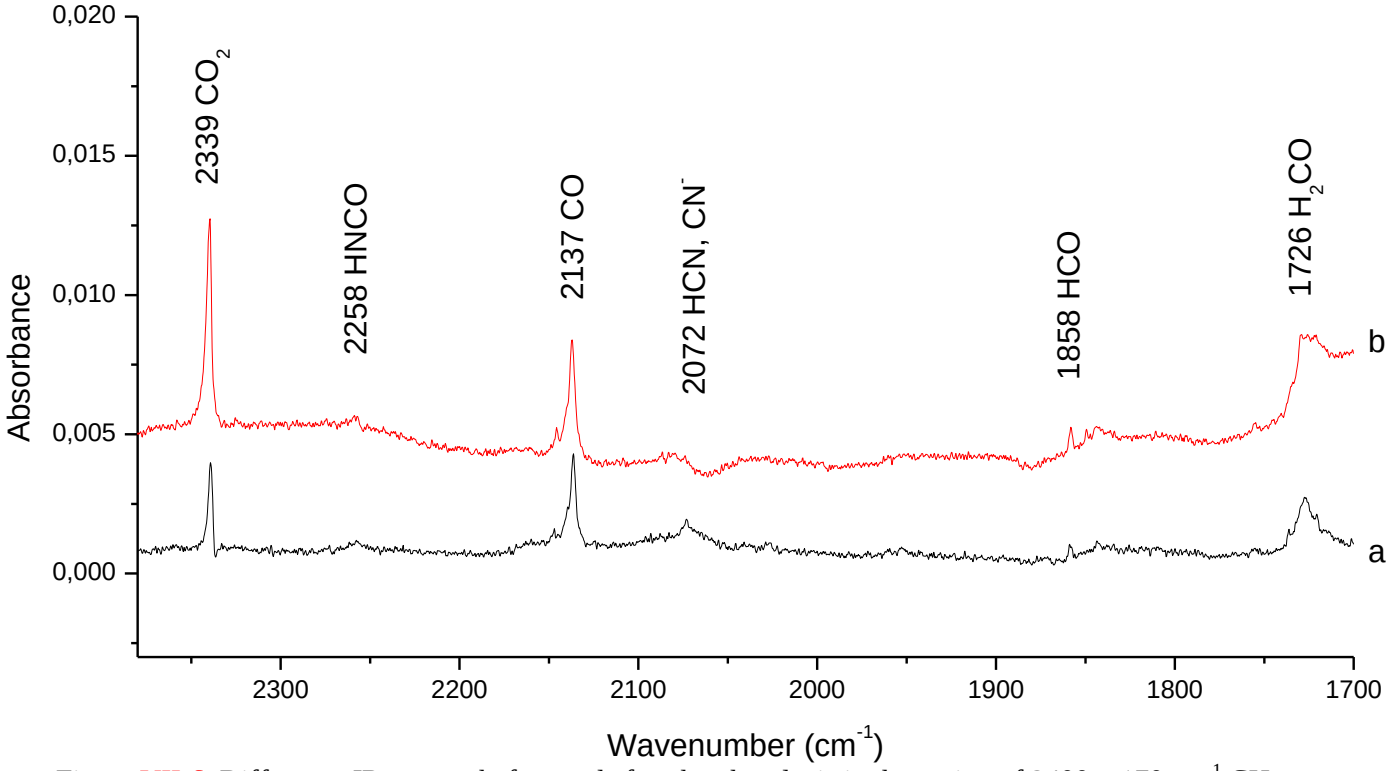

Figure VII-6. Difference IR spectra before and after the photolysis in the region of 2400 – 170 cm^{-1} CH_4-NH_3-H_2O with different ratios: a) 250/7/0.05; b) 250/7/1

It should be underlined that all these species such as CO_2, CO, HCO, and H_2CO have been already detected in irradiated CH_4-H_2O ices while either HCN or CN^- are observed only in mixed CH_4-NH_3-H_2O irradiated ices. No species with NO functional group have been detected after the photolysis of CH_4-NH_3-H_2O ices. The band attributions are provided in table VII-1.

Table VII-1. Attributions of photoproducts found in the CH_4-NH_3-H_2O ices after the photolysis

Position (cm^{-1})	Assignment	Reference
609	CH_3	Lin et al.[20]
729	C_2H_2-complex or radical	-
737	C_2H_2	Lin et al.[20]
808	C_2H_6-complex or radical	-
822	C_2H_6	Lin et al.[20]
884	CH_3NH_2	-
912	Propylene	Kim & Kaiser[12] Es-sebbar et al.[15]
951	C_2H_4	Lin et al.[20]
1372	C_2H_6	Lin et al.[20]
1384	C_2H_5	-
1437	C_2H_6	Lin et al.[20]
1463	C_2H_6	Lin et al.[20]
1496	H_2CO	Khoshkhoo et al.[21]
1511	NH4+, NH_2	Zins & Krim[22]
1726	H_2CO	Khoshkhoo et al.[21]
1858	HCO	Ewing et al.[23]
2072	HCN, CN^-	Noble et al.[18] Mencos & Krim[19]
2137	CO	Leroi et al.[24]
2258	HNCO	Theule et al.[16] Raunier et al.[17]
2339	CO_2	Nxumalo et al.[25]

VII.4. Heating

Considering the fact that in the both samples of CH_4-NH_3-H_2O with different water concentrations the formed amount of photoproducts seems the same, the further evolution of these products during the heating is analyzed for the sample with the lower concentration of water due to the fact that the absorption of water is much lower in the region of 1000 – 550 cm^{-1} allowing a better attribution of species.

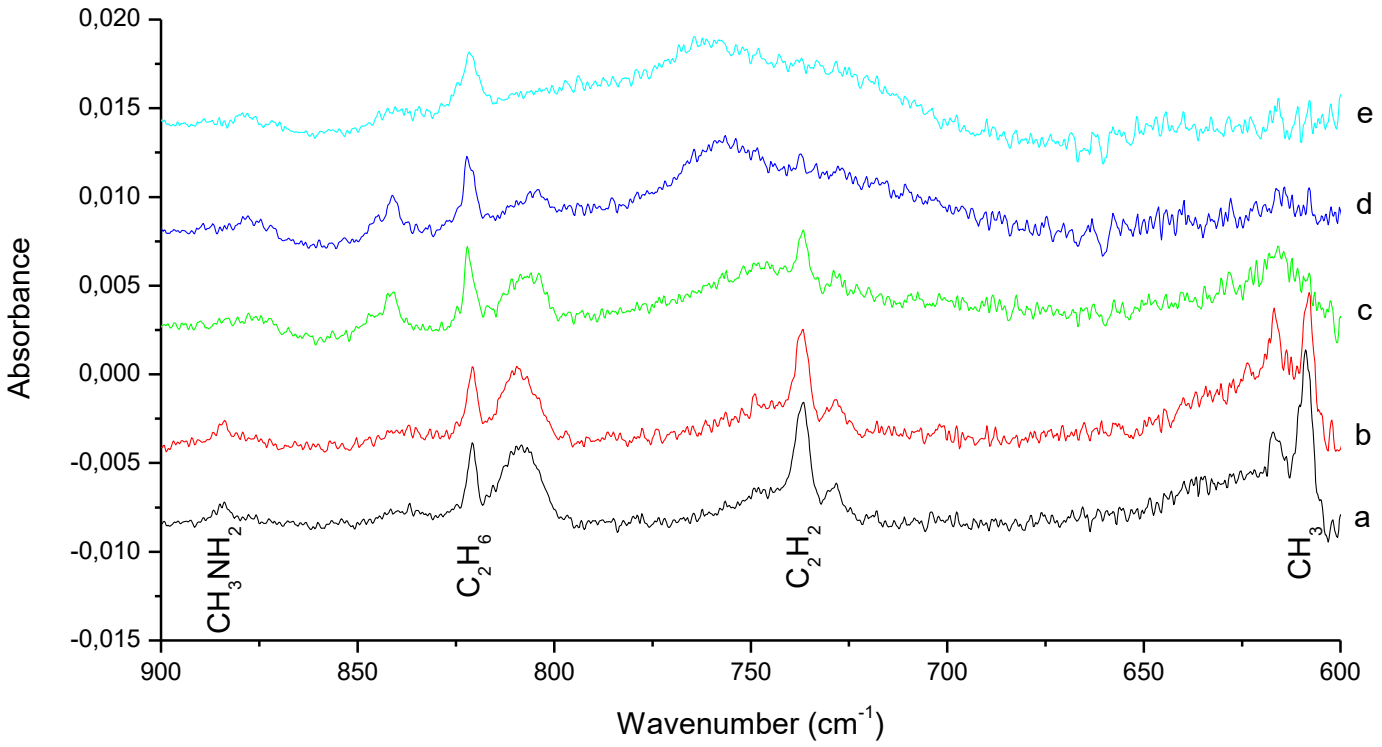

Figure VII-7. The changes in IR spectra of CH_4-NH_3-H_2O ice after the photolysis in the region of 1000 – 500 cm^{-1} at different temperatures: a) 3K; b) 10K; c) 20K; d) 30K; e) 40K

Figure VII-7 shows an evolution of photoproducts in irradiated CH_4-NH_3-H_2O ice in 3 – 40K temperature range in the 1000 - 500 cm^{-1} spectral range. There is a visible decrease in signal intensity of bands attributed to CH_3, while in the same time no increase in a C_2H_6 species is observed (band 822 cm^{-1}) while heating the sample up to 40K, by contrast in irradiated CH_4-H_2O ices the decrease of CH_3 signal may be linked to the increase of that of C_2H_6. This shows that in the irradiated CH_4-NH_3-H_2O ice the CH_3 radical might be involved in other chemical reactions rather than CH_3-CH_3 recombination. One of the reaction products derived from the disappearance of CH_3 from the heated ice could be species characterized by band at 840 cm^{-1} which appears between 20 and 30K and completely disappears at temperatures higher than 40K, which can be due to the desorption of the species. Similarly C_2H_2 (736 cm^{-1}) signal decreases when the ice is heated from 3 to 30K and disappears at temperatures higher than 40K. The intensity of the band attributed to CH_3NH_2 (884 cm^{-1}) slightly increases between 3 and 10K, and becomes wider at higher temperatures. The spectral region between 1000 and 1600 is completely perturbed by the huge absorption signals due to the reactants water, methane and ammonia. However, in the spectral region between 1700 and 2300 some IR signal evolutions are noticed during the heating of the irradiated sample. Looking at the figure VII-8 the band of interest is at 2072 cm^{-1}, which increases in intensity and widens by increase of temperature. Many studies have already shown that HCN and CN^- absorb in this region. However, the absorption band of the CN^- is wider than that of HCN. We think that

the heating of the irradiated ice allow the formation of HCN and also its conversion into CN- through acid-base reaction:

$$HCN + NH_3 \rightarrow CN^- + NH_4^+ \quad \text{(VII-2)}$$

$$HCN + H_2O \rightarrow CN^- + H_3O^+ \quad \text{(VII-3)}$$

Similarly the band attributed to HNCO (2258 cm^{-1}) disappear during the heating of the sample while a new wide band appears at 2156 cm^{-1} clearly at 40K and it can be attributed to OCN^- formed through similar acid-base reactions involving HNCO, NH3 and H2O, as follows:

$$HNCO + NH_3 \rightarrow OCN^- + NH_4^+ \quad \text{(VII-4)}$$

$$HNCO + H_2O \rightarrow OCN^- + H_3O^+ \quad \text{(VII-5)}$$

The intensity of the band attributed to H_2CO (1726 cm^{-1}) increases during the heating of the sample, while that of HCO (1860 cm^{-1}) decreases, while a new signal appears at 1845 cm^{-1}, which may correspond to HOCO. Previous studies have already shown that HOCO in solid phase is characterized by an absorption in this region.[26] Consequently, HCO may involve during the irradiated ice into the formation of H_2CO or HOCO:

$$HCO + H \rightarrow H_2CO \quad \text{(VII-6)}$$

$$HCO + OH \rightarrow HOCO + H \quad \text{(VII-7)}$$

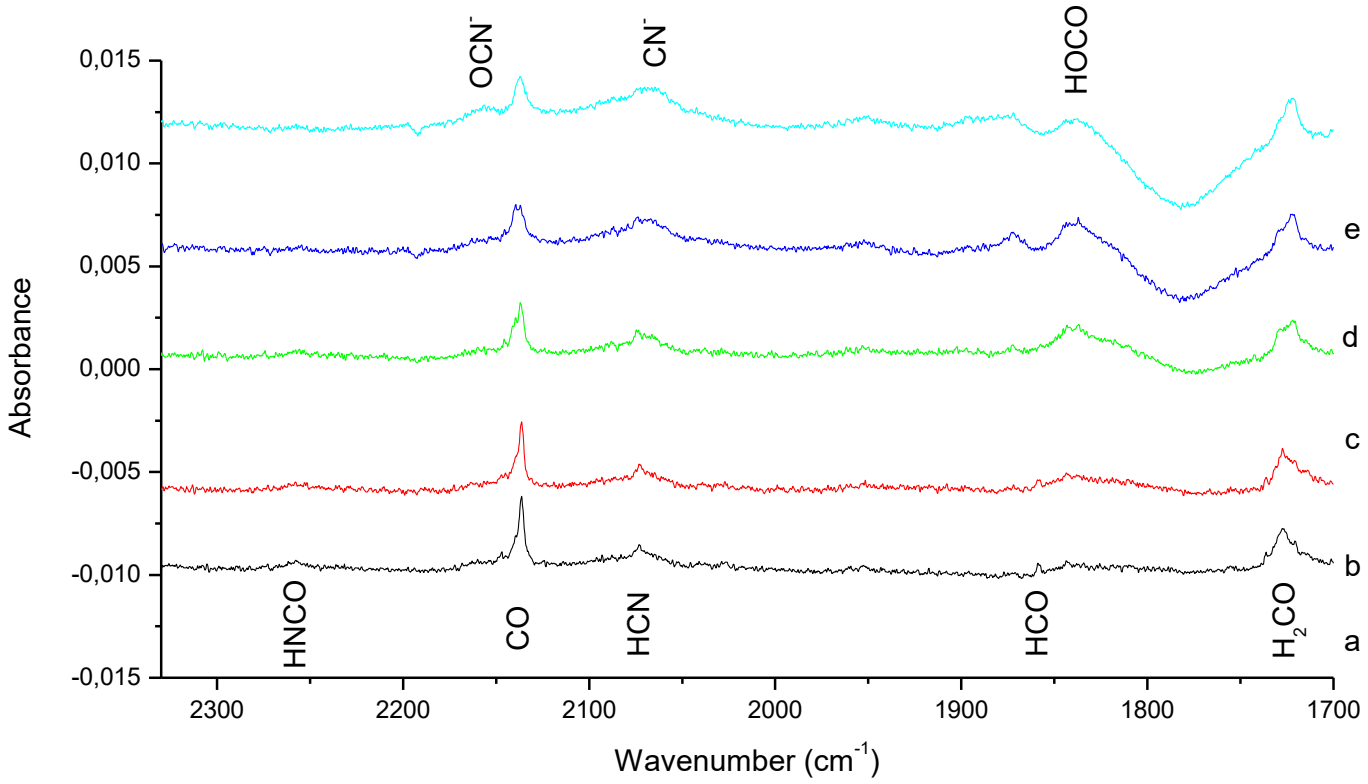

Figure VII-8. The changes in IR spectra of CH_4-NH_3-H_2O ice after the photolysis in the region of 2300 – 1700 cm^{-1} at different temperatures: a) 3K; b) 10K; c) 20K; d) 30K; e) 40K

While already mentioned in the previous chapters, the desorption of the methane starts around 50K and that of ammonia around 110K. The recorded IR spectra in this temperature range show a possible polymerization in the sample making the possible attribution to evolution of photoproducts impossible. However, it is possible to analyze the reaction products in the irradiated ice at temperatures higher than 120K as shown in figure VII-9 in the whole spectral range.

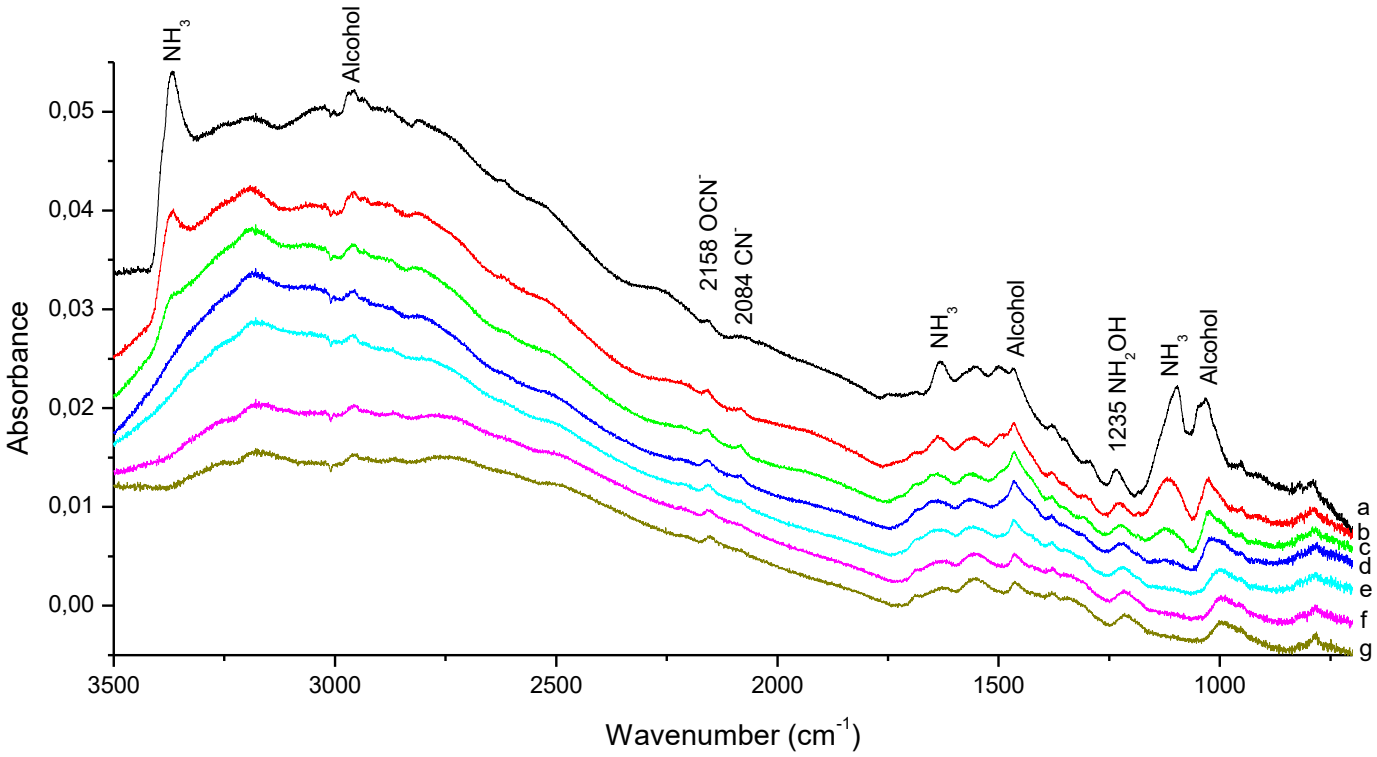

Figure VII-9. The changes in IR spectra of CH_4-NH_3-H_2O ice after the photolysis at different temperatures: a) 120K; b) 130K; c) 140K; d) 150K; e) 160K; f) 170K; g) 180K

From figure VII-9 we can easily attribute bands to NH_3, NH_2OH and alcoholic species, in addition to CN^- and OCN^-. We notice that the band due to the ammonia decrease between 120 and 140K and completely disappear at temperatures higher than 150K while the bands of species with OH function remain until 180K! At this point of the study we reach the limit of IR spectroscopy in the characterization of the solid phase reactions occurring in the irradiated and heated CH_4-NH_3-H_2O ices. In fact, we can use the IR spectroscopy to describe species easily detectable at low temperature in range between 3 and 40K as shown in figures VII-4 – VII-8. However at temperatures between 40 and 180K attribution of the species of the reaction products should be complemented by mass spectroscopy. I present the mass spectrum of the irradiated CH_4-NH_3-H_2O ices and heated to 140K and average temperature corresponding to the starting point of desorption of many heavy species shown in figure VII-10.

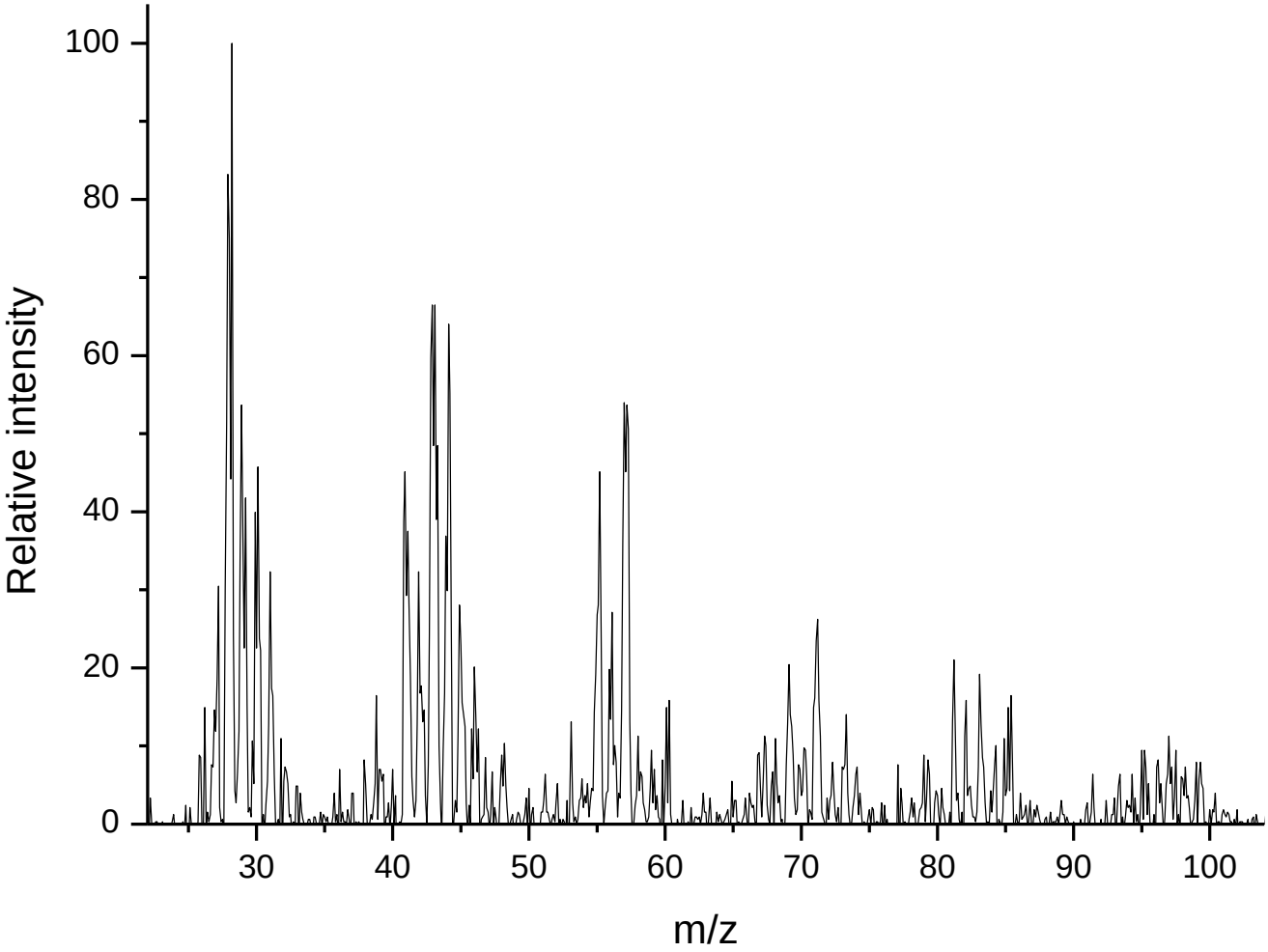

Figure VII-10. Mass fragmentation spectra of the detected desorbed species recorded in the gas phase at 140K

We have already shown that the heating of the irradiated CH_4-H_2O under our experimental conditions allows a detection of species which the highest mass is in the 55 – 62u range and we have attributed these masses to fragmentation from heavy alcoholic species such as propanol or metoxymethanol. Adding ammonia in the CH_4-H_2O ice leads to the formation of very heavy species which masses are in the range between 65 – 85u range. We saw higher masses between 90 and 100u, but they will not be considered for this study as they show very low intensities and thus need proper future investigations. In order to investigate all the complex organic species formed during the desorption of the irradiated CH_4-NH_3-H_2O ice, table VII-2 summary the mass fragments of species involving one, two, three, four and five C-C, C-N, C-O and N-O bonds. This table would help in the assignment of the species desorbing into the gas phase from the recorded mass spectra.

Table VII-2: Summary of mass fragments from unsaturated to fully saturated with different amount of atoms

Mass range	24 - 33	36 - 47	48 - 61	60 - 75	72 – 89	84-103
Fragments	C-C C-N C-O N-O	C-C-C C-C-N C-C-O C-N-O	C_2-C-C C_2-C-N C_2-C-O C_2-N-O	C_3-C-C C_3-C-N C_3-C-O C_3-N-O	C_4-C-C C_4-C-N C_4-C-O C_4-N-O	C_5-C-C C_5-C-N C_5-C-O C_5-N-O

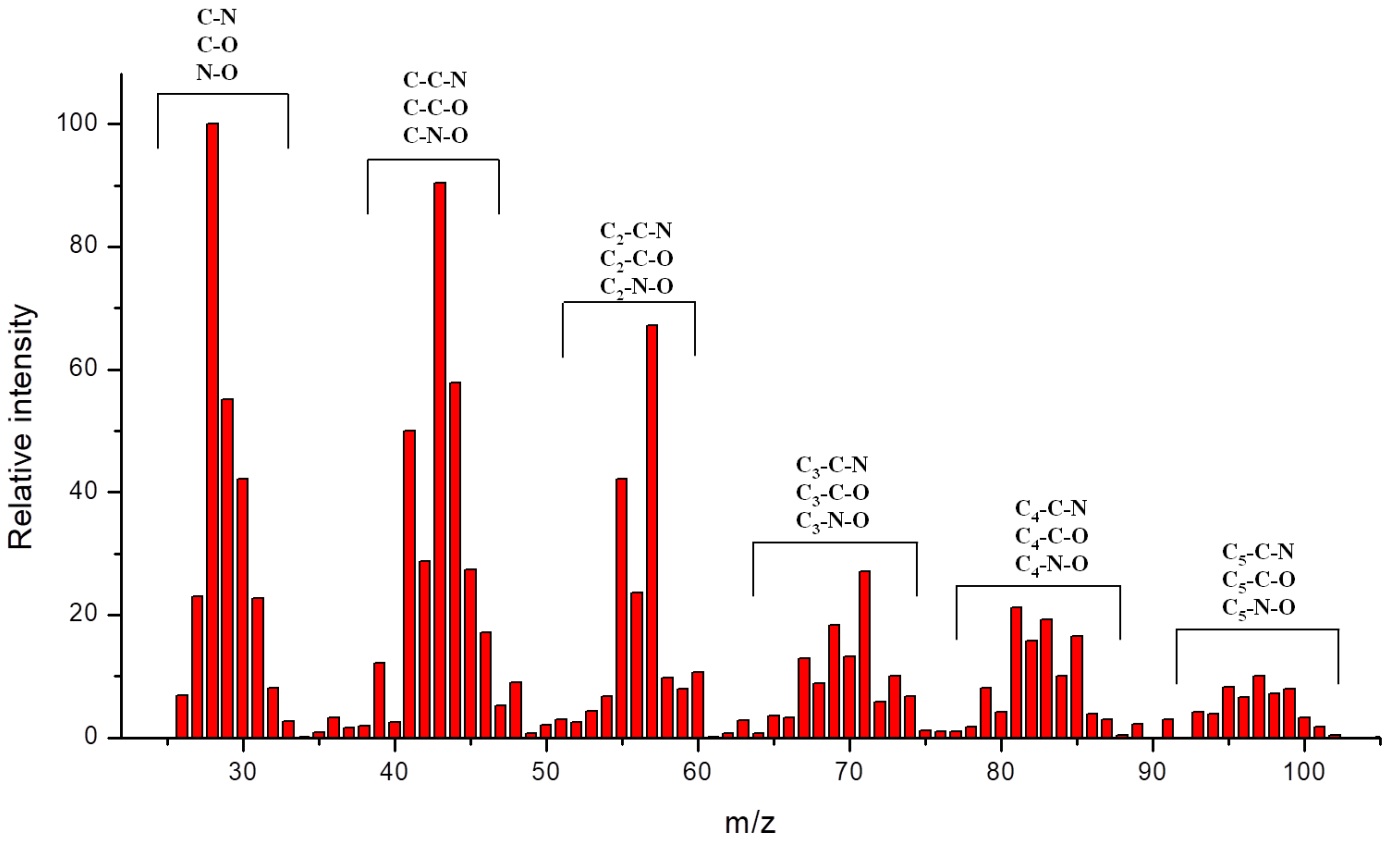

Figure VII-11. Mass fragmentation spectra of the detected desorbed species recorded in the gas phase at 140K with ranges of bond attributions.

Figure VII-11 shows mass fragmentation patterns with different attributed heavier molecular groups. Since the temperature of the recorded spectrum is 140K, alka[e]nes (C-C) are not considered as one of the possible molecular species, since their desorption temperatures are lower than 100K. To desorption temperatures higher than 100K, the complex organic molecules should at least have C-N, C-O or N-O bonds. Consequently, in the most intense first group (24 – 33u), there are possible fragmentations of species containing C-N, C-O and N-O bonds, such as CH_3NH_2, CH_3OH and NH_2OH which have been observed in the recorded IR spectra. Some heavier mass fragments can also be suggested provided in the table VII-3 with the detected mass fragments and possible molecules that have high intensity of the corresponding fragments.

Table VII-3: Detected mass fragments with possible molecular attributions

Mass	Fragment	Molecule
57	C_2H_3NO C_3H_5O C_3H_7N	Isocyanatomethane 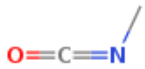 Allyl alcohol 
71	C_3H_5NO C_4H_7O C_4H_7N	3-Buten-2-ol 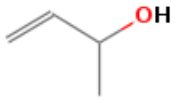 2-Propenamide 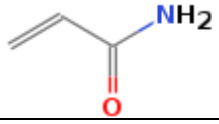
81	C_4H_3NO C_5H_5O C_5H_7N	
83	C_4H_5NO C_5H_7O C_5H_9N	5-methyl-isoxazole 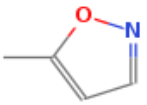 1,4-Pentadien-3-ol 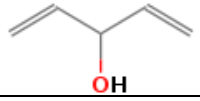
85	C_4H_7NO C_5H_9O $C_5H_{11}N$	4,5-dihydro-2-methyl-oxazole 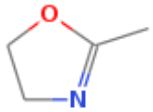 2-Pyrrolidinone 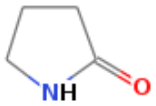 trans-Crotonamide 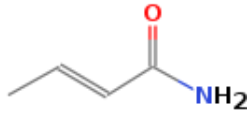 Methacrylamide 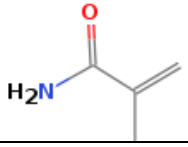

All these organic compounds have been chosen based on their chemical bonds (C-N, C-O and N-O) and also as they show mass fragmentations in correlation with our reference mass spectra. For example, if a molecule has a fragment with the mass 85 with a given intensity, it should not have another fragment at 75u with higher intensity, and so on…For these two reasons table VII-4 show molecular fragmentation of the potential species we proposed that are formed under our experimental conditions: UV@3K + thermal processing of CH_4-NH_3-H_2O interstellar ice analogs.

Table VII-4. Mass fragmentation spectra of suggested molecules

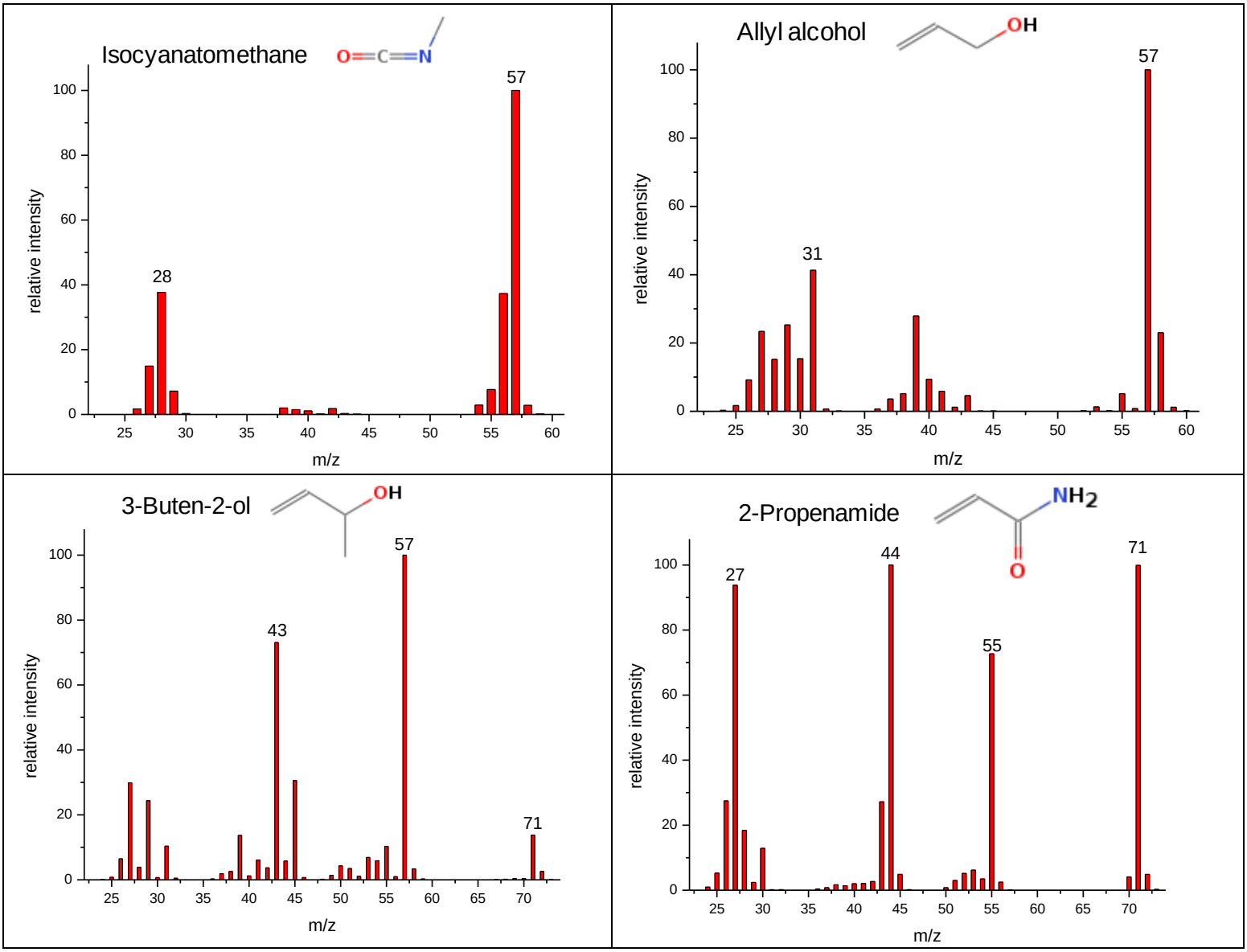

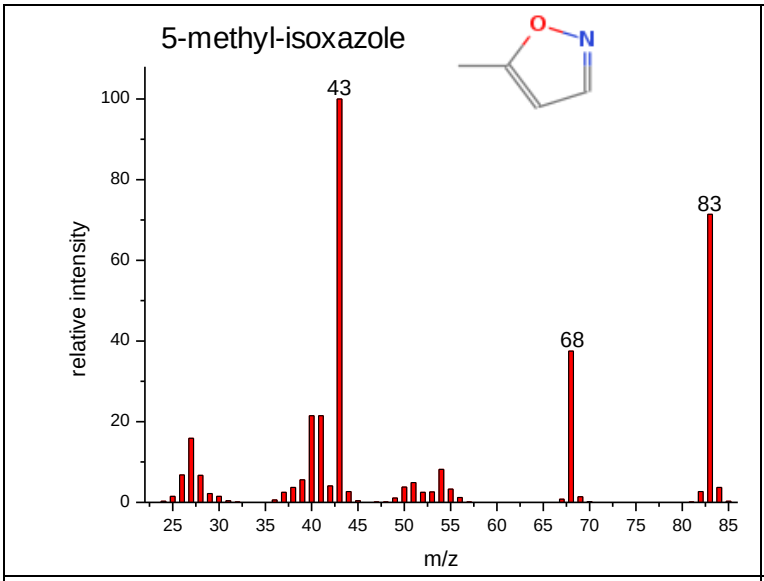
5-methyl-isoxazole
O
N
43
83
68
relative intensity
m/z

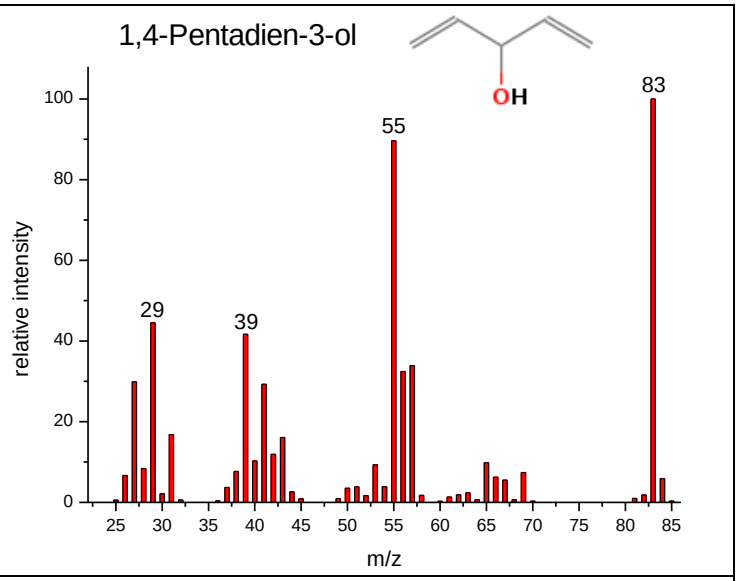
1,4-Pentadien-3-ol
OH
83
55
29
39
relative intensity
m/z

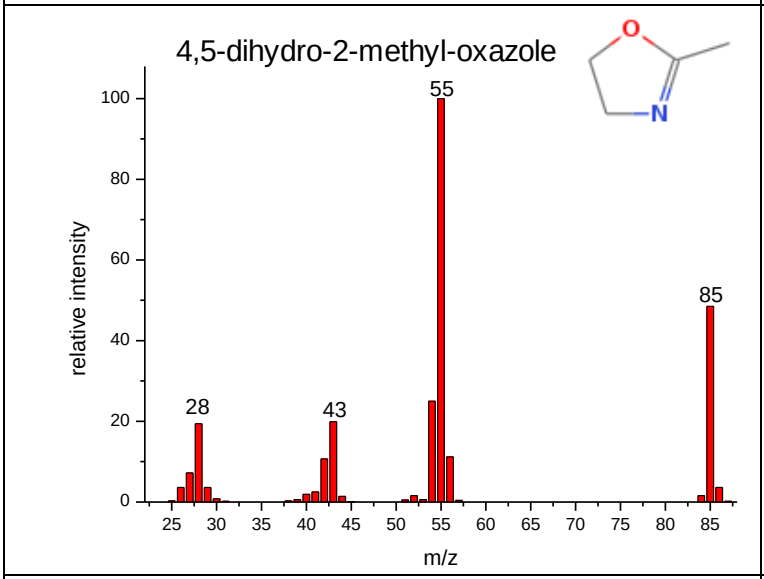
4,5-dihydro-2-methyl-oxazole
O
N
55
85
28
43
relative intensity
m/z

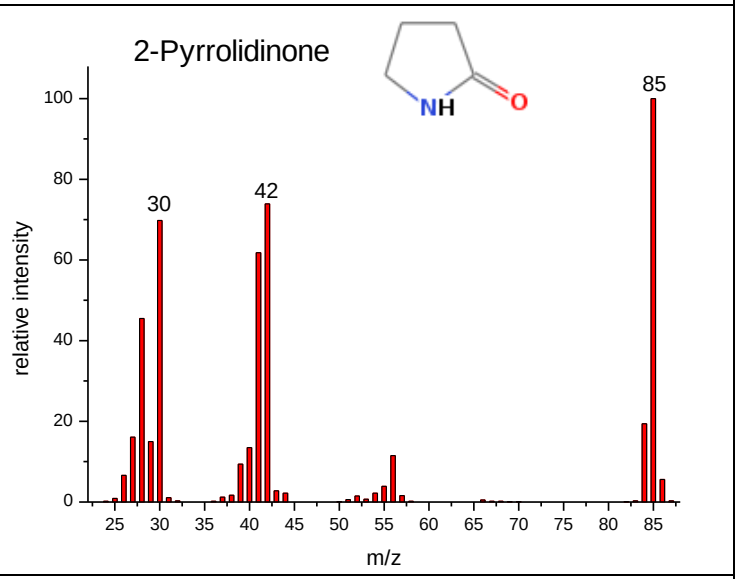
2-Pyrrolidinone
NH
O
85
30
42
relative intensity
m/z

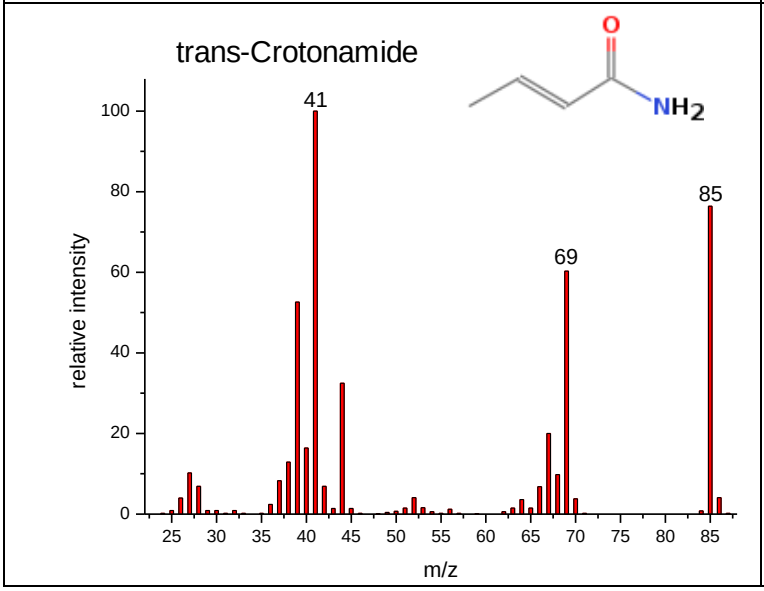
trans-Crotonamide
O
NH2
41
85
69
relative intensity
m/z

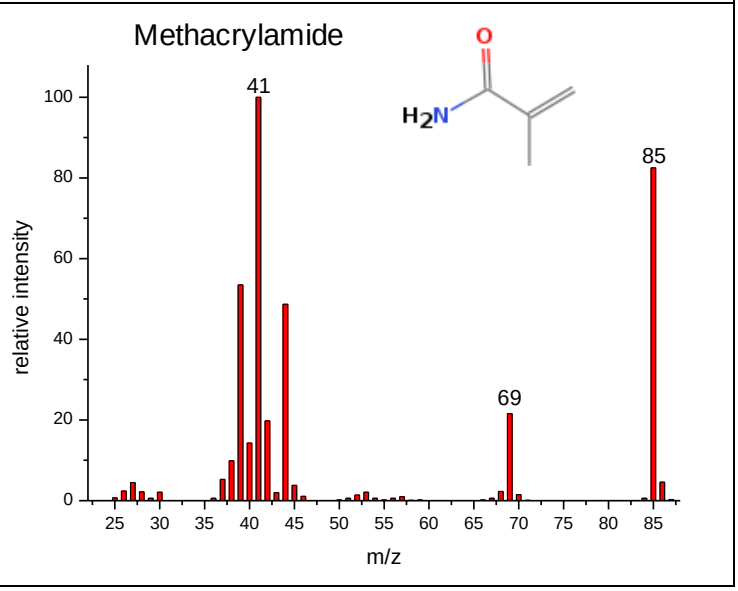
Methacrylamide
O
H2N
41
85
69
relative intensity
m/z

VII.5. Transformation pathways

From our experimental results we can propose many reaction mechanisms starting from simple species derived from fragmentation of NH_3, CH_4 and H_2O to form complex organic molecules. We have already shown that fragmentation of ammonia to the formation of NH_2, NH and H:

$$h\nu + NH_3 \rightarrow NH + H_2 / 2H \quad \text{(VII-8)}$$

$$h\nu + NH_3 \rightarrow NH_2 + H, \quad \text{(VII-9)}$$

Similarly, the fragmentation of CH_4 leads to the formation of CH_3, CH_2 and probably CH, in addition to atomic and molecular hydrogen:

$$h\nu + CH_4 \rightarrow CH_3 + H, \quad \text{(VII-10)}$$

$$h\nu + CH_4 \rightarrow CH_2 + H_2 / 2H, \quad \text{(VII-11)}$$

From these fragments, methylamine can be formed though the radical recombination:

$$CH_3 + NH_2 \rightarrow CH_3NH_2 \quad \text{(VII-12)}$$

Reaction VII-12 is radical recombination and then barrierless, however it cannot be the only reaction pathway to form methylamine regarding the low amount of CH_3 and NH_2 in the irradiated ice. Other reactions can take place through the insertion of CH_2 into N-H bond of ammonia and NH insertion into methane:

$$CH_2 + NH_3 \rightarrow H–CH_2–NH_2 \quad \text{(VII-13)}$$

$$NH + CH_4 \rightarrow CH_3–NH–H \quad \text{(VII-14)}$$

These two reactions allow a transformation from radical-molecule to molecule and should have a huge activation energy. However they involve radical species with low concentrations in the irradiated sample and huge amounts of stable molecules forming the ice, namely NH_3 and CH_4. These reactions are possible in solid phase during the photolysis processing which allows overcoming their energy barriers. CH_3NH_2 can be link to HCN due to the equilibrium between Formation and photo-destruction of methylamine:

$$h\nu + CH_3NH_2 \rightarrow CH_2NH + H_2 / 2H, \quad \text{(VII-15)}$$

$$h\nu + CH_2NH \rightarrow HCN + H_2 / 2H \quad \text{(VII-16)}$$

We have already shown that the species such as NH_2OH are formed in the irradiated NH_3-H_2O ices and alka[e]ne and alcoholic species are formed in the irradiated CH_4-H_2O ices. By

combining IR and mass spectroscopy analysis of the heated irradiated CH_4-NH_3-H_2O ices, we have shown that more complex organic molecules involving C-N-O, C-C-N-O and C-C-C-N-O bonds may be formed. Simple species have been already characterized at low temperatures through IR spectroscopy:

- In CH_4-H_2O rich environments: HCO, H_2CO, CH_3OH, and probably CH_3O and CH_2OH (intermediates for the formation of CH_3OH through H_2CO + H), CH_3CH_2OH, CH_3, CH_3CH_2, C_2H_2, C_2H_4, C_2H_6.
- In NH_3-H_2O rich environments: NH, NH_2, N_2, NH_2OH and probably NH_3O (less stable isomeric form of NH_2OH).
- In CH_4-NH_3-H_2O mixed environments: in addition to the species mentioned above, CH_3NH_2, HCN, HNCO, HOCO and CN-, OCN- formed at higher temperatures through thermal processing.

Consequently the products detected during the sublimation of the irradiated CH_4-NH_3-H_2O mixed ice would derive from radical-radical or radical-molecule reactions. In such situation many reaction pathways involving the species formed in the three environments could be proposed.

As the formation of CH_3CH_2OH can be due to the radical recombination CH_3 + CH_2OH or CH_3CH_2 + OH, more complex species containing C, N and O such as HNCO would form through:

$$NH + HCO \rightarrow HNHCO \rightarrow HNCO + H \qquad \text{(VII-17)}$$

Many of these reaction pathways should be investigated by theoretical modeling in order to have a clear description of the formation of organic compounds more complex than HNCO and proposed in table VII-3.

VII.6. Conclusions

This chapter has been based on previous analysis carried out for separate irradiated NH_3-H_2O and CH_4-H_2O ices. Our main results show that the addition of water might improve the formation of NH_2 and CH_3 radicals and their recombination into CH_3NH_2 allowing the detection of this molecule in the IR spectra. Other formed species detected were HCN which is a derivative from methylamine and HNCO which could be due to the reaction NH + HCO. Heating the sample to temperatures above 120K formation of anions such as OCN^- and CN^- was observed. With the combination of IR and mass spectrometry more complex organic species reaching masses up to 100u are characterized. However, theoretical modeling are needed to propose reaction pathways leading to the formation of these species through chemical interactions between photoproducts detected in separate irradiated NH_3-H_2O and CH_4-H_2O ices.

Bibliography

[1] Kuan Y.-J., Charnley S. B., Huang H.-C., Tseng W.-L., Kisiel Z., 2003. ApJ, 593, 848.
[2] Snyder L. E., Lovas F. J., Hollis J. M., Friedel D.N, Jewell P. R., Remijan A., Ilyushin V. V., Alekseev E. A., Dyubko S. F., 2005. ApJ, 619, 914.
[3] Glavin D. P., Dworkin J. P., Aubrey A., Botta O., Doty III J.H., Martins Z., Bada J. L., 2006. M&PS, 41, 889.
[4] Botta, O., Glavin, D., Kminek, G., Bada, J. 2002, OLEB, 32, 143.
[5] Elsila J. E., Dworkin J. P., Bernstein M. P., Martin M. P., Sandford S. A., 2007. ApJ, 660, 911.
[6] Kaiser R. I., Stockton A. M., Kim Y. S., Jensen E. C., Mathies R. A., 2013. ApJ, 765, 111
[7] Fourikis N., Takagi K., Morimoto M., 1974. Astrophys. J. 191, L139.
[8] Requena-Torres M. A., Martín-Pintado J., Rodríguez-Franco A., Martín S., Rodríguez-Fernández N. J., de Vicente P., 2006. Astron. Astrophys. 455, 971
[9] Remijan A., Snyder L. E., Liu S.-Y., Mehringer D., Kuan Y.-J., 2002. Astrophys. J. 576, 264.
[10] Cheung A. C., Rank D. M., Townes C. H., Thornton D. D., Welch W. J., 1968. Phys. Rev. Lett. 21, 1701.
[11] Gardner E. P. & McNesby J. R., 1980. J. Photochem., 13, 353.
[12] Kim Y. S. and Kaiser R. I., 2011. ApJ, 729:68.
[13] Theulé P., Borget F., Mispelaer F., Danger G., Duvernay F., Guillemin J. C., Chiavassa T., 2011. A&A, 534, A64.
[14] Förstel M., Bergantini A., Maksyutenko P., Góbi S., Kaiser R. I., 2017. ApJ, 845:83.
[15] Es-sebbar Et-t., Alrefae M. and Farooq A., 2014. JQSRT, 133, 559.
[16] Theule P., Duvernay F., Ilmane A., Hasegawa T., Morata O., Coussan S., Danger G. and Chiavassa T., 2011. A&A 530, A96.
[17] Raunier S., Chiavassa T., Marinelli F., Allouche A. and Aycard J.-P., 2003. J. Phys. Chem. A, 107, 9335.
[18] Noble J. A., Theule P., Borget F., Danger G., Chomat M., Duvernay F., Mispelaer F. and Chiavassa T., 2013. MNRAS 428, 3262.
[19] Mencos A. and Krim L., 2016. MNRAS 460, 1990.
[20] Lin M.Y., Lo J.I., Lu H.C., Chou S.L., Peng Y.C., Cheng B.M., Ogilvie J. F., 2014. J. Phys. Chem. A, 118, 3438.
[21] Khoshkhoo H., Nixon E.R., 1973. Spectrochimica Acta Part A: Molecular Spectroscopy, 29, 4, 603
[22] Zins E. L. and Krim L., 2013. RSC Advances, 3, 10285
[23] Ewing G.E., Thompson W.E., Pimentel G.C., 1960. J.Chem.Phys. 32, 927
[24] Leroi G. E., Ewing G. E., Pimentel G. C., 1964. J.Chem.Phys., 40, 2298
[25] Nxumalo L.M., Ford T.A., 1994. J.Mol.Struc., 327, 145.
[26] Jacox M. E., 1988. J. Chem. Phys., 88, 4598.
[27] Bennett C. J., Jones B., Knox E., Perry J., Kim Y. S., Kaiser R. I., 2010. ApJ, 723:641.

General conclusions and overview

One of the main objectives of this thesis was building an experimental system having a capability to investigate the reactivity and formation of reactive radicals and monitor their evolutions during the temperature variance in low temperature and pressure. In doing so, the main study consisted of the investigation of irradiated interstellar ice analogs containing ammonia and methane. Considering that interstellar ices contain water, the simulated experimental ices were introduced with water molecules to study the possible water catalytic effects in formation of radical and complex stable species. Prior to working on the three body system NH_3-CH_4-H_2O each of the two systems were studied separately: photolysis of NH_3-H_2O and CH_4-H_2O.

The photolysis of NH_3-H_2O has been carried out in both diluted (isolated in neon matrix) and condensed phases. Diluted phase investigations lead to the formation of several photoproducts such as NH_2, NH_2OH, cis and trans HONO, HO_2, HON, HNO, NO, N_2O and NO_2, while in the condensed bulk phase the only photoproducts detected are N_2, NH_2 and NH_2OH. Bulk ice NH_3 + H_2O, with the addition of 2 % of water, photolysis made possible the NH_3 + OH → NH_2 + H_2O reaction to occur increasing the formation of NH_2 radical showing a catalytic role played by H_2O molecules in enhancing NH_2 formation during the photolysis processing. Further on, by heating the sample to higher temperatures, the formation of stable species NH_2OH was observed. Similarly, a different approach was used to produce the amino NH_2 radical using hydrogenation of the atomic nitrogen, using the different N_2-H_2 gas ratios in the microwave discharge. Co-depositing the amount of NH_2 radical (formed through the hydrogenation of nitrogen atom) in conjunction with water, formation of NH_2-H_2O complex was observed shifted from NH_2 band, proving the formation of more stable complex. This confirmed that the opposite reaction NH_2 + H_2O → NH_3 + OH is not possible.

While the photolysis of NH_3-H_2O ices leads to the formation of stable species NH_2OH, it is still puzzling that this simple molecule is not yet detected in space. Having this in mind an experimental study was carried out to study the behavior of NH_2OH in interstellar ice analogs. The experimental results show clearly that the chemical transformation of NH_2OH occurring in the solid phase at relatively lower temperatures before the desorption processes of NH_2OH from the mantle of interstellar icy grains might be the main cause of the very low abundance of hydroxylamine in space and then it might explain its non-detection. Knowing that the NH_2OH desorption temperatures range from 160 to 190K, it was showed, through this study, there is a competition between NH_2OH desorption into the gas phase and its chemical transformation in the solid sample, occurring at relatively lower temperature and leading to the formation of HNO, NH_3 and O_2. From these experimental results, it was proved that the chemical transformation of NH_2OH starts occurring in solid phase at 130K, a temperature far lower than that of NH_2OH desorption and this may reduce considerably the abundance of NH_2OH molecules releasing in the gas phase. We also show that this NH_2OH chemical transformation is due mainly to the presence

of high amount H_2O and NH_2OH aggregates. Finally, these results might be the primary reasons to the non-detectability of hydroxylamine in space.

Following the photolysis study of NH_3-H_2O ices, a similar study was carried out with methane. It was shown that the similar catalytic behavior takes place in methane-water ice during the photolysis process as observed in ammonia-water ices. The increase of 2% of water shows the increase in production of methyl radical though the additional reaction $CH_4 + OH \rightarrow CH_3 + H_2O$. While during the photolysis of NH_3 and NH_3-H_2O ices lead to the formation of a very few reaction products, NH_2, N_2 and NH_2OH, the UV irradiation of CH_4-H_2O is a source of many more complex molecules, mainly alka[e]ne, HCO, H_2CO, CH_3OH, CH_3CH_2OH in addition to different fragments derived H_2O and CH_4. It was shown that the simultaneous presence in the same sample of these latter photofragments such as CH_3 and OH radicals leads to more complex organic compounds during the sample heating. The heat treatment further on revealed the formation of larger alcoholic species – propanol (non-detected in the ISM) and metoxymethanol (just recently detected in the ISM - in December 2017)...

The puzzling non-detection of larger alcohols like propanol or allyl alcohol in the ISM leads us to perform the study of the hydrogenation process of alcohols and aldehydes involving triple, double and single CC bonds under the ISM conditions. The hydrogenation of the simplest aldehyde H_2CO to form CH_3OH suggests a possible alcohol formation pathway through its aldehyde counterpart. Propynal and propanal have been observed in the ISM where H addition reactions are predominant while neither propargyl nor propanol alcohols have been detected. Pure aldehyde and alcohol ices formed at 10 K have been bombarded by H-atoms, showing that unsaturated alcohols can be reduced to fully or partially saturated alcohols while unsaturated aldehydes such as propynal and propenal are exclusively reduced to fully saturated aldehyde, propanal. This study shows that there is no link between larger aldehydes and their corresponding reduced alcohols via successive H-addition occurring in solid phase at cryogenic temperatures. By combining the two studies UV processing of CH_4-H_2O ices and H-addition reaction on aldehyde ices we conclude that larger alcohols would form exclusively under energetic processing and should be searched for in regions with high fluxes of UV or cosmic ray radiations such as the hot cores and corinos rather than dark cold molecular clouds.

The last chapter was devoted to the experimental study on the photolysis of NH_3-CH_4-H_2O ices. This work showed that the addition of water leads to the formation of NH_2 and CH_3 and their main recombination products CH_3NH_2 which was detected in low temperature solid ices through IR spectrometry. Another formed species included the reduced derivative of methylamine HCN and HNCO. At higher temperatures the IR spectra show the transformation of HCN and HNCO into the CN^- and OCN^- ions in addition to other IR signals of more complex species. With this experiment we reach the identification limit by IR spectroscopy of these complex species due to the fact that all the absorption bands become wider and overlap. To overcome this problem, we have chosen the combination of IR and mass spectrometry in order to identify the complex organic species formed during the irradiation of NH_3-CH_4-H_2O ice. We

show that very large species can be formed with masses up to 100u. We have proposed some potential organic molecules which may be formed under our experimental conditions, however, theoretical modeling are needed to propose reaction pathways involving photoproducts detected in separate irradiated NH_3-H_2O and CH_4-H_2O ices.

Résumé: L'eau joue un rôle fondamental dans la photochimie du milieu interstellaire (MIS), à travers la formation d'espèces très réactives comme OH. Les radicaux OH peuvent par la suite interagir avec d'autres molécules hydrogénées pour reformer H_2O par abstraction d'hydrogène: R-H + OH → R* + H_2O. Dans le cadre de ce travail de thèse, nous avons étudié l'influence des photons VUV sur des analogues de glace interstellaire NH_3-H_2O, CH_4-H_2O, NH_3-CH_4-H_2O. Nous montrons que l'incorporation d'une petite quantité d'eau dans ces glaces augmente considérablement la formation de radicaux réactifs comme NH_2 et CH_3 pendant le processus de photolyse et que le chauffage des glaces binaires irradiées telles que NH_3-H_2O et CH_4-H_2O conduit à la formation de NH_2OH et d'espèces alcooliques plus complexes comme le propanol et le métoxyméthanol. Nous avons également entamé d'autres études en parallèle sur le l'évolution thermique des glaces de NH_2OH d'une part et la formation de propanol par voies énergétiques (irradiation VUV) et non énergétique (réaction d'addition H) d'autre part afin de tenter d'expliquer la non-détection des ces espèces organiques dans le milieu interstellaire. Nos résultats montrent que les molécules d'hydroxylamine subissent une transformation thermique avant d'atteindre leurs températures de désorption tandis que les alcools plus complexes que le méthanol sont formés exclusivement par voies énergétique, ce qui suggère qu'ils ne devraient être présents que dans les régions à forts flux de rayonnements UV ou cosmiques et non dans les nuages moléculaires froids. L'étude des glaces mixtes irradiées NH_3-CH_4-H_2O a montré la formation à basse température d'espèces plus exotiques telles que HNCO, CH_3NH_2 et HCN en plus des anions OCN^- et CN^- formés à des températures plus élevées. En combinant les spectrométries IR et de masse, nous avons réussi à identifier des composés organiques très complexes déjà détectés ou activement recherchés dans le MIS.

Mots clés: Spectroscopie IRTF, Spectroscopie de Masse, Phase solide, Photons VUV, Radicaux activés, MOC-Molécules organiques complexes. Nuages moléculaires, Molécules hydrogénées, Températures cryogéniques.

Abstract: Water plays a fundamental role in the photochemistry of the interstellar medium (ISM), through OH radical formation. Highly reactive, OH radicals can interact with other H-containing species to form H_2O through a hydrogen abstraction reaction: R-H + OH → R^* + H_2O. In the present work, we have investigated the VUV processing on NH_3-H_2O, CH_4-H_2O, NH_3-CH_4-H_2O interstellar ice analogs. We show that the incorporation of small amount of water in these ices greatly increases the formation of reactive NH_2 and CH_3 radicals during the photolysis processing. Thermal treatments of irradiated NH_3-H_2O and CH_4-H_2O ices lead to the formation of NH_2OH and larger alcoholic species such as propanol and metoxymethanol. Further studies of thermal processing of NH_2OH ice and formation of propanol through energetic (VUV irradiation) and non-energetic (surface H-addition reaction) processing were carried out in the context of this thesis in order to try explaining their non-detection in the interstellar medium. Our results show that hydroxylamine molecules undergo thermal transformations before reaching its desorption temperatures while large alcohols are formed exclusively through energetic processing which suggests that they should be present only in regions with high fluxes of UV or cosmic ray radiations such as the hot cores and corinos rather than in the dark cold molecular clouds. Our study of the irradiated mixed NH_3-CH_4-H_2O ices showed the formation of more exotic species such as HNCO, CH_3NH_2 and its derivative HCN at low temperatures in addition to OCN^- and CN^- anions formed at higher temperatures. By combining the IR and mass spectrometries, we managed to identify very large complex organic compounds already detected or tensively sought throughout the ISM.

Keywords: FTIR spectroscopy, Mass spectroscopy, solid phase, VUV Photons, Activated radicals, COM-complex Organic Molecules, Molecular clouds, H-containing molecules, cryogenic temperatures